MODELLING STIFFNESS AND SHEAR STRENGTH OF COMPACTED SUBGRADE SOILS

ZHONG HAN

Thesis submitted to the
Faculty of Graduate and Postdoctoral Studies
in partial fulfillment of the requirements
for the Doctorate in Philosophy degree in Civil Engineering

Department of Civil Engineering
Faculty of Engineering
University of Ottawa

The Doctor of Philosophy in Civil Engineering is a joint program between Carleton University and University of Ottawa, which is administered by the Ottawa-Carleton Institute for Civil Engineering

ABSTRACT

Compacted soils are frequently used as subgrade for pavements as well as commercial and residential buildings. The stiffness and shear strength properties of compacted soils, which are collectively denoted as Ω in this thesis, fluctuate with moisture content changes that result from the influence of environmental factors such as the evaporation and infiltration. For example, mechanistic pavement design methods require the information of resilient modulus (M_R), which is the soil stiffness behavior under cyclic traffic loading, and its variation with respect to the soil moisture content determined from laboratory tests or estimation methods. Significant advances have been made during the last five decades to understand and model the variation of the Ω with respect to soil moisture content and soil suction (s) based on the principles of mechanics of unsaturated soils. There are a variety of models presently available in the literature relating the Ω to the s using different approaches. There are however uncertainties extending these models for predicting Ω - s relationships when they are used for a larger soil suction range. In addition, the good performance of these models are only valid for certain soil types for which they were developed and calibrated.

Studies presented in this thesis are directed towards developing a unified methodology for modelling the relationship between the Ω and the s using limited while easy-to-obtain information. However, more emphasis has been focused on the M_R - s relationships of pavement subgrade soils considering the need for the application of the mechanistic pavement design methods in Canada. The following studies have been conducted:

(i) State-of-the-art review on existing equations in the literature for the M_R - s relationships is summarized. A comparison study is followed to discuss the strengths and limitations of these equations;

(ii) A unified methodology for modelling the Ω - s relationships is proposed. Experimental data on 25 different soils are used to verify the proposed unified methodology. The investigations are applied on small strain shear modulus, elastic

modulus, and peak and critical shear strength. Good predictions are achieved for all of the investigated soils;

(iii) Performance of the proposed methodology is examined for the M_R - s relationships using experimental data of 11 subgrade soils. Reasonably good predictions are achieved for all of the subgrade soils;

(iv) Extensive experimental investigations are conducted on the M_R - s relationships for several subgrade soils collected from various regions in Canada. Experimental results suggest non-linear variation in the M_R with respect to s, moisture content and the external stress. The measured results are modelled using the proposed methodology with adequate success;

(v) Additional experimental investigations are performed to determine the variation of the elastic modulus (E) and unconfined compression strength (q_u) with the s and the gravimetric moisture content (w) for several Canadian subgrade soils. An approach, which is developed extending the proposed unified methodology, is used to normalize the measured M_R - w, E - w and q_u - w relationships. It is shown that the normalized M_R - w, E - w and q_u - w relationships exhibit remarkable similarity and can be well described using the proposed approach. Such similarity in the normalized Ω - moisture content relationships are also corroborated using the experimental data on several other soils reported in the literature.

The proposed unified methodology alleviates the need for the determination of the Ω - s relationships which requires elaborate testing equipment that needs the supervision of trained personnel and is also time-consuming and expensive. In addition, experimental programs in this thesis provide detailed experimental data on the M_R, E, q_u, and soil-water characteristic curves of Canadian subgrade soils. These data will be helpful for the better understanding of the hydro-mechanical behavior of the Canadian subgrade soils and for the implementation of the mechanistic pavement design method in Canada. The simple tools presented in this thesis are promising and encouraging for implementing the mechanics of unsaturated soils into conventional geotechnical engineering practice.

ACKNOWLEDGEMENTS

Studies presented in this thesis were conducted at the Department of Civil Engineering, University of Ottawa under the supervision of Prof. Sai K. Vanapalli. I am proud to say that Dr. Vanapalli is not only my supervisor, but also my Guruji for my research as well as my life. His encouragement, insightful suggestions, and continuous supports have enlightened my way towards exploring the mysteries of unsaturated soils and have broadened my horizon and vision.

The financial supports received from the China Scholarship Council (CSC) - University of Ottawa joint scholarship, the Natural Sciences and Engineering Research Council of Canada (NSERC), and the Ministry of Transportation of Ontario (MTO) are gratefully acknowledged.

My appreciations extend to my colleagues at the University of Ottawa for their friendship, company and support. They are: Jules, Celestin, Won, Fathi, Hana, Naresh, Javad, Singyu, Shunchao, Xueming, Mohammed, Yunlong, Ping, Hongyu, Junping, Penghai, Jiaying. Special thanks go to Dr. Weilie Zou, Professor at Wuhan University, China for his kind help and suggestions on this thesis; and to Mihambanou and Amina, undergraduate students at the University of Ottawa and Vinicius and Bruno, exchange undergraduate students from Brazil for their assistance during the experimental investigations.

I am extremely thankful for my parents, who wholeheartedly encouraged their only child to go Canada to pursuit his studies and dreams, and supported his every decision in his life. They have been courageous in accepting several challenges during the last four years, without their grownup son at home. This thesis would not have been possible without their love, support and inspiration. I humbly dedicate this thesis to my parents, Jingyan and Hong.

LIST OF CONTENTS

LIST OF FIGURES

LIST OF TABLES

CHAPTER ONE

GENERAL INTRODUCTION

1.1 Background

Pavements form the major infrastructure for land transportation systems that are of critical importance to the regional and global economy. Typical pavement structure constitutes of one or more layers of compacted granular base and sub-base placed over compacted subgrade and sealed with rigid or flexible surfacing (Brown 1996). Figure 1.1 shows a typical pavement structure.

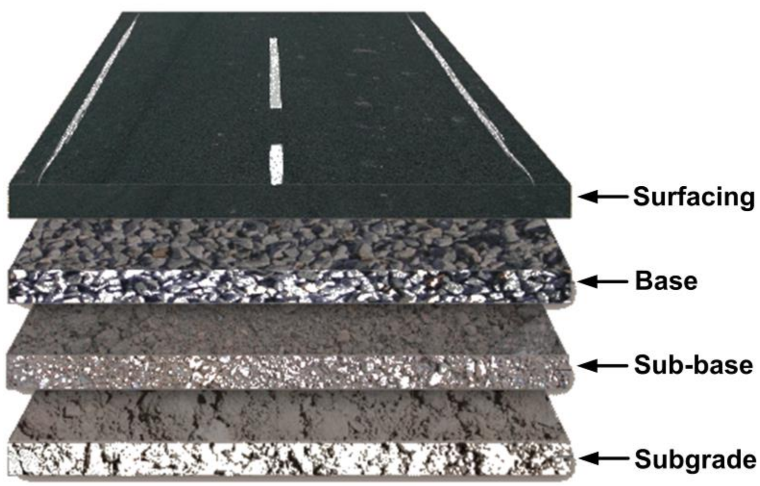

Figure 1.1 Typical pavement structure

Two failure criteria widely used in the design of pavement and the assessment of pavement service life are:

(i) Fatigue cracking at the bottom of the surfacing;
(ii) Permanent deformation at the surface of the subgrade layer that leads to rutting.

The stiffness behavior of the pavement layers under cyclic traffic loading has been identified as the key parameter for the rational analysis of both the fatigue cracking and rutting which arise respectively due to the repeated recoverable deformation and the accumulation of permanent deformation (Brown and Selig 1991).

Traffic loading in pavement analysis is conventionally simplified as a cyclic deviator stress (σ_d). The application of the σ_d results in permanent strain (ε_p) and resilient strain (ε_r) within pavement materials. The definition of resilient modulus (M_R), which is widely accepted in the literature, was originally introduced by Seed et al. (1962) as the ratio of the σ_d to the ε_r. This definition is also adopted by AASHTO (1986) pavement design guide. Since then M_R has been widely used as the key soil stiffness parameter in the mechanistic pavement design methods to:

(i) Rationally characterize the resilient behavior of the pavement materials;
(ii) Analyze the fatigue failure of the surface layer;
(iii) Dimension the multilayer system of the pavement structure.

Pavement base, sub-base and subgrade materials are compacted materials that typically stay in an unsaturated condition and are subjected to the environmental factors such as the wetting-drying and freeze-thaw cycles. The environmental factors pose significant influence on the moisture content and soil suction (s) variations within the pavement structure, which in turn, influence the strength and stiffness of pavement materials.

Research studies undertaken since 1970's have highlighted strong relationships between the shear strength and stiffness properties (collectively noted as Ω) of unsaturated soils with respect to the s (Fredlund et al. 1978, Edil et al. 1981, Wu et al. 1984, Alonso et al. 1990, Vanapalli et al. 1996, Drumm et al. 1997, Khalili et al. 2004, Ng and Yung 2008, Sawangsuriya et al. 2009a, Khosravi and McCartney 2012, Oh and Vanapalli 2013, Alonso et al. 2013, Lu and Kaya 2014, Hoyos et al. 2015). It is therefore recommended to use s as one of the key parameters to interpret and predict the response of the Ω of unsaturated soils to the soil moisture content fluctuations.

The M_R of pavement materials is sensitive to many other factors in addition to s which include applied stress level, moisture content, soil type, soil fabric and structure, and testing protocol (Puppala 2008, Malla and Joshi 2008). The variation of the M_R with respect to the moisture content is widely determined and used in practice because the measurement of the moisture content is convenient, quick and reliable (Li and Selig 1994, Drumm et al. 1997, Khoury et al. 2013). However, the M_R - moisture content relationships are highly soil-type-dependent and hence difficult to characterize (Heath et al. 2004, Ng et al. 2013).

Sauer and Monismith (1968), Edris and Lytton (1976), Fredlund et al. (1977), and Edil and Motan (1979) are pioneers who extended the mechanics of unsaturated soils for the interpretation and prediction of the variation of the M_R with respect to the s. Such an approach is promising, rational and reliable to better understand and determine the influence of seasonal moisture regime fluctuations on the M_R. Experimental investigations in recent years highlighted the influence of the s on the M_R of various pavement materials (Khoury and Zaman 2004, Yang et al. 2008, Thom et al. 2008, Khoury et al. 2011, Ng et al. 2013, Sivakumar et al. 2013, Ng and Zhou 2014, Abu-Farsakh et al. 2015, Salour and Erlingsson 2015). Reliable determination of the variation of M_R with respect to soil suction from experimental methods is time consuming and needs sophisticated equipment as well as trained personnel. Due to these reasons, several researchers proposed various equations in the literature to predict the M_R - s relationships for different pavement materials (Lytton 1995, Yang et al. 2005, Liang et al. 2008, Sawangsuriya et al. 2009a, Cary and Zapata 2011, Ng et al. 2013, Ba et al. 2013, Nokkaew et al. 2014). These studies have provided valuable information for better understanding the influence of the s on the M_R.

The presently used models are capable of providing reasonable predictions for the pavement materials for which they have been developed. Reliable model parameters are however required for extending these models for other pavement materials. These model parameters are typically derived from regression analysis performed on extensive experimental data on the M_R - s relationships which are cumbersome to obtain (Vanapalli and Han 2014). For this reason, there is an urgent need for a methodology that can be used for reliably predicting the M_R - s relationships for a wide range of soils using simple soil properties and easy-to-estimate model parameters.

Ontario is one of the largest province in Canada which significantly contributes to the Canadian economy. Ontario has approximately 16,600 km of provincial highway and 2,756 bridges. In the 2015-2016 fiscal year, \$2.4 billion has been allocated by the Ontario government towards the rehabilitation and expansion of provincial highways and bridges to stimulate and strengthen economic growth. The traditional pavement design methods that are used in Ontario and other provinces in Canada are empirical in approach and may not guarantee satisfactory pavement performance over a long term. In addition, maintenance costs of these pavements can be exorbitant. Significant savings could be achieved by implementing mechanistic pavement design methods which can improve the quality of newly constructed highways and reduce future deterioration and rehabilitation works.

The Ministry of Transportation of Ontario (MTO) is one of the pioneers of the North American government agencies to adopt the new mechanistic-based pavement design method: Mechanistic-Empirical Pavement Design Guide (MEPDG) which was developed under the National Cooperative Highway Research Program (NCHRP 1-37A) (Stolle et al. 2009), for the design and rehabilitation of pavements in Ontario. The successful implementation of the MEPDG depends on high quality testing data on the M_R of typical Ontario local pavement materials. The determination of the M_R for use in the MEPDG should also consider the influence of applied stress level and moisture content.

1.2 Objective

Studies presented in this thesis aim at developing a unified methodology based on the mechanics of unsaturated soils to rationally interpret and predict the evolution of Ω of unsaturated soils with respect to s. Such a methodology can be used for predicting M_R - s relationships for pavement materials considering various influencing factors such as the external stress, soil type, soil structure and fabric, and testing technique for pavement design practice following mechanistic design methods. It also can be applied to predict the variation of other mechanical properties, such as the shear strength τ, small strain shear modulus G_0, elastic modulus E with s to serve the rational design and analysis of geotechnical infrastructure for which these mechanical properties are needed. The unified methodology is simple in formulation, easy to use and compatible with the existing prediction methodologies used in engineering practice.

Extensive experimental data on the mechanical properties of soils varying from cohesionless sands and silts to lean and highly expansive clays that are available in the literature are collected and used for the development and validation of the proposed methodology. In addition, comprehensive experimental investigations are conducted to determine the M_R, E and unconfined compression strength q_u of several typical subgrade soils collected from different locations in Canada (1 soil from Saskatchewan, and 3 soils from Ontario). The experimental data are used to validate the proposed methodology. These data are also valuable for assisting the implementation of the MEPDG in Ontario pavement design practice.

1.3 Novelty

The developments in the research area of the mechanics of unsaturated soils since the 1950's have contributed to different approaches for interpreting and predicting the mechanical properties of unsaturated soils. There are at least 46 different equations proposed for the τ (Vanapalli 2009), seven equations proposed for the E, 15 equations proposed for the G_0 (Oh and Vanapalli 2014) and 30 equations proposed for the M_R (Han and Vanapalli 2016a). These approaches have significantly contributed to our present understanding of the stiffness and shear strength behaviors of unsaturated soils. However, implementation of these approaches into the geotechnical engineering practice requires the calibration of various model parameters involved in these equations by performing regression analysis using extensive experimental data. Experimental determination of the Ω - s relationship is time-consuming, cumbersome, and expensive. Moreover, it is difficult for practitioners to make engineering judgement choosing the most suitable approach for predicting a specific Ω - s relationship. Lack of judgement introduces uncertainties especially when users have limited knowledge with respect to the strengths and limitations of a specific equation. The experimental difficulties along with the diversity and complexity of the prediction methods pose major obstacles for the implementation of the mechanics of unsaturated soils in conventional geotechnical practice.

The studies presented throughout this thesis contribute towards analyzing the variation of different mechanical properties of unsaturated soils with respect to soil suction using a unified methodology. Several novelties of the methodology introduced in this thesis are summarized below:

(i) For using this methodology, only limited experimental data including the SWCC and the Ω values at saturated condition and one referencing unsaturated condition are needed. The required experimental data can be determined from conventional tests;

(ii) Only one model parameter is involved in the formulation of the proposed methodology, which is found to be constant. This further waives the calibration process and therefore alleviates the need for an extensive amount of experimental data;

(iii) The proposed methodology is validated using experimental data of more than 30 different soils on various mechanical properties (including shear strength and elastic moduli at different strain levels and drainage conditions) derived using different testing techniques (e.g., direct shear, triaxial, bender element, resonant column, plate load and cyclic loading tests) from all regions of the world. It is found that the proposed methodology is capable of providing reliable predictions for all of the soils taking account the various influencing factors such as the soil type, soil structure and fabric, hydraulic hysteresis, anisotropy, and testing technique.

Currently, there are limited experimental studies available in the literature that provide detailed information on the M_R of typical Canadian subgrade soils. Experimental program presented in this thesis for determining the variation of the M_R, E and q_u with s for four Canadian subgrade soils yields first-hand testing data that can be used not only to validate the proposed methodology, but also to contribute to our understanding of the resilient behavior of typical Canadian subgrade soils. Such experimental studies and resulting data will contribute to the characterization of the pavement materials and the rational implementation of the MEPDG in the design of pavements in Canada.

In addition, an approach is developed based on the proposed methodology to normalize the Ω - moisture content relationships obtained in this thesis. It is found that, for the same soil, the normalized Ω - moisture content relationships for different mechanical properties show remarkable similarities and can be suitably fitted by the proposed approach for normalization. It is therefore suggested to use Ω - moisture content relationships that are easy to obtain to predict the Ω - moisture content relationships that are difficult to obtain. The similarity in the normalized Ω - moisture content relationships are also corroborated using experimental data on several other soils reported in the literature. The proposed normalization approach is the first of its kind that contributes to further simplify the prediction of the Ω - moisture content relationships.

1.4 Layout

This thesis is organized in a format of "a collection of manuscripts". The thesis consists of seven chapters. Chapter one provides a general introduction to the manuscripts summarized in this thesis while Chapter seven provides overall summary and discussions for the presented studies as well as suggestions for future work.

Chapters two through six are five different manuscripts published in or submitted to the peer-reviewed journals themed in geotechnical engineering. In order to maintain the integrity of each of the manuscripts while organizing them into a thesis, some minor changes are made with respect to text, numbering of equations, figures and main- and sub-titles. The notation used for each manuscript are different considering the requirements of different journals. Therefore, a table of notation is provided at the beginning of each chapter for clarification purposes.

The main content of the seven chapters are briefly described as follows:

(i) Chapter One presents the background, objective, novelty and layout of this thesis;

(ii) Chapter Two consists of a comprehensive state-of-the-art review on the experimental determination of resilient modulus of unsaturated soils, the various characteristics of the M_R - s relationships, and the equations available in the literature for predicting M_R - s relationships. A comparison study using six different existing equations to provide predictions of the M_R for three different soils is presented to discuss the strengths and limitations of the current equations. This chapter is the manuscript "State-of-the-Art: Prediction of resilient modulus of unsaturated subgrade soils" authored by Zhong Han and Sai K. Vanapalli that is published in *ASCE International Journal of Geomechanics* in 2016;

(iii) Chapter Three proposes a unified methodology for predicting the Ω - *s* relationships. Experimental data available in the literature on a total of 25 soils that include 8 cohesionless soils and 17 cohesive soils are used to verify the unified methodology. The investigated Ω include small strain shear modulus, elastic modulus, peak shear strength, and critical shear strength. It is found that the unified methodology is capable of providing reasonable predictions for all the different soils and mechanical properties. This chapter is the manuscript "Stiffness and shear strength of unsaturated soils in relation to soil-water characteristic curve" authored by Zhong Han and Sai K. Vanapalli that is published in *Géotechnique* in 2016;

(iv) Chapter Four validates the performance of the proposed methodology for predicting the resilient modulus - soil suction relationships. The information needed for prediction includes the SWCC, M_R at saturated condition and optimum moisture content condition. The methodology is verified using 16 sets of experimental data derived from 11 different soils. Reasonably good predictions are achieved for all the soils. This chapter is the manuscript "Model for predicting the resilient modulus of unsaturated subgrade soil using the soil-water characteristic curve" authored by Zhong Han and Sai K. Vanapalli that is published in *Canadian Geotechnical Journal* in 2015;

(v) Chapter Five presents an extensive experimental program on determining the M_R - *s* relationships for several subgrade soils collected from various regions in Canada. Experimental results suggest non-linear variation in the M_R with respect to *s*, moisture content and the external stress. The measurements on the M_R - *s* relationships are reasonably well predicted using the proposed methodology. This chapter is the manuscript "Relationship between resilient modulus and suction for compacted subgrade soils" authored by Zhong Han and Sai K. Vanapalli that that is published in *Engineering Geology* in 2016;

(vi) Chapter Six introduces additional experimental investigations using modified unconfined compression tests to determine the *E* and q_u, and their variations with *s* and gravimetric moisture content (*w*) for several Canadian subgrade soils. An approach is proposed to normalize the measured M_R - w, E - w and q_u - w relationships. It is observed that these normalized relationships are remarkably similar for the different mechanical properties of the same soil and they can be well fitted by the proposed approach. The observed similarity can be used to predict the Ω - w relationships that are difficult to measure (such as M_R - w relationships) from those that are easy to measure (such as E - w and q_u - w relationships). This has been verified using the experimental data from the tested subgrade soils. This chapter is the manuscript "Normalizing variation of soil stiffness and shear strength with moisture content" authored by Zhong Han and Sai K. Vanapalli that has been submitted to *ASCE Journal of Geotechnical and Geoenvironmental Engineering* in March 2016 for review and possible publication;

(vii) Chapter Seven presents overall summary, discussions and suggestions for the future research.

1.5 Related publications

Journal Publications:

1. **Han, Z**., and Vanapalli, S. K. (2016). Stiffness and shear strength of unsaturated soils in relation to soil-water characteristic curve. *Géotechnique*, 66(8): 627-647. DOI: 10.1680/geot./15-P-104.
2. **Han, Z.**, and Vanapalli, S. K. (2016). State-of-the-Art: Prediction of resilient modulus of unsaturated subgrade soils. *ASCE International Journal of Geomechanics*, 16(4): 04015104. DOI: 10.1061/(ASCE)GM.1943-5622.0000631.
3. **Han, Z.**, and Vanapalli, S. K. (2016). Relationship between resilient modulus and suction for compacted subgrade soils. *Engineering Geology*, 211: 85-97. DOI: 10.1016/j.enggeo.2016.06.020.
4. Vanapalli, S. K., and **Han, Z**. (2016). Modelling the mechanical properties of a compacted glacial till. *Indian Geotechnical Journal*. DOI: 10.1007/s40098-016-0183-9.

5. **Han, Z.**, and Vanapalli, S. K. (2015). Model for predicting the resilient modulus of unsaturated subgrade soil using the soil-water characteristic curve. *Canadian Geotechnical Journal*, 52(10): 1605-1619. DOI: 10.1139/cgj-2014-0339.
6. **Han, Z.**, and Vanapalli, S. K. Normalizing variation of soil stiffness and shear strength with moisture content. Submitted to *ASCE Journal of Geotechnical and Geoenvironmental Engineering* (under review).

Conference Publications:

7. **Han, Z.**, Ren, J. P., Faria, A. and Vanapalli, S. K. (2016). Modelling the resilient modulus of Ontario subgrade soils considering the environmental influences. In *Proceedings of the GeoVancouver2016, the 69th Annual Canadian Geotechnical Conference*, Vancouver, Canada.
8. **Han, Z.**, and Vanapalli, S. K. (2015). Prediction of the resilient modulus of unsaturated base-course materials. In *Proceedings of the IFCEE 2015*, San Antonio, USA. Geotechnical Special Publication 256, IFCEE 2015, Edited by M. Iskander, M. T. Suleimanand, J. B. Anderson and D. F. Laefer, 2112-2121. DOI: 10.1061/9780784479087.195.
9. **Han, Z.**, Mihambanou, B., and Vanapalli, S. K. (2015). Two-step approach for estimating the resilient modulus of pavement subgrade taking account the influence of moisture regime. In *Proceedings of the 2015 ASCE Airfield & Highway Pavement Conference*, Miami, USA. DOI: 10.1061/9780784479216.076.
10. **Han, Z.**, and Vanapalli, S. K. (2015). Resilient modulus - suction correlations for several subgrade soils from China. In *Proceedings of the 2015 Asia-Pacific Conferences on Unsaturated Soils*, Guilin, China, Unsaturated Soil Mechanics from Theory to Practice, Edited by Z. Chen, C. Wei, D. Sun, and Y. Xu, CRC Press, 247-252. DOI: 10.13140/RG.2.1.4162.1526.
11. **Han, Z.**, and Vanapalli, S. K. (2014). Predicting the variation of resilient modulus with respect to suction using the soil-water characteristic curve as a tool. In *Proceedings of the ASCE 2014 GeoCongress Conference*, Atlanta, Georgia, USA, Geotechnical Special Publication 234, Geo-Characterization and Modeling for

Sustainability, Edited by M. Abu-Farsakh, X. Yu, and L. R. Hoyos, 1463-1472. DOI: 10.1061/9780784413272.143.

12. **Han, Z.**, and Vanapalli, S. K. (2014). Prediction of the variation of the resilient modulus with respect to the soil suction for three granular materials using three methods. In *Proceedings of the 2014 GeoShanghai Conference*, Shanghai, China, Geotechnical Special Publication 239, Pavement Materials, Structures, and Performance, Edited by B. Huang, and S. Zhao, 414-423. DOI: 10.1061/9780784413418.041.
13. **Han, Z.**, and Vanapalli, S. K. (2014). Semi-empirical model for predicting the resilient modulus of unsaturated fine-grained soils using the soil-water characteristic curve. In *Proceedings of the 6th International Conference on Unsaturated Soils*, Sydney, Australia, Unsaturated Soils: Research & Applications, Edited by N. Khalili, A. Russell, and A. Khoshghalb, CRC Press, 797-803. DOI: 10.1201/b17034-113.
14. Vanapalli, S. K., and **Han, Z.** (2014). Application of the unsaturated soil mechanics in the design of pavements. In *Proceedings of the 6th International Conference on Unsaturated Soils*, Invited Paper, Sydney, Australia, Unsaturated Soils: Research & Applications, Edited by N. Khalili, A. Russell, and A. Khoshghalb, CRC Press, 1799-1805. DOI: 10.1201/b17034-263.
15. **Han, Z.**, and Vanapalli, S. K. (2013). Comparison between three different models for predicting the variation of the resilient modulus of subgrade soils with respect to soil suction. In *Proceedings of the 66th Canadian Geotechnical Conference & 11th Joint CGS/IAH-CNC Groundwater Conference*, Montreal, Canada. DOI: 10.13140/RG.2.1.4686.4405.
16. Vanapalli, S. K., and **Han, Z.** (2013). Prediction of the resilient modulus of unsaturated fine-grained soils. In *Proceedings of the 4th International Conference on Advances in Civil Engineering*, NCR, India, Advances in Engineering and Technology. Edited by B. S. Harish, and V. V. Das, Elsevier, a division of Reed Elsevier India Pvt. Ltd, 876-887. DOI: 10.13140/RG.2.1.3889.2881.

CHAPTER TWO

STATE-OF-THE-ART REVIEW

2.0 Background-Information

The contents presented in this chapter are from the manuscript of the publication:

Han, Z., and Vanapalli, S. K. (2016). State-of-the-Art: Prediction of resilient modulus of unsaturated subgrade soils. *ASCE International Journal of Geomechanics*. DOI: 10.1061/(ASCE)GM.1943-5622.0000631.

The symbols used in this chapter are summarized in Table 2.0.

Table 2.0 Symbols used in Chapter Two

Symbols	
a	minimum of log (M_R / M_{ROPT})
b	maximum of log (M_R / M_{ROPT})
c	compressibility factor,
c_{ld} and m_{ld}	intercept and slope of the σ_d versus log (M_R) relationship
DDR	dry density ratio
e	void ration
f	saturation factor ($1 < f < 1 / \theta$)
G_s	specific gravity
I_p	plasticity index
J_1	first stress invariant
k_m, k, k_s, k_{us}, k_1, k_2, k_3, k_4, k_5, m_b, K_1, K_2, a, n, m	model parameters
M_0	M_R value at reference stress state when $(u_a - u_w) = 0$
MDD	maximum dry density
M_R	resilient modulus
n	model parameter of Fredlund and Xing (1994) SWCC model
p	net mean stress
p_a	atmosphere pressure
p_r	reference pressure
q_{cyc}	cyclic shear stress
RC	relative compaction
RCM	percent of recycled clay masonry

Table 2.0 Symbols used in Chapter Two

Symbols	
S	degree of saturation
subscript $_{OPT}$	corresponding parameter value at optimum moisture content condition
u_a	pore-air pressure
w_L	liquid limit
α and β	Henkel pore water pressure parameters
α_1, β_1, κ, ξ,	model parameters
γ_d	dry density
ΔM_R	changes in M_R
$\Delta u_{w\text{-}sat}$	build-up of pore-water pressure under saturated conditions
$\Delta\theta_{bT}$	changes in θ_b due to temperature
$\Delta\theta_{b\psi}$	changes in θ_b due to soil suction
$\Delta\psi$	relative change of soil suction with respect to ψ_0 due to build-up of pore-water pressure under unsaturated conditions
ε_p	permanent strain
ε_q	deviator strain
ε_r	resilient strain
ε_v	volumetric strain
Θ	normalized volumetric water content
θ	volumetric water content
θ_b	bulk stress
θ_d	volumetric water content along the drying curve
θ_{net}	net bulk stress
θ_s	saturated volumetric water content
θ_w	volumetric water content along the wetting curve
σ_c	confining stress
σ_{cnet}	net confining stress
σ_d	cyclic deviator stress
σ_m	mean normal stress
τ_{oct}	octahedral shear stress
τ_{ref}	reference shear stress
χ	Bishop's effective stress parameter
ψ	soil suction
ψ_0	initial soil suction
ψ_b	air-entry value

2.1 Introduction

Pavements are the most widely used geotechnical structures in land transportation systems throughout the world. The structure of a typical pavement foundation is formed with compacted granular materials placed over compacted subgrade soils (Brown 1996). Two key criteria that are used in the design of pavement layers are the fatigue cracking at the bottom of the surface layer and the permanent deformation at the surface of the subgrade soils (Figure 2.1). The fatigue cracking failure is found closely related to the resilient behavior of the pavement materials in response to the traffic loading (Seed et al. 1962).

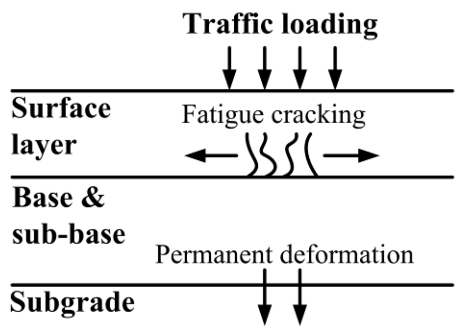

Figure 2.1 Schematic of a typical asphalt pavement structure

Traffic loading in pavement analysis is conventionally simplified as a cyclic deviator stress (σ_d). The repeated application of the σ_d results in permanent strain (ε_p) and resilient strain (ε_r) within pavement materials as shown in Figure 2.2. The resilient modulus (M_R), which was initially recommended as per AASHTO (1986) pavement design guide, has been widely used since then as the key soil property in the mechanistic pavement design methods to rationally characterize the resilient behavior of the pavement materials, analyze the fatigue failure of the surface layer, and dimension the multilayer system of the pavement structure. The definition of M_R has been introduced in the literature by Seed et al. (1962) as the ratio of the σ_d to the ε_r.

$$M_R = \frac{\sigma_d}{\varepsilon_r} \tag{2.1}$$

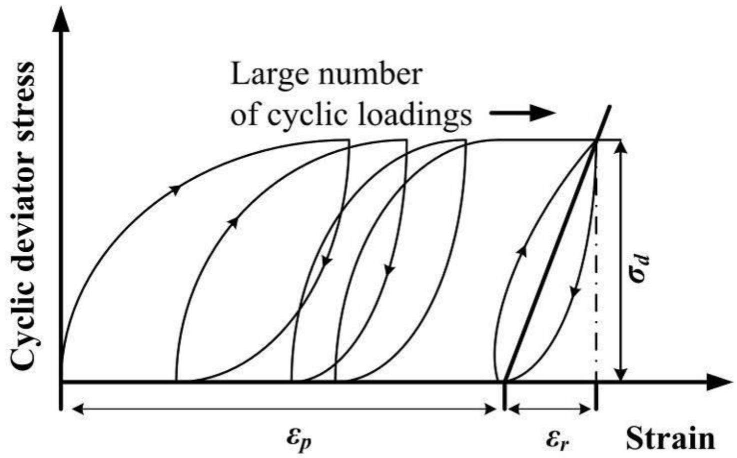

Figure 2.2 Response of soils to cyclic deviator stress

Pavement base / sub-base materials and subgrade soils are typical compacted soils that stay in an unsaturated condition and are subjected to environment influences. Environmental factors contribute to moisture regime and soil suction (ψ) variations within the pavement structure, which in turn, influence the strength and stiffness of pavement materials. Several research studies in recent years have demonstrated the strong correlations between the mechanical properties of unsaturated soils and the ψ (Fredlund et al. 1978, Edil et al. 1981, Wu et al. 1984, Alonso et al. 1990, Vanapalli et al. 1996, Drumm et al. 1997, Khalili et al. 2004, Ng and Yung 2008, Sawangsuriya et al. 2009a&b, Khosravi and McCartney 2012, Oh and Vanapalli 2013, Alonso et al. 2013, Lu and Kaya 2014, Hoyos et al. 2015). It is therefore recommended to use ψ as a key parameter to interpret and predict the response of the mechanical behavior of unsaturated soils to the soil moisture regime fluctuations. Experimental investigations in recent years highlighted the influence of the ψ on the M_R of various pavement materials (Khoury and Zaman 2004, Yang et al. 2008, Thom et al. 2008, Khoury et al. 2011, Khoury et al. 2012, Ng et al. 2013, Sivakumar et al. 2013, Ng and Zhou 2014, Abu-Farsakh et al. 2015, Salour and Erlingsson 2015). However, reliable determination of the M_R using experimental methods with soil suction control is time consuming, needs sophisticated equipment as well as trained personnel. Due to these reasons, several researchers proposed various equations in the literature to predict the M_R - ψ correlations (Lytton 1995, Yang et al. 2005, Liang et al. 2008, Sawangsuriya et al. 2009a, Cary and Zapata 2011, Ng et al. 2013, Ba et al. 2013, Nokkaew et al. 2014, Han and Vanapalli 2015). These equations can be used in pavement design to taking account for the influence of environmental factors.

The influence of several factors on the M_R of granular materials and subgrade soils are well documented in the literature (LeKarp et al. 2000, George 2004). However, a comprehensive state-of-the-art review of the equations for interpreting and predicting the variation of the M_R with respect to the ψ for pavement materials remains outstanding. In this chapter, various equations available in the literature that were proposed in this direction are summarized into three groups; namely, (i) empirical relationships, (ii) constitutive models incorporating the soil suction into applied shearing or confining stresses, and (iii) constitutive models extending the independent stress state variable approach. Two equations from each of the groups are selected to predict the variation of the M_R with respect to ψ for three compacted subgrade soils. The predictions are compared with the measured results. In addition, predictions for one subgrade soil by the six selected equations are plotted as surfaces presenting resilient modulus - cyclic stress - soil suction relationships for more rigorous comparisons. Strengths and limitations of the three summarized equation groups are reviewed based on the comparison studies. The state-of-the-art summary and comparison studies presented in this chapter are helpful to assist practicing engineers to choose appropriate equations for the reliable prediction of the resilient modulus taking account the influence of the soil suction.

2.2 Measurement of resilient modulus - soil suction correlations

Repeated load triaxial tests (RLTTs) are widely used to determine the M_R of pavement materials (Uzan 1985, Tian et al. 1998). There are a variety of standard testing protocols that can be followed to determine the M_R (e.g., AASHTO T292-91, AASHTO T307-99, NCHRP 1-28A (Witczak 2003)). These testing protocols have certain differences with respect to sequences of applying loading stresses, measurement of deformations, specimen preparation and conditioning methodology before and during the testing procedure. More detailed information of the various testing protocols are summarized by Puppala (2008). Several researchers incorporated various soil suction measurement or control techniques into the RLTTs to investigate the influence of the ψ on the M_R of pavement materials. For example, the ψ of the specimens can be measured after the completion of RLTTs using filter paper method or null pressure plate method which are both simple and inexpensive (Fredlund et al. 1977, Yang et al. 2005, Liang et al. 2008, Azam et al. 2013). However, such methods are user dependent and sensitive to testing protocols (Power et al. 2008, Power and Vanapalli 2010). Also, the applied stress on the specimens influences the soil suction (Vanapalli et al. 1999, Ng and Pang 2000). Due to the differences in the applied stress levels between the RLTTs and the soil suction measurement tests, the measured soil suction may not precisely represent the soil suction within the specimens during the RLTTs.

In recent years, modified cyclical triaxial testing systems equipped with various techniques (e.g., thermal dissipation sensor, psychrometer, suction probe, axis-translation technique etc.) are used to measure or control the soil suction during the RLTTs for obtaining reliable test results on the variation of the M_R with soil suction (Gupta et al. 2007, Yang et al. 2008, Craciun and Lo 2010, Cary and Zapata 2011, Ng et al. 2013, Sivakumar et al. 2013). Such modified triaxial testing systems are expensive, cumbersome and require trained professionals to conduct the tests. In addition, several weeks are typically required to achieve equilibrium conditions with respect to the each applied suction value for fine-grained unsaturated soils if axis-translation technique is employed (Khoury et al. 2011, Ng et al. 2013).

2.3 Prediction of resilient modulus - soil suction correlations

The Mechanistic-Empirical Pavement Design Guide (MEPDG, ARA, Inc., ERES, 2004) recommends using Equation 2.2 to estimate the M_R at Optimum Moisture Content (OMC) condition (M_{ROPT}) taking account the influence of the applied stresses.

$$M_R = k_1 p_a \left(\frac{\theta_b}{p_a}\right)^{k_2} \left(\frac{\tau_{oct}}{p_a} + 1\right)^{k_3} \tag{2.2}$$

where p_a = atmosphere pressure (i.e., 101.3 kPa), θ_b = bulk stress, τ_{oct} = octahedral shear stress, k_1, k_2 and k_3 = model parameters.

Equation 2.3 is used in MEPDG to calibrate the M_{ROPT} values considering the influence of seasonal moisture content fluctuations.

$$\log\left(\frac{M_R}{M_{ROPT}}\right) = a + \frac{b-a}{1+\exp[\ln(-\frac{b}{a}) + k_m(S - S_{OPT})]} \qquad (2.3)$$

where S = degree of saturation (in decimals), S_{OPT} = degree of saturation at OMC condition (in decimals), a = minimum of log (M_R / M_{ROPT}), b = maximum of log (M_R / M_{ROPT}), k_m = regression parameter. Parameter values a = − 0.5934, b = 0.4, k_m = 6.1324 are suggested for fine-grained soils, and parameter values a = − 0.3123, b = 0.3, k_m = 6.8157 are suggested for coarse-grained soils.

Equation 2.3 is an empirical relationship that was derived from extensive experimental data (Zapata et al. 2007). This equation is widely implemented in practice as it i) uses parameters a, b, and k_m with specific values which do not need calibration; ii) only requires the information of the M_{ROPT} and S that are conventionally determined. The variations of the (M_R / M_{ROPT}) with respect to the (S − S_{OPT}) predicted by Equation 2.3 for fine- and coarse-grained soils are shown in Figure 2.3.

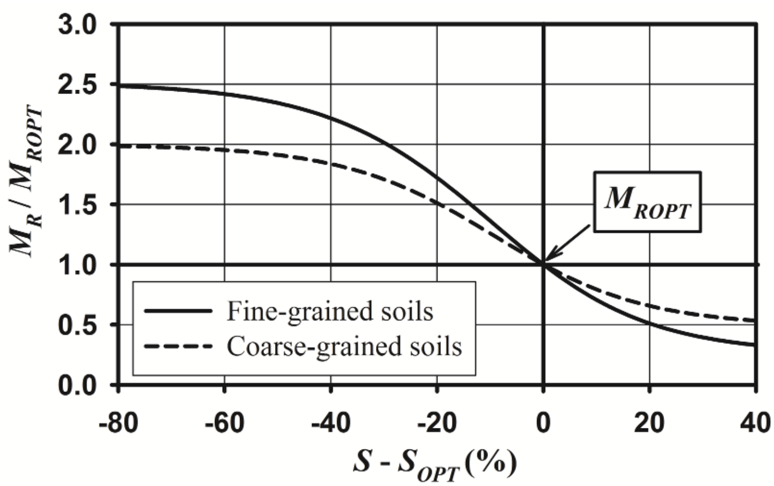

Figure 2.3 Predicted M_R / M_{ROPT} with respect to variation in moisture content by Equation 2.3

Recent studies show that the M_R - moisture content relationship is highly soil-type-dependent and hence is difficult to precisely characterize using either empirical or mechanistic methods (Heath et al. 2004, Ng et al. 2013). Sauer and Monismith (1968), Edris and Lytton (1976), Fredlund et al. (1977), Edil and Motan (1979) were the pioneers who suggested using soil suction as the fundamental parameter to interpret the response of resilient behavior of pavement materials to soil moisture content variations. Over the past four decades, various equations have been proposed in the literature to predict the M_R - ψ correlations for different pavement materials. These equations can be categorized into three groups (namely; *Group A*, *Group B*, and *Group C*) based on the different approaches used to take account the influence of the soil suction.

2.3.1 Group A. Empirical relationships

Empirical relationships are simple equations that are used to simulate the measured M_R - ψ correlations for specific soils. Such equations do not provide theoretical justification but are developed based on statistical analysis performed on large data base of experimental results for soils with approximately similar properties. Some empirical equations available in the literature are summarized below (soils are classified as per AASHTO M-145 soil classification system).

Johnson et al. (1986) proposed Equation 2.4 which was derived for sandy soils.

$$M_R = 1.35 \times 10^6 \times (101.36 - \psi)^{2.36} (J_1)^{3.25} (\gamma_d)^{3.06} \tag{2.4}$$

where J_1 = the first stress invariant, γ_d = dry density; M_R is in (MPa), ψ and J_1 are in (kPa), γ_d is in (Mg/m^3).

Parreira and Gonçalves (2000) proposed Equation 2.5 which was derived for a lateritic soil (A-7-6) from Brazil over the soil suction range of 0 to 87500 kPa.

$$M_R = 14.10 \sigma_d^{0.782} \psi^{0.076} \tag{2.5}$$

where M_R is in (MPa), σ_d is in (kPa), ψ is in (kPa).

Ceratti et al. (2004) proposed Equation 2.6 which was derived for a lateritic soil (A-7-6) from Brazil over an in-situ soil suction range of 0 to 14 kPa.

$$M_R = 142 + 16.9\psi \tag{2.6}$$

where M_R is in (MPa) and ψ is in (kPa).

Doucet and Doré (2004) proposed Equation 2.7 which was derived for several partial crushed and crushed granular materials from Quebec, Canada.

$$M_R = 1060\theta_b - 8700\psi + 57000 \tag{2.7}$$

where ψ and M_R are in (kPa).

Sawangsuriya et al. (2009a) proposed Equations 2.8 and 2.9 which were derived for four fine-grained subgrade soils (two A-4 soils and two A-7-6 soils) from Minnesota, USA over the soil suction range of 0 to 10000 kPa.

$$M_R / M_{RSAT} = \text{-}5.61 + 4.54\log(\psi) \tag{2.8}$$

$$M_R / M_{ROPT} = \text{-}0.24 + 0.25\log(\psi) \tag{2.9}$$

where $M_{RSAT} = M_R$ at saturation condition; ψ is in (kPa).

Ba et al. (2013) proposed Equation 2.10 which was derived for four unbound granular base materials from Senegal over the soil suction range of 0 to 100 kPa.

$$M_R / M_{ROPT} = 0.385 + 0.267\log(\psi) \tag{2.10}$$

where ψ is in (kPa).

Note that Equation 2.3 was also developed following this approach to relate M_R with S. When the soil-water characteristic curve (SWCC, which describes the S - ψ relationships) is known, Equation 2.3 can also be extended to predict M_R - ψ correlations. Empirical equations are widely used in practice as they are easy to apply. For example, for prediction, Equations 2.8, 2.9, and 2.10 only require the experimental data of M_{ROPT} or M_{RSAT} which can be determined using conventional equipment without soil suction control, no additional tests are required.

Several investigators proposed constitutive models to predict the M_R by relating applied stresses using model parameters. The power law equations proposed by Moossazadeh and Witczak (1981) (Equation 2.11), Uzan (1985) (Equation 2.12), and the ARA, INC., ERES (2004) (Equation 2.2) are the commonly used constitutive models.

$$M_R = k_1 (\frac{\sigma_d}{p_a})^{k_2} \tag{2.11}$$

$$M_R = k_1 p_a (\frac{\theta_b}{p_a})^{k_2} (\frac{\tau_{oct}}{p_a})^{k_3} \tag{2.12}$$

Equations 2.2, 2.11, 2.12 and other equations developed following similar formulations can be revised to take account the influence of soil suction using two different approaches. One approach is to include the contribution of the soil suction into applied confining or shearing stresses (*Group B*); the other approach is based on using the independent stress state variable approach (*Group C*).

2.3.2 Group B. Constitutive models incorporating the soil suction into applied shearing or confining stresses

Several constitutive models available in the literature that incorporate the soil suction into applied shearing or confining stresses are summarized below.

Loach (1987) proposed Equatin 2.13 which was derived for three fine-grained soils from UK over the soil suction range of 0 to 100 kPa.

$$M_R = \frac{\sigma_d}{k_1} [\frac{c\sigma_c + \psi}{\sigma_d}]^{k_2} \tag{2.13}$$

Jin et al. (1994) proposed Equation 2.14 which was derived for two granular base materials from Rhode Island, USA.

$$\Delta M_R = K_1 K_2 \theta_b^{K_2-1}(\Delta\theta_{bT} + \Delta\theta_{b\psi}) \quad (2.14)$$

Lytton (1995) proposed Equation 2.15 for granular base materials. Equation 2.15 was further verified using experimental data derived from nine granular base materials from Texas, USA by Gu et al. (2014).

$$M_R = k_1 p_a (\frac{\theta_b - 3f\theta\psi}{p_a})^{k_2} (\frac{\tau_{oct}}{p_a})^{k_3} \quad (2.15)$$

Heath et al. (2004) proposd Equation 2.16 which was derived for a typical granular base material from California, USA.

$$M_R = k_1 p_a [\frac{(\theta_b / 3) - u_a + \chi\psi}{p_a}]^{k_2} (\frac{\sigma_d}{p_a})^{k_3} \quad (2.16)$$

Yang et al. (2005) proposd Equation 2.17 which was derived for two fine-grained subgrade soils (one A-7-5 soil and one A-7-6 soil) from Taiwan, China over the soil suction range of 0 to 10000 kPa.

$$M_R = k_1(\sigma_d + \chi\psi)^{k_2} \quad (2.17)$$

Liang et al. (2008) proposed Equation 2.18 which was derived for two fine-grained subgrade soils (one A-4 soil and one A-6 soil) over the suction range of 150 to 380 kPa. Equation 2.18 was also validated using eight sets of experimental data on fine-grained soils from the literature.

$$M_R = k_1 p_a (\frac{\theta_b + \chi\psi}{p_a})^{k_2} (1 + \frac{\tau_{oct}}{p_a})^{k_3} \quad (2.18)$$

Oh et al. (2012) proposed Equation 2.19 which was derived for granular base and subgrade soils from Florida, USA.

$$M_R = k_1 p_a (\frac{\theta_b + 3k_4\psi\theta}{p_a})^{k_2} (\frac{\tau_{oct}}{p_a} + 1)^{k_3} \quad (2.19)$$

Sahin et al. (2013) proposed Equation 2.20 for granular base materials.

$$M_R = k_1 p_a [\frac{\theta_b - 3f\theta(\psi_0 + \beta \frac{\theta_b}{3} + \alpha\tau_{oct})}{p_a}]^{k_2} (\frac{\tau_{oct}}{p_a} + 1)^{k_3} \tag{2.20}$$

Notations in Equations 2.13 through 2.20: K_1, K_2, k_1, k_2, k_3, k_4 = model parameters, c = compressibility factor, σ_c = confining stress, ΔM_R = changes in M_R, $\Delta\theta_{b\psi}$ = changes in θ_b due to soil suction, $\Delta\theta_{bT}$ = changes in θ_b due to temperature, θ = volumetric water content, f = saturation factor ($1 < f < 1/\theta$), u_a = pore-air pressure, χ = Bishop's effective stress parameter, ψ_0 = initial soil suction, α and β = Henkel pore water pressure parameters.

These summarized models are developed based on either Bishop's effective stress concept or unsaturated soils (Bishop 1959; for example, Equations 2.16, 2.17, and 2.18) or micro-mechanics theory and thermo-dynamic laws (Fung 1977; for example, Equations 2.14, 2.15, 2.19, and 2.20).

2.3.3 Group C. Constitutive models extending the independent stress state variable approach

Several constitutive models availabe in the literature, which consider the soil suction as a stress state variable that influences the mechanical behavior of unsaturated soils independently, are summarized below.

Fredlund et al. (1977) proposed Equation 2.21 which was developed for a glacial till from Saskatchewan, Canada over the soil suction range of 0 to 1000 kPa. In Equation 2.21, c_{ld} is the intercept, m_{ld} is the slope of the σ_d versus log (M_R) relationship, c_{ld} and m_{ld} are functions of ψ.

$$\log M_R = c_{ld} - m_{ld}(\sigma_d) \tag{2.21}$$

Oloo and Fredlund (1998) prposed Equation 2.22 for coarse-grained soils and Equations 2.23 and 2.24 for fine-grained soils.

$$M_R = k\theta_b^{m_b} + k_s\psi \tag{2.22}$$

$$M_R = k_2 - k_3(k_1 - \theta_b) + k_s\psi \text{ when } k_1 > \theta_b \tag{2.23}$$

$$M_R = k_2 + k_4(\theta_b - k_1) + k_s\psi \text{ when } k_1 < \theta_b \tag{2.24}$$

Gupta et al. (2007) proposed Equations 2.25 and 2.26 which were derived for four fine-grained subgrade soils (two A-4 soils and two A-7-6 soils) from Minnesota, USA over the soil suction range of 10 to 10000 kPa.

$$M_R = k_1 p_a \left(\frac{\theta_b - 3k_4}{p_a}\right)^{k_2} \left(k_5 + \frac{\tau_{oct}}{p_a}\right)^{k_3} + \alpha_1 \psi^{\beta_1} \tag{2.25}$$

$$M_R = k_1 p_a \left(\frac{\theta_b}{p_a}\right)^{k_2} \left(1 + \frac{\tau_{oct}}{p_a}\right)^{k_3} + k_{us} p_a \Theta^{\kappa} \psi \tag{2.26}$$

Khoury et al. (2009) proposed Equation 2.27 which was derived for several subgrade soils (ranging from A-4 to A-7) from Oklahoma, USA over the soil suction range of 0 to 6000 kPa.

$$M_R = k_1 p_a \left(\frac{\theta_b}{p_a}\right)^{k_2} \left(k_4 + \frac{\tau_{oct}}{p_a}\right)^{k_3} + \alpha_1 \psi^{\beta_1} \tag{2.27}$$

Caicedo et al. (2009) proposed Equation 2.28 which was derived for three non-standard granular base materials from Andes Cordillera, Colombia over the soil suction range of 0 to 200 kPa.

$$M_R = k_1 p_a \left(1 + k_2 \frac{\sigma_d}{p_a}\right) \left(\frac{\psi}{p_a}\right)^{k_3} \frac{f(e)}{f(0.33)} \tag{2.28}$$

Khoury et al. (2011) proposed Equation 2.29 which was derived for a manufactured soil with soil suction levels similar to a silty soil. The hysteresis behaviour in the M_R with respect to soil suction was considered within the soil suction range of 0 to 100 kPa.

$$M_R = \left[k_1 p_a \left(\frac{\theta_b}{p_a}\right)^{k_2} \left(1 + \frac{\tau_{oct}}{p_a}\right)^{k_3} + (\psi - \psi_0) \times \left(\frac{\theta_d}{\theta_s}\right)^{\left(\frac{1}{n}\right)}\right] \times \left(\frac{\theta_d}{\theta_w}\right) \tag{2.29}$$

Cary and Zapata (2011) proposed Equation 2.30 which was derived for a granular soil (A-1-a) and a clayey sand (A-4) from Arizona, USA over the soil suction range of 0 to 250 kPa. Equation 2.30 was further verified using experimental data of two sandy subgrade soils (one A-4 soil and one A-2-4 soil) from Sweden over the soil suction range of 0 to 450 kPa by Salour et al. (2014).

$$M_R = k_1 P_a (\frac{\theta_{net} - 3\Delta u_{w-sat}}{p_a})^{k_2} (\frac{\tau_{oct}}{p_a} + 1)^{k_3} (\frac{\psi_0 - \Delta\psi}{p_a} + 1)^{k_4} \tag{2.30}$$

Ng et al. (2013) proposed Equation 2.31 which was derived for a subgrade soil (A-7-6) from Hong Kong, China over the soil suction rang of 0 to 250 kPa.

$$M_R = M_0 (\frac{p}{p_r})^{k_1} (1 + \frac{q_{cyc}}{p_r})^{k_2} (1 + \frac{\psi}{p})^{k_3} \tag{2.31}$$

Azam et al. (2013) proposed Equation 2.32 which was derived for four recycled unbound granular materials from Australia over the soil suction range of 0 to 10 kPa.

$$M_R = k (\frac{\sigma_m}{p_a})^{k_1} (\frac{\tau_{oct}}{\tau_{ref}})^{k_2} (\frac{\psi}{p_a})^{k_3} [\frac{DDR(1 - k_4 RCM / 100)}{100}]^{k_5} \tag{2.32}$$

Han and Vanapalli (2015) proposed Equation 2.33 which was derived based on the experimental results of eleven different compacted fine-grained subgrade soils that were tested following various protocols. Model parameter ξ was found equal to 2.0 for all the examined subgrade soils.

$$\frac{M_R - M_{RSAT}}{M_{ROPT} - M_{RSAT}} = \frac{\psi}{\psi_{OPT}} (\frac{S}{S_{OPT}})^{\xi} \tag{2.33}$$

Notations in Equations 2.21 through 2.33: k, k_s, k_{us}, k_1, k_2, k_3, k_4, k_5, α_1, β_1, κ, m_b, ξ = model parameters, $\Theta = \theta / \theta_s$ = normalized volumetric water content, θ_s = saturated volumetric water content, e = void ration, $f(e) = (1.93 - e)^2 / (1 + e)$, θ_d = volumetric water content along the drying curve, θ_w = volumetric water content along the wetting curve, n = model parameter obtained from Fredlund and Xing (1994) SWCC model, $\theta_{net} = \theta_b - 3u_a$ = net bulk stress, $\Delta u_{w\text{-}sat}$ = build-up of pore-water pressure under saturated conditions, $\Delta\psi$ = relative change of soil suction with respect to ψ_0 due to build-up of pore-water pressure under unsaturated conditions, $p = (\theta_b/3 - u_a)$ = net mean stress, p_r = reference pressure = 1 kPa, q_{cyc} = cyclic shear stress, $M_0 = M_R$ value at reference stress state when $(u_a - u_w) = 0$, $(p - u_a) = p_r$ and $q_{cyc} = p_r$, DDR = dry density ratio (%), RCM = percent of recycled clay masonry (%), τ_{ref} = reference shear stress, σ_m = mean normal stress = $\theta_b/3$, ψ_{OPT} = soil suction at OMC.

Model parameters with same notations (e.g., k_1, k_2, k_3) are used in Equations 2.2, 2.11, 2.12 and Equations 2.13 through 2.33 for simplicity purposes. These model parameters in different equations however may have different physical meaning as well as values.

It should be noted that apart from the M_R, the volumetric strain (ε_v) and the deviator strain (ε_q) under cyclic loading can also be used for characterizing the resilient behavior of pavements. The variations of ε_v and ε_q with ψ can also be predicted using the approaches described in *Groups B* and *C*. Prediction models for ε_v and ε_q however are beyond the scope of this chapter. More discussions on this topic are available in Nowamooz et al. (2011) and Ho et al. (2014a&b).

Some common concerns with respect to the prediction equations are discussed below:

1) The M_R - ψ correlation of a specific pavement material tested following certain techniques can be reasonably simulated using a simple empirical equation. However, there are uncertainties using the same empirical equation for other soils and other testing scenarios. Also, empirical equations are only suitable for a certain soil suction range; prediction results beyond this range may not be reliable. For example, at saturation condition when $\psi = 0$, Equation 2.5 predicts $M_{RSAT} = 0$ while Equations 2.8, 2.9, and 2.10 predict M_{RSAT} values which equal to negative infinity. Due to such limitations, empirical equations are not suggested for rigorous analysis or numerical simulations as they likely contribute to instability problems. The constitutive models are comparatively more flexible to reproduce different M_R - ψ correlations using various model parameters. Reliable calibration of the model parameters for different pavement materials is based on

performing regression analysis on large amount of experimental data, which however could be time consuming and expensive.

2) Most of the summarized constitutive models are revisions of Equations 2.2, 2.11, or 2.12. At saturation condition (ψ = 0), some of these constitutive models reduce to Equation 2.2, 2.11, 2.12 or similar formulations and predict M_{RSAT}. For instance, when ψ = 0, Equation 2.17 is similar to Equation 2.11, Equations 2.15, 2.16 are similar to Equation 2.12, and Equations 2.18, 2.19, 2.20, 2.26, 2.29, 2.30 are similar to Equation 2.2. These revised equations can be represented using the following formulations:

$$M_R = \begin{cases} M_{RSAT} \times f_1(\psi), & f_1(0) = 1 \\ M_{RSAT} + f_2(\psi), & f_2(0) = 0 \end{cases} \tag{2.34}$$

where $f_1(\psi)$ and $f_2(\psi)$ are the functions representing the contribution of the soil suction towards the M_{RSAT}.

In the pavement construction practice, materials are normally compacted at or near OMC to achieve maximum density and assure better performance (Zaman et al. 2010). Equations 2.2, 2.11, and 2.12 were proposed and generally used for M_{ROPT}. Several studies, based on various pavement materials, suggested specific values and estimation approaches for model parameters k_1, k_2, and / or k_3 in Equations 2.2, 2.11, and 2.12 to predict the M_{ROPT} (e.g., Hossain 2008, Stolle et al. 2009, Caliendo 2012, Shaqlaih et al. 2013). However, the model parameters for the M_{ROPT} are not suitable for the M_{RSAT}. Referring the M_{ROPT} values for predicting M_R - ψ correlations is common in empirical equations (Equations 2.3, 2.8, and 2.10) as M_{ROPT} is conventionally determined. Same approach can also be extended for constitutive models. Equation 2.33 allows the direct use of M_{ROPT} for prediction. The M_{ROPT} can be expressed using any stress-dependent constitutive models (e.g., Equations 2.2, 2.10 and 2.11) to take into account the influence of applied stresses on the M_R - ψ correlations (Han and Vanapalli 2015).

3) Incorporating the soil suction into applied stresses (*Group B*) is typically based on Bishop's effective stress concept for unsaturated soils using parameter χ, or micro-mechanics theory and thermodynamic laws using parameter f. Determination of the χ and

f needs experimental investigations which could be cumbersome and expensive. Some investigators therefore suggested using empirical relationships to estimate χ and f (Khalili and Khabbaz 1998, Heath et al. 2004, Khalili et al. 2004, Yang et al. 2006, Liang et al. 2008, Nokkaew et al. 2014). Concerns are however raised as using empirical relationships may introduce additional uncertainties into the predictions (Cary and Zapata 2011).

Model parameters used in summarized constitutive equations are different from those used in Equations 2.2, 2.11, and 2.12 both in terms of physical meaning as well as values. For example, the k_2 used in Equation 2.11 describes the response of the M_R to the applied shearing stress σ_d; the k_2 used in Equation 2.17 however describes the response of M_R to a stress state composed of σ_d and ψ. The k_2 used in Equation 2.2 describes the relationship between M_R and the applied confining stress θ_b; the k_2 used in Equation 2.17 however describes the relationship between M_R and a stress state composed of θ_b and ψ. The differences in the physical meaning of the model parameters not only translate to different values but also cause changes to other model parameters. Therefore, estimation methods of the model parameters used in Equations 2.2, 2.11, and 2.12 which were well established and documented in the literature may not be suitable for the equations categorized in *Group B* and *Group C.*

4) The M_R - ψ correlations show non-linear increasing trend within lower suction range. Such trend however may not be continued to higher suction range. Edil and Motan (1979) reported that the M_R of several clay and sand-clay mixtures from Wisconsin, USA increased with soil suction approximately up to 800 kPa, beyond which the M_R started to decrease. Ceratti et al. (2004) reported that the M_R of a lateritic soil from Brazil increased with the soil suction up to 1000 kPa. Further soil suction increases did not contribute to significant increase in the M_R. Such behaviors of the M_R may be attributed to the more effective contribution of soil suction on wetted contacted area of the soil particles within the low soil suction range (boundary effect zone and the transition zone) to the soil strength and stiffness properties (Vanapalli et al. 1996). Within high soil suction range (residual zone), the moisture content is significantly low and the wetted contact area of soil particles is limited. There is breakage of the capillary menisci which limits or ceases the contribution of soil suction towards the M_R (Caicedo et al. 2009). In addition, hysteresis effects, which

are also generally attributed to the influence of the moisture regime, are widely reported for the M_R of different pavement materials (Parreira and Gonçalves 2000, Khoury and Zaman 2004, Khoury et al. 2011, Ng et al. 2013). There are significant differences between the M_R values measure from specimens tested following drying process and those measured following wetting process. It is reasonable and necessary to incorporate the influence of the moisture regime in the prediction of the M_R - ψ correlations. The influence of moisture regime is considered in some summarized equations through using parameters χ, f, θ, S or Θ. Equations neglecting the influence of moisture regime may encounter limitations such as i) predicting continuous increasing trend in M_R over the entire soil suction range, and ii) incapable of taking account the hysteresis effects.

2.4 Comparisons and discussions

Two equations from each of the three groups: Equations 2.3 and 2.8 from *Group A* which are empirical relationships; Equations 2.17 and 2.18 from *Group B* which are constitutive models incorporating the soil suction into applied shearing or confining stresses; Equations 2.27 and 2.31 from *Group C* which are constitutive models extending the independent stress state variable approach; are chosen for comparison studies. Equation 2.3 was developed from large number of testing data on different soils and is one of the most widely used equations in the pavement design practice; Equation 2.8 well predicted the M_R of four representative subgrade soils from Minnesota, USA (Sawangsuriya et al. 2009a); Equations 2.17, 2.18, 2.27, and 2.31 on the other hand are constitutive models that were verified with experimental data on a variety of soil types.

Experimental data derived from three different subgrade soils with similar soil properties (Yang et al. 2005, Gupta et al. 2007, and Ng et al. 2013; all the soils are classified as A-7-6 soils according to AASHTO M-145) are selected to provide comparisons between the measured M_R and the predicted M_R using the selected equations. The soil properties, compaction characteristics and experimental details of the three subgrade soils are summarized in Table 2.1. Figure 2.4 shows the measured SWCC for the three soils (symbols) and the predicted SWCC (lines) using the Fredlund and Xing (1994) equation.

$$S = 1/\{\ln[2.718 + (\psi/a)^n]\}^m \tag{2.35}$$

where a, m, n = model parameters. The comparisons between the predicted and measured M_R values are carried out following the combinations shown in Table 2.2.

Table 2.1 Details of the three soils used in this study

Details	Pulverized Mudstone from Taiwan (PM)	Decomposed Tuff from Hong Kong (DT)	Silty Clay Loam from Minnesota (SCL)
Source	Yang et al. (2005)	Ng et al. (2013)	Gupta et al. (2007)
Classification[1]	A-7-6	A-7-6	A-7-6
w_L (%)	50	43	42
I_p (%)	23	14	24
MDD (Mg/m^3)	18	17.6	15.8
OMC (%)	17	16.3	22
G_s	2.67	2.73	2.69
RC (%)	100	100	98
M_R testing procedure	AASHTO T292-91	AASHTO T307-99	NCHRP 1-28A
Suction measurement	Filter paper method	Axis-translation technique	Thermal dissipation sensor
Shearing and confining stresses (kPa)	σ_d = 21, 48, 103; σ_c = 21	q_{cyc} = 30, 40, 55, 70; σ_{cnet} = 30	σ_d = 28, 49, 92; σ_c = 14

Note: [1] Classified as per AASHTO M-145 soil classification system.
Notations: w_L = liquid limit, I_p = plasticity index, MDD = maximum dry density, G_s = specific gravity, RC = relative compaction, σ_{cnet} = net confining stress = $(\sigma_c - u_a)$.

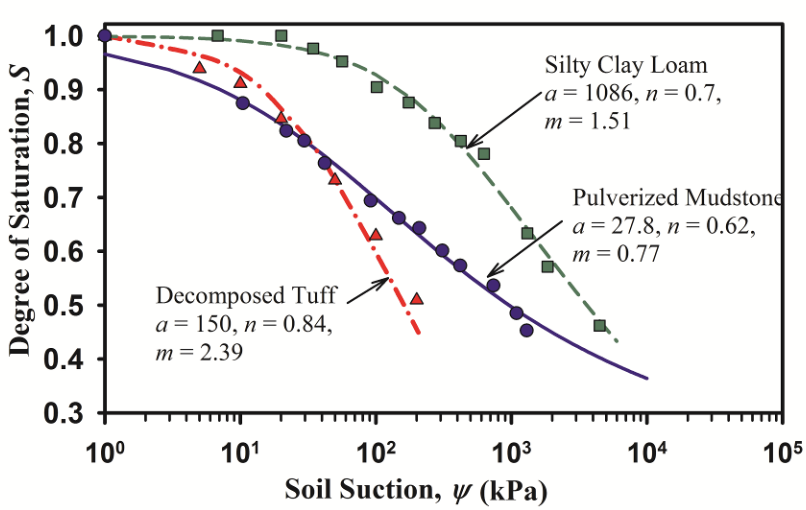

Figure 2.4 SWCC of the three soils used in this study

Table 2.2 Combinations of the comparisons

Equation	Pulverized Mudstone Yang et al. (2005)	Decomposed Tuff Ng et al. (2013)	Silty Clay Loam Gupta et al. (2007)
Group A	Equations 2.3 and 2.8	Equations 2.3 and 2.8	Equation 2.3
Group B	Equation 2.18	Equations 2.17 and 2.18	Equations 2.17 and 2.18
Group C	Equations 2.27 and 2.31	Equation 2.27	Equation 2.31

Note: Selected equations are not used to predict the measurements from the same study.

2.4.1 Comparisons for empirical equations from Group A

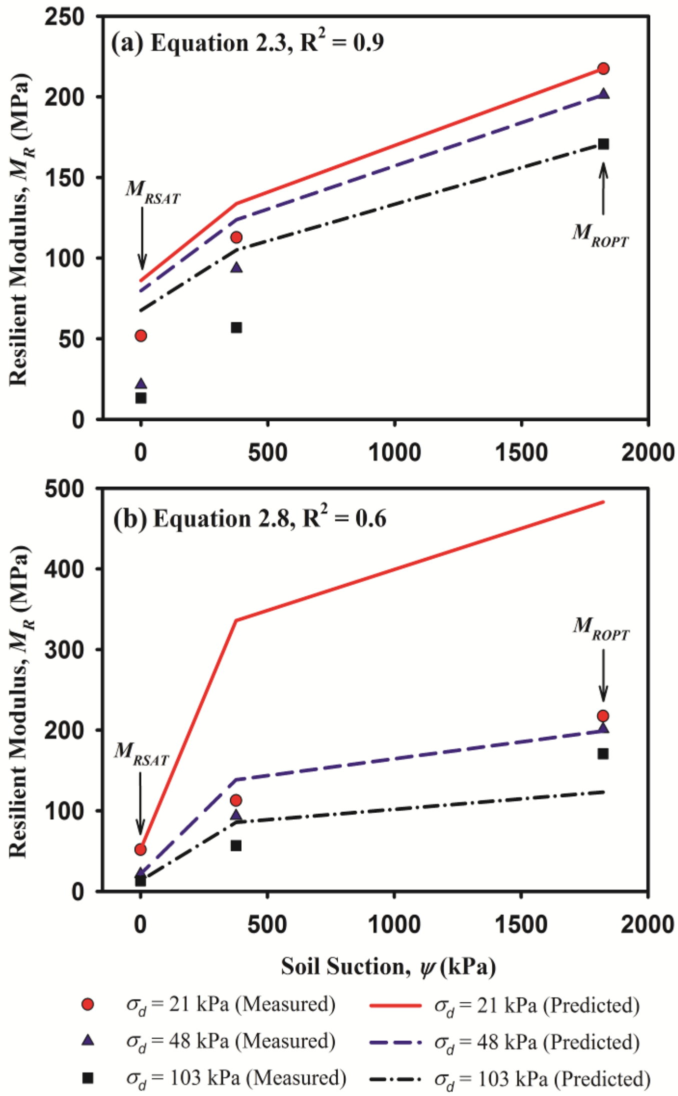

Figure 2.5 Comparisons between variation of the M_R with soil suction of the PM measured by Yang et al. (2005) and predicted by (a) Equation 2.3, (b) Equation 2.8

Figures 2.5, 2.6, and 2.7 show the comparisons between the measured M_R and the predictions using empirical Equation 2.3 and / or Equation 2.8 for the Pulverized Mudstone (PM), Decomposed Tuff (DT), and Silty Clay Loam (SCL) respectively. Figure 2.8 shows the overall predictions provided by the two equations.

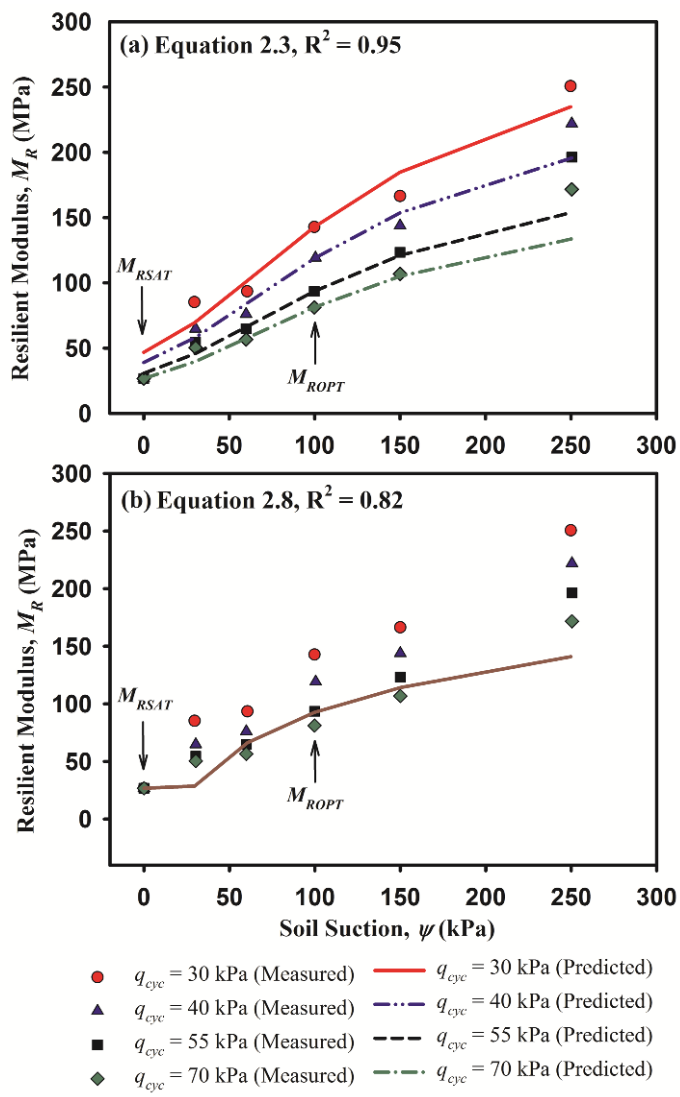

Figure 2.6 Comparisons between the variation of the M_R with soil suction of the DT measured by Ng et al. (2013) and predicted by (a) Equation 2.3, (b) Equation 2.8

The measured M_R - ψ correlations for the three soils show non-linear characteristics and are reasonably predicted using Equations 2.3 and 2.8. Witczak et al. (2002) suggested subjective criteria for goodness predictions based on the coefficient of determination (R^2) values. An excellent fit can be defined as $R^2 \geq 0.9$, a good fit covers the R^2 range of 0.7 to

0.89, while a fair fit is defined as $0.4 \leq R^2 \leq 0.69$. According to this criteria, Equation 2.3 provides excellent prediction for the PM and DT (Figures 2.5a and 2.6a,), good prediction for the SCL (Figure 2.7), and an overall good prediction (Figure 2.8). It is observed that Equation 2.3 tends to over predict the M_R values of the PM and SCL on the wet side of the OMC (where soil suction is lower than the OMC condition), and under predict the M_R values of the SCL for the dry side of the OMC (where soil suction is higher than the OMC condition). Equation 2.3 tends to over-predict most of the experimental data as shown in Figure 2.8.

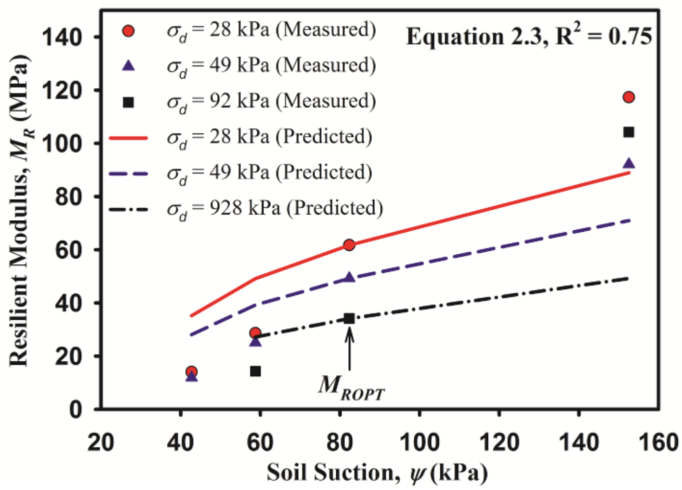

Figure 2.7 Comparisons between the variation of the M_R with soil suction of the SCL measured by Gupta et al. (2007) and predicted by Equation 2.3

Equation 2.8 provides fair prediction for the PM (Figure 2.5b), good prediction for the DT (Figure 2. 6b), and an overall fair prediction (Figure 2.8). It is observed that the predictions of Equation 2.8 are sensitive to the M_{RSAT}. Small differences in the M_{RSAT} contribute to significant variations in the predicted M_R at higher soil suction values as shown in Figure 2.5b. On the other hand, the measured M_{RSAT} of the DT is a constant irrespective of the different cyclic stresses (q_{cyc}). The measured M_R at other soil suction levels is influenced by the q_{cyc} (Ng et al. 2013). The predictions do not reflect the influence of the applied stresses but are identical at different q_{cyc} values (see Figure 2.6b). Equation 2.8 tends to under-predict most of the experimental data as shown in Figure 2.8.

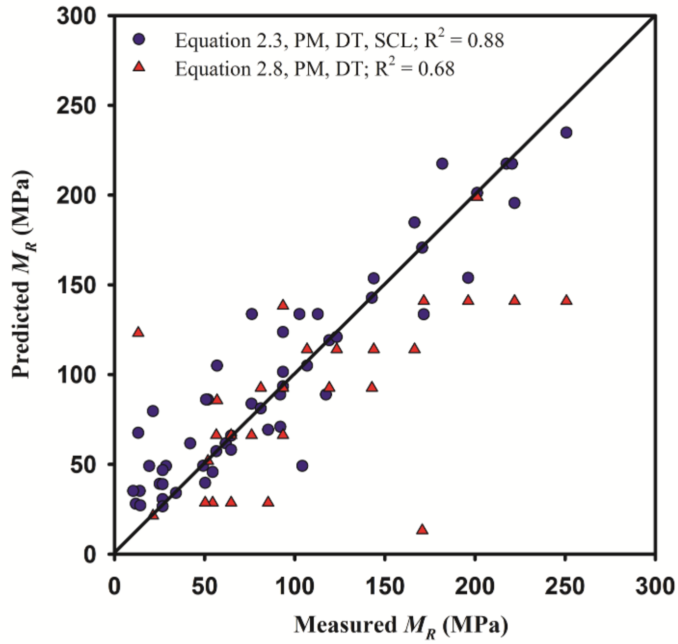

Figure 2.8 Overall predictions provided by Equations 2.3 and 2.8 in comparison with the measured values

2.4.2 Comparisons for constitutive models from Group B

Yang et al. (2006) and Liang et al. (2008) suggested estimating the χ values in Equations 2.17 and 2.18 using the empirical equation proposed by Khalili and Khabbaz (1998).

$$\chi = \begin{cases} \left(\dfrac{\psi}{\psi_b}\right)^{-0.55} & \text{when } \psi \geq \psi_b \\ 1 & \text{when } \psi \leq \psi_b \end{cases} \tag{2.36}$$

where ψ_b = air-entry value (i.e., soil suction beyond which air starts to enter the largest pores in the soil). The ψ_b values are 7 kPa for the PM (Yang et al. 2006), 60 kPa for the DT (Ng et al. 2013), and 70 kPa for the SCL (Gupta et al. 2007). The model parameters used in Equations 2.17 and 2.18 for the three soils are listed in Table 2.3 along with the respective R^2 values. Figures 2.9, 2.10 and 2.11 show comparisons between the measured and predicted M_R values for the three soils, using Equation 2.17 and / or Equation 2.18. Figure 2.12 shows the overall predictions.

Table 2.3 Regression parameters of Equations 2.17 and 2.18

Equations		Decomposed Tuff	Silty Clay Loam	Pulverized Mudstone
Equation 2.17 where M_R, ψ and σ_d are in (kPa)	k_1	274.2	111.5	-
	k_2	1.24	1.27	
	R^2	0.5	0.26	
Equation 2.18 where M_R, ψ, θ_b and τ_{oct} are in (kPa)	k_1	296.8	168.9	744.2
	k_2	3.6	5.79	3.12
	k_3	- 6.69	- 9.07	- 5.5
	R^2	0.96	0.93	0.93

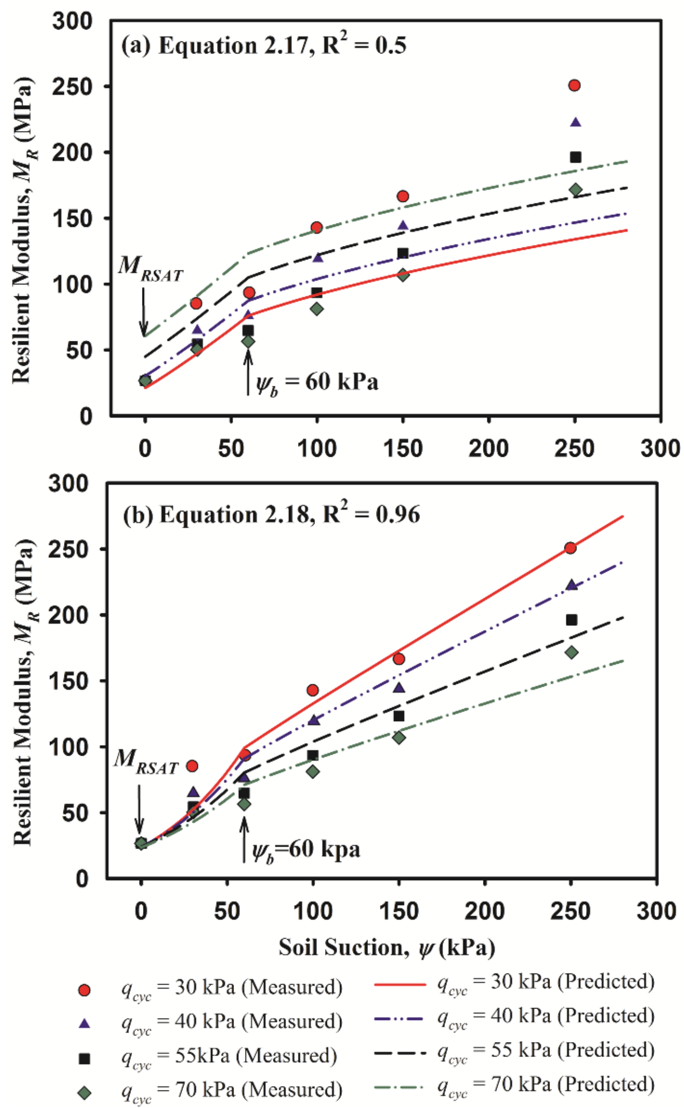

Figure 2.9 Comparisons between the variation of the M_R with soil suction of the DT measured by Ng et al. (2013) and predicted by (a) Equation 2.17, (b) Equation 2.18

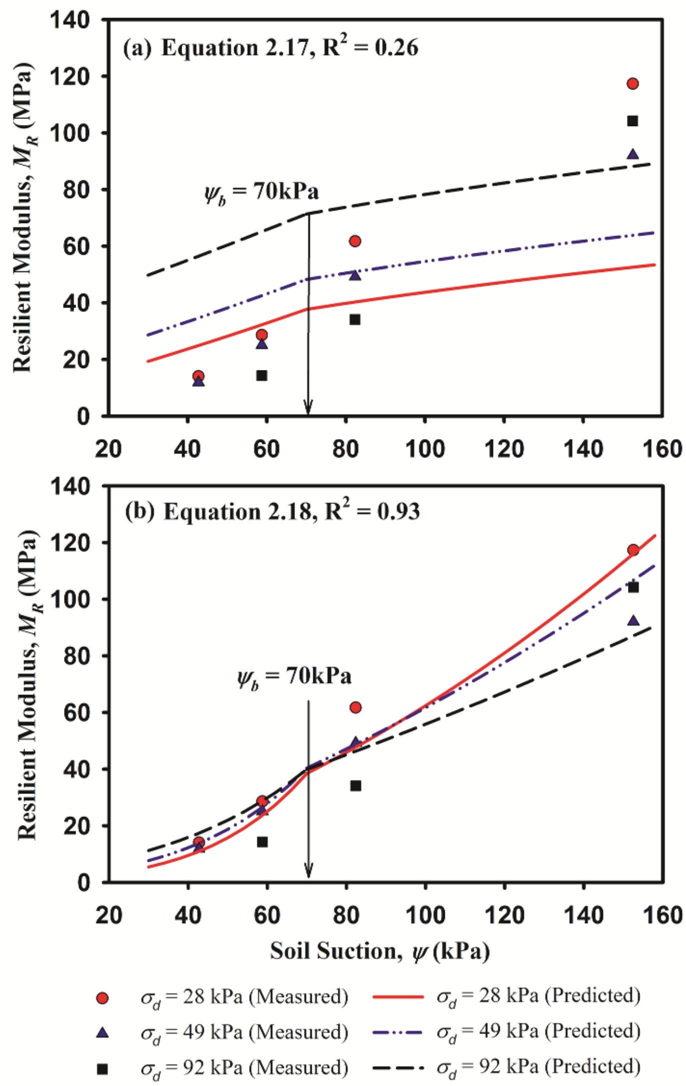

Figure 2.10 Comparisons between the variation of the M_R with soil suction of the SCL measured by Gupta et al. (2007) and predicted by (a) Equation 2.17, (b) Equation 2.18.

Equations 2.17 and 2.18 predict non-linear variations of the M_R with respect to the soil suction for the three soils. It can be observed from Figures 2.9, 2.10 and 2.11 that the predicted M_R - ψ curves are steeper when soil suction is lower than the ψ_b, the predicted curves flatten when soil suction is greater than the ψ_b. Such a behavior can be in part attributed to the use of parameter χ which varies with soil suction as predicted by Equation 2.36.

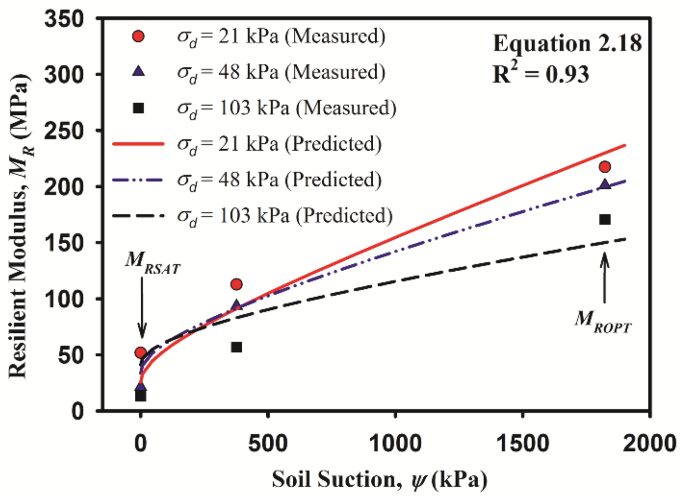

Figure 2.11 Comparisons between the variation of the M_R with soil suction of the PM measured by Yang et al. (2005) and predicted by Equation 2.18

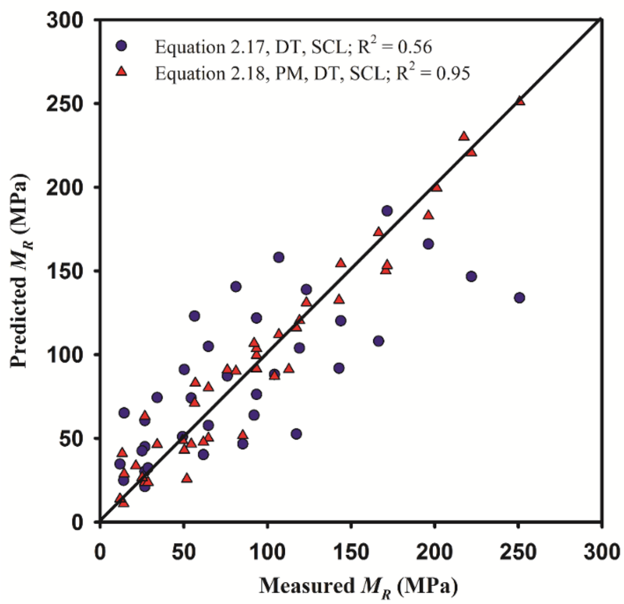

Figure 2.12 Overall predictions provided by Equations 2.17 and 2.18 in comparison with the measured values

The measured M_R values of the three soils increase with increasing soil suction but decrease with increasing applied shearing stresses q_{cyc} and σ_d (Figures 2.9, 2.10 and 2.11). Equation 2.17 reasonably captures the increase in the M_R with ψ. It predicts increasing M_R with increasing q_{cyc} and σ_d, which is however contrary to the measurements. Such results can be attributed to the formulation of Equation 2.17 which uses a single model parameter k_2 to predict the behavior of the M_R with respect to both σ_d and ψ. Positive k_2 values derived from regression analysis in this study (see Table 2.3) indicate that M_R increases with both σ_d and ψ. Negative k_2 values however will indicate a decreasing trend in the M_R with both σ_d and ψ. The softening behavior of the M_R with increasing applied shearing stresses for fine-grained soils was observed and discussed by some investigators in the literature (Ceratti et al. 2004, Ng et al. 2013, Sivakumar et al. 2013). The hardening behavior of the M_R was also reported (Parreira and Gonçalves 2000, Yang et al. 2008). Equation 2.17 is more suitable to predict the M_R - ψ correlations for subgrade soils that exhibit hardening behavior with respect to applied shearing stresses.

Equation 2.18 predicts the variations of the M_R with soil suction and shearing stress using model parameters k_2 and k_3 respectively. The positive k_2 values and negative k_3 values derived from the regression analysis (see Table 2.3) reasonably capture the measured behavior of the M_R and consequently contribute to better predictions. However, the predicted behavior of the M_R with respect to the σ_d for the PM and SCL are not consistent. The predicted M_R values increase with increasing σ_d at soil suction range lower than ψ_b but decrease with increasing σ_d at soil suction range higher than ψ_b (see Figures 2.10b and 2.11). Such a behavior may be attributed to the use of bulk stress θ_b (θ_b = 3σ_c + σ_d) in Equation 2.18 which also increases with σ_d.

2.4.3 Comparisons for constitutive models from Group C

The variation of the M_R with respect to the ψ is predicted using model parameters α_1, β_1 in Equation 2.27 and model parameter k_3 in Equation 2.31. Estimation of the model parameters k_1, k_2, k_3, k_4, α_1 and β_1 in Equation 2.27 requires the experimental data of the M_R under various applied confining / shearing stresses and soil suction values. At saturation condition (i.e., ψ = 0), Equation 2.27 reduces to:

$$M_{RSAT} = k_1 p_a (\frac{\theta_b}{p_a})^{k_2} (k_4 + \frac{\tau_{oct}}{p_a})^{k_3} \tag{2.37}$$

Thus, Equation 2.27 is simplified as Equation 2.38 and used in this study.

$$M_R = k_1 p_a (\frac{\theta_b}{p_a})^{k_2} (k_4 + \frac{\tau_{oct}}{p_a})^{k_3} + \alpha_1 \psi^{\beta_1} = M_{RSAT} + \alpha_1 \psi^{\beta_1} \tag{2.38}$$

Table 2.4 Regression parameters of Equations 2.38 and 2.31

Equations		DT	SCL	PM
Equation 2.38 where M_R and ψ are in (kPa)	α_1	1352		1157
	β_1	0.89	-	0.66
	R^2	0.90		0.98
Equation 2.31 where M_R, p, q_{cyc} and ψ are in (kPa)	k_1	1.0	1.0	1.0
	k_2	− 0.65	− 0.1	− 0.46
	k_3	1.01	1.72	0.51
	M_0	8.32	0.23	4.07
	R^2	0.98	0.92	0.96

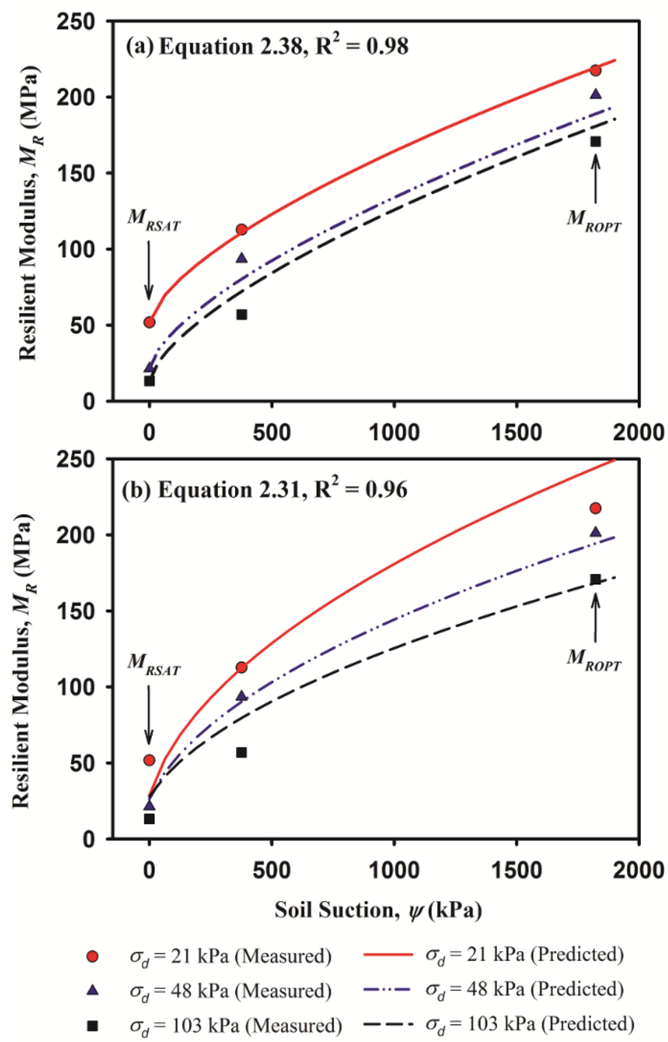

Figure 2.13 Comparisons between the variation of the M_R with soil suction of the PM measured by Yang et al. (2005) and predicted by (a) Equation 2.38, (b) Equation 2.31

Ng et al. (2013) suggested that the M_R increases linearly with respect to the confining stress (p) for pavement subgrades. Similar suggestion was also proposed by Fredlund et al. (1977). Thus, a value of k_1 equals to 1.0 is used in Equation 2.31 assuming linear M_R - p relationship for the SCL and PM. Other model parameters M_0, k_2 and k_3 in Equation 2.31 are derived from the regression analysis. Table 2.4 summarizes the model parameters used for Equations 2.31 and 2.38 and their respective R^2 values. Figures 2.13, 2.14, and 2.15 show comparisons between the measured M_R values and the predicted M_R values using Equations 2.31 and / or 2.38 for the PM, DT, and SCL. Figure 2.16 shows the overall predictions.

Both Equations 2.31 and 2.38 provide excellent predictions ($R^2 \geq 0.9$) according to Witczak et al. (2002) for the experimental data shown in Figure 2.16. It can be observed from Figures 2.13a and 2.14 that Equation 2.38 predicts variations of the M_R regardless of the influence of applied shearing stresses q_{cyc} or σ_d. This in part can be attributed to the second term of Equation 2.38 (i.e., $\alpha_1 \psi^{\beta_1}$) which takes into account the influence of the soil suction while neglects the influence of the applied stresses. Equation 2.31 on the other hand, predicts different non-linear M_R - ψ relationships at various levels of shearing stress for the PM and SCL as shown in Figures 2.13b and 2.15.

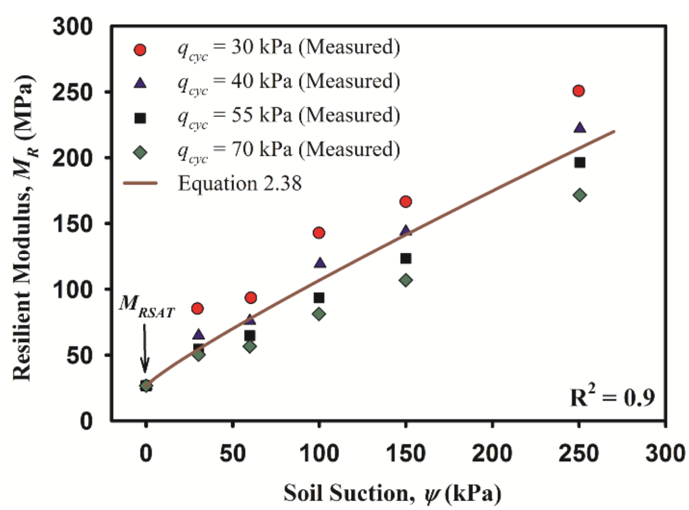

Figure 2.14 Comparisons between the variation of the M_R with soil suction of the DT measured by Ng et al. (2013) and predicted by Equation 2.38

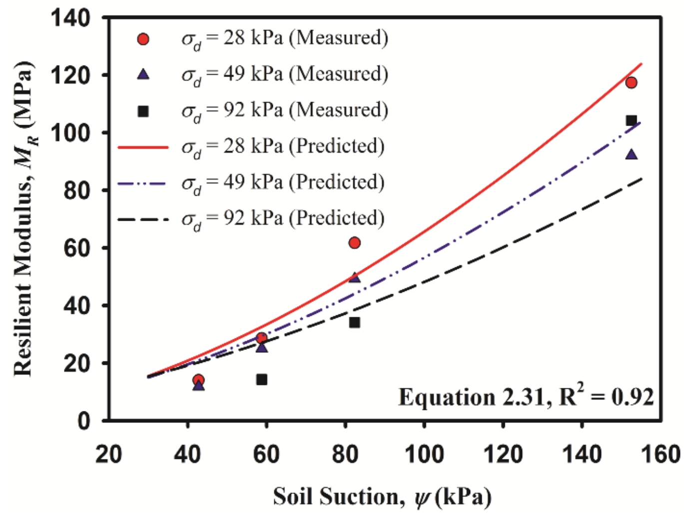

Figure 2.15 Comparisons between the variation of the M_R with soil suction of the SCL measured by Gupta et al. (2007) and predicted by Equation 2.31

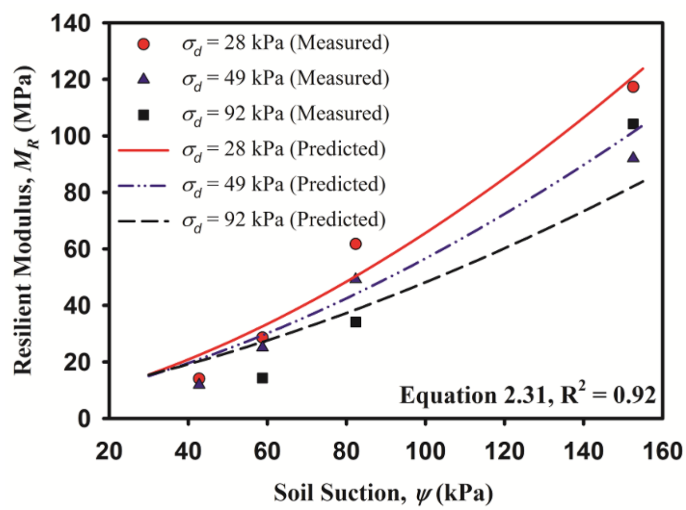

Figure 2.16 Overall predictions provided by Equations 2.38 and 2.31 in comparison with the measured values

2.4.4 Comparisons presented in resilient modulus - cyclic stress - soil suction space

Comparisons between the measured M_R of the DT (Ng et al. 2013) and the predicted M_R using the six selected equations are shown in Figure 2.17 in the M_R - q_{cyc} - ψ space. The model parameters used in Equations 2.17, 2.18, 2.31 and 2.38 are listed in Tables 2.3 and 2.4 (Model parameter values used for Equation 2.31 were suggested by Ng et al. 2013).

The shape of the surfaces predicted using empirical relationships (i.e., Equations 2.3 and 2.8) depends on (i) constant model parameters and, (ii) referenced M_R values (M_{ROPT} in Equation 2.3, M_{RSAT} in Equation 2.8). The shape of the surfaces predicted using constitutive models (i.e., Equations 2.17, 2.18, 2.27 (2.38), and 2.31) is controlled by (i) methodologies used to take account the contribution of the soil suction, (ii) applied stresses (e.g., θ_b, σ_d, τ_{oct}, p, q_{cyc} etc.) formulated in the prediction equation, and (iii) model parameters (e.g., model parameters k_1, k_2, k_3, k_4, M_0 etc.) that need to be calibrated from experimental data.

Generally, constitutive models are flexible in fitting the non-linear variations of the M_R with respect to the applied stresses and soil suction. Constitutive models extending Bishop's effective stress concept for unsaturated soils predict surfaces with distinctly different shapes prior to and after the air-entry value (see Figures 2.17c and 2.17d). The constitutive models extending the independent stress state variable approach predict smooth surfaces (see Figures 2.17e and 2.17f) and better fit the measured M_R - q_{cyc} - ψ relationships for subgrade soils.

It is important to note that reasonable predictions using constitutive models are possible when the model parameters are derived from regression analysis performed on a large experimental database. Different model parameter values are required for the same constitutive model for different soils (see Tables 3 and 4). Also, regression parameters may only be reliable for the applied stress and soil suction range of the experimental database. The predicted M_R - ψ correlations using the six selected equations (Equations 2.3, 2.8, 2.17, 2.18, 2.27 (2.38), and 2.31) show a continuous non-linear increasing trend with the soil suction (see Figures 2.9, 2.10, 2.11, 2.13, 2.14, 2.15, and 2.17). As discussed earlier, the loss of strength and stiffness that occurs at higher soil suction values may not be reasonably predicted.

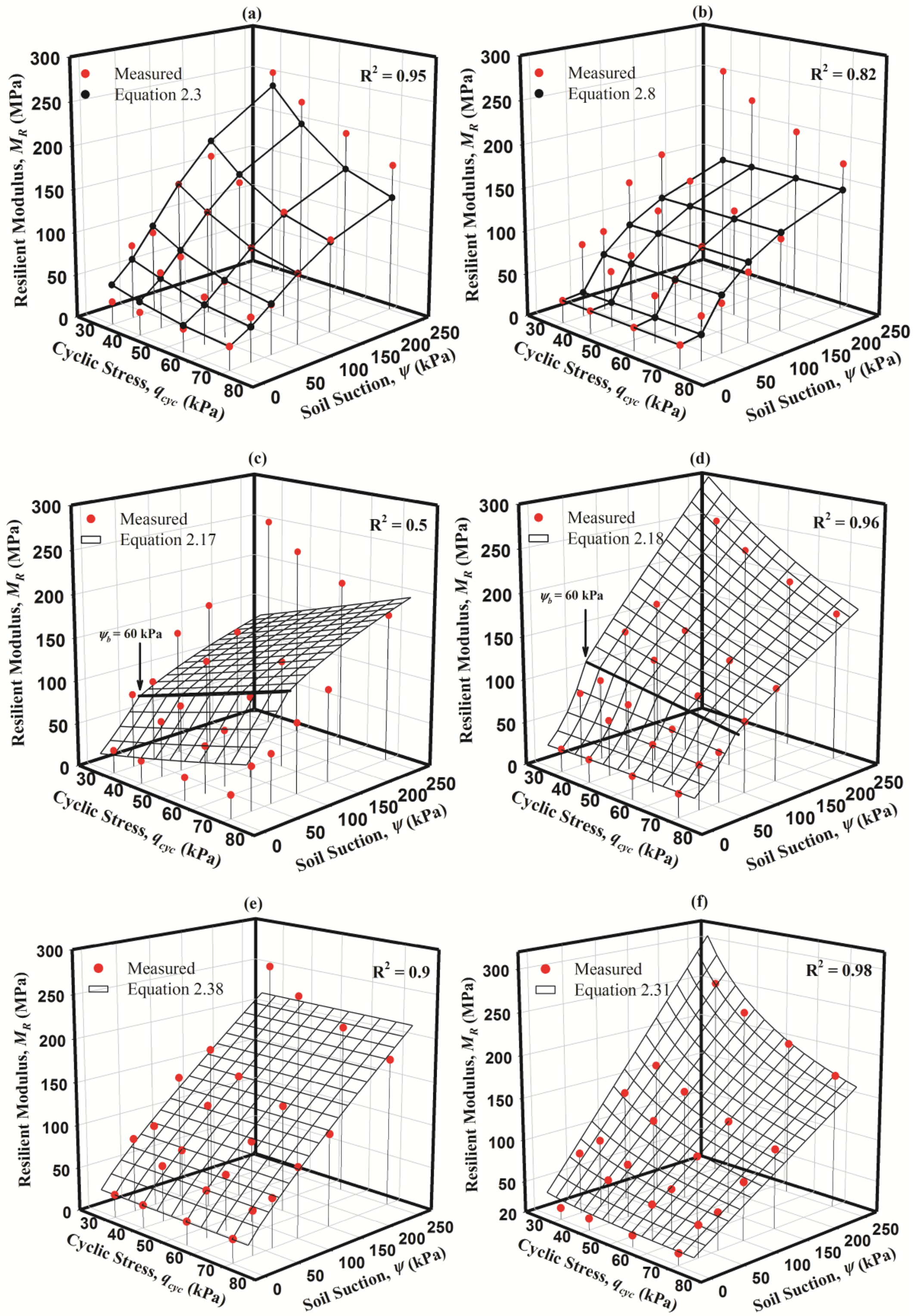

Figure 2.17 Comparisons between the M_R of the DT measured by Ng et al. (2013) and predicted by (a) Equation 2.3, (b) Equation 2.8, (c) Equation 2.17, (d) Equation 2.18, (e) Equation 2.27 (2.38), and (f) Equation 2.31 in the M_R - q_{cyc} - ψ space

2.5 Summary and conclusions

Various empirical relationships and constitutive models available in the literature to predict the variation of the M_R with respect to soil suction are summarized into three groups: Group A, empirical relationships; Group B, constitutive models incorporating the soil suction into the applied shearing or confining stresses; and Group C, constitutive models extending the independent stress state variable approach.

Several comments are provided for the summarized equations:

(i) Empirical relationships are easy and economical for use in practice, but are only suitable for certain soils for a limited soil suction range. Constitutive models are more flexible to consider various factors that influence the M_R and provide reasonably good predictions if the model parameters are calibrated using extensive experimental data. The calibrated model parameters for a particular soil for specific soil suction and applied stress ranges may not be suitable for other soils or even the same soil when it is subjected to different applied stress and soil suction.

(ii) Most constitutive models proposed to predict the M_R - ψ relationships are revised from conventional constitutive models. However, model parameters for conventional models which were well documented cannot be directly extended into the improved models for prediction;

(iii) It is important to incorporate moisture regime (can be represented by gravimetric / volumetric water contents or degree of saturation) into the constitutive models to rationally predict the M_R - ψ relationships. Neglecting the influence of moisture content may result in unreasonable predictions of the M_R at a large soil suction range and not being able to take account the influence of hysteresis effects.

Two equations that are widely used from each of the three summarized equation groups are selected to predict the M_R of three subgrade soils with similar soil properties in order to understand their strengths and limitations. Empirical relationships Equations 2.3 and 2.8 predict unique M_R - ψ relationships for the three soils regardless of the soil type. Equation

2.3 tends to over-predict the experimental data, while Equation 2.8 tends to under-predict the experimental data and is sensitive to the M_{RSAT} values. Constitutive models Equations 2.17 and 2.18 that incorporate the soil suction into applied stresses using Bishop's effective stress concept for unsaturated soils predict different M_R - ψ relationships for soil suction ranges before and after the air-entry value. They reasonably predict the non-linear variation of the M_R with respect to the ψ; but the variation in the M_R with respect to the applied stress is not properly addressed. Constitutive equations 2.27 and 2.31 that extend the independent stress state variable approach are able to reasonably take account the influence of soil suction and provide reliable predictions within boundary effect and transition zones. However, Equation 2.38, which is the simplified form of Equation 2.27, does not consider the influence of the applied stress on the M_R - ψ relationships.

Pavement design methodology in recent years has advanced from using empirical or semi-empirical methods to computer-aided design using numerical analysis which is based on the mechanistic models. It is important to use suitable and rigorous constitutive models for determining the variations of the M_R with applied stress levels and soil suction in the numerical analysis of pavement structure. It is recommended to propose and use constitutive models that provide reasonable predictions based on conventional soil properties (e.g., M_{ROPT}, S_{OPT}) using well defined model parameters. Such constitutive models can better assist the rational of design of pavement structures.

CHAPTER THREE

PREDICTING STIFFNESS AND SHEAR STRENGTH OF UNSATURATED SOILS

3.0 Background-Information

The contents presented in this chapter are from the manuscript of the publication:

Han, Z., and Vanapalli, S. K. (2016). Stiffness and shear strength of unsaturated soils in relation to soil-water characteristic curve. *Géotechnique*. DOI: 10.1680/geot./15-P-104.

The symbols used in this chapter are summarized in Table 3.0.

Table 3.0 Symbols used in Chapter Three

Symbols	
a, n, m	model parameters for Fredlund & Xing (1994) SWCC equation
a_w	area of pore-water
c	apparent cohesion
c'	effective cohesion
E	elastic modulus
e	void ratio
e_0	initial void ratio
G_s	specific gravity
G_0	small strain shear modulus
I_p	plastic index
k_1 through k_{12}, κ, ω	model parameters for stress-dependent equations
M_R	resilient modulus
OCR	over consolidation ratio
P_a	atmosphere pressure
p_{net}	net mean stress
q	deviator stress
q_c	deviator stress at critical state
q_p	peak deviator stress
R^2	coefficient of determination
S_r	water degree of saturation
S_r^e	effective degree of saturation
S'_r	residual water degree of saturation or microscopic water degree of saturation

Table 3.0 Symbols used in Chapter Three

Symbols	
subscript $_{sat}$	corresponding parameters at saturation condition
subscript $_{ref}$	corresponding parameters at reference condition
s	suction
s_{ae}	air-entry suction
s^r	residual suction
u_a	pore-air pressure
v	velocity of shear wave
w_{comp}	compaction moisture content
w_L	liquid limit
w_n	natural water content
w_{opt}	optimum moisture content
Γ	suction-related variable
θ_b	bulk stress
ξ	exponent parameter
ρ	bulk density
σ	total stress
σ'	Bishop-type effective stress
σ_n	normal stress
σ_c	confining stress
τ_p	peak shear strength
τ_{oct}	octahedral shear stress
ϕ'	effective angle of friction
χ	Bishop effective stress parameter
Ω	stiffness or shear strength properties

3.1 Introduction

The stiffness - suction and shear strength - suction relationships for unsaturated soils are non-linear and sensitive to various factors such as the external stress, moisture regime, soil type, hydraulic hysteresis, soil structure, aging and testing technique. The soil-water characteristic curve (SWCC), which represents the moisture regime - suction relationship, is frequently used in the interpretation and prediction of the stiffness - suction and shear strength - suction relationships (Alonso et al., 1990; Fredlund & Rahardjo, 1993; Vanapalli et al., 1996; Gallipoli et al., 2003; Wheeler et al., 2003; Thu et al., 2007; Sawangsuriya et al., 2009b; Gens, 2010; Alonso et al., 2013).

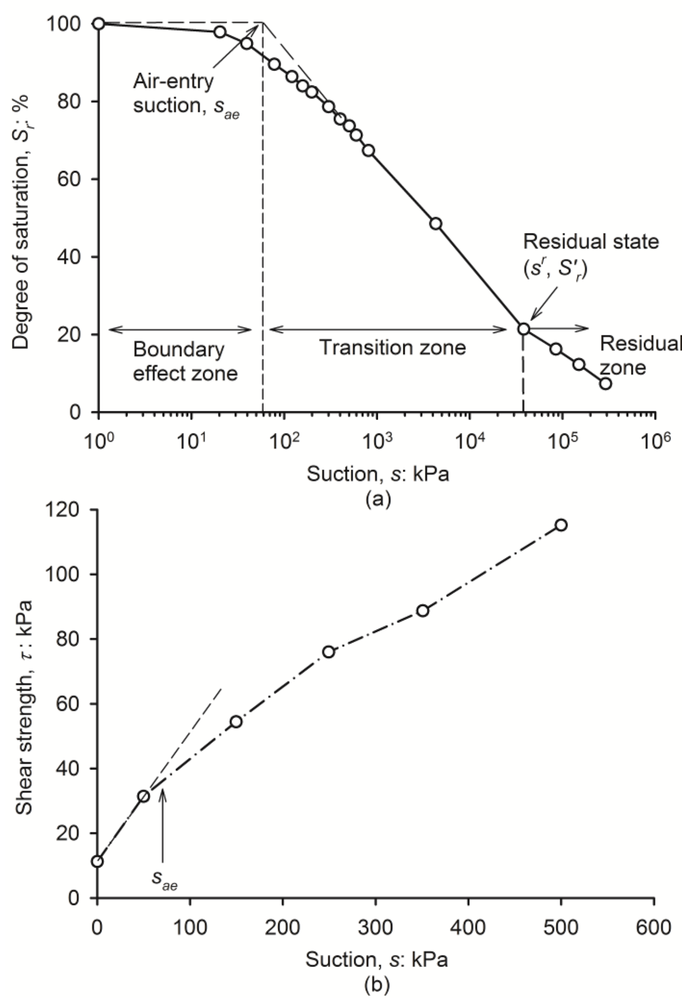

Figure 3.1 Compacted glacial till: (a) SWCC; (b) τ_p - s relationships

Figs 3.1(a) and 3.1(b) show an example, for a glacial till from Saskatchewan, Canada (liquid limit w_L = 35.5%, plastic index I_p = 18.7%, optimum moisture content w_{opt} = 16.3%), the SWCC and the peak shear strength (τ_p) - suction (s) relationship obtained from suction-controlled multistage direct shear tests under a net normal stress of 25 kPa (data from Vanapalli et al., 1996). The relationship between the SWCC and the τ_p shown in Figs 3.1(a) and 3.1(b) is corroborated by the testing data of other soils from the literature on the relationships between the SWCC and the stiffness and shear strength properties. The key characteristics of these relationships can be summarized as follows.

(i) The SWCC can be divided into three zones; namely, boundary effect, transition and residual zones (Vanapalli et al., 1999; see Fig. 3.1(a)). Within the boundary effect zone, soil pores are saturated with capillary water under suction. It is likely there may be some air in the form of occluded bubbles, which is not continuous. As suction exceeds the air-entry suction (s_{ae}), air starts to enter the largest soil pores and subsequently drain the capillary water out of the soil. In this stage of desaturation, both air phase and water phase are continuous; however, liquid phase flow and capillary effect tends to decrease with increasing suction. When suction exceeds the residual suction (s^r), the amount of capillary water and the contribution of capillary effect and suction towards the skeleton constitutive stress become negligible. Water transports in the soil pores only in the form of vapor as the water phase retreats to the micro-pores and becomes discontinuous in the residual zone of desaturation. In this stage, the rate of the desaturation of water becomes remarkably slower regardless of the large suction increase. This characteristic can be recognized from the flattened part of the SWCC at large suction values.

(ii) It is well recognized from experimental investigations that the stiffness and shear strength properties exhibit non-linear evolution with suction and water degree of saturation (see Fig. 3.1(b) and also in Escario & Sáez, 1986; Wheeler & Sivakumar, 1995; Vanapalli et al., 1996; Cunningham et al., 2003; Ng & Yung, 2008; Jotisankasa et al., 2009; Oh et al., 2009; Lu & Kaya, 2014; Sivakumar et al., 2013; Ng & Zhou, 2014, Morales et al., 2015). Such a behaviour can be related to the variation of the capillary water and its associated capillary effect and suction, which contributes to the changes in the skeleton constitutive stress and therefore, the stiffness and shear strength properties (Lu & Likos, 2006, Baker & Frydman, 2009; Alonso et al., 2010). Within the boundary effect zone, the soil system stays in a stage of capillary saturation and can be treated as a continuum medium. The increasing suction fully contributes to the constitutive stress of the soil skeleton, resulting in a significant increase in the stiffness and shear strength properties. The contribution of suction becomes less efficient with further suction increase and the corresponding drainage of the capillary water in the transition zone, which results in a less significant increase in the stiffness and shear strength properties.

It should be noted that, apart from the suction, the physicochemical inter-particle forces such as the van der Waals and cementation forces also influence the mechanical properties (Lu & Likos, 2006; Baker & Frydman, 2009). The physicochemical inter-particle forces are different for different soil types. Their influence on the soil mechanical behaviour for natural soils may be secondary compared with that of suction within the lower suction range. At higher suction range, the influence of suction decreases with decreasing capillary water and the physicochemical inter-particle forces start to dominate. For example, the stiffness and shear strength for cohesionless soils such as gravels and sands usually decrease in the residual zone of desaturation due to the decrease in the contribution of the suction and the weak physicochemical inter-particle forces (Wu et al., 1984; Escario et al., 1989; Oh et al., 2009; Ghayoomi & McCartney, 2011). However, for cohesive soils, stiffness and shear strength behaviour in the high suction range varies for different soil types. Decreasing, constant or increasing trends of stiffness and shear strength behaviour are respectively reported for various soils (Escario et al., 1989; Cunningham et al., 2003; Geiser et al., 2006). It would be rather difficult to clearly determine or distinguish the boundary suction value or moisture regime where the influence of the physicochemical forces outweigh that of the suction. However, it is reasonable to assume, for natural soils, that the capillary effect and suction govern i) the mechanical behaviour of cohesionless soils over the whole suction range, and ii) the mechanical behaviour of cohesive soils in the lower suction range where liquid flow is typically predominant, especially the in-situ suction range which is typically between 0 kPa and 600 kPa (Cui & Delage, 1996; Vanapalli et al., 1996; Khalili & Khabbaz, 1998). Within higher suction range, physicochemical inter-particle forces should be taken into account, in addition to suction, for the reasonable interpretation of the mechanical behaviour of cohesive soils.

(iii) The area of pore-water (a_w) is the factor used to upscale the suction (s) from a pore-scale stress to a macroscopic stress ($a_w s$) that contributes to the constitutive stress and consequently, the mechanical properties of unsaturated soils (Fung, 1977; Vanapalli et al., 1996; Lu, 2008; Nuth & Laloui, 2008; Alonso et al., 2010; Khalili & Zargarbashi, 2010). The water degree of saturation (S_r) is frequently used to approximate the a_w due to the difficulties concerning the direct measurement of the a_w. Several studies suggested directly using S_r as the parameter χ in the expression of the Bishop-type effective stress σ' (i.e. $\sigma' = \sigma - u_a + \chi s$, where σ is the total stress, u_a is the pore-air pressure; Bishop, 1959) (Wheeler et al., 2003; Coussy, 2004; Nuth & Laloui, 2008). Some studies, on the other hand, proposed using effective degree of saturation (S_r^e) as the parameter χ to highlight the role of capillary water and the associated capillary effect, in the contribution of suction towards the skeleton constitutive stress (Romero & Vaunat, 2000; Tarantino & Tombolato, 2005; Sawangsuriya et al., 2009b; Alonso et al., 2010; Lu et al., 2010). The S_r^e is generally defined by equation (3.1).

$$S_r^e = \frac{S_r - S_r'}{1 - S_r'} \tag{3.1}$$

There are different interpretations of the parameter S'_r. The S'_r can be defined as residual water degree of saturation below which the liquid flow ceases and vapor flow prevails (Fredlund & Rahardjo, 1993). Such interpretation assumes that the amount of adsorptive water that has minor influence on the mechanical properties can be indicated by the residual water degree of saturation. The S'_r can be determined either from the SWCC as the point separating transition zone and residual zone (see Fig. 3.1(a), Vanapalli et al., 1999; Fredlund, 2006), or as the corresponding S_r at a specified suction value (e.g., 1500 kPa as per van Genuchten, 1980; 3000 kPa as per Vanapalli et al., 1996). Another interpretation of S'_r is attributed to the dual-porosity structure of soils assuming that water stored in macro-pores is mainly capillary water while water stored in micro-pores is mainly adsorptive water (Romero et al., 1999; Alonso et al., 2010, Alonso et al. 2013). The amount of adsorptive water (S'_r) therefore equals to that of the micro-pores and is referred to as microscopic water degree of saturation (Alonso et al., 2010). The microscopic water degree of saturation can be determined from pore-size analyzing techniques such as the mercury intrusion tests. It is suggested that the micro-pore content is negligible for coarse-grained soils but increases with soil plasticity for cohesive soils (Alonso et al., 2013). Factors S_r and S_r^e are also widely used in the interpretation and prediction of stiffness - suction and shear strength - suction relationships for unsaturated soils applying the independent stress state variable approach (Fredlund et al., 1996; Vanapalli et al., 1996; Hamid & Miller, 2009; Oh et al., 2009; Sawangsuriya et al., 2009b).

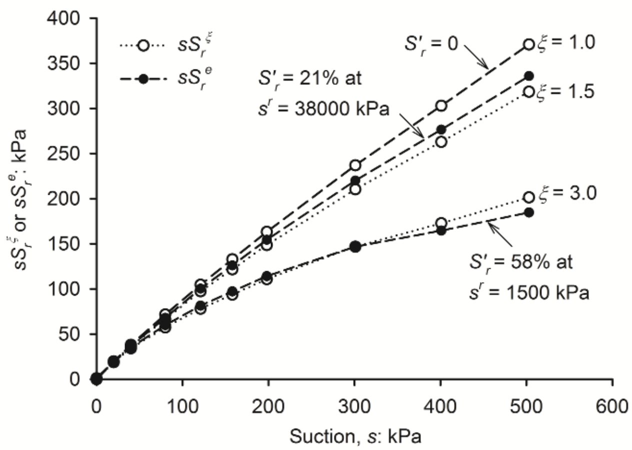

Figure 3.2 Variations of sS_r^ξ and sS_r^e with respect to suction for the glacial till

One approximation of the S_r^e is the exponential degree of saturation S_r^ξ where ξ is the exponent (Vanapalli et al., 1996; Alonso et al., 2010). Fig. 3.2 shows, based on the measured SWCC of the glacial till (see Fig. 3.1(a)), the sS_r^e - s relationships plotted using different S'_r values (S'_r = 0; or S'_r = 58% if s^r = 1500 kPa, as per van Genuchten, 1980; or S'_r = 21%, if S'_r is determined at the boundary of transition zone and residual zone where s^r = 38000 kPa, as per Fredlund & Rahardjo, 1993), and the sS_r^ξ - s relationships plotted using different ξ values (s is in kPa and S_r is in decimal when calculating the sS_r^ξ and sS_r^e in Fig. 3.2). It can be observed that both sS_r^e - s and the sS_r^ξ - s relationships are non-linear, which are similar to the behaviour of the stiffness - suction relationships and shear strength - suction relationships (see Fig. 3.1(b) for example). The sS_r^ξ - s relationships and sS_r^e - s relationships may behave differently within higher suction range (i.e. sS_r^e decreases to 0 while sS_r^ξ may increase to unrealistically high values when S_r drops below S'_r; Alonso et al., 2010). However, there are potential benefits of using S_r^ξ to approximate S_r^e within lower suction ranges if the ξ values can be reliably determined with adequate ease. This is because the determination of the S'_r i) could be rather subjective, if S'_r is considered as the residual water degree of saturation (Kim & Borden, 2011) or ii) needs additional experimental determination of the pore-size distribution, if S'_r is considered as microscopic degree of saturation (Alonso et al., 2010). The substantial difference between the S_r^e and the S_r^ξ is that the S_r^e, defined by equation (3.1), is a soil physical state parameter that should be measured or determined through various experiments corresponding to the different interpretations of the S'_r. The S_r^ξ, on the other hand, is a mathematical formulation other than a soil physical state parameter that purely serves to approximate the value of the S_r^e. The exponent ξ therefore is empirical in nature and should be determined from the regression analysis that best fits the value of S_r^ξ to that of S_r^e within lower suction range for a specific soil.

This chapter proposes a methodology to interpret and predict the stiffness - suction and shear strength - suction relationships within lower suction range using their similarities with the sS_r^ξ - s relationships, which could be derived from the SWCC. The methodology is presented as a normalized function to consider the various influencing factors including external stress, soil structure, hydraulic hysteresis, anisotropy and testing technique. Experimental data on the stiffness and shear strength properties and the SWCC derived from 25 different soils varying from cohesionless sands and silts to cohesive glacial tills and expansive clays are used to verify the proposed methodology and calibrate the ξ. It is found that the methodology can satisfactorily describe and predict the stiffness - suction and shear strength - suction relationships using a ξ value of 1.0 for cohesionless soils with little to no clay content, and a ξ value of 2.0 for cohesive soils with higher clay content.

3.2 A methodology for modelling the stiffness and shear strength of unsaturated soils

Soil stiffness and shear strength properties respond to external stress differently. Elastic deformation under external stress can be mainly attributed to the bending of soil particles and the flattening of the inter-particle and inter-packets contacts. Physical processes happening during shearing, on the other hand, are generally slippage and friction at contacts, particle crushing, and particle rearrangement (dilation or contraction). Therefore, the relationships between the stiffness and shear strength properties and the external stress should be described using different theories or equations (see several stress-dependent equations summarized in Table 3.1, which were proposed for shear strength τ, small strain shear modulus G_0, elastic modulus E, and resilient modulus M_R). The influence of suction on the elastic deformation and shearing however is similar. The meniscus water lenses restrains the physical processes of straining that leads to elastic deformation or plastic shear failure. The contribution of the meniscus water lenses is similar to a stabilizing agent or pre-consolidation stress (Alonso et al., 1990; Wheeler et al., 2003; Khalili et al., 2004; Sheng et al., 2008; Sheng 2011; Khalili & Zargarbashi, 2010). For this reason, it is rational and also possible to describe the stiffness - suction and shear strength - suction relationships using a unified methodology.

3.2.1 Development of the proposed methodology

There are different types of equations for predicting stiffness and shear strength properties of unsaturated soils. One type of equations incorporating factor sS_r^{ξ} and can be written as:

$$\Omega = \Omega_{sat} + \Gamma s S_r^{\xi} \tag{3.2}$$

where Ω_{sat} represents the stiffness or shear strength at saturation condition, Γ is a suction-related variable that indicates the influence of various factors such as the external stress, testing technique, soil structure on the contribution of sS_r^{ξ} towards the Ω. Equation (3.2) presents a smooth transition from saturated condition to unsaturated condition as $\Omega = \Omega_{sat}$ when s = 0. Table 3.1 summarises several equations proposed extending the mode illustrated in equation (3.2) for different stiffness and shear strength properties of unsaturated soils.

The Γ for shear strength can be simply assumed equal to tan ϕ' within low suction range (Fredlund et al., 1996; Vanapalli et al., 1996; Khalili & Khabbaz, 1998; see equation (3.2)). However, the determination of Γ for stiffness properties is rather cumbersome. For example, if equations (3.3.4), (3.3.6), or (3.3.8) in Table 3.1 were to be extrapolated for prediction, extensive experimental data derived under different suction and external stress levels would be required to calibrate the Γ and ξ values using regression analysis. Different Γ values may also be required for the same soil if influence of other factors, such as the external stress, soil structure, and testing technique, has to be taken into account. It may not be possible to accurately estimate the Γ without extensive experimental investigations for stiffness properties. In addition, both Γ and S_r^{ξ} in equation (3.2) control the predicted Ω - s relationships. The S_r^{ξ} is to approximate the S_r^{e} and subsequently the a_w. It indicates the contribution of s (through the formulation of sS_r^{ξ}) to the constitutive stress and therefore to the Ω. The Γ is used to regulate the Ω - s relationships taking account of different influencing factors. It is important to distinguish the different contributions of Γ and S_r^{ξ} in equation (3.2) in describing the Ω - s relationships when determining the Γ and ξ values. However, regression analysis is only useful to best-fit the equations to experimental results but may not yield reasonable Γ and ξ values in terms of their respective contributions as different combinations of Γ and ξ values may provide equally good-fit, especially when the experimental data is limited. Such uncertainties may also be encountered by other equations presented in formulations other than equation (3.2) within which different parameters jointly influence the Ω - s relationships.

Table 3.1 Summary of equations for predicting stiffness and shear strength

Index	Stress-dependent equations	Equations proposed for unsaturated soils
τ	$\tau = c' + \sigma_n \tan\phi'$ (3.3.1) Mohr-Coulomb equation	$\tau = c' + (\sigma_n - u_a)\tan\phi' + sS_r^{\xi}\tan\phi'$ (3.3.2) Vanapalli et al. (1996)
G_0	$G_0 = k_1(\sigma_c)^{k_2}$ (3.3.3) Mitchell & Soga (2005)	$G_0 = k_3(\sigma_c - u_a)^{k_4} + \Gamma_{G0} sS_r^{\xi}$ (3.3.4) Sawangsuriya et al. (2009b)
E	$E = k_5 P_a (\frac{\sigma_c}{P_a})^{k_6}$ (3.3.5) Duncan & Chang (1970)	$E = E_{sat} + \Gamma_E sS_r^{\xi}$ (3.3.6) Oh et al. (2009)
M_R	$M_R = k_7 P_a (\frac{\theta_b}{P_a})^{k_8} (\frac{\tau_{oct}}{P_a} + 1)^{k_9}$ (3.3.7) ARA, INC., ERES (2004)	$M_R = k_{10} P_a (\frac{\theta_b - 3u_a}{P_a})^{k_{11}} (\frac{\tau_{oct}}{P_a} + 1)^{k_{12}} + \Gamma_R sS_r^{\xi}$ (3.3.8) Gupta et al. (2007)

Notations: k_1 through k_{12} = model parameters, $k_1 = \kappa f(e)(\mathrm{OCR})^{\omega}$, $k_3 = \kappa f(e)$, $f(e)$ = function of void ratio e, OCR = over consolidation ratio, κ, ω = model parameters, c' = effective cohesion, ϕ' = effective angle of friction, σ_n = normal stress, σ_c = confining stress, P_a = atmosphere pressure, θ_b = bulk stress, τ_{oct} = octahedral shear stress, E_{sat} = elastic modulus at saturation condition, Γ_{G0}, Γ_E, Γ_R = suction-related variables for G_0 (Γ_{G0}), E (Γ_E), and M_R (Γ_R).

An alternative way is to eliminate the parameter Γ from equation (3.2). If Ω - s and S_r - s relationships at one reference suction level s_{ref} (i.e. (s_{ref}, Ω_{ref}) and (s_{ref}, $S_{r,ref}$)) are known or can be determined, and substituted into equation (3.2), equation (3.4) can be arrived.

$$\Omega_{ref} = \Omega_{sat} + \Gamma S_{r,ref}^{\xi} s_{ref} \tag{3.4}$$

Equation (3.4) can be substituted into equation (3.2) to eliminate Γ and derive equation (3.5).

$$\frac{\Omega - \Omega_{sat}}{\Omega_{ref} - \Omega_{sat}} = \frac{s}{s_{ref}} \left(\frac{S_r}{S_{r,ref}}\right)^{\xi} \tag{3.5}$$

The S_r corresponding to s can be estimated from the SWCC. In this chapter, the Fredlund & Xing (1994) model developed using three parameters a, n, and m is used for describing the SWCC (equation (3.6)).

$$S_r = \left\{ 1/\ln[2.718 + (\frac{s}{a})^n] \right\}^m \tag{3.6}$$

A graphical procedure based on a hypothetical soil example can assist to illustrate the development of the methodology. The SWCC of the hypothetical soil shown in Fig. 3.3(a) is plotted using equation (3.6) with parameter values of a = 160, n = 1.63, m = 0.68. The air-entry suction s_{ae} of the soil is 70 kPa. The Ω - s relationship for the hypothetical soil shown in Fig. 3.3(b) is plotted from a simple exponential function $\Omega = 21 + 71.9 \times (1 - 0.995^s)$ where units for Ω and s are assumed as MPa and kPa. This hypothetical Ω - s relationship described by the exponential function is chosen because it is linear when s is less than the s_{ae} and turns non-linear when s exceeds the s_{ae}. Such a behavior is typical for stiffness and shear strength properties in response to suction. Fig. 3.3(c) shows the sS_r^{ξ} - s relationships calculated from the SWCC using different ξ values (s is in kPa and S_r is in decimal for calculating the sS_r^{ξ}). The sS_r^{ξ} - s curves also exhibit very similar characteristics to that of the Ω - s curve shown in Fig. 3.3(b). The sS_r^{ξ} - s curves can present different shapes using different ξ values. Higher ξ value (e.g., ξ = 3.0) indicates a moderate non-linear increase followed by non-linear decrease; lower ξ value (e.g., ξ = 1.0) however indicates a significant non-linear increase. Based on the characteristics of the sS_r^{ξ} - s curve shown in Fig. 3.3(c), it is reasoned that the sS_r^{ξ} - s curve, using a suitable ξ, can closely reproduce the Ω - s curve.

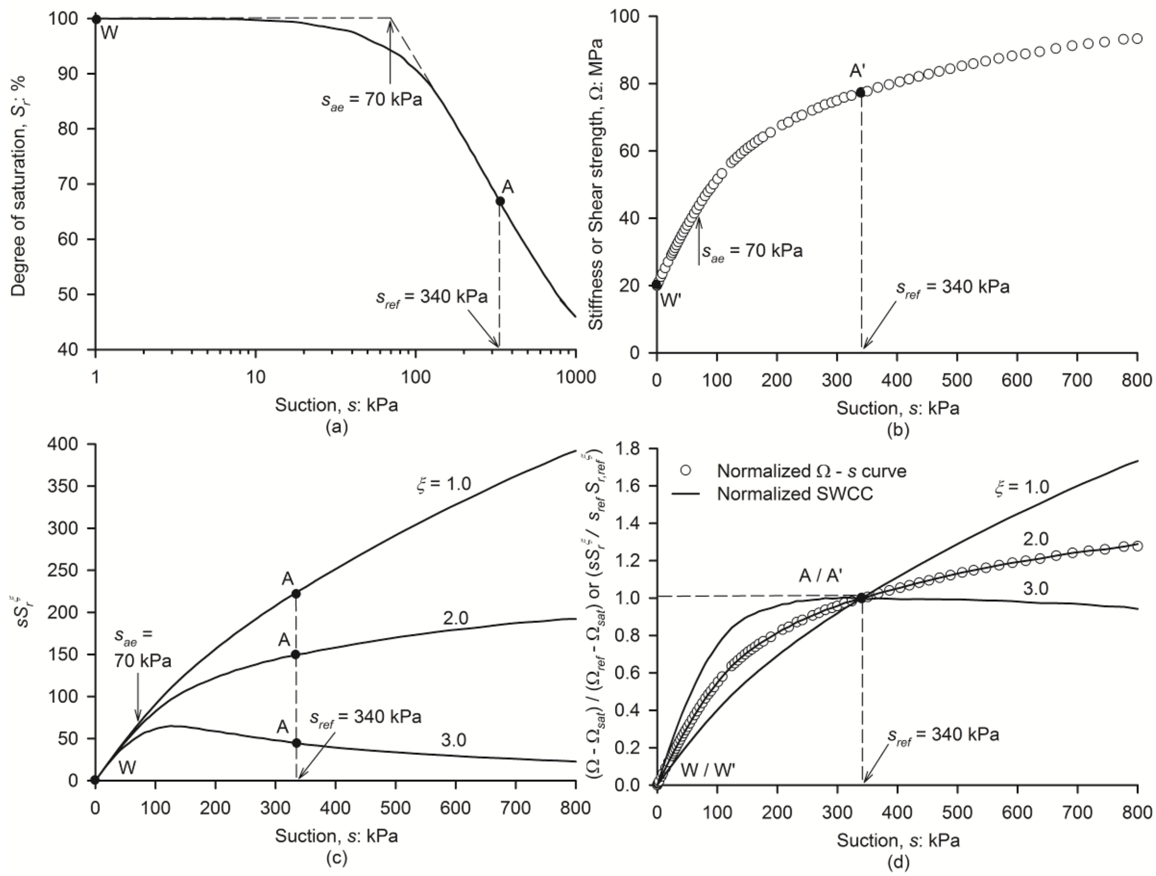

Figure 3.3 Variations of (a) S_r, (b) Ω, (c) sS_r^{ξ} and (d) normalized Ω and normalized sS_r^{ξ} with respect to suction

Let us choose two points on both the SWCC (see Fig. 3.3(a)) and the Ω - s curve (Fig. 3.3(b)). One point is at saturation condition (i.e. point W (s = 0, S_r = 100%) in Fig. 3.3(a) and point W' (s = 0, $\Omega = \Omega_{sat}$) in Fig. 3.3(b)), and the other point is the reference point mentioned in equation (3.5) which is taken at a random suction value (for example, at s_{ref} = 340 kPa, point A (s_{ref}, $S_{r,ref}$) in Fig. 3.3(a) and point A' (s_{ref}, Ω_{ref}) in Fig. 3.3(b)). Expression $(\Omega - \Omega_{sat}) / (\Omega_{ref} - \Omega_{sat})$, which is the left-hand side of equation (3.5) can be applied to normalize the Ω - s curve in Fig. 3.3(b) while the expression $(sS_r^{\xi} - 0) / (s_{ref}S_{r,ref}^{\xi} - 0)$, which equals to the right-hand side of equation (3.5) ($sS_r^{\xi} = 0$ at $s = 0$) can be applied to normalize the sS_r^{ξ} - s curves in Fig. 3.3(c). The two expressions are essentially identical as per the procedure used for normalization. The resultant normalized curves are shown in Fig. 3.3(d). All curves in Figs 3.3(b) and 3.3(c) are normalized to the same scale and are dimensionless. Again, different ξ values control the shape of the normalized sS_r^{ξ} - s curves (referred to as normalized SWCC). A suitable ξ value can be determined from regression analysis by best fitting the normalized SWCC to the normalized Ω - s curve. In this hypothetical example, the normalized SWCC, using a ξ value of 2.0, can best reproduce the normalized Ω - s curve.

For using equation (3.5), only data of Ω at two suction values (i.e. Ω_{sat} at s = 0 and Ω_{ref} at $s = s_{ref}$) are required. If the conventional stress-dependent models (e.g., equations (3.3.1), (3.3.3), (3.3.5) and (3.3.7) in Table 3.1) were used to predict the Ω_{sat} and Ω_{ref}, the influence of external stress on the Ω - s relationships can be taken into account. These details are discussed in later sections of the chapter.

It should be noted that the factor sS_r^{ξ} or sS_r^{e} used in equation (3.5) facilitates the extrapolation of the non-linearity of the SWCC to describe Ω - s relationships. Factors sS_r^{ξ} and sS_r^{e} are also widely used in equations proposed following both effective stress approach (e.g., Lu & Likos, 2006; Nuth & Laloui, 2008; Alonso et al., 2010) and independent stress state variable approach (e.g., Vanapalli et al., 1996; Oh et al., 2009; Sawangsuriya et al., 2009b) for predicting Ω - s relationships. However, there are certain differences between the proposed equation (3.5) and the equations developed following the two well-known approaches. Effective stress approach equations generally use sS_r^{ξ} or sS_r^{e} to calculate the quantifiable contribution of suction towards the constitutive stress. Equations of this kind are usually developed from conventional stress-dependent equations based on effective stress analysis without introducing additional parameters. The Ω_{sat} and Ω_{ref} in equation (3.5), are suggested to be measured directly or predicted using conventional stress-dependent models without modifications to the constitutive stress, which suggests that the proposed equation (3.5) is developed based on total stress analysis. The independent stress state variable approach equations introduce quantifiable items typically formulated with sS_r^{ξ} or sS_r^{e} along with other additional parameters into conventional stress-dependent models to predict the Ω - s relationships. Equation (3.5), on the other hand, alleviates the need for the determination and calculation of additional parameters or any quantifiable items by using a normalized form and a reference point.

3.2.2 Reference point

The stiffness or shear strength at a reference suction (s_{ref}, Ω_{ref}) is required to implement the proposed methodology. Fig. 3.4 illustrates, for the hypothetical soil in Fig. 3.3, the fit of the normalized SWCC to the normalized Ω - s curve using three reference points chosen from the SWCC and the Ω - s curve at different suction values (i.e. points A / A' at intermediate s of 340 kPa, points B / B' at lower s of 125 kPa near the s_{ae}, points C / C' at higher s of 800 kPa, see Figs 3.4(a) and 3.4(b)). The ξ value that best-fits the normalized SWCC to the normalized Ω - s curve at reference points A / A' is used (i.e. $\xi = 2.0$, see Fig. 3.3(d)). It can be observed from Fig. 3.4(c) that the fit is not influenced by the choice of the reference point. In other words, the ξ and the performance of the proposed methodology are not sensitive to the choice of the reference point.

Caution however should be maintained because the measurements of the stiffness and shear strength at different suction values are not always strictly distributed along a smooth curve as shown in Fig. 3.4(b). Experimental errors and the associated scatter at various levels exist and depend on many external and internal factors. Possible errors embedded in the reference points may affect the overall performance of the proposed methodology. Thus, high-quality and reliable experimental data at reference points are important to guarantee the performance of the proposed methodology.

The reference point can be chosen facilitating the protocols of engineering practice. For example, compacted soils used in geotechnical structures such as pavement layers, foundation subgrades, and embankments are usually compacted at optimum moisture content to achieve maximum density for ensuring favourable engineering performance. For this reason, the shear strength and stiffness at optimum moisture content condition are conventionally measured in practice and can be conveniently chosen as the reference points (Brown, 1996; Sivakumar et al., 2013; Ng et al., 2013; Ng & Zhou, 2014). Natural soils are also likely to achieve an equilibrium condition with the external environment after a certain period of time (Gens 2010, Blight 2013). The stiffness and shear strength at such an equilibrium condition are also typically measured in practice and are suitable to be used as the reference points.

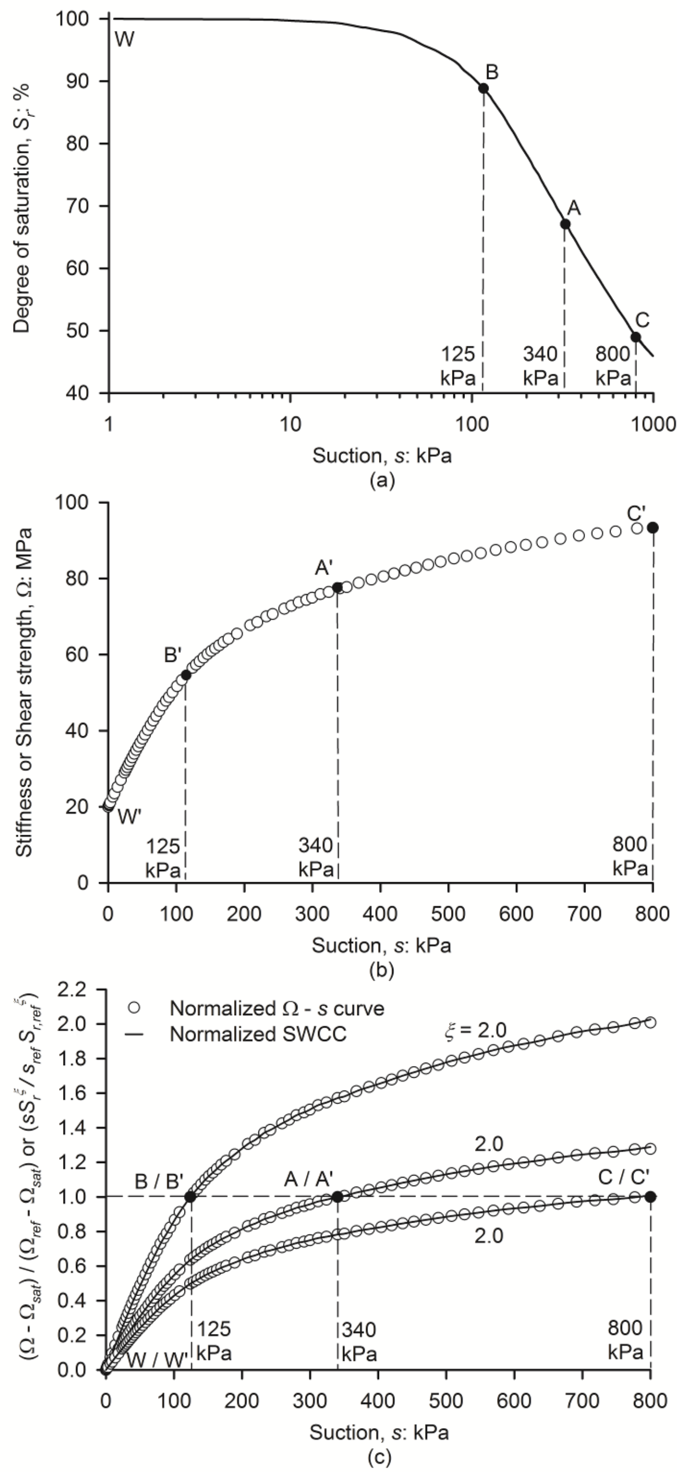

Figure 3.4 Influence of the selected reference points from the (a) SWCC and (b) Ω - *s* relationships on the (c) prediction

3.3 Calibration of ξ and performance of the methodology

Graphically, the parameter ξ fits the normalized SWCC to the normalized Ω - s curves. Mathematically, ξ is a model parameter that can be used in the factor S_r^{ξ} to approximate the factor S_r^{e} within the lower suction range. Both interpretations suggest the empirical nature of parameter ξ and therefore the need for adequate amount of experimental data for the reliable calibration of the parameter ξ.

Experimental data obtained from 25 different soils varying from coarse-grained sand to expansive clay are used in this study to examine the performance of the proposed methodology and to calibrate the parameter ξ. These experimental data are on various stiffness and shear strength parameters (including peak and critical shear strength, and different elastic modulus at various strain levels). The influence of various factors is also highlighted in the experimental data (e.g., external stress, soil structure, testing technique, hydraulic hysteresis, and anisotropy). Such combinations of the experimental data contribute to reduce any possible bias for validating the proposed methodology. The 25 different soils are categorized into two groups (i.e. 8 cohesionless soils in one group and 17 cohesive soils in another group). The cohesionless soil group includes sands and sand mixtures (%sand $\geq$ 50%), and silts with none to very low clay content (typically %clay < 10%). The cohesive soil group includes silts with higher plasticity (typically plasticity index I_p% $\geq$ 12) or clay content (typically %clay $\geq$ 10%), lean clays and active expansive clays. Details of the chosen soils and their corresponding stiffness and shear strength parameters are summarized in Table 3.2 and Table 3.3, respectively.

Different silts have been categorized into two groups based on the fact that silt is a material that falls between sands and clays. The mechanical behaviour of silt could be similar to either cohesionless or cohesive soils depending on the clay content and clay mineralogy and activity. There are no definite or universally recognized criteria available to precisely differentiate silts from cohesionless or cohesive soils in the literature. Clay particles which are small in dimension but large in specific surface area, significantly influence the hydro-mechanical behaviour of unsaturated soils. The choice of the clay content (represented by the %clay) and clay mineralogy and activity (represented by the I_p) as criteria to categorize the silts in this study is based on the fact that both factors significantly influence the amount of adsorbed water that determines the S'_r (Gens & Alonso, 1992; Fredlund & Rahardjo, 1993; Gallipoli et al., 2003; Blight, 2013). Although the criteria could be subjective, it is demonstrated in the later sections that the mechanical behaviour of the respective silts can be described identically using the proposed methodology with other sands or clays categorized in the same group.

The information of the SWCC is necessary for implementing the proposed methodology. The SWCC of the 25 chosen soils are fitted using equation (3.6). Fitting parameters of equation (3.6) for the soils are listed in Table 3.4 along with the testing techniques used to obtain the SWCC.

Table 3.2 Details of cohesionless soils used in this study

ID	Soil type & properties	Index & testing technique
1	Minnesota silt, sand% = 11.9, silt% = 82.4, clay% = 5.7, G_s = 2.69, w_{comp}% = w_{opt}% = 13.5	Small strain shear modulus; bender element
2	California clayey sand, sand% = 59, silt% = 23, clay% = 18, G_s = 2.7, w_{opt}% = 13.5, w_{comp}% = 13.5, or 9.5, or 17.5	
3	Silty sand, sand% = 70, silt% = 30, clay% = 0, G_s = 2.71, w_{comp}% = w_{opt}% = 13.5	Small strain shear modulus; resonant column
4	Hopi silt, sand% ≥ 50, w_{comp}% = 32	Elastic modulus; unconfined compression
5	Coarse sand, sand% > 90, G_s = 2.65	Elastic modulus; model footing loading
6	Kidston tailings, sand% = 47, silt% = 51, clay% = 2, consolidated from slurried condition	Peak shear strength; direct shear
7	Bourke silt, sand% = 46, silt% = 54, clay% = 0, G_s = 2.65, w_{comp}% = w_{opt}% = 12.5	Critical shear strength; Triaxial
8	Sand-kaolin mixture, sand% = 75, silt% = 7.5, clay% = 17.5, G_s = 2.64, w_{comp}% = w_{opt}% = 12.7	

References: 1 - 2, Sawangsuriya et al. (2009b); 3, Hoyos et al. (2015); 4, Lu & Kaya (2014); 5, Oh et al. (2009); 6, Rassam & Williams (1999); 7 - 8, Khalili & Zargarbashi (2010);

Notations: w_{comp}% = compaction moisture content, w_{opt}% = optimum moisture content, G_s = specific gravity, sand% = percentage of sand, silt% = percentage of silt, clay% = percentage of clay.

Table 3.3 Details of cohesive soils used in this study

ID	Soil type & properties	Index &testing technique
9	Minnesota RLF clay, w_L% = 42, I_p% = 24, sand% = 8.9, silt% = 63.8, clay% = 27.3, G_s = 2.69, w_{comp}% = w_{opt}% = 22	Small strain shear modulus; bender element
10	Minnesota MR clay, w_L% = 26, I_p% = 9, sand% = 36.3, silt% = 45.3, clay% = 14.5, G_s = 2.66, w_{comp}% = w_{opt}% = 16	
11	Minnesota fat clay, w_L% = 85, I_p% = 52, sand% = 3.1, silt% = 21.2, clay% = 75.2, G_s = 2.75, w_{comp}% = w_{opt}% = 27.5	
12	Decomposed tuff, w_L% = 43, I_p% = 14, sand% = 24, silt% = 72, clay% = 4, G_s = 2.73, w_{comp}% = w_{opt}% = 16.3	
13	Bonny silt, w_L% = 25, I_p% = 4, sand% = 16.1, silt% = 69.9, clay% = 14, w_{comp}% = 29	Elastic modulus; unconfined compression
14	BALT silt, w_L% = 27.4, I_p% = 5.8, w_{comp}% = 29	
15	Iowa silt, w_L% = 33.7, I_p% = 11.3, sand% = 15, silt% = 70, clay% = 15, w_{comp}% = 27	
16	Golden silt, w_L% = 31, I_p% = 14, w_{comp}% = 22	
17	Denver clay stone, w_L% = 44, I_p% = 21, clay% = 55, w_{comp}% = 39	
18	Georgia kaolinite, w_L% = 44, I_p% = 18, clay% = 35, w_{comp}% = 45	
19	Denver bentonite, w_L% = 118, I_p% = 73, clay% = 90, w_{comp}% = 32	
20	Nanyang expansive soil, w_L% = 58.3, I_p% = 31.8, sand% = 6.7, silt% ≈ 68.5, clay% ≈ 24.8, w_{comp}% = 17, w_{opt}% = 21.4	Elastic modulus & peak shear strength; Triaxial
21	Bukit Timah Granite, w_L% = 47, I_p% = 18, sand% = 49, silt% = 25, clay% = 26, G_s = 2.66, w_{comp}% = w_{opt}% = 15	Elastic modulus & peak shear strength; Direct shear
22	Zaoyang expansive soil, w_L% = 50.5, I_p% = 31, sand% = 3, silt% = 48, clay% = 39, w_{comp}% = 20.5	Elastic modulus, peak & critical shear strength; direct shear & triaxial
23	Glacial till, w_L% = 35.5, I_p% = 18.7, sand% = 28, silt% = 42, clay% = 30, w_{opt}% = 16.3, w_{comp}% = 13, or 16.3, or 19.6	Peak shear strength; direct shear
24	SJ10 clay, w_L% = 33, I_p% = 12, natural specimens sampled at w_n% = 18	Peak shear strength; triaxial
25	SJ11 clay, w_L% = 25, I_p% = 6, natural specimens sampled at w_n% = 13	

References: 9 - 11, Sawangsuriya et al. (2009b); 12, Ng & Yung (2008); 13 - 19, Lu & Kaya (2014); 20, Miao et al. (2002); 21 Rahardjo et al. (2011); 22, Zhan (2003), Zhan & Ng (2006); 23, Vanapalli et al. (1996), Vanapalli et al. (1999); 24 - 25, Khalili et al. (2004); Notations: w_L% = liquid limit, I_p% = plasticity index, w_n% = natural water content.

Table 3.4 Details of the SWCC of the soils

ID	Soil type		Model parameters a	n	m	Testing technique
1	Minnesota silt		37	1.24	0.73	Measured during bender element tests
2	California clayey sand	w_{opt}, standard	134	0.83	0.72	
		w_{opt} – 4%, standard	43.4	0.99	0.56	
		w_{opt} + 4%, standard	300	0.88	1.39	
		w_{opt}, enhanced	82.2	0.85	0.5	
		w_{opt}, reduced	30	1.21	0.25	
3	Silty sand		46	0.86	1.2	Pressure plate apparatus
4	Hopi silt		30.82	1.83	0.87	Drying cake method
5	Coarse sand		7.8	4.80	8.00	Tempe cell
6	Kidston tailing-A		3.63	3.14	0.78	Pressure plate apparatus
	Kidston tailing-B		14.1	1.78	1.07	
7	Bourke silt		Not fitted			Measured during triaxial tests
8	Sand-kaolin mixture					
9	Minnesota RLF clay		154.3	0.82	0.84	Measured during bender element tests
10	Minnesota MR clay		400	0.96	0.79	
11	Minnesota fat clay		278.5	0.93	0.48	
12	Decomposed tuff		60	0.98	1.35	Pressure plate apparatus
13	Bonny silt		23.37	1.23	1.12	Drying cake method
14	BALT silt		19.1	1.10	0.99	
15	Iowa silt		26.3	1.75	1.15	
16	Golden silt		69	0.75	0.80	
17	Denver clay stone		77	1.10	0.94	
18	Georgia kaolinite		164	1.95	1.14	
19	Denver bentonite		73	1.48	0.63	
20	Nanyang expansive soil		412.4	1.10	1.46	Pressure plate apparatus
21	Bukit Timah Granite		171.1	0.62	0.77	
22	Zaoyang expansive soil		35.22	4.55	0.10	
23	Glacial till	w_{opt}, 25 kPa	200	0.76	0.73	
		w_{opt} – 3.3%, 25 kPa	45.22	0.75	0.68	
		w_{opt} + 3.3%, 25 kPa	526	0.91	0.85	
		w_{opt}, 75 kPa	505	0.83	0.78	
		w_{opt}, 200 kPa	922	0.88	0.83	
24	SJ10 clay		180	0.84	0.39	
25	SJ11 clay		150	0.94	0.41	

3.3.1 Performance on cohesionless soils

Cohesionless soils with little or no clay content usually present large and inner-connected pore structure, low specific surface area and micro-pore contents, and therefore have low water retention capacity and adsorbed water content. It is reasonable to assume that the S'_r, either interpreted as the residual water degree of saturation or microscopic water degree of saturation, is negligible for cohesionless soils (Alonso et al., 2013). Neglecting the S'_r (i.e. $S'_r = 0$) leads to relationship $S_r^{\xi} \approx S_r^{e} = S_r$ (as per equation (3.1)) and therefore $\xi = 1.0$. As a first assumption, a ξ value of 1.0 is used for cohesionless soils. Experimental data on the 8 cohesionless soils listed in Table 3.2 are used to validate the proposed methodology taking account of various influencing factors.

General performance and influence of the reference points

Sawangsuriya et al. (2009b) performed bender element tests on a compacted silt from Minnesota (soil 1) to determine the small strain shear modulus (G_0). Specimens were compacted, saturated, and then brought to different higher suction values to determine the G_0. Strain level experienced during the measurement of G_0 using bender element test typically is 0.001% (Atkinson, 2000; Ng & Yung, 2008). The SWCC and G_0 were measured simultaneously under a net confining stress ($\sigma_c - u_a$) of 35 kPa. Lu & Kaya (2014) performed modified unconfined compression tests (referred to as "drying cake" method) on a compacted Hopi silt (soil 4) to determine the elastic modulus (E). Specimens were compacted to nearly saturated condition, air-dried to different lower water contents, and then measured for the E values. The strain level experienced during the determination of the E using "drying cake" method is about 1.5% which is typically the strain level applied in conventional soil testing (Atkinson, 2000).

Figs 3.5(a) and 3.5(b) show the measured and fitted SWCC of the Minnesota silt and the Hopi silt. Figs 3.5(c) and 3.5(d) show the measured G_0 - s and E - s relationships. Three reference points at different suction levels on the SWCC and stiffness - suction relationships are respectively selected for the Minnesota silt (points D / D', E / E', and F / F') and the Hopi silt (points G / G', H / H', and I / I'). Applying equation (3.5) using i) the fitted SWCC shown in Figs 3.5(a) and 3.5(b), ii) the stiffness at saturation condition and reference conditions shown in Figs 3.5(c) and 3.5(d), and iii) a ξ value of 1.0, Figs 3.5(e) and 3.5(f) show the comparisons between the normalized SWCC (calculated using right-hand side of equation (3.5), shown in lines) and the normalized G_0 - s and E - s relationships (calculated using left-hand side of equation (3.5), shown in symbols). It can be observed from Figs 3.5(e) and 3.5(f) that the proposed methodology can reasonably simulate the normalized G_0 - s and E - s relationships despite the differences in the soil types and the stiffness parameters.

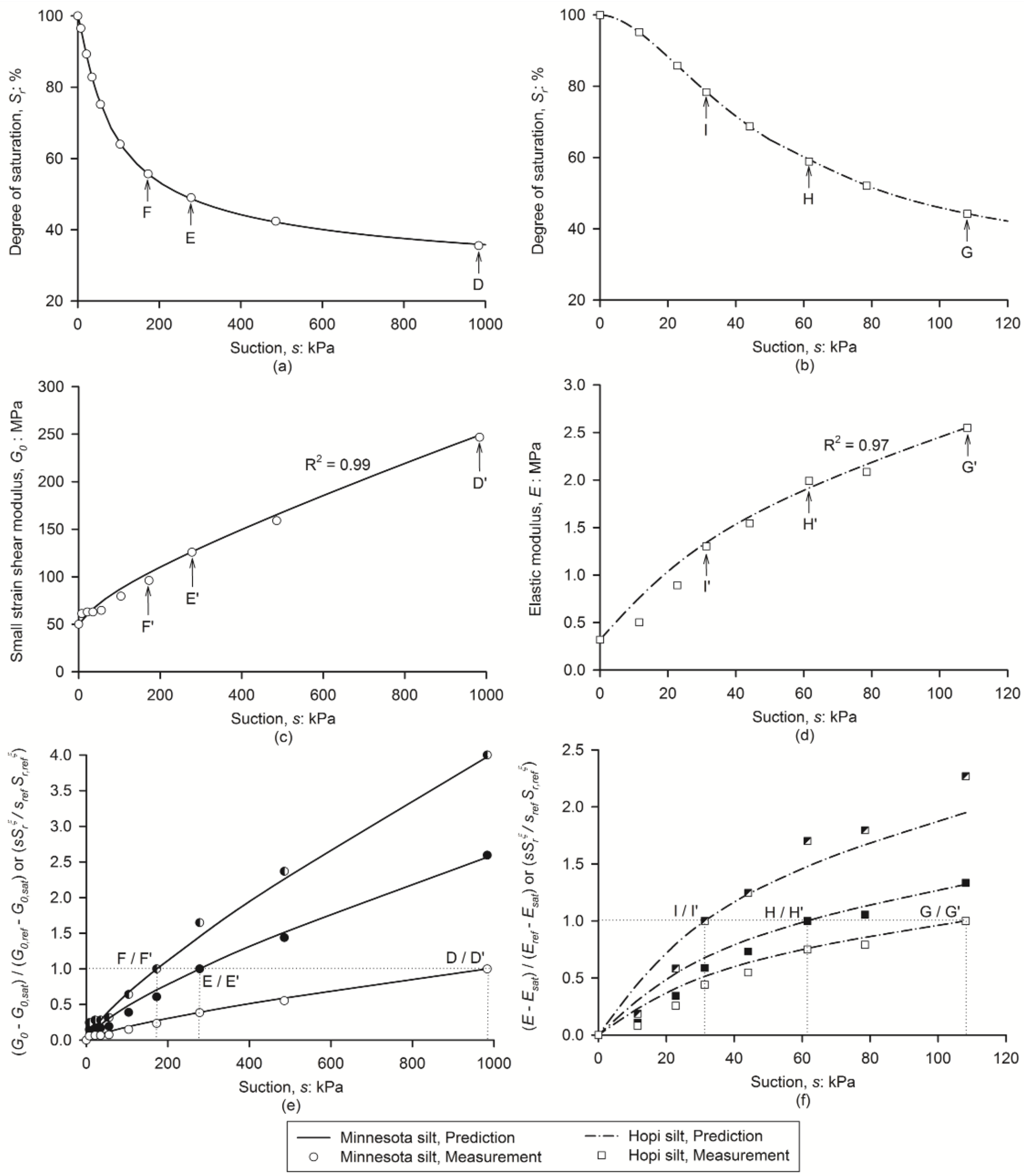

Figure 3.5 Minnesota silt and Hopi silt: (a) and (b) SWCC; (c) and (d) Ω - *s* relationships; (e) and (f) influence of reference points

The performance of the proposed methodology is not significantly influenced by the selection of the reference points as they produce similar predictions (see Figs 3.5(e) and 3.5(f)). Differences between the predictions are mainly caused by the slight scatter of the experimental data. These observations are consistent with the results of the hypothetical example shown in Fig. 3.4. A common rule therefore is adopted to use the Ω corresponding to the highest s value of the measured Ω - s relationships as the reference points (e.g., points D / D' for Minnesota silt and points G / G' for Hopi silt in Fig. 3.5). Such a choice of reference points also will limit the ratio on both sides of equation (3.5) to the scale typically between 0 and 1 (as shown in Figs 3.5(e) and 3.5(f)) and therefore facilitate the comparison and illustration. The predictions of the Ω - s relationships using reference points D / D' and G / G' for the two soils are shown in Figs 3.5(c) and 3.5(d) along with the corresponding coefficient of determination (R^2) values. In order to facilitate comparing the quality of the prediction, several subjective criteria based on the R^2 values are adopted. Witczak et al. (2002) suggested excellent prediction as R^2 greater than 0.9, good prediction as R^2 between 0.7 and 0.9, fair prediction as R^2 between 0.4 and 0.7. Smith (1986) suggested meaningful correlation as R greater than 0.8 (i.e. R^2 greater than 0.64). In this study, Witczak et al. (2002) criteria are used with fair prediction criterion modified as R^2 between 0.64 and 0.7. According to such criteria, excellent predictions are achieved for both soils as can be observed from Figs 3.5(c) and 3.5(d).

Soil structure

Bender element tests following the same procedure used for the Minnesota silt (soil 1) were also performed on the California clayey sand (soil 2) compacted at three initial water contents (w_{opt} + 4%, w_{opt}, and w_{opt} − 4%) using three compaction energies (enhanced, standard, and reduced energies) to determine the G_0 considering the influence of compaction-induced soil structures (Sawangsuriya et al., 2009b). Fig. 3.6(a) shows the measured and fitted SWCC for specimens compacted using standard energy but different initial water contents. Fig. 3.6(b) shows the measured G_0 - s relationships and the predictions using the proposed methodology. Soil tends to form different structures corresponding to different initial compaction moisture contents (generally flocculated structure is formed at dry of optimum while dispersed structure is formed at wet of optimum) and show different hydro-mechanical behaviour (e.g., differences in water retention capacities as well as shear strength and stiffness) (Wheeler & Sivakumar, 1995; Vanapalli et al., 1996; Ng & Pang, 2000; Tarantino & Tombolato, 2005; Suriol & Lloret, 2007; Alonso et al., 2013). Same observations can be made on the Minnesota silt with respect to SWCC and G_0 - s relationships from Fig. 3.6.

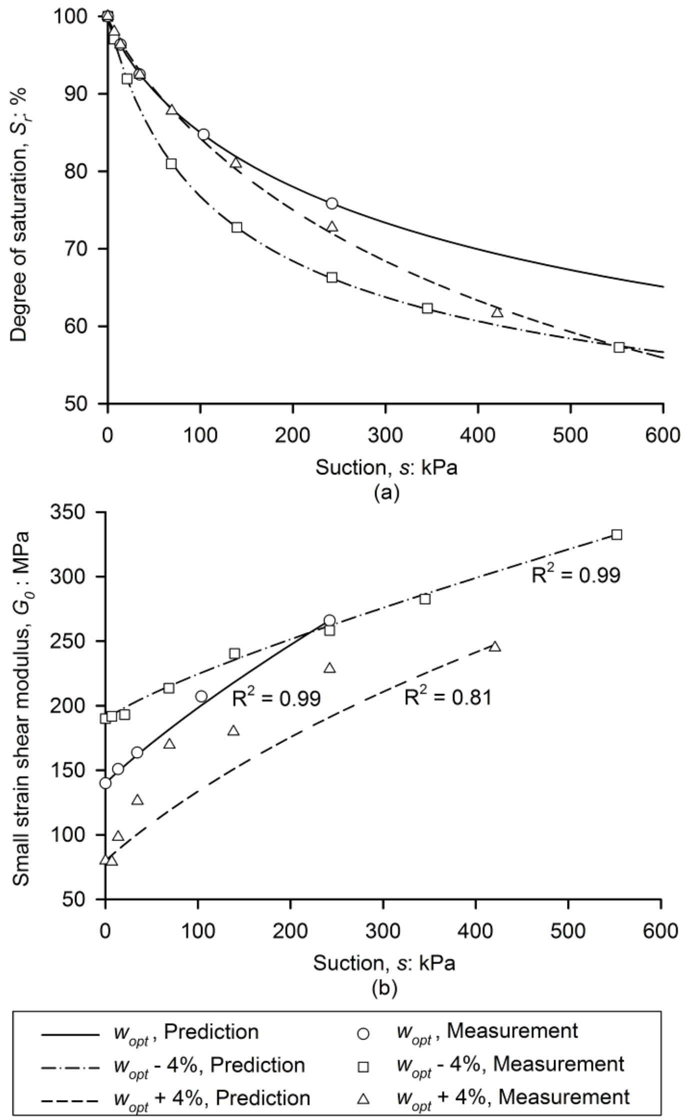

Figure 3.6 California clayey sand compacted at different initial water contents: (a) SWCC; (b) G_0 - s relationships

Similarly, Fig. 3.7 shows the comparisons between the measurements and the predictions of the specimens compacted at w_{opt} using different energies. Although results show little variance in the SWCC (Fig. 3.7(a)), the differences in the G_0 are significant (Fig. 3.7(b)).

The predictions shown in Figs 3.6(b) and 3.7(b) suggest that the proposed methodology can well predict (five excellent predictions with $R^2 \geq 0.9$ and one good prediction with $R^2 \geq 0.7$) the G_0 - s relationships for the California clayey sand with different compaction-induced structures.

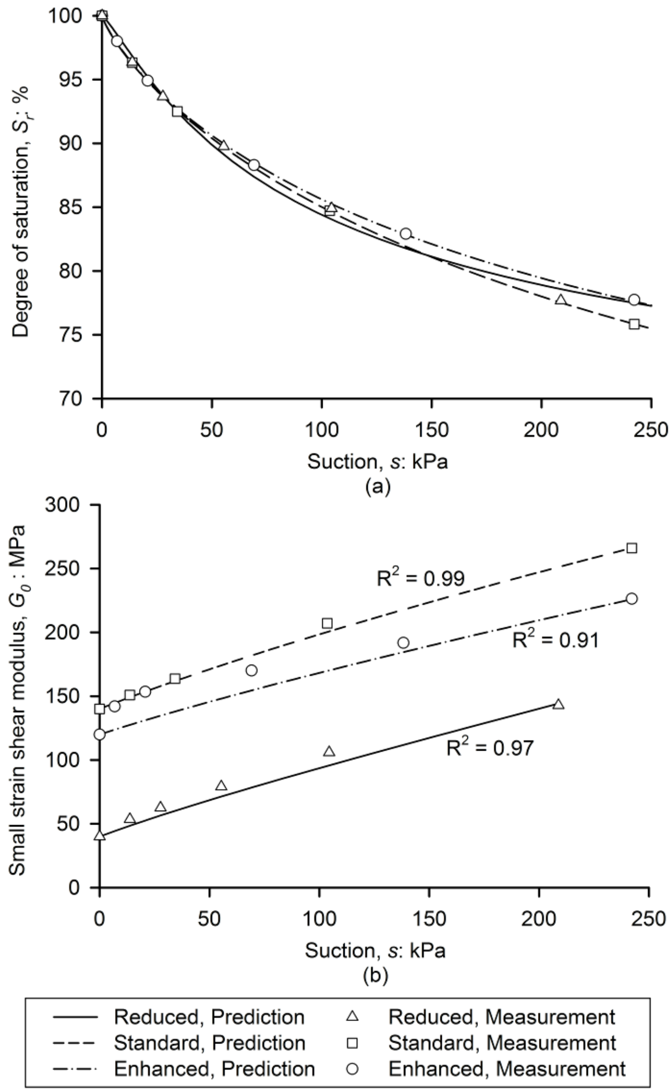

Figure 3.7 California clayey sand compacted using different energies: (a) SWCC; (b) G_0 - s relationships

External stress

The stiffness / shear strength - suction relationships and stiffness / shear strength - external stress relationships show coupled characteristics (Vanapalli & Han, 2014). Experimental data obtained for a silty sand (soil 3), a coarse sand (soil 5), and two Kidston tailings (soil 6) on the G_0, E, and τ_p respectively are used to check the performance of the proposed methodology concerning the influence of the external stress. The G_0 of the silty sand is measured from resonant column test performed on compacted specimens equilibrated to different levels of $(\sigma_c - u_a)$ and s within the shear strain level of 0.002% (Hoyos et al., 2015). The τ_p values of the two Kidston tailings collected from different locations (referred to as Kidston tailing-A and Kidston tailing-B in Table 3.2) are measured from direct shear tests performed on reconstituted specimens consolidated from slurried condition. Specimens were consolidated to different suction values and then subjected to direct shear under different $(\sigma_n - u_a)$ values (Rassam & Williams, 1999). The E values of the coarse sand are back-calculated from the load - settlement curves derived from model footing tests performed on the coarse sand with suction control (Vanapalli & Mohamed, 2007; Oh et al., 2009). Square model footings with two dimensions (100 by 100 mm and 150 by 150 mm) are used in the tests. The loading of the different model footings results in different stress levels (i.e. different stress bulbs) in the sand beneath the model footings, and therefore different load - settlement curves and E values. Such E values represent the elastic behavior of the coarse sand at higher strain levels as the settlement used for back-calculation is as high as 10 mm (Oh et al., 2009).

The influence of external stress can be considered in the proposed methodology by expressing the Ω_{sat} and Ω_{ref} in equation (3.5) using conventional stress-dependent equations such as equations (3.3.1), (3.3.3), (3.3.5) and (3.3.7) in Table 3.1. The $G_{0,sat}$ and $G_{0,ref}$ (at s = 400 kPa) of the silty sand can be expressed as the function of $(\sigma_c - u_a)$ (equation (3.3.3)) while he $\tau_{p,sat}$ and $\tau_{p,ref}$ (at s = 100 kPa) of the Kidston tailings can be written as a function of $(\sigma_n - u_a)$ using Mohr-Coulomb equation (equation (3.3.1)). Details of the stress-dependent equations and their parameters for the silty sand, Kidston tailings and other soils used in later sessions of this chapter are listed in Table 3.5. Substituting i) the Ω_{sat} and Ω_{ref} expressed as stress-dependent equations, ii) the fitted SWCC shown in Fig. 3.8(a), and iii) ξ = 1.0 into equation (3.5) provides smooth surfaces in the G_0 - $(\sigma_c - u_a)$ - s space (Fig. 3.8(b)) and τ_p - $(\sigma_n - u_a)$ - s space (Figs 3.8(c) and 3.8(d)). The measured G_0 varies nonlinearly with both ($\sigma_c - u_a$) and s, while the measured τ_p varies linearly with ($\sigma_n - u_a$) but non-linearly with s. These features are reasonably captured by the predicted surfaces using the equation (3.5) (two excellent prediction with $R^2 \geq 0.9$ and one good prediction with $R^2 \geq 0.7$).

Table 3.5 Parameters of stress-dependent equations for Ω_{sat} and Ω_{ref}

Soil ID & type		Equations	Ω_{sat}	Ω_{ref}
3, Silty sand	G_0	$G_0 = k_1(\sigma_c - u_a)^{k_2}$	$k_1 = 1.33$, $k_2 = 0.54$	$k_1 = 57.4$, $k_2 = 0.09$
6, Kidston tailing-A	τ_p	$\tau_p = c' + (\sigma_n - u_a)\tan\phi'$	$c' = 0$, $\phi' = 41.7^o$	$^*c = 37.7$, $\phi' = 41.7^o$
6, Kidston tailing-B			$c' = 0$, $\phi' = 40.7^o$	$^*c = 48.9$, $\phi' = 40.7^o$
12, Decomposed tuff	v_{hh}	$v = k_1(\sigma_c - u_a)^{k_2}$	$k_1 = 47.37$, $k_2 = 0.2$	$k_1 = 111.6$, $k_2 = 0.32$
	v_{hv}		$k_1 = 47.72$, $k_2 = 0.2$	$k_1 = 112.1$, $k_2 = 0.32$
	v_{vh}		$k_1 = 42.02$, $k_2 = 0.2$	$k_1 = 94.25$, $k_2 = 0.32$
20, Nanyang expansive soil	q_p	$q_p = z + p_{net}M$	$z = 83.22$, $M = 0.84$	$z = 217.4$, $M = 0.84$
	E	$E = k_5 P_a (\frac{\sigma_c - u_a}{P_a})^{k_6}$	$k_5 = 0.18$, $k_6 = 0.54$	$k_5 = 0.31$, $k_6 = 0.15$
21, Bukit Timah Granite	τ_p	$\tau_p = c' + (\sigma_n - u_a)\tan\phi'$	$c' = 13$, $\phi' = 30^o$	$^*c = 303.8$, $\phi' = 30^o$
	E	$E = k_5 P_a (\frac{\sigma_n - u_a}{P_a})^{k_6}$	$k_5 = 0.13$, $k_6 = 0.24$	$k_5 = 0.24$, $k_6 = 0.4$

Notations: $z = 6c'\cos\phi' / (3 - \sin\phi')$, $M = 6\sin\phi' / (3 - \sin\phi')$, p_{net} = net mean stress, c = apparent cohesion; Units: G_0 and E in MPa; τ_p, c, q_p, p_{net}, ($\sigma_c - u_a$) and ($\sigma_n - u_a$) in kPa; v in m/s; P_a = 100 kPa; *Apparent cohesion c is used to replace effective cohesion c' for unsaturated shear strength.

Fig. 3.9 shows, for the coarse sand, the comparisons between the measurements (in symbols) and the predictions (continuous lines) if the measured values (i.e. E_{sat} and E_{ref} at s = 6 kPa) are directly substituted into equation (3.5) as Ω_{sat} and Ω_{ref} values. Excellent predictions are achieved for this case. The comparisons shown in Figs 3.8 and 3.9 suggest that i) the methodology can reasonably describe the Ω - external stress - suction relationships for cohesionless soils; and ii) it is flexible to use any suitable stress-dependent equations to express the Ω_{sat} and Ω_{ref} and therefore include the influence of external stress into the prediction.

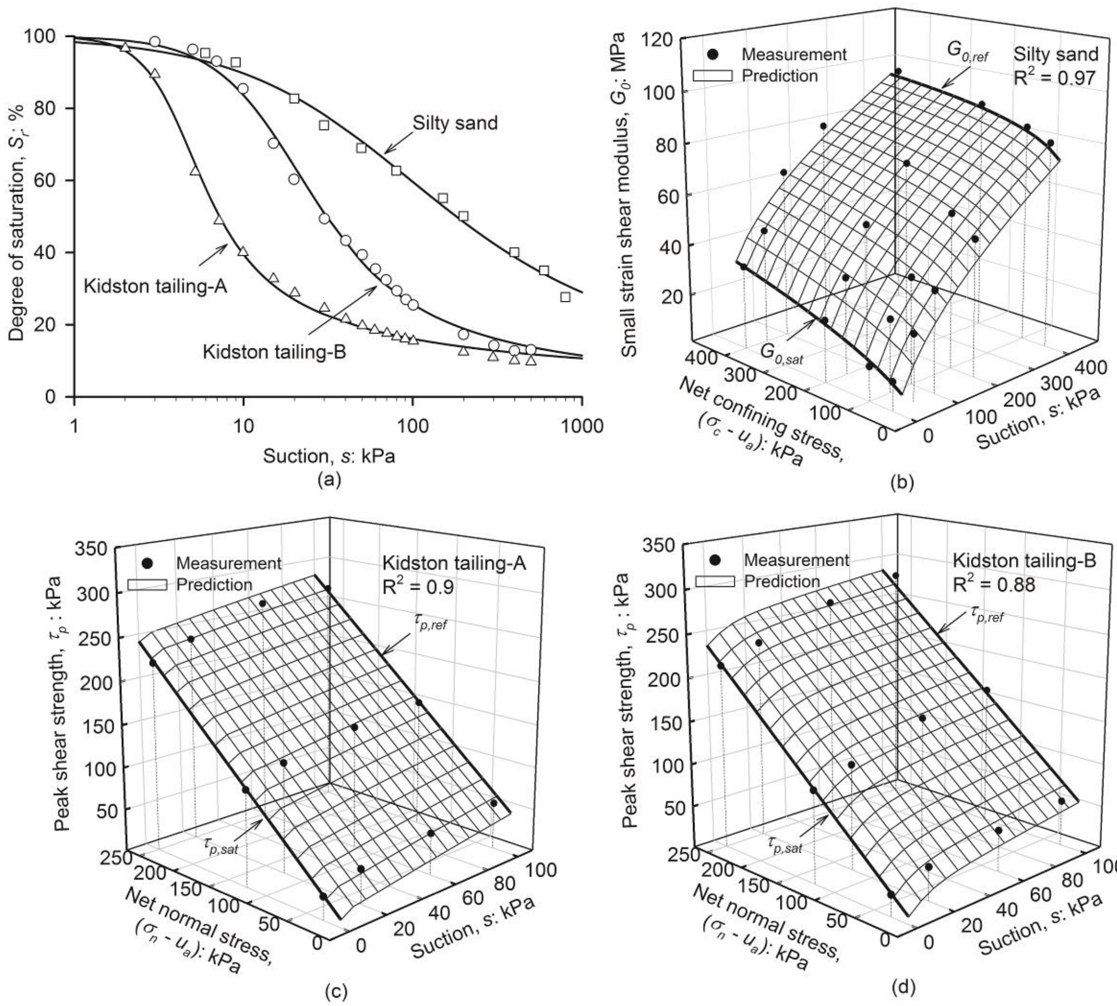

Figure 3.8 Silty sand and Kidston tailings: (a) SWCC; (b) G_0 - s relationships for the silty clay; τ_p - s relationships for (c) Kidston tailing-A and (d) Kidston tailing-B

Hydraulic Hysteresis

Khalili & Zargarbashi (2010) performed suction controlled triaxial tests on Bourke silt (soil 7) and sand-kaolin mixture (soil 8) to investigate the influence of hydraulic hysteresis on the critical shear strength and effective stress parameter χ. Multistage triaxial tests were performed on specimens which were initially saturated and consolidated to different higher suction levels following the drying path. When suction reached 300 kPa, the wetting path was thereafter followed by reducing the suction while adjusting the deviator stress (q) to maintain the soil stay on the critical state line. The q applied to load the specimens to the critical state (q_c) can be used to indicate the critical shear strength. Figs 3.10(a) and 3.10(b) show the hysteresis loops of the measured SWCC and q_c - suction relationships of the two soils. Reference points are chosen at highest suction level (i.e. s = 300 kPa, points K / K' for the Bourke silt, points J / J' for the sand-kaolin mixture) where drying and wetting curves join.

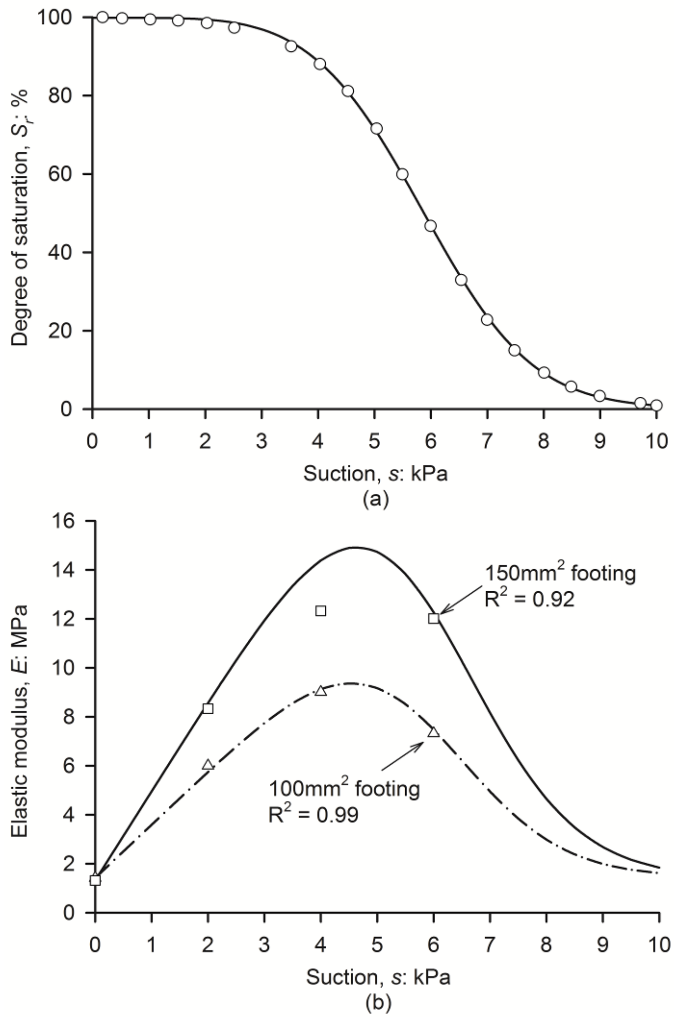

Figure 3.9 Coarse sand: (a) SWCC; (b) *E* - *s* relationships

The S_r and q_c values at s = 0 on the wetting curves, which are necessary for implementing the equation (3.5), were not measured in the original study. The S_r on the wetting curve at s = 0 usually cannot fully recover to 100% due to the entrapped air bubbles that are formed and separated during the flooding of the soil pores. The presence of entrapped air bubbles at s = 0 may influence the soil mechanical behaviour; however, discussion on this topic is beyond the scope of this chapter. An assumption is made in this chapter that there is no hydraulic hysteresis effect at saturation condition (i.e. S_r = 1.0 and $q_{c,sat}$ is a constant on both drying and wetting curves at s = 0). Similar assumptions are also used in other studies (e.g., Wheeler et al., 2003; Sheng et al., 2008; Gallipoli, 2012; Gallipoli et al., 2015). Figs 3.10(c) and 3.10(d) show the comparisons between the normalized SWCC and the normalized q_c - s relationships (using ξ =1.0 in equation (3.5)) for the two soils. Excellent predictions with $R^2 \geq 0.9$ are achieved for both soils.

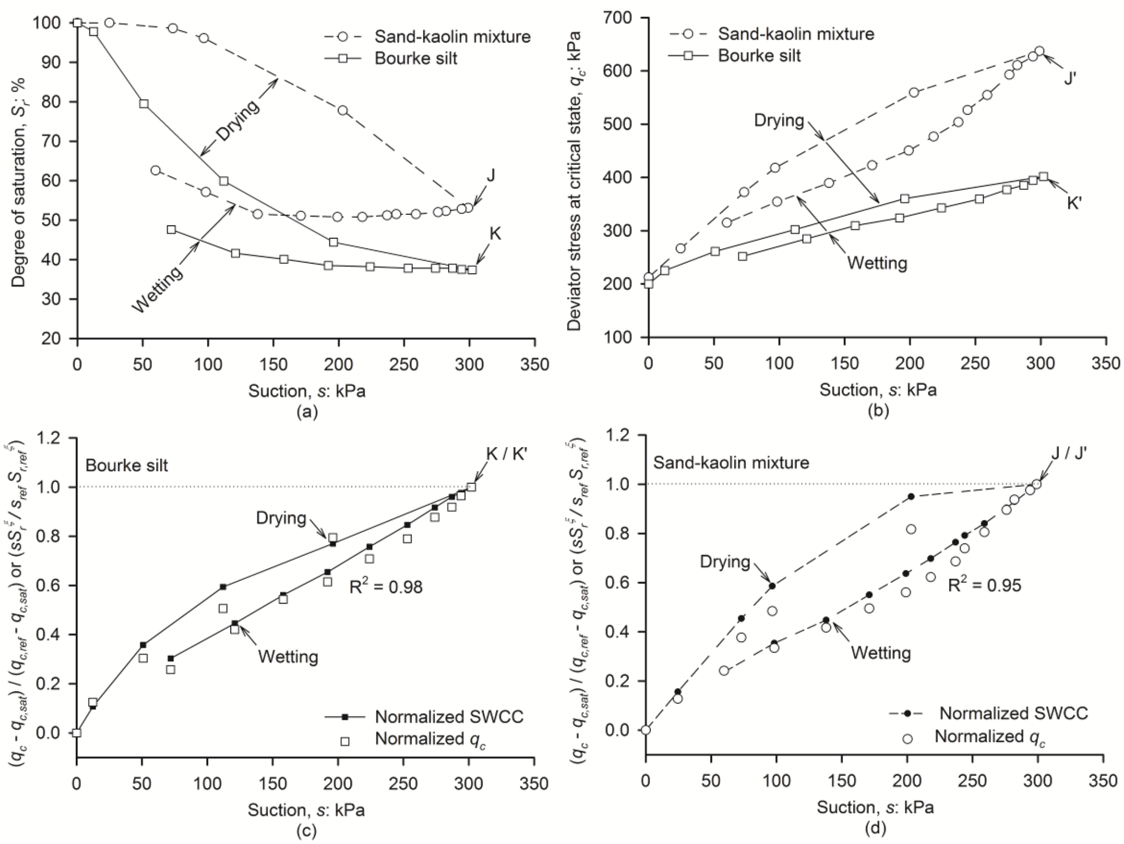

Figure 3.10 Bourke silt and sand-kaolin mixture: (a) SWCC; (b) q_c - s relationships; (c) predictions for the Bourke silt; (d) predictions for the sand-kaolin mixture

3.3.2 Performance on cohesive soils

Calibration of the ξ and general performance

For cohesive soils, the increased amount of clay particles contributes to the following: i) more water is adsorbed to the surface of clay particles; ii) the dimension of the macro-pores decreases while the amount of micro-pores increases; and iii) clays tend to form aggregated structures that are likely to trap water in the intra-aggregate micro-pores (Fredlund & Rahardjo, 1993; Delage et al., 1996; Barbour, 1998; Tarantino & Tombolato, 2005; Romero & Simms, 2008; Alonso et al., 2013).

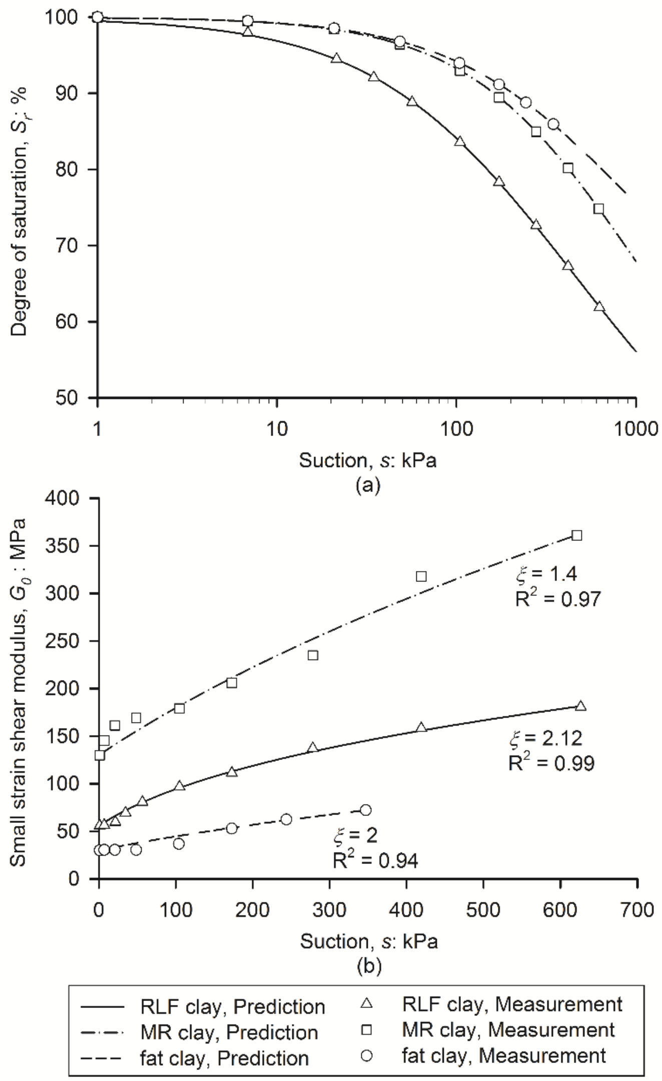

Figure 3.11 RLF clay, MR clay and fat clay: (a) SWCC; (b) G_0 - s relationships

The S'_r within cohesive soils becomes significant and therefore should be taken into account. Considering $S'_r > 0$ in equation (3.1) leads to relationship $S_r^{\xi} \approx S_r^{e} < S_r$ and therefore $\xi > 1.0$. Due to the empirical nature of the ξ, its values for cohesive soils should be determined from regression analysis. The experimental data derived from a total of 12 different cohesive soils on small strain shear modulus (soils 9 - 11), elastic modulus (soils 13 - 19) and shear strength (soils 24 - 25) are used to calibrate the ξ value (see Table 3.3). Experimental data of the rest 5 cohesive soils (soils 12 and 20 - 23 in Table 3.3) are used to test the performance of equation (3.5) using the calibrated ξ. The G_0 values of soils 9 - 11 were determined following the experimental procedures described for soil 1

(Sawangsuriya et al., 2009b) and the E values of soils 13 - 19 were determined following the experimental procedures described for soil 4 (Lu & Kaya, 2014). The SJ10 clay and SJ11 clay samples were natural samples collected from different depths. Samples were equilibrated to different suction levels under a net confining stress ($\sigma_c - u_a$) of 200 kPa in triaxial apparatus and then sheared (Khalili et al., 2004). The peak deviator stress (q_p) applied during the shearing is used to indicate the peak shear strength of these two clays.

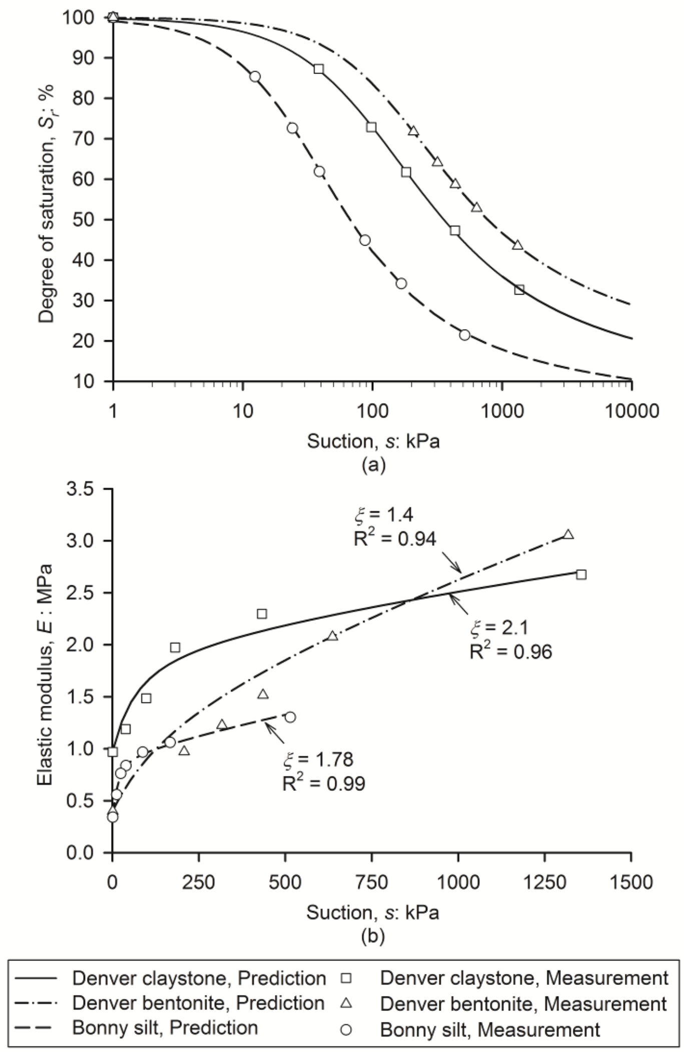

Figure 3.12 Denver claystone, Denver bentonite and Bonny silt: (a) SWCC; (b) *E* - *s* relationships

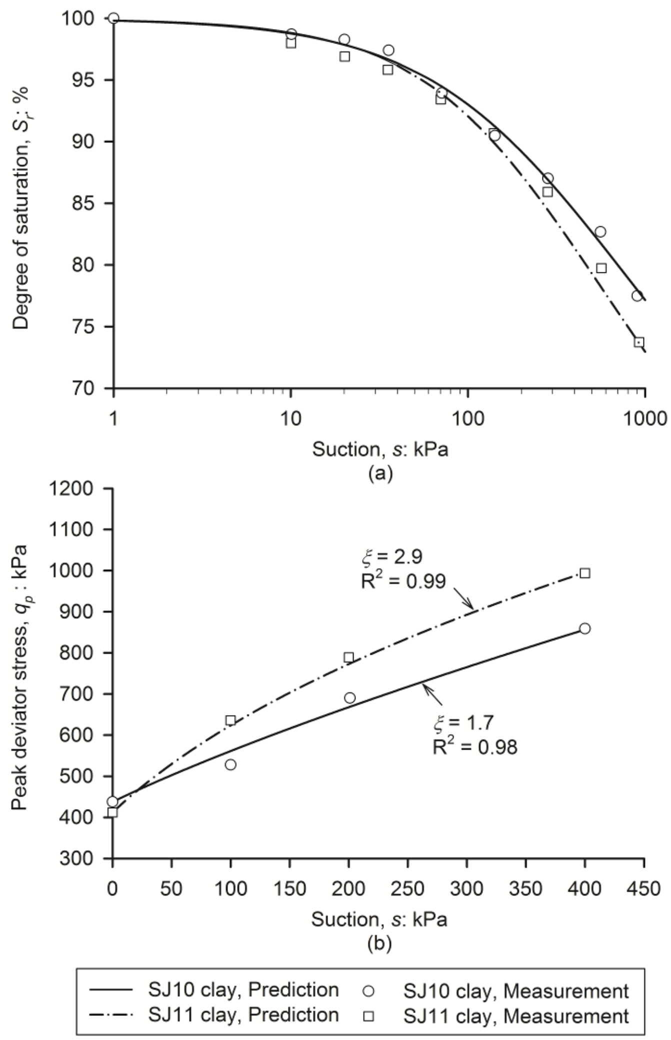

Figure 3.13 SJ10 clay and SJ11 clay: (a) SWCC; (b) q_p- s relationships

Figs 3.11 - 3.13 show, for some of the 12 soils, the SWCC and comparisons between the measured Ω - *s* relationships and the predictions using the proposed methodology. It can be noted that the measured Ω - *s* relationships for different cohesive soils are well predicted.

Table 3.6 summarises, for all the 12 soils, the ξ values derived from regression analysis that best-fit the predictions of equation (3.5) to the measurements and the corresponding R^2 values and quality of prediction as per Witczak et al. (2002) criteria. The ξ values are generally greater than 1.0 which is consistent with the summarized analysis. The ξ values vary within a narrow range between 1.0 and 3.0 as shown in Table 3.6. Some previous studies in the literature which adopted factor S_r^{ξ} for predicting different stiffness or shear strength of unsaturated cohesive soils also suggested similar ξ range (Vanapalli & Fredlund, 2000; Garven & Vanapalli, 2006, Han & Vanapalli, 2015). The variation of ξ however seems less correlated to the soil types or plasticity. This could be attributed to the experimental error and the resulting scatter embedded in the measurements of the SWCC or Ω - s relationship, which influences the regression analysis and the resulting ξ value. In order to determine the optimum value of the ξ that provides the most favorable predictions, the measurements on the Ω - s relationships at various suction levels are required in the regression analysis.

Table 3.6 Values of ξ and R^2 for 12 different cohesive soils

Soil ID & type	ξ from regression analysis			ξ = 2.0	
	ξ	R^2	Quality *	R^2	Quality *
9, Minnesota RLF clay	2.12	0.99	Excellent	0.99	Excellent
10, Minnesota MR clay	1.40	0.97	Excellent	0.96	Excellent
11, Minnesota fat clay	1.30	0.95	Excellent	0.94	Excellent
13, Bonny silt	1.78	0.99	Excellent	0.91	Excellent
14, BALT silt	2.07	0.91	Excellent	0.91	Excellent
15, Iowa silt	1.38	0.82	Good	0.75	Good
16, Golden silt	2.47	0.99	Excellent	0.98	Excellent
17, Denver clay stone	2.10	0.96	Excellent	0.96	Excellent
18, Georgia kaolinite	1.10	0.80	Good	0.70	Good
19, Denver bentonite	1.40	0.94	Excellent	0.80	Good
24, SJ10 clay	1.70	0.98	Excellent	0.98	Excellent
25, SJ11 clay	2.90	0.99	Excellent	0.98	Excellent

*Quality of prediction is reviewed as per criteria: excellent, $R^2 \geq 0.9$; good, $0.7 \leq R^2 < 0.9$; fair, $0.64 \leq R^2 < 0.7$.

A unique ξ value of 2.0, which falls between 1.0 and 3.0, could also be used in equation (3.5) for cohesive soils i) in favor of simplicity for use in engineering practice or ii) when comprehensive measurements on the Ω - s relationships are not available. For such a scenario, only one measurement of Ω - s relationship (i.e. reference point (s_{ref}, Ω_{ref})) is needed to implement equation (3.5) as there is no need for regression analysis to determine the ξ. Table 3.6 also summarizes the corresponding R^2 values and quality of prediction if a ξ value of 2.0 is used for all the 12 soils. It can be observed that there is a reduction in the R^2 and soils show different sensitivity to the variation in the ξ (for example, soil 19 show higher sensitivity to ξ (R^2 reduced from 0.94 to 0.8) than soil 10 (R^2 reduced from 0.97 to

0.96) given the same change in the ξ from 1.4 to 2.0). In general, the reduction in the R^2 and quality of prediction as shown in Table 3.6 is not significant. In other words, a value of ξ equal to 2.0 could be conveniently used with adequate confidence for cohesive soils in equation (3.5), especially when experimental data on Ω - s relationship are rather limited. In the following analysis, a constant ξ value of 2.0 is assumed for the remainder 5 cohesive soils (soils 12 and 20 - 23 in Table 3.3). It has been proved in later sections of this chapter that the proposed methodology provides favorable predictions for cohesive soils using ξ = 2.0.

Anisotropy, soil structure and external stress

Ng & Yung (2008) performed bender element tests on a decomposed tuff (soil 12) to investigate the influence of anisotropy on the $(\sigma_c - u_a)$ - s - G_0 relationships (the strain level for G_0 is 0.001%). Compacted specimens were consolidated to different $(\sigma_c - u_a)$ and s levels in a triaxial cell. The velocities of the shear wave v (m/s) penetrating the specimens via three paths (i.e. v_{hh}, velocity of shear wave penetrating horizontally with horizontal polarisation; v_{hv}, velocity of shear wave penetrating horizontally with vertical polarisation; v_{vh}, velocity of shear wave penetrating vertically with horizontal polarisation) were recorded and used to indicate the corresponding $G_{0,hh}$, $G_{0,hv}$, and $G_{0,vh}$ values as per relationships $G_{0,hh} = \rho v_{hh}^2$, $G_{0,hv} = \rho v_{hv}^2$, and $G_{0,vh} = \rho v_{vh}^2$ (ρ is the bulk density of the penetrated media). Similar to the analysis of the silty sand (soil 2), the v_{sat} (i.e. $v_{hh,sat}$, $v_{vh,sat}$, $v_{hv,sat}$) and v_{ref} (i.e. $v_{hh,ref}$, $v_{vh,ref}$, $v_{hv,ref}$ at s = 200 kPa) can be related to external stress using a simple stress-dependent equation similar to equation (3.3.3) (see details in Table 3.5). Substituting i) the v_{sat} and v_{ref}, ii) the fitted SWCC of the decomposed tuff shown in Fig. 3.14(a), and iii) ξ = 2.0 into equation (3.5), Figs 3.14 (b), 3.14(c) and 3.14(d) show the predicted surfaces in the $(\sigma_c - u_a)$ - s - v spaces in comparison with the measurements. It can observed that the anisotropy influences the absolute values of the v_{vh}, v_{hv}, v_{hh} and their variations with $(\sigma_c - u_a)$ and s. These relationships are reasonably well predicted (excellent predictions with $R^2 \geq 0.9$) using the proposed methodology.

Vanapalli et al. (1996) performed multistage suction-controlled direct shear tests on glacial till specimens (soil 23) compacted at three moisture contents (w_{opt} + 3.3%, w_{opt}, w_{opt} – 3.3%) and sheared under three net normal stresses (25 kPa, 75 kPa, 200 kPa) to investigate the influence of compaction-induced soil structure and external stress on the SWCC and the τ_p - s relationships. Fig. 3.15 shows the measured and predicted SWCC and τ_p - s relationships. Similar to the results for the California clayey sand (soil 1) shown in Fig. 3.7, different soil structures resulted from different compaction moisture contents pose significant influence on the SWCC and τ_p - s relationships under the net normal stress of 25 kPa (Figs 3.15(a) and 3.15(c)). The influence of net normal stress on the SWCC and τ_p - s relationships of specimens compacted at w_{opt} can also be inspected from Figs 3.15 (b) and 3.15(d). The predictions shown in Fig. 3.15 well simulate the τ_p - s relationships in response to different soil structures and external stresses (excellent predictions with $R^2 \geq 0.9$).

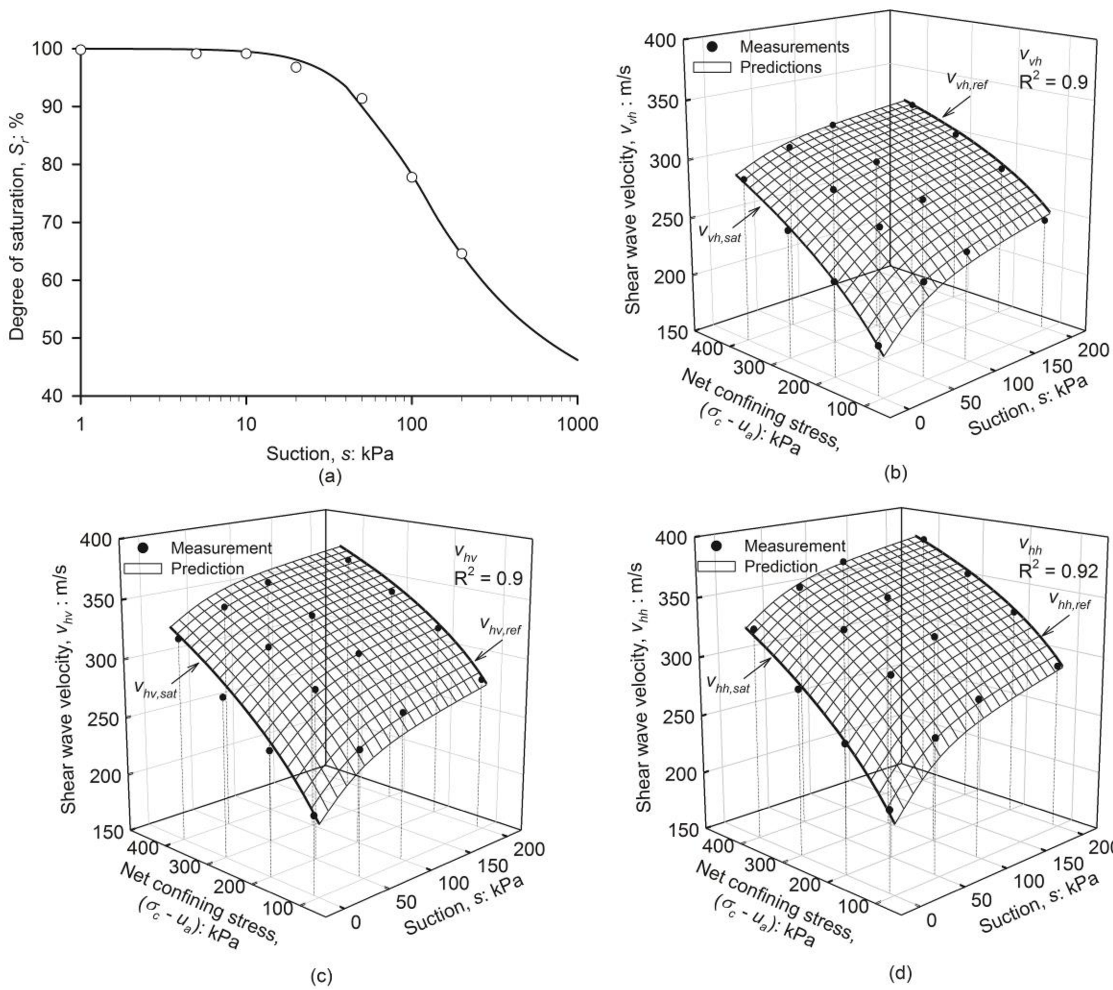

Figure 3.14 Decomposed tuff: (a) SWCC; v - s relationships for (b) v_{vh}; (c) v_{hv}; (d) v_{hh}

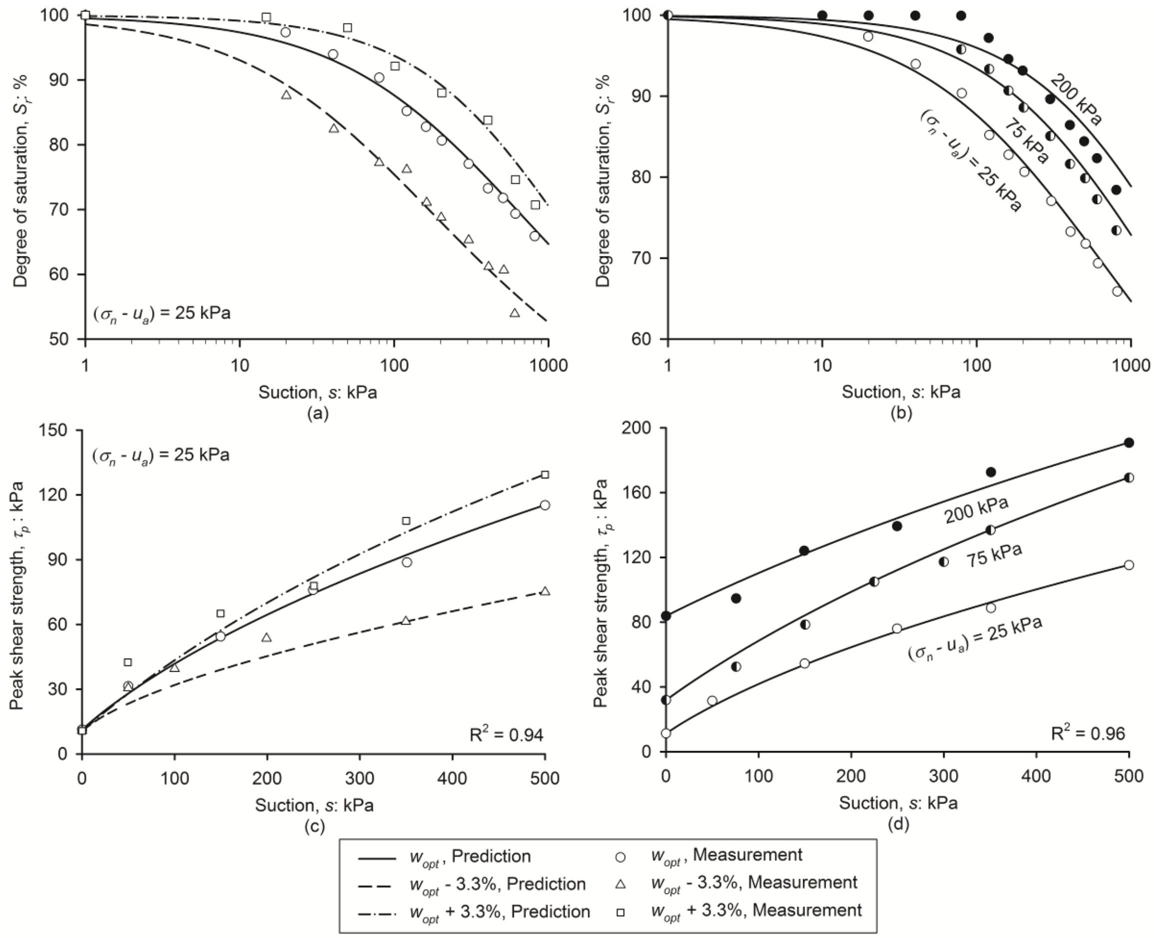

Figure 3.15 Glacial till: response of SWCC with (a) compaction moisture content; (b) net normal stress; response of τ_p - s relationships with (c) compaction moisture content; (d) net normal stress

Stiffness and shear strength of the same soil

The experimental data of both elastic modulus and shear strength determined from Nanyang expansive soil (soil 20), Bukit Timah Granite (soil 21) and Zaoyang expansive soil (soil 22) are used to verify the performance of the methodology on the same soil but different properties. The slope of the stress - strain curves within the axial strain level of 1% derived from triaxial tests can be used to calculate the elastic modulus based on the assumption that soils stay elastic within the low axial strain level (Lu & Kaya, 2014). In addition, 1% is also the frequent strain level encountered in conventional soil testing (Atkinson, 2000). This procedure is adopted in this study to determine the elastic modulus of the Nanyang expansive soil (soil 20) tested by Miao et al. (2002) and the Zaoyang expansive soil (soil 22) tested by Zhan (2003). Compacted specimens of these two soils were consolidated in suction-controlled triaxial apparatus to different ($\sigma_c - u_a$) and s levels and sheared under drained condition. The measured stress - strain curves of these two soils are used to i) determine the q_p (indicating peak shear strength of triaxial specimens), and ii) back calculate the E values within the strain level of 1%. Experimental data on the τ_p and critical shear strength (τ_c) of the compacted Zaoyang expansive soil derived from suction controlled direct shear tests under the net normal stress of 50 kPa (Zhan & Ng, 2006) are also used to check the performance of the methodology. Rahardjo et al. (2011) performed suction controlled direct shear tests on Bukit Timah Granite specimens (soil 21) which were compacted, saturated and consolidated to different ($\sigma_n - u_a$) and s levels to determine the τ_p. Numerical analysis were performed in the same study to simulate the direct shear tests using different trial E values. The trial E values used in the numerical analysis that best simulated the shear stress - horizontal displacement curves derived from the direct shear tests were assumed to be the E values of the Bukit Timah Granite (Rahardjo et al., 2011). Such E values determined from numerical analysis represent the elastic behavior of the Bukit Timah Granite at higher strain levels typically experienced during the direct shear tests (2% - 5% for example).

Figs 3.16 and 3.17 show, for the Nanyang expansive soil and Bukit Timah Granite respectively, the SWCC and the measurements of the stiffness / shear strength - external stress - suction relationships in comparison with the predictions (Ω_{sat} and Ω_{ref} are expressed as stress-dependent equations in equation (3.5), see details in Table 3.5). Fig. 3.18 shows the SWCC and the measured and predicted variations of the τ_p, q_p and E with respect to s for Zaoyang expansive soils. The comparisons shown in Figs 3.16, 3.17, and 3.18 suggest that the proposed methodology is able to reliably predict different stiffness and shear strength properties for the same soil (excellent or good predictions are achieved).

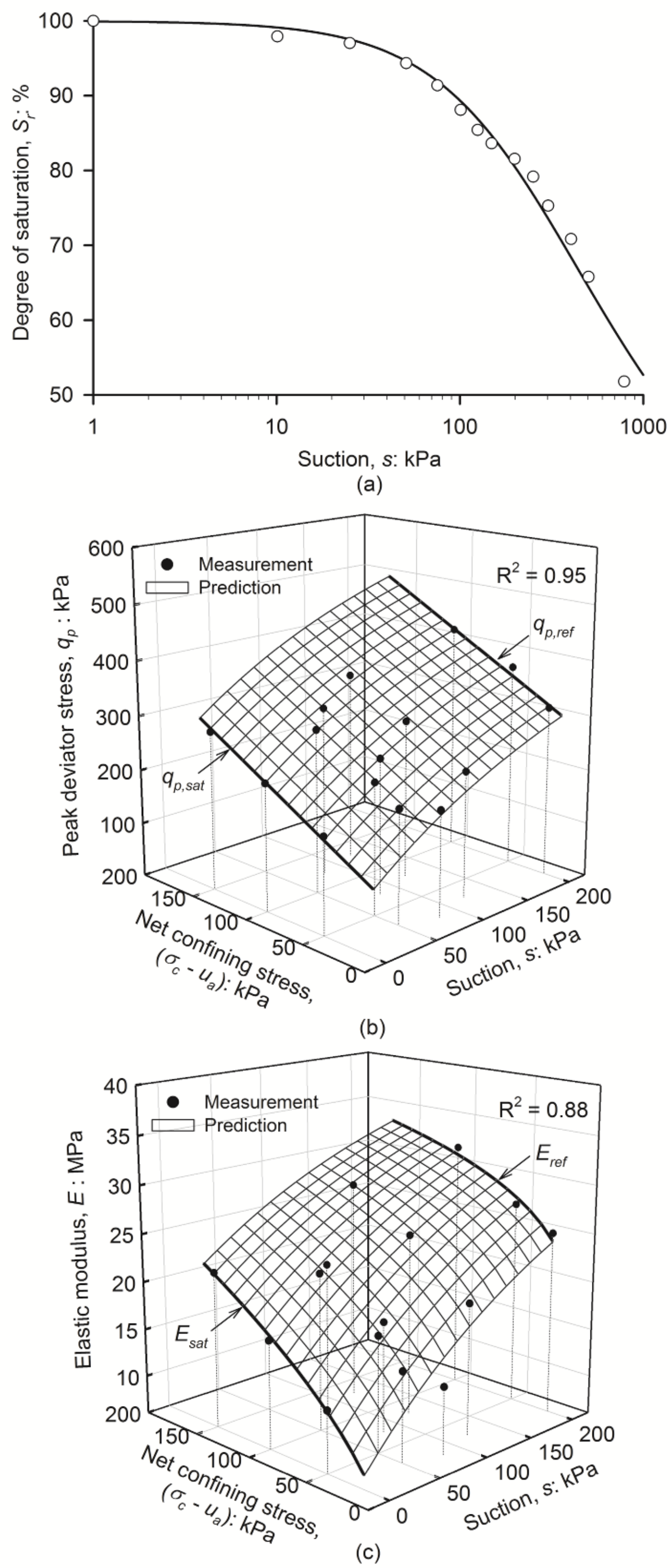

Figure 3.16 Nanyang expansive soil: (a) SWCC; (b) q_p - s relationships; (c) E - s relationships

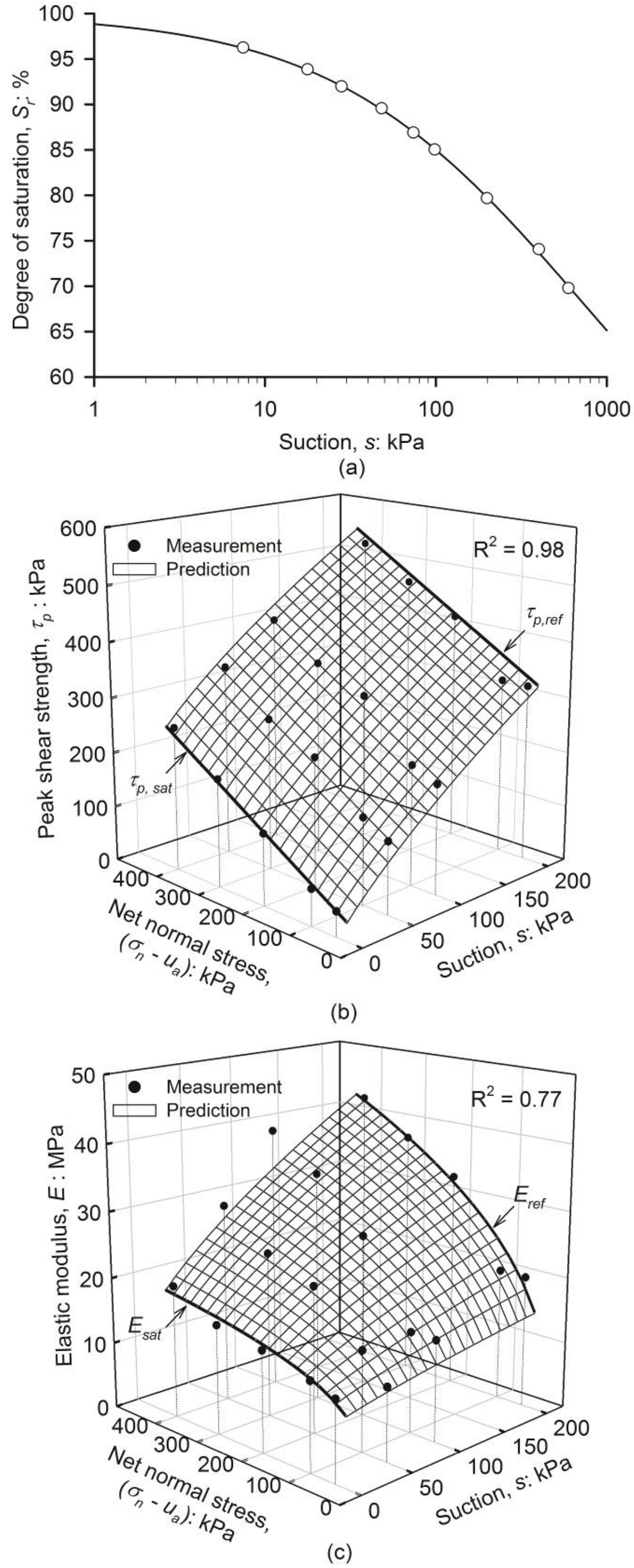

Figure 3.17 Bukit Timah granite: (a) SWCC; (b) τ_p - s relationships; (c) E - s relationships

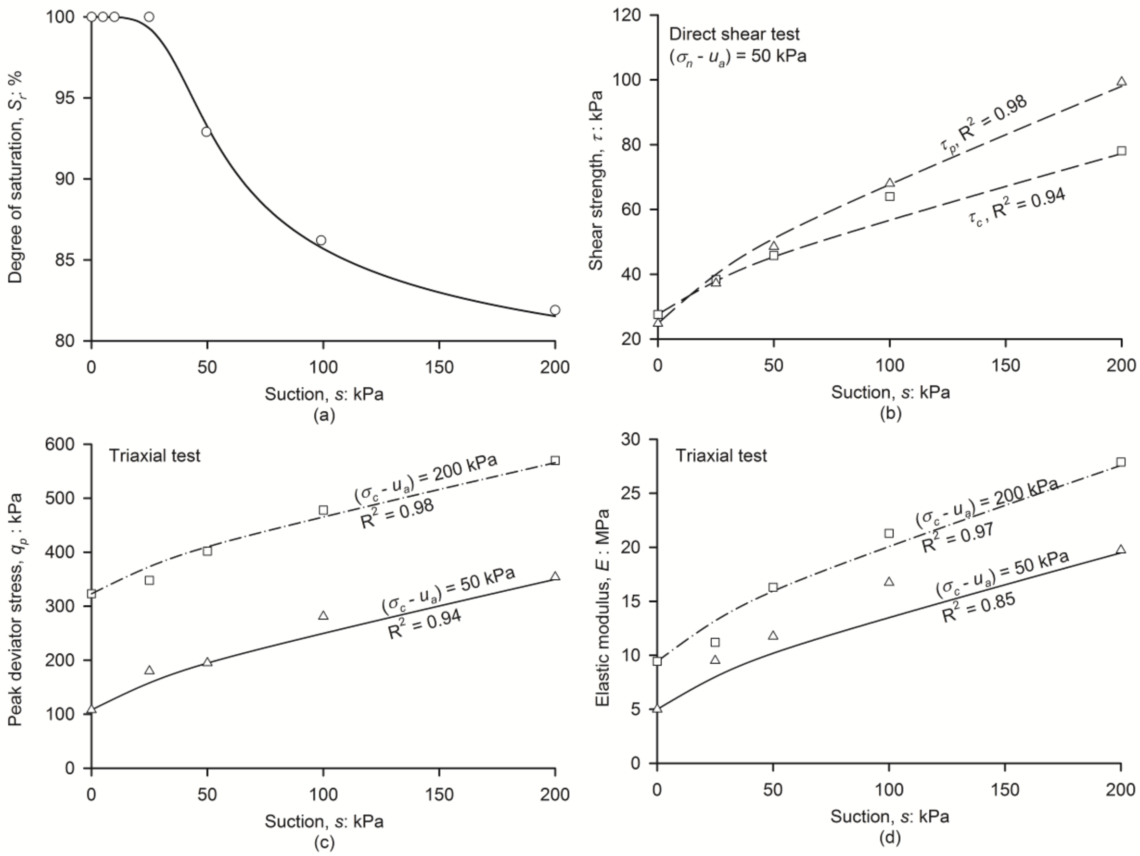

Figure 3.18 Zaoyang expansive soil: (a) SWCC; (b) τ_p - s relationships; (b) q_p - s relationships; (d) E - s relationships

Relationship between S_r^e and S_r^ξ

The proposed methodology is able to provide reasonable predictions for different stiffness and shear strength properties for all the 8 cohesionless soils (using $\xi = 1.0$) and 17 cohesive soils (using $\xi = 2.0$) in the present study. This suggests that factors S_r and S_r^2 can be reasonably used to approximate the factor S_r^e within lower suction range for cohesionless soils and cohesive soils, respectively. Using S_r to approximate S_r^e for cohesionless soils is straightforward and can be used as per the earlier discussion. However, using S_r^2 to approximate S_r^e for cohesive soils needs more discussion and justification.

Fig. 3.19 shows the variations of S_r, S_r^2 and S_r^e with respect to s for six cohesive soils. The S'_r of these six soils were determined using different approaches. The S'_r of the glacial till (soil 23) and Nanyang expansive soil (soil 20) were suggested at suction of 3000 kPa and

1500 kPa respectively (Vanapalli et al., 1996; Miao et al., 2002; see Figs 3.19(a) and 3.19(b)). The S'_r of the Denver bentonite (soil 19) is determined using the graphical method described in Vanapalli et al. (1999) (Lu & Kaya, 2013; Fig. 3.19(c)). The S'_r of the Boom clay (w_L% = 55.7, I_p% = 28.8, sand% = 18, silt% = 30, clay% = 52) compacted at higher and lower densities (Figs 3.19(d) and 3.19(e)) and the S'_r of the Barcelona silty clay (w_L% = 30.5, I_p% = 11.8, sand% = 26, silt% = 50, clay% = 24) compacted at initial void ratio e_0 of 0.538 (Fig. 3.19(f)) were suggested to be equal to the micro-pore contents that were measured using mercury intrusion tests (data of Boom clay and Barcelona silty clay were measured by Suriol et al., 1998; Romero, 1999; Barrera, 2002; data used in this chapter were gathered from Alonso et al., 2010 & 2013). It is noted that using the suggested S'_r values and the resulting S_r^e values, the stiffness or shear strength properties of the six soils were all rationally interpreted or predicted (Vanapalli et al., 1996; Miao et al., 2002; Alonso et al., 2010 & 2013; Lu & Kaya, 2013 & 2014). It can be observed from Fig. 3.19 that the values of S_r^2 are close to that of the S_r^e for all the cohesive soils with the s value up to several hundreds of kPa, which is the typical suction range encountered in engineering practice (Vanapalli et al., 1996; Fredlund, 2006). The analysis of results support using ξ = 2.0 in the proposed methodology for unsaturated cohesive soils.

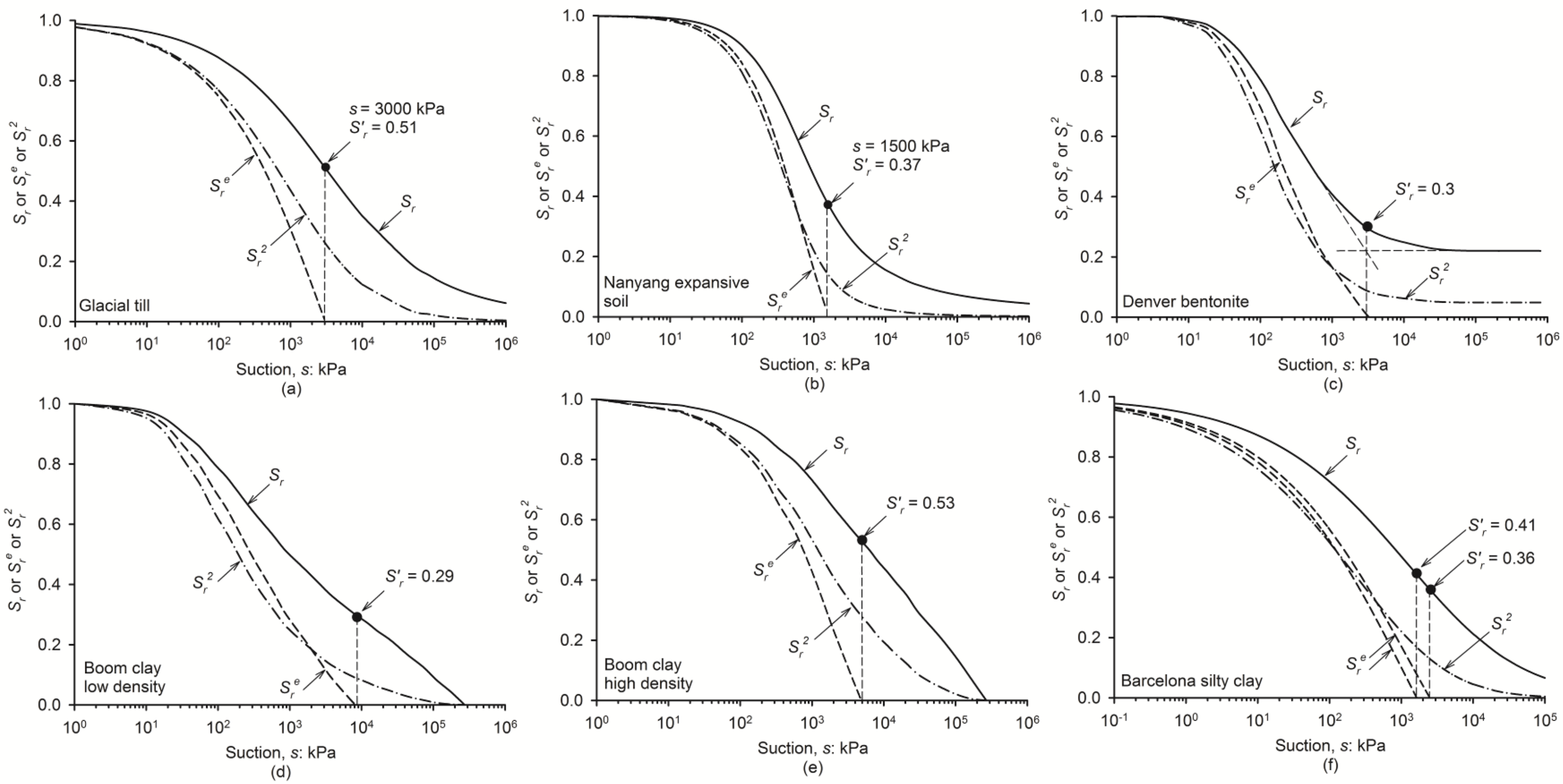

Figure 3.19 S_r - s, S_r^2 - s and S_r^e - s relationships for (a) glacial till; (b) Nanyang expansive soil; (c) Denver bentonite; (d) low density Boom clay; (e) high density Boom clay; (f) Barcelona silty clay

3.4 Discussion

The non-linearity of the SWCC is related to the non-linearity of the stiffness / shear strength - suction relationships using the proposed methodology in this chapter. The accuracy of using S_r - s relationships defined by SWCC to simulate the actual S_r - s relationships within the soil specimens subjected to stiffness / shear strength experiments however are dependent on the level of similarity between the experimental conditions applied during the SWCC tests and that applied during the stiffness / shear strength experiments. The SWCC of soils used in this chapter were measured using different approaches (see in Table 3.4) taking account the influence of various factors (including external stress, hydraulic hysteresis, soil structure etc.) to simulate, at various levels of reliabilities, the actual S_r - s relationships for the stiffness / shear strength experiments. Although there are no significant inconsistencies between the experimental measurements and the predictions produced by the proposed methodology using the SWCC, caution however should be exercised with respect to the determination or estimation of the SWCC to rationally represent the actual S_r - s relationships.

The methodology proposed in this chapter is suggested to be applied for unsaturated soils only within the low suction range (e.g., boundary effect and transition zones of desaturation). This is because i) the methodology and the suggested ξ values are only validated using experimental data within lower suction ranges where suction and capillary effect is believed to dominate the soil behaviour, and ii) considering sole influence of suction at higher suction range (e.g., residual zone of desaturation) may not be reliable as the influence of other physico-chemical forces may become significant within higher suction range.

Reliable predictions are achieved for the various stiffness and shear strength properties of the 25 different soils using a unified equation (3.5). It is therefore reasonable to conclude that the suction appears to influence the stiffness and shear strength properties similarly within lower suction range, although it has been shown that the external stresses influence the stiffness and shear strength properties differently. This conclusion is consistent with the discussion presented in earlier sections of this chapter. The subjective criteria suggested in this chapter is based on clay content and plasticity index to distinguish silts between cohesionless soils (%clay < 10) and cohesive soils (%clay ≥ 10 and / or I_p% ≥ 12). This criteria works well with equation (3.5) using ξ = 2.0 for cohesive soils and ξ = 1.0 for cohesionless soils for predictions. On the other hand, in order to achieve most reliable predictions, additional experimental investigations on the Ω - s relationships are necessary to determine the ξ values from regression analysis. Such practice is suggested for mixed soils or silts especially when knowledge on their mechanical behaviour is limited.

3.5 Conclusions

A new methodology is proposed in this chapter such that the stiffness and shear strength properties of unsaturated soils can be interpreted and predicted using a unified normalized function. The methodology relates the non-linearity of the SWCC to the non-linearity of the stiffness - suction and strength - suction relationships using i) a parameter ξ and ii) measurements of stiffness or shear strength properties at saturation condition and one unsaturated condition (reference condition). Validations of the proposed methodology using experimental data of different stiffness and shear strength properties derived at various strain levels for 8 cohesionless and 17 cohesive soils suggest that the methodology (i.e. equation (3.5)) can reasonably well interpret and predict the behaviour of stiffness and shear strength within lower suction range taking account of various influencing factors. A unique ξ value of 1.0 and 2.0 are respectively suggested for cohesionless and cohesive soils. The proposed methodology can be used as a convenient prediction model in geotechnical engineering practice as it only requires limited testing results and does not need calibration.

CHAPTER FOUR

PREDICTING THE RESILIENT MODULUS OF COMPACTED SUBGRADE SOILS

4.0 Background-Information

The contents presented in this chapter are from the manuscript of the publication:

Han, Z., and Vanapalli, S. K. (2015). Model for predicting the resilient modulus of unsaturated subgrade soil using the soil-water characteristic curve. *Canadian Geotechnical Journal*, 52(10): 1605-1619. DOI: 10.1139/cgj-2014-0339.

The symbols used in this chapter are summarized in Table 4.0.

Table 4.0 Symbols used in Chapter Four

Symbols	
a, b, k_m, k_{us}, k_1, k_2, k_3, k_4, k_5, k_6, k_7, k_8, k_9, k_{10}, k_{11}, k_{12}, k_{13}, m, n	model parameters
c'	cohesion under saturated conditions
E	modulus of elasticity
e	void ration
G_s	specific gravity
I_p	plasticity index
M_R	resilient modulus
p_a	atmosphere pressure
S	degree of saturation
subscript $_{OPT}$	corresponding parameter value at optimum moisture content condition
subscript $_{sat}$	corresponding parameter value at saturated condition
subscript $_{unsat}$	corresponding parameter value at unsaturated condition
u_a	pore-air pressure
u_w	pore-water pressure
w	gravimetric water content
w_L	liquid limit

Table 4.0 Symbols used in Chapter Four

Symbols	
α_E, β_E, κ, ξ, φ,	model parameters
$\Delta u_{w\text{-}sat}$	build-up of pore-water pressure under saturated conditions
ε_r	resilient strain
θ	volumetric water content
θ_b	bulk stress
θ_{net}	net bulk stress
ρ_{dmax}	maximum dry density
σ_d	deviator stress
τ_{oct}	octahedral shear stress
ϕ'	angle of internal friction under saturated condition
ψ	soil suction

4.1 Introduction

The definition of the resilient modulus (M_R) was originally introduced into the literature by Seed et al. (1962) as the ratio of the applied deviator stress (σ_d) to the resilient strain (ε_r, i.e., the recoverable strain corresponding to the σ_d). The M_R is more widely used in mechanistic pavement design methods to characterize the resilient behavior of pavement materials, dimension the multilayer system of a pavement structure, and analyze the fatigue cracking typically initiated at the bottom of the asphalt or concrete surface layers (Brown 1996, Ng et al. 2013).

The M_R of pavement subgrade soil is sensitive to many factors including applied stress level, moisture regime, soil type, soil fabric / structure, and testing protocols (Puppala 2008, Malla and Joshi 2008). The variation of the M_R with respect to the moisture content is widely determined and used in practice because the measurement of moisture content is convenient, fast and reliable (Li and Selig 1994, Drumm et al. 1997, Khoury et al. 2013). However, the M_R - moisture content relationships for both base course and subgrade soil are highly soil-type-dependent and hence difficult to characterize using either empirical or mechanistic methods (Heath et al. 2004, Ng et al. 2013). Subgrade soils are usually compacted soils that typically stay in an unsaturated condition during their entire service life. The soil suction (ψ), which contributes to the stiffness and strength of the soil body, is significantly influenced by moisture regime changes associated with the environmental factors (Uzan 1998, Quintus and Killingsworth 1998, Ceratti et al. 2004). Sauer and Monismith (1968), Edris and Lytton (1976), Fredlund et al. (1977), and Edil and Motan (1979) are pioneers who extended the mechanics of unsaturated soils for the interpretation and prediction of the variation of the M_R with respect to the ψ. Such an approach is promising to better understand and determine the influence of seasonal moisture regime fluctuations on the M_R.

Extensive experimental investigations were conducted by several researchers during the past decade using advanced testing techniques to measure the M_R - ψ relationships and propose models for predictions (Khoury and Zaman 2004, Yang et al. 2005, Liang et al. 2008, Yang et al. 2008, Sawangsuriya et al. 2009a, Craciun and Lo 2010, Cary and Zapata

2011, Nowamooz et al. 2011, Ng et al. 2013, Sivakumar et al. 2013, Sahin et al. 2013, Azam et al. 2013, Salour et al. 2014). These studies have provided valuable information for better understanding the influence of the ψ on the M_R. The proposed models are capable of providing reliable predictions for the pavement materials for which they have been developed. Extending these models for other pavement materials however needs reliable model parameters. These model parameters are typically derived from regression analysis performed on extensive experimental data of the M_R - ψ relationships (Vanapalli and Han 2014). There is a need for a model that can be used for reliably predicting the M_R - ψ relationships for a wide range of soils using simple soil properties and easy-to-estimate model parameters.

In this chapter, a model is developed using the experimental data of various compacted fine-grained subgrade soils from the literature. The M_R values at two conditions (i.e., saturation condition, M_{RSAT} and optimum moisture content condition, M_{ROPT}) that can be measured from conventional repeated load triaxial tests (RLTTs), along with the soil-water characteristic curve (SWCC) and the ψ at optimum moisture content condition (ψ_{OPT}) are required in the proposed model for prediction. The required information can be obtained from experiments following conventional testing methods. The model uses only one fitting parameter (ξ) to predict the M_R - ψ relationships. There is good agreement between the experimentally determined M_R - ψ relationships and the predicted results for 16 sets of testing data derived from 11 different subgrade soils (in total, 210 testing results) using a single-valued ξ for all the soils. The proposed model is promising for use in pavement design practice as it alleviates the need for determining the M_R - ψ relationships which is cumbersome, expensive, and time-consuming.

4.2 Background

4.2.1 Experimental determination of the M_R - ψ relationships

RLTTs, following various testing protocols such as AASHTO T292-91, AASHTO TP46-94, AASHTO T307-99 (American Association of State Highway and Transportation Officials), NCHRP 1-28A (National Cooperative Highway Research Program, Witczak 2003), are widely used to determine the M_R of pavement materials (Uzan 1985, Tian et al.

1998). Several researchers incorporated various soil suction measurement or control techniques into the RLTTs to investigate the influence of the ψ on the M_R. For example, the ψ of the specimens can be measured after the completion of RLTTs using filter paper method or null pressure plate method, which are both simple and inexpensive (Fredlund et al. 1977, Odezugo et al. 1994, Yang et al. 2005, Liang et al. 2008, Azam et al. 2013). However, soil suction measurements from these methods are user dependent, sensitive to testing protocols and neglect the influence of the applied stress on the ψ (Ng and Pang 2000, Power et al. 2008, Power and Vanapalli 2010, Ng et al. 2012). In recent years, modified cyclic triaxial testing systems equipped with various techniques (e.g., thermal dissipation sensor, psychrometer, suction probe, axis-translation technique) are used to measure or control the soil suction during the RLTTs for obtaining reliable testing results (Gupta et al. 2007, Yang et al. 2008, Craciun and Lo 2010, Cary and Zapata 2011, Ng et al. 2013, Sivakumar et al. 2013). Trained professionals are required to conduct these tests. In addition, considerably long period of time (several days to weeks) is required to achieve equilibrium condition with respect to applied soil suction for fine-grained soils prior to determining the M_R values (Khoury et al. 2011, Ng et al. 2013).

Details of 11 compacted fine-grained subgrade soils that were tested by different researchers for investigating the influence of the ψ on the M_R are summarized in Table 4.1. In the present study, the experimental data derived from the 11 soils summarized in Table 4.1 is used to develop and verify the proposed model. The selection of the published testing data from the literature is based on unbiased guidelines that include; (i) different M_R and ψ testing methods were used to determine the M_R - ψ relationships for the selected soils, (ii) the selected soils provided adequate information to describe the M_R - ψ relationships in addition to using it for the development of the proposed model, (iii) for certain soils where large amount of testing data is available, only some data sets were selected to avoid space limitations of presenting graphical relationships, (iv) all the selected soils are conventional subgrade soils. Problematic soils such as expansive / collapsible / sensitive soils are excluded as they are not typically used as pavement subgrade soil without proper treatments and thus are beyond the scope of the present study.

Table 4.1 Soil properties and experimental techniques of the subgrade soils used in this study for investigating the M_R - ψ relationships

Reference & Location	Soil No.	Soil ID	Atterberg Limits w_L (%)	Atterberg Limits I_p (%)	Compaction Characteristics OMC (%)	Compaction Characteristics ρ_{dmax} (kg/m^3)	G_s	Classification USCS	Classification AASHTO	Soil suction Range (kPa)	Soil suction Testing technique	M_R testing protocol
Fredlund et al. (1977), Saskatchewan, Canada	1	Glacial till	34	17	16.5	1767	2.77	CL	A-6	0-900	Pressure plate	STP1[1]
Zaman and Khoury (2007), Oklahoma, USA	2	Burleson	55	30	23.5	1532	N/A	CH	A-7-6	0-5000	Filter paper	AASHTO T307-99
	3	Renfrow	35	20	16.5	1690	N/A	CL	A-6			
Ceratti et al. (2004), Porto Alegre, Brazil	4	Weathered shale	44	21	21	1670	N/A	CL	A-7-6	0-1500	Filter paper	AASHTO TP46-94
Yang et al. (2005), Taiwan, China	5	Lateritic soil	54	20	18	1760	2.71	MH	A-7-5	0-11000	Filter paper	AASHTO T292-91
	6	Mudstone	50	23	17	1800	2.67	CL-CH	A-7-6			
Gupta et al. (2007), Minnesota, USA	7	Red wing	28	11	13.5	1790	2.69	CL	A-4	0-20000	Axis-translation & Thermal dissipation sensor	NCHRP 1-28A
	8	Red lake falls	42	24	22	1580	2.69	CL	A-7-6			
	9	MnRoad	26	9	16	1779	2.66	CL	A-4			
	10	Duluth slope	85	52	27.5	1440	2.75	CH	A-7-6			
Ng et al. (2013), Hong Kong, China	11	Decomposed tuff	43	14	16.3	1760	2.73	ML	A-7-6	0-250	Axis-translation & Suction probe	STP2[2]

Notation: w_L = liquid limit, I_p = plasticity index, OMC = optimum moisture content, ρ_{dmax} = maximum dry density, G_s = specific gravity, N/A = data not available in the reference, USCS = Unified soil classification system, AASHTO = American association of state highway and transportation officials, NCHRP = National cooperative highway research program, STP = Special testing protocol.

Note: [1]STP1, Specimens were loaded at 20 repetitions/min with a loading duration of 0.1s for 100 repetitions; [2]STP2, Specimens were loaded at 60 repetitions/min with a loading duration of 0.1s for 100 repetitions; no conditioning phase was applied for STP1 or STP2.

4.2.2 Predicting the M_R of unsaturated pavement materials

Many factors such as the soil type, soil fabric / structure, applied stress level, compaction effort and hysteresis influence the M_R - ψ relationship which exhibits high non-linear characteristics (more discussions are available in Vanapalli and Han 2014). Several approaches were proposed in the literature to predict the M_R taking account the influence of the ψ. The widely used Mechanistic-Empirical Pavement Design Guide (ARA, INC., ERES 2004) suggests using Eq. 4.1 to predict the M_{ROPT} values. This is based on the considerations that (i) pavement materials are typically compacted at optimum moisture content (OMC) and maximum dry density (ρ_{dmax}) condition to assure better engineering performance in pavement construction practice, (ii) there are several studies reported in the literature that provide testing data of M_{ROPT} along with the k_1, k_2 and k_3 values that can be used in Eq. 4.1 for various pavement materials (Khazanovich et al. 2006, Hossain 2008, Stolle et al. 2009).

$$M_R = k_1 p_a \left(\frac{\theta_b}{p_a}\right)^{k_2} \left(\frac{\tau_{oct}}{p_a} + 1\right)^{k_3} \tag{4.1}$$

where p_a = atmosphere pressure, θ_b = bulk stress, τ_{oct} = octahedral shear stress, k_1, k_2 and k_3 = model parameters. Eq. 4.2, which is an empirical relationship that describes the variation of the M_R with respect to the degree of saturation (S), is used in the ARA, INC., ERES (2004) to predict the M_R taking account the influence of the moisture content.

$$\log\left(\frac{M_R}{M_{ROPT}}\right) = a + \frac{b-a}{1+\exp[\ln(-\frac{b}{a}) + k_m(S - S_{OPT})]} \tag{4.2}$$

where S_{OPT} = degree of saturation at OMC condition, a, b, k_m = model parameters. Parameter values a = -0.5934, b = 0.4, k_m = 6.1324 are suggested for fine-grained soils, while parameter values a = -0.3123, b = 0.3, k_m = 6.8157 are suggested for coarse-grained soils. Eq. 4.2 can be extended to predict the M_R - ψ relationship using the SWCC, which defines the relationship between the ψ and the S.

There are several other empirical relationships in the literature proposed for estimating the M_R - ψ relationship for regional or local pavement materials. For example, Sawangsuriya et al. (2009a) proposed Eq. 4.3 and Eq. 4.4 for four different local subgrade soils from Minnesota, USA (soils 7 - 10 in Table 1).

$$M_R / M_{RSAT} = \text{-}5.61 + 4.54 \log(\psi) \tag{4.3}$$

$$M_R / M_{ROPT} = \text{-}0.24 + 0.25 \log(\psi) \tag{4.4}$$

Ba et al. (2013) proposed Eq. 4.5 to estimate the M_R for four local granular materials from Senegal.

$$M_R / M_{ROPT} = 0.385 + 0.267 \log(\psi) \tag{4.5}$$

Empirical relationships are simple and economical for use in practice. Such empirical relationships are developed from limited experimental results using regression analysis without providing explanations to the phenomenological behavior. They are only suitable for soils for which they have been developed, thus are less reliable to be extended to other testing scenarios and soil types. Several investigators proposed semi-empirical models which relate various influencing factors using different model parameters to alleviate these limitations. For example, Liang et al. (2008) incorporated the effect of the ψ into bulk stress (θ_b) using Bishop's effective stress parameter χ (Bishop 1959) and improved Eq. 4.1 into Eq. 4.6.

$$M_R = k_4 p_a \left(\frac{\theta_b + \chi\psi}{p_a}\right)^{k_5} \left(1 + \frac{\tau_{oct}}{p_a}\right)^{k_6} \tag{4.6}$$

where k_4, k_5 and k_6 = model parameters. Gupta et al. (2007) considered the independent contribution of the ψ to the M_R and proposed Eq. 4.7.

$$M_R = k_7 p_a \left(\frac{\theta_b}{p_a}\right)^{k_8} \left(1 + \frac{\tau_{oct}}{p_a}\right)^{k_9} + k_{us} p_a S^{\varphi} \psi \tag{4.7}$$

where k_{us}, φ, k_7, k_8 and k_9 = model parameters. Cary and Zapata (2011) modified Eq. 4.1 into Eq. 4.8 by incorporating the influence of the ψ as an additional term and considering (i) the excitation of positive pore-water pressure (u_w) under saturated condition ($\Delta u_{w\text{-}sat}$), and (ii) the variation of the ψ under unsaturated condition ($\Delta\psi$) during the cyclic loading.

$$M_R = k_{10} p_a \left(\frac{\theta_{net} - 3\Delta u_{w-sat}}{p_a}\right)^{k_{11}} \left(\frac{\tau_{oct}}{p_a} + 1\right)^{k_{12}} \left(\frac{\psi - \Delta\psi}{p_a} + 1\right)^{k_{13}} \tag{4.8}$$

where $\theta_{net} = \theta_b - 3u_a$ = net bulk stress, u_a = pore-air pressure, k_{10}, k_{11}, k_{12}, and k_{13} = model parameters.

Semi-empirical models provide greater flexibility and reliability in predicting the M_R - ψ relationships for different soils through the use of model parameters such as χ, k_{us}, φ, and k_4 through k_{13} in Eq. 4.6 through Eq. 4.8. However, two major concerns arise towards using these semi-empirical models.

(i) Semi-empirical models provide good predictions for different soils based on the reasonable determination of model parameters. The model parameters are reliable when they are derived from a large experimental data base using regression analysis. Obtaining high quality and reliable experimental data however is time-consuming, expensive therefore may not be practical for many pavement design agencies. In some scenarios, model parameter values used in a semi-empirical model that provide reasonable predictions for one soil may not be suitable for another soil that belongs to the same group of soil classification or in some cases for the same soil but tested under different scenarios (Vanapalli and Han, 2014).

(ii) Semi-empirical models for M_R - ψ relationships are mostly modifications of Eq. 4.1 or its similar forms proposed by other researchers (e.g., Moossazadeh and Witczak 1981, Uzan 1985). The definitions of the model parameters and their values in these models however are different in spite of similar forms of the proposed models. For example, the k_1, k_2, and k_3 values used in Eq. 4.1 to predict the M_{ROPT} for one soil (which is required by the ARA, INC., ERES 2004) cannot be directly used in Eq. 4.6 as k_4, k_5, k_6 values, or in Eq. 4.7 as k_7, k_8, k_9 values, or in Eq. 4.8 as k_{10}, k_{11}, k_{12} values, to predict the M_R - ψ relationships for the same soil. In other words, the values of M_{ROPT} and the model parameters k_1, k_2, k_3, which are commonly determined or estimated in practice and well documented in the literature, could not be directly used in these semi-empirical models to predict M_R - ψ relationships.

The above discussions highlight the need for a model with limited number of model parameters that can be universally used with confidence for the reliable prediction of the variation of the M_R with respect to the ψ for different subgrade soils.

4.2.3 Predicting unsaturated soil properties using the SWCC

The SWCC has been frequently used as a tool in the prediction of the non-linear variation of unsaturated soil properties with respect to soil suction, such as coefficient of permeability (Fredlund et al. 1994, Simms and Yanful 2001), shear strength (Vanapalli et al. 1996, Fredlund et al. 1996), stiffness (Thu et al. 2007, Oh et al. 2009, Rosenbalm and Zapata 2013), and bearing capacity (Vanapalli and Mohamed 2007, Oh and Vanapalli 2011). The incorporation of the SWCC in the prediction of unsaturated soil properties helps to take into account of the influence of moisture content on the contribution of ψ towards unsaturated soil properties. Model parameters of the equations developed following this approach are strongly related to the conventional soil properties and thus are convenient for prediction or estimation. For example, Eq. 4.9 proposed by Vanapalli et al. (1996) uses the SWCC and one model parameter (κ) to predict the shear strength of unsaturated soils (τ_{unsat}).

$$\tau_{unsat} = c' + (\sigma_n - u_a)\tan\phi' + \psi S^{\kappa}\tan\phi' \tag{4.9}$$

where c' = cohesion under saturated conditions, ($\sigma_n - u_a$) = net normal stress, ϕ' = angle of internal friction under saturated condition. Also, Eq. 4.10 has been used by Oh et al. (2009), Vanapalli and Oh (2010) to predict the variation of modulus of elasticity (E_{unsat}) from its saturated value (E_{sat}) using SWCC and two model parameters (α_E and β_E).

$$E_{unsat} = E_{sat}[1 + \alpha_E \frac{\psi}{(p_a/100)}(S^{\beta_E})] \tag{4.10}$$

Figure 4.1 shows the distribution of the model parameter κ used in Eq. 4.9 with the plasticity index (I_p) for 9 different fine-grained soils (Garven and Vanapalli 2006). The κ values were distributed in a narrow range between 1 and 3. It is convenient to use simple relationships to predict κ from I_p such as those proposed by Vanapalli and Fredlund (2000), Garven and Vanapalli (2006). Similarly, for predicting the modulus of elasticity using Eq. 4.10, a β_E value of 2 was suggested for fine-grained cohesive soils. The model parameter α_E in Eq. 4.10 was strongly related to the I_p values (Vanapalli and Oh 2010).

In this chapter, a new model is proposed for the prediction of the variation of the M_R of compacted fine-grained subgrade soils with respect to the ψ using the SWCC as a tool.

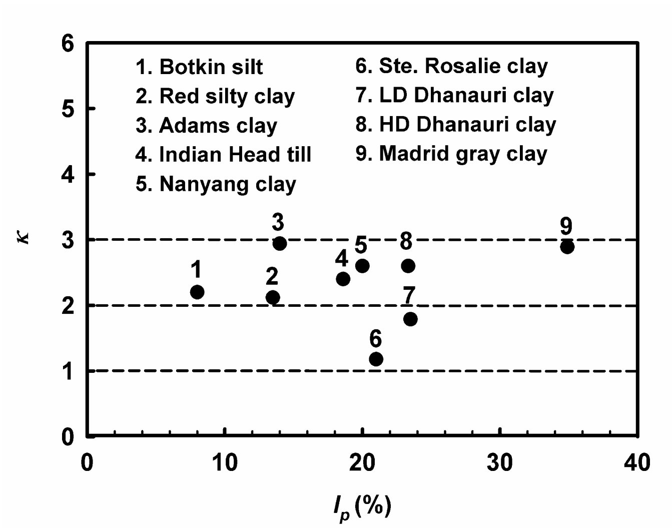

Figure 4.1 Distribution of κ with I_p (Modified after Garven and Vanapalli 2006)

4.3 Model formulation

Han and Vanapalli (2014) proposed Eq. 4.11 for predicting the M_R of compacted subgrade soils using the SWCC and two parameters ξ and ζ.

$$M_R = M_{RSAT} + \zeta \psi S^{\xi} \tag{4.11}$$

Eq. 4.11 can also be expressed in a different form as shown in Eq. 4.12.

$$\zeta = \frac{M_R - M_{RSAT}}{\psi S^{\xi}} \tag{4.12}$$

Substituting M_{ROPT} and the corresponding soil suction (ψ_{OPT}) and degree of saturation (S_{OPT})

in Eq. 4.12 yields Eq. 4.13.

$$\zeta = \frac{M_{ROPT} - M_{RSAT}}{\psi_{OPT} S_{OPT}^{\xi}} \tag{4.13}$$

Eq. 4.14 can be derived by substituting Eq. 4.13 in Eq. 4.11.

$$\frac{M_R - M_{RSAT}}{M_{ROPT} - M_{RSAT}} = \frac{\psi}{\psi_{OPT}} (\frac{S}{S_{OPT}})^{\xi} \tag{4.14}$$

The ratio of the S (i.e., S / S_{OPT}) equals to the ratio of the gravimetric water content w (i.e., w / w_{OPT}) or the ratio of the volumetric water content θ (i.e., θ / θ_{OPT}) (w_{OPT} and θ_{OPT} are the corresponding values of w and θ at OMC) based on the volume-mass relationships $w = Se / G_s$ and $\theta = Se / (1 + e)$ assuming the void ratio (e) is constant. Eq. 4.14 thus can be expressed in terms of w (Eq. 4.15) or θ (Eq. 4.16).

$$\frac{M_R - M_{RSAT}}{M_{ROPT} - M_{RSAT}} = \frac{\psi}{\psi_{OPT}} (\frac{w}{w_{OPT}})^{\xi} \tag{4.15}$$

$$\frac{M_R - M_{RSAT}}{M_{ROPT} - M_{RSAT}} = \frac{\psi}{\psi_{OPT}} (\frac{\theta}{\theta_{OPT}})^{\xi} \tag{4.16}$$

The S, w, and θ values (including S_{OPT}, w_{OPT}, and θ_{OPT} values) can be estimated from the SWCC using various models such as those proposed by Brooks and Corey (1964), van Genuchten (1980), and Fredlund and Xing (1994). In this study, Fredlund and Xing (1994) model (Eq. 4.17) is used to predict the SWCC.

$$S = \frac{\theta}{\theta_{SAT}} = \frac{w}{w_{SAT}} = \left\{ 1 / \ln[2.718 + (\frac{\psi}{a})^n] \right\}^m \tag{4.17}$$

where w_{SAT} and θ_{SAT} are the corresponding values of w and θ at saturated condition; a, n, m = model parameters. A unique equation (Eq. 18) can be obtained by substituting Eq. 4.17 in Eq. 4.14, Eq. 4.15 or Eq. 4.16.

$$\frac{M_R - M_{RSAT}}{M_{ROPT} - M_{RSAT}} = \frac{\psi}{\psi_{OPT}} \left\{ \frac{\ln[2.718 + (\frac{\psi_{OPT}}{a})^n]}{\ln[2.718 + (\frac{\psi}{a})^n]} \right\}^{m \times \xi} \tag{4.18}$$

Eq. 4.18 is used in the present study for predicting the M_R - ψ relationships. The information including M_{ROPT}, ψ_{OPT}, M_{RSAT}, and SWCC (i.e., model parameter a, n, m values) is needed in Eq. 4.18. Several reasons are provided for using Eq. 4.18 towards the reliable prediction of the M_R with respect to the ψ.

(i) The M_{ROPT} and M_{RSAT} can be determined using conventional RLTTs. The M_{ROPT} values can also be estimated using Eq. 4.1 or other models (e.g., Moossazadeh and Witczak 1981, Uzan 1985). This alleviates the need for performing soil-suction-controlled RLTTs to determine the M_R - ψ relationships. The ψ_{OPT} can be measured using simple techniques such as the filter paper method, null pressure plate or estimated using relationships with other soil properties (Tarantino and Tombolato 2005, Vanapalli and Oh 2011).

(ii) Eq. 4.18 is presented in a normalized form. Such formulation helps to take into account of the influence of several key factors such as the testing method, soil type and structure on the M_R, ψ and SWCC without introducing extra model parameters. Upon using Eq. 4.1 or other stress dependent models for estimating the M_{ROPT} values, the influence of applied stress level on the M_R - ψ relationships can be introduced into the prediction.

(iii) The M_{RSAT} of subgrade soil is found to be less sensitive to the applied stress level compared with the M_{ROPT}. For example, the M_R values of two subgrade soils from Taiwan (soils 5 and 6 in Table 4.1) tested near saturated condition show little variation with deviator stress (Yang et al. 2005). The M_{RSAT} of a decomposed tuff from Hong Kong (soil 11 in Table 4.1) and four subgrade soils from Minnesota (soils 7 - 10 in Table 4.1) are reported to be constant values regardless of the applied stress levels (Sawangsuriya et al. 2009a, Ng et al. 2013). Similar observations on the M_{RSAT} were also reported by Loach (1987), Salour et al. (2014) for several subgrade soils from Europe. The M_R values of a clayey soil and a lean clay from Oklahoma (soils 2 and 3 in Table 4.1) are approximately the same at saturated condition regardless of the different compaction moisture contents and the resulting different soil fabric / structure (Zaman and Khoury 2007). In other words, the soil fabric / structure and applied stress level appear to have little or negligible influence on the M_{RSAT}. Similar observations were also reported by Vanapalli et al. (1996) for shear strength of saturated soils with different soil fabric / structure. Based on these observations, the M_{RSAT} can be reasonably assumed as a constant value in Eq. 4.18 for prediction without introducing significant errors. This assumption is further validated in later sections of this chapter.

(iv) Several investigators reported that the soil suction decreases during the application of the cyclic loading (Yang et al. 2008, Craciun and Lo 2010, Sivakumar et al. 2013). Such behavior can be attributed to the accumulation of the non-recoverable plastic strain and the pore air dissolving into the pore water (Thom et al. 2008). However, the influence of the cyclic loading on the ψ and SWCC depends on many factors and hence is difficult to evaluate or estimate. On the other hand, subgrade soils after compaction are typically subjected to wetting or drying process before achieving equilibrium condition with the environment (Uzan 1998, Yang et al. 2005). The SWCC measured during drying process (desorption of water, referred to as drying SWCC) is found to be different from the one measured during wetting process (absorption of water, referred to as wetting SWCC) (Fredlund and Rahardjo 1993). Such hysteresis behavior introduces extra difficulties in predicting the ψ using the SWCC. Besides, the measurement of wetting SWCC is time-consuming and difficult in comparison to that of the drying SWCC. Due to these reasons, several researchers used the drying SWCC or the moisture content - ψ relationships measured after the RLTTs (referred to as apparent SWCC) to estimate or determine the ψ values of the specimens (Fredlund et al. 1977, Khoury and Zaman 2004, Nowamooz et al. 2011, Ba et al. 2013). ARA, INC., ERES (2004) also suggests using the drying SWCC to estimate the ψ values. In this study, the drying SWCC or the apparent SWCC measured for the various soils listed in Table 4.1 are used in Eq. 4.18 for prediction.

(v) The use of the model parameter ξ is to characterize the influence of the S, w, or θ on the M_R - ψ relationships. It is similar to the model parameter κ in Eq. 4.9 and the model parameter β_E in Eq. 10. Figure 4.2 illustrates the influence of the ξ on the predicted M_R - ψ relationships for a Hong Kong decomposed tuff (soil 11 in Table 4.1, Ng et al. 2013) using

Eq. 4.18. Eq. 4.17 was used for fitting the SWCC using the measured values as shown in Figure 4.2(A). The variation of the measured M_R values with respect to the ψ for σ_d = 33.33 kPa and σ_c = 30 kPa stress level is compared with the predictions of Eq. 4.18 using different ξ values (see Figure 4.2B). The ξ value controls the shape of the prediction lines on the M_R versus ψ plot. Higher ξ values (e.g., ξ = 1.5 and 2.5) predict higher M_R values when ψ is less than ψ_{OPT} and lower M_R values when ψ is greater than ψ_{OPT}, comparing with lower ξ values (e.g., ξ = 0.01 and -2.0). Also, higher ξ values provide a non-linear decreasing trend while lower ξ values result in a non-linear increasing trend when ψ is greater than ψ_{OPT}. The ξ values can be both positive and negative as shown in Figure 4.2(B) to predict different non-linear M_R - ψ relationships. A ξ value of zero however predicts linear M_R - ψ relationship. It should be noted that, besides ξ, SWCC has a significant influence on the shape of the predicted M_R - ψ relationships. More discussions with respect to the ξ values are presented in later sections of the chapter.

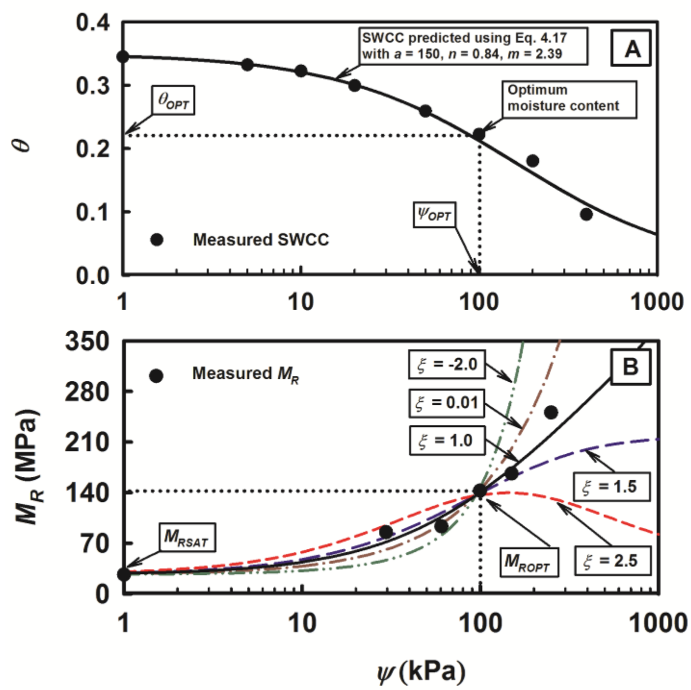

Figure 4.2 Measured and predicted (A) SWCC and (B) variation of M_R with respect to ψ for a subgrade soil from Hong Kong (Data from Ng et al. 2013).

4.4 Validation of the proposed model

A total of 16 sets of data derived from 11 different compacted fine-grained subgrade soils (210 testing data points) listed in Table 4.1 are used to validate and test the performance of the proposed model. Soil 2 was tested under three different scenarios, resulting in three sets of data; soils 3, 5 and 6 were tested under two scenarios, resulting in two sets of data. All other soils were tested to produce one set of data. The tested soils were divided into two groups. The first group includes six soils (i.e., soils 2, 4, 5, 7, 8 and 11) with nine sets of data. These test data sets were used to validate the proposed model and determine the ξ value. The second group includes five soils (i.e., soils 1, 3, 6, 9 and 10) with seven sets of data which were used to test the performance of the proposed model. The experimental data are assigned to the two groups in such a way that each one of them contains experimental data of M_R and ψ that was derived using different testing protocols. Different soils tested by the same investigators are also evenly assigned to both groups (see Table 4.1 for more details). Such an approach helps to validate the proposed model without introducing any bias. The details of the SWCC of the 11 soils listed in Table 4.1 are summarized in Table 4.2. The values of the SWCC model parameters a, n, and m in Eq. 4.17 for each soil are listed in Table 4.2 with the respective coefficient of determination (R^2) values. The summarized a, n, and m values will be used in Eq. 4.18 for predicting the M_R.

Zaman and Khoury (2007) prepared specimens for experiments using three different approaches: Approach (i), specimens were compacted at OMC – 4% then wetted to achieve different higher moisture contents up to OMC + 4%; Approach (ii), specimens were compacted at OMC + 4% then dried to different lower moisture contents up to OMC – 4%; Approach (iii), specimens were compacted at OMC then either wetted to different higher moisture contents up to OMC + 4%, or dried to different lower moisture contents up to OMC – 4%. After the specimens were prepared, RLTTs were performed, followed by the measurement of ψ using the filter paper method. Soil 2 (Burleson soil) was prepared following approaches (i), (ii) and (iii) while soil 3 (Renfrow soil) was prepared using approaches (i) and (ii). Thus, soil 2 yields three sets of data on the M_R and SWCC while soil 3 yields two sets (see Table 4.2).

Table 4.2 Details of the SWCC of the subgrade soils

Soil No. and ID	Eq. 4.17				SWCC type	Testing technique
	a	n	m	R^2		
1. Glacial till	95.8	2.67	0.39	0.98	Apparent SWCC, *w*-type[1]	Pressure plate
2. Burleson	1054	0.69	0.97	0.83	Apparent SWCC, Approach. (i), *w*-type	Filter paper
	2000	1.34	0.72	0.90	Apparent SWCC, Approach. (ii), *w*-type	
	1700	0.73	0.92	0.90	Apparent SWCC, Approach. (iii), *w*-type	
3. Renfrow	231.5	0.75	0.62	0.98	Apparent SWCC, Approach. (i), *w*-type	Filter paper
	3000	1.49	0.90	0.86	Apparent SWCC, Approach. (ii), *w*-type	
4. Weathered shale	1000	0.59	0.94	0.94	Drying SWCC, *w*-type	Filter paper
5. Lateritic soil	19.9	0.65	0.28	0.98	Drying SWCC, *w*-type	Pressure plate
6. Mudstone	27.8	0.62	0.77	0.99		
7. Red wing	66.4	0.89	1.14	0.99	Drying SWCC, θ-type[2]	Pressure plate
8. Red lake falls	1086	0.7	1.51	0.99		
9. MnRoad	920	0.72	1.36	0.99		
10. Duluth slope	3456	0.7	2.13	0.99		
11. Decomposed tuff	150	0.84	2.39	0.98	Drying SWCC, θ-type	Pressure plate

Note: [1]SWCC describing the w - ψ relationship is denoted as *w*-type; [2]SWCC describing the θ - ψ relationship is denoted as θ-type.

Burleson soil (soil 2) from Oklahoma, USA (Zaman and Khoury 2007)

The testing methods of Burleson soil (soil 2) and Renfrow soil (soil 3) are detailed as approaches (i), (ii) and (iii). Representative M_R values at σ_d = 28 kPa and σ_c = 41 kPa loading condition are used to investigate the influence of the moisture content and soil suction on the M_R of the Burleson soil and Renfrow soil (Zaman and Khoury 2007). According to the testing results of Zaman and Khoury (2007), the M_R of Burleson soil specimens prepared using approaches (i), (ii) and (iii) converged to a unique value of approximately 20 MPa at close to saturated condition. Thus, a value of M_{RSAT} = 20 MPa is used in Eq. 4.18. Similar observations were also valid for the Renfrow soil which shows a M_{RSAT} value of 25 MPa. Burleson soil is used here to validate the model (Eq. 4.18) and Renfrow soil is used in a later section to test the performance of the proposed model. Figure 4.3 shows the measured and predicted SWCC and M_R of the Burleson soil using Eq. 4.17

and Eq. 4.18. The SWCC shows different shapes due to the differences in soil structure that arise from the different initial compaction moisture contents (Figure 4.3A). Specimens compacted at wet of OMC with dispersed soil structure show higher water retention capacity, which is in agreement with the observations of Vanapalli et al. (1999) and Ng and Pang (2000). The proposed model Eq. 4.18 provides predictions with $R^2 \geq 0.87$ for the Burleson soil using the same ξ value of 2.1 as shown in Figure 4.3.

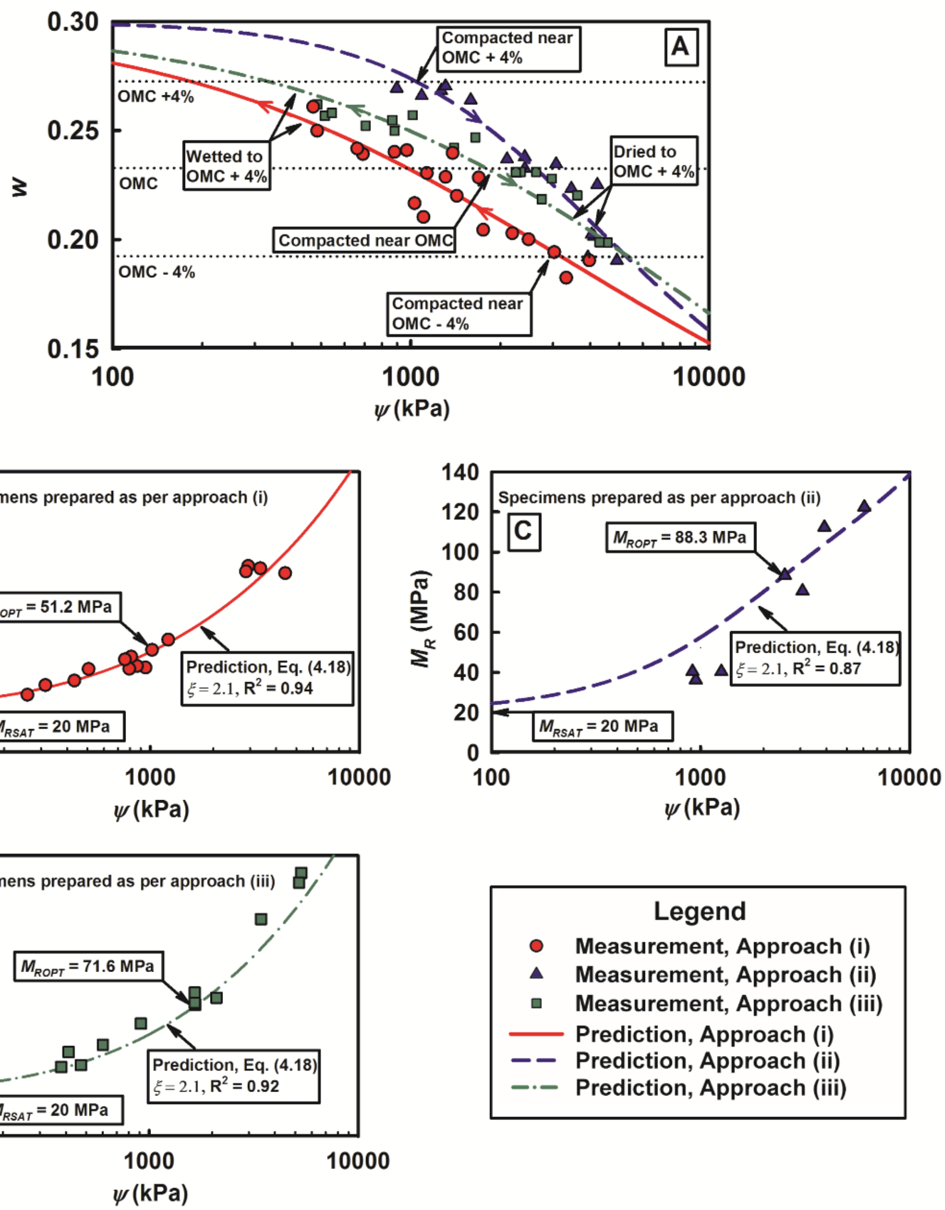

Figure 4.3 Measured and predicted (A) SWCC and (B), (C), (D) variation of M_R with respect to ψ for Burleson soil from Oklahoma (Data from Zaman and Khoury 2007)

Weathered shale (soil 4) from Porto Alegre, Brazil (Ceratti et al. 2004)

The specimens of the weathered shale (soil 4) were compacted at OMC, or compacted at OMC then wetted to OMC + 2%, or compacted at OMC then dried to OMC - 2%, before subjecting to M_R tests. The M_R tests were conducted at σ_d = 12.4 kPa, 24.8 kPa, 37.3 kPa, 49.7 kPa, 62.0 kPa and σ_c = 24.8 kPa loading conditions. Figure 4.4 shows the measured and predicted SWCC and M_R using Eq. 4.17 and Eq. 4.18. The M_{ROPT} values were predicted using Eq. 4.1 while a constant M_{RSAT} value of 50 MPa was used in Eq. 4.18 for prediction (Figure 4.4B). A ξ value of 2.8 is determined from regression analysis (R^2 = 0.8) based on the experimental data.

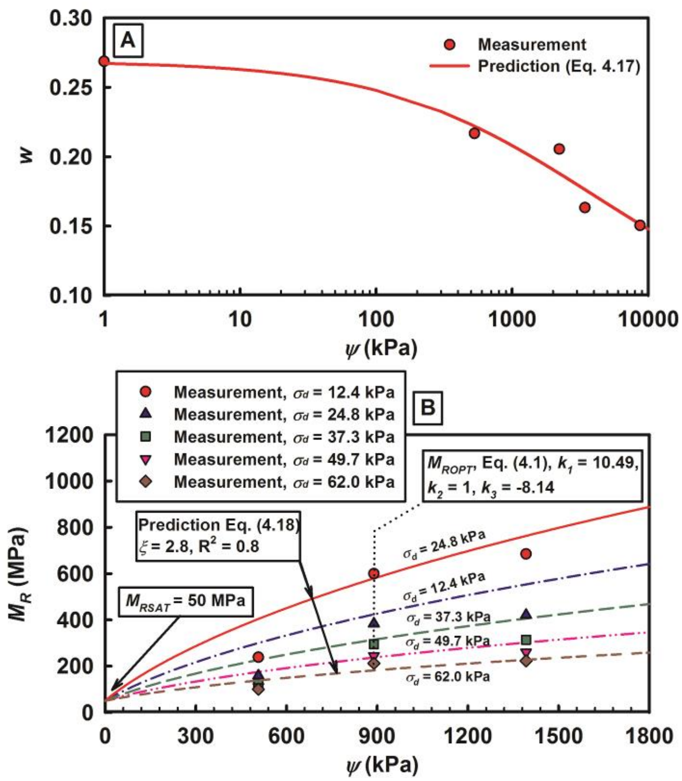

Figure 4.4 Measured and predicted (A) SWCC and (B) variation of M_R with respect to ψ for a weathered shale from Brazil (Data from Ceratti et al. 2004)

A lateritic soil (soil 5) from Taiwan, China (Yang et al. 2005)

The lateritic soil (soil 5) and the mudstone (soil 6) from the experimental investigations of Yang et al (2005) were compacted at OMC or compacted at OMC then wetted to different higher moisture contents before subjecting to the RLTTs. Three different energies were used to compact the soils to relative compaction (RC = ρ_d / ρ_{dmax}, ρ_d = dry density) values of 100%, 95% and 88% (Yang et al. 2005). Pavement materials are usually compacted at RC ≥ 95% as per design and quality control requirements. The experimental data derived from specimens compacted at RC = 100% and 95% are thus chosen for investigation in this study. Specimens were tested at σ_d = 21 kPa, 34 kPa, 48 kPa, 69 kPa, 103 kPa and σ_c = 21 kPa loading conditions. The M_{RSAT} values of the lateritic soil and the mudstone are chosen as 40 MPa and 10 MPa respectively, which are the average values of specimens tested near saturation condition (Yang et al. 2005). The lateritic soil is used here to validate the model (Eq. 4.18) and the mudstone is used in the later section to test the model. The SWCC of the lateritic soil measured by Yang et al. (2006) is shown in Figure 4.5A. Figure 4.5B shows an example of the comparisons between the measured M_R at σ_d = 103 kPa, σ_c = 21 kPa and predictions using Eq. 4.18 with a ξ value of 2.0. Figure 4.6 shows in the M_R - ψ - σ_d space the distribution of the measured M_R values and the *3D* surfaces predicted using Eq. 4.18. According to Figure 4.6, a ξ value of 2.0 provides predictions with R^2 ≥ 0.96 for specimens compacted at RC = 100% and 95%.

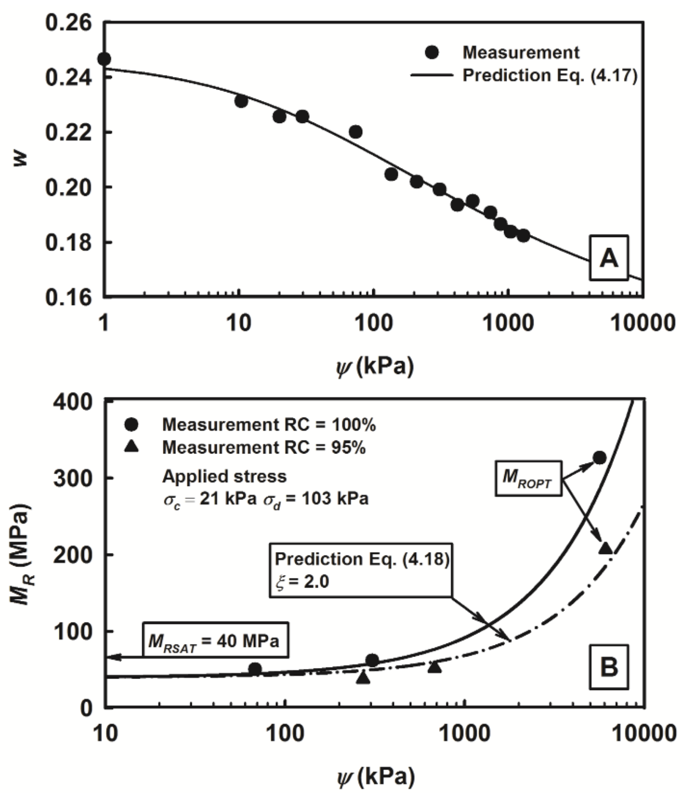

Figure 4.5 Measured and predicted (A) SWCC and (B) variation of M_R with respect to ψ for a lateritic soil from Taiwan (Data from Yang et al. 2005)

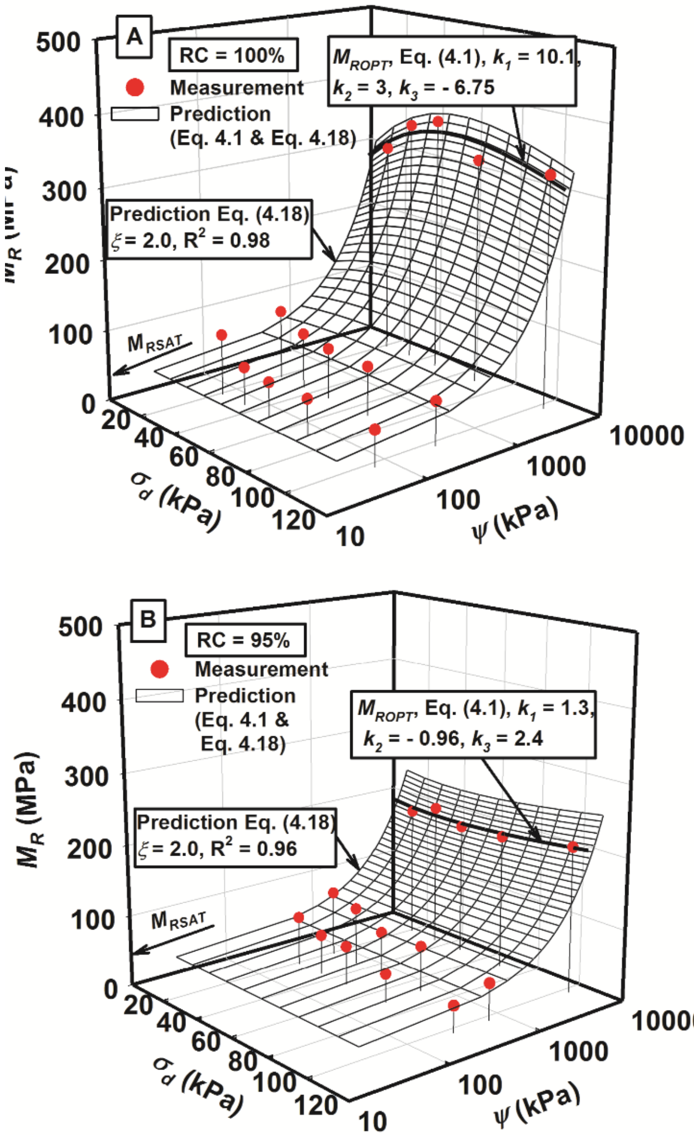

Figure 4.6 Comparisons between the measured and predicted M_R - ψ - σ_d relationships for a lateritic soil from Taiwan compacted at (A) RC = 100% and (B) RC = 95% (Data from Yang et al. 2005)

Two subgrade soils (Red wing and Red lake falls, soils 7 and 8) from Minnesota, USA (Gupta et al. 2007)

Four subgrade soils, namely; Red wing, Red lake falls, MnRoad, Duluth slope (soils 7 through 10 in Table 4.1) were tested by Gupta et al. (2007) using triaxial testing apparatus equipped with axis-translation technique and thermal dissipation sensor for soil suction control and measurement. Specimens were compacted at OMC, saturated and then brought to different higher soil suction values before the RLTTs. The experimental data of specimens compacted at RC = 98% and tested under σ_d = 30 kPa, 50 kPa, 70 kPa, 100 kPa and σ_c = 14.5 kPa loading conditions were used in this study. The measured M_{RSAT} values for Red wing, Red lake falls, MnRoad, Duluth slope are 33 MPa, 12 MPa, 15 MPa, 12 MPa respectively regardless of the applied stress levels (Sawangsuriya et al. 2009a). The M_{ROPT} values of the four soils are predicted using Eq. 4.1. The Red wing and Red lake falls soils are used to validate the model (Eq. 4.18) and the MnRoad and Duluth slope soils are used for testing the model.

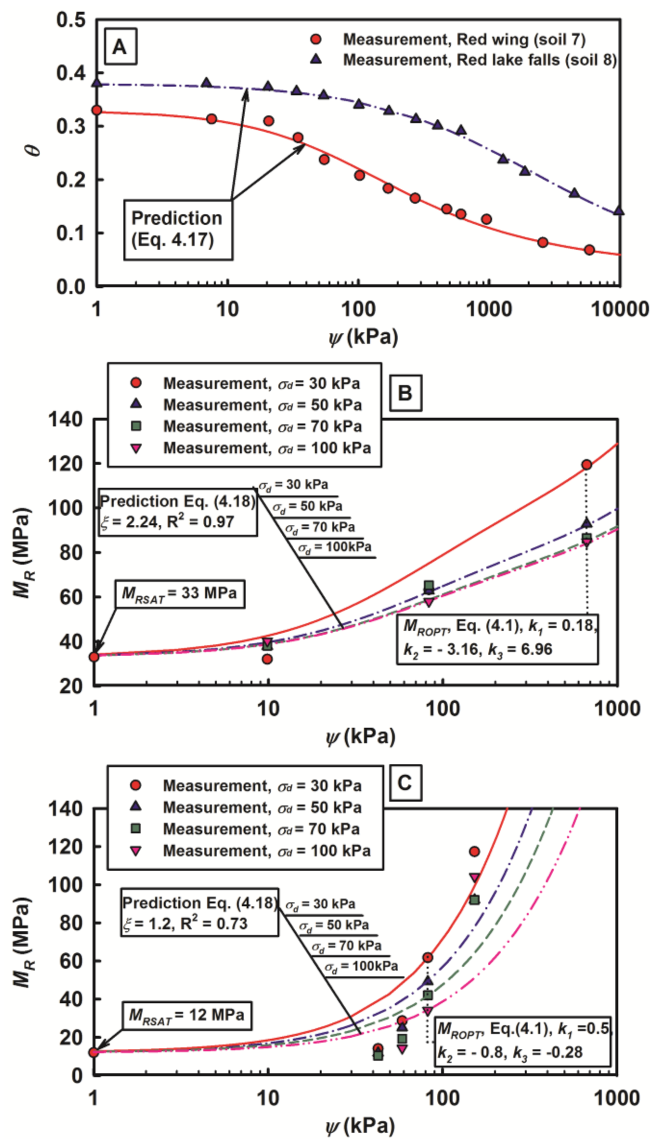

Figure 4.7 Measured and predicted (A) SWCC and the variation of M_R with respect to ψ for (B) Red wing soil and (C) Red lake fall soil (Data from Gupta et al. 2007)

The SWCC of the Red wing and Red lake falls soils are shown in Figure 4.7A. Figures 4.7B and 4.7C show respectively the predictions by Eq. 4.18 along with the measured values for Red wing and Red lake falls soils. Eq. 4.18 provides predictions with $R^2 = 0.97$ using a ξ value of 2.24 for the Red wing soil while it provides predictions with $R^2 = 0.73$ using a ξ value of 1.2 for the Red lake fall soil. Figure 4.8 shows in the M_R - ψ - σ_d space the distribution of the measured M_R values and the *3D* surface predicted using Eq. 4.18 for the Red wing soil.

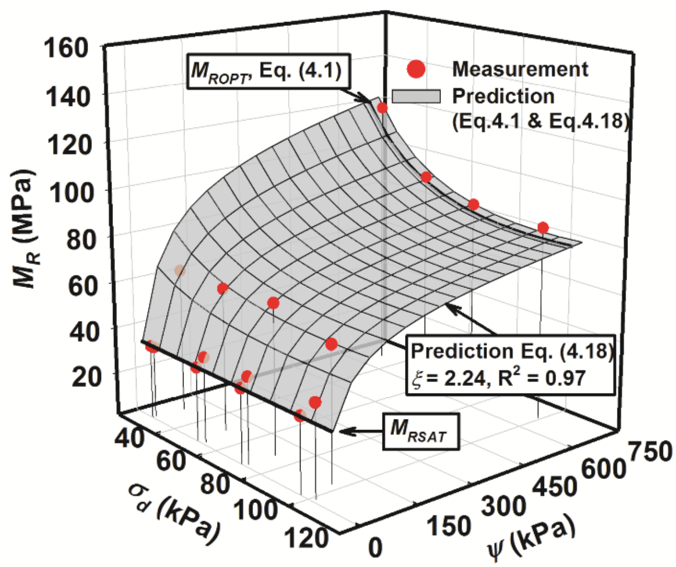

Figure 4.8 Comparisons between the measured and predicted M_R - ψ - σ_d relationships for Red wing soil from Minnesota (Data from Gupta et al. 2007)

A decomposed tuff (soil 11) from Hong Kong, China (Ng et al. 2013)

The decomposed tuff (soil 11) specimens were compacted at OMC, wetted or dried to different soil suction values and then subjected to the M_R tests. The M_R values were determined under the stress levels of σ_d = 33.3 kPa, 44.4 kPa, 61.1 kPa, 77.8 kPa and σ_c = 30 kPa. The measured M_{RSAT} value was approximately 26.7 MPa regardless of the applied stress levels. Eq. 4.1 was used to predict the M_{ROPT} values. The SWCC of the decomposed tuff is shown in Figure 4.2A. Figure 4.9A shows the predictions of Eq. 4.18 for the decomposed tuff using a ξ value of 0.6 (R^2 = 0.98). The predictions are also shown in Figure 4.9B in the M_R - ψ - σ_d space in comparison with the measurements.

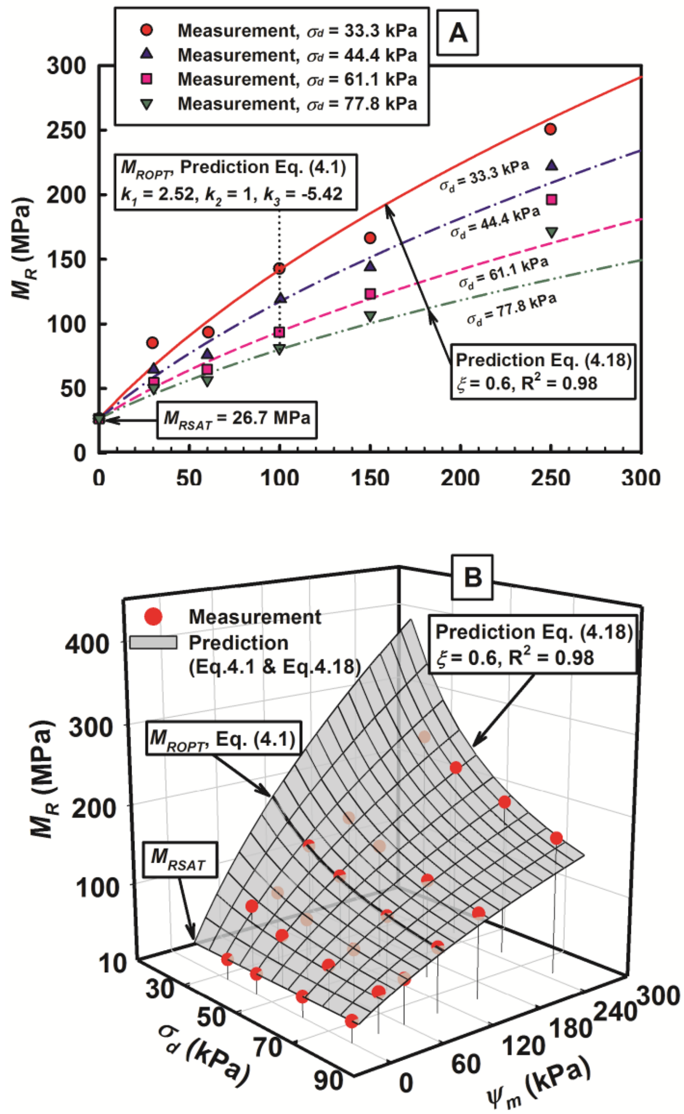

Figure 4.9 Measured and predicted variation of M_R with respect to ψ using Eq. 4.18 in (A) M_R - ψ plot and (B) M_R - ψ - σ_d plot for the decomposed tuff from Hong Kong (Data from Ng et al. 2013)

As can be observed from the measurements and predictions of several soils shown in the M_R - ψ - σ_d space (lateritic soil in Figure 4.6, Red wing soil in Figure 4.8, decomposed tuff in Figure 4.9), the M_R - ψ relationship and the M_R - σ_d relationship show coupled influence (i.e., the M_R - ψ relationship is influenced by the σ_d while the M_R - σ_d relationship is also influenced by the ψ). By introducing the stress dependent model (Eq. 4.1) for predicting the M_{ROPT} values, the proposed model is capable of predicting the coupled influences.

4.5 Model parameter ξ

Figure 4.10 shows the distribution of the ξ values with respect to the I_p for soils 2, 4, 5, 7, 8 and 11 (9 sets of experimental data). The ξ values fall into a narrow range between 1 and 3 except for soil 11 (decomposed tuff, ξ = 0.6). This is similar to the distribution of the κ values shown in Figure 4.1. Instead of provide relationship between ξ values and I_p, a simple median value of ξ equal 2.0 was found to provide reasonable predictions for soils 2, 4, 5, 7, 8 and 11. Table 4.3 lists the R^2 values correspond to different ξ values derived from regression analysis, and the R^2 values correspond to a unique ξ value of 2.0. A subjective criteria suggested by Witczak et al. (2002) for the goodness of prediction based on the R^2 values is used in this study to evaluate the predictions by Eq. 4.18 (See Table 4.3 footnote). As can be seen from Table 4.3 that Eq. 4.18, using various ξ values derived from regression analysis, provides good to excellent predictions for all the experimental data. On the other hand, the goodness of predictions provided by Eq. 4.18, using a unique ξ value of 2.0, is not significantly reduced.

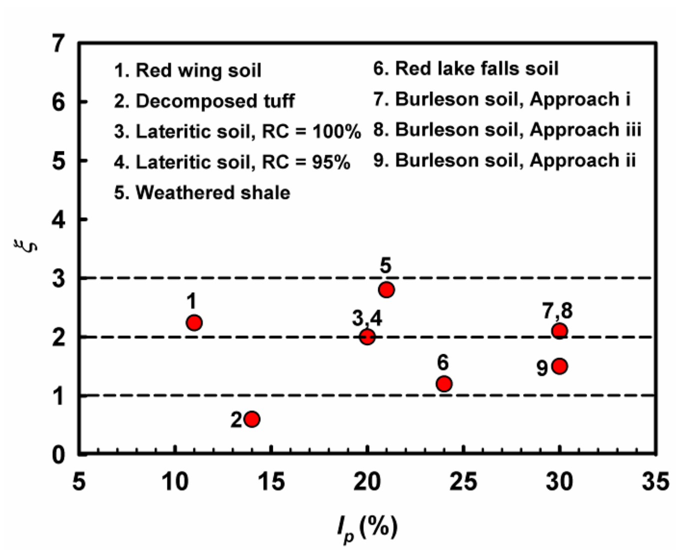

Figure 4.10 Distribution of the model parameter ξ with respect to I_p for soils 2, 4, 5, 7, 8 and 11

The predictions of the Red lake falls (soil 8) and the decomposed tuff (soil 11) are comparatively less accurate than other soils when using ξ = 2.0 for prediction (see Table 4.3). A closer look into the behavior of the Red lake falls shows that the M_R of this soil is highly sensitive with respect to the ψ (i.e., small reduction in the ψ leads to significant drop in the M_R, see Figure 4.7C). As shown in Figure 4.2, lower ξ values indicate a significant increase in the M_R with respect to the ψ than higher ξ values. It appears that a lower ξ value than 2.0 is required for soils which are more sensitive to ψ changes. On the other hand, among soils used to develop the proposed model (soils 2, 4, 5, 7, 8 and 11), the decomposed tuff (soil 11) is classified as silt with low plasticity (i.e., ML, according to USCS) The remainder of the soils are classified as clayey soils or silt with high plasticity (see Table 4.1). The mechanical behavior of ML soils can reflect characteristics of either cohesionless soils or cohesive soils (Fredlund and Rahardjo 1993). Garven and Vanapalli (2006), Vanapalli and Oh (2010) suggested respectively a value of 1.0 for model parameters κ and β_E in Eq. 4.9 and Eq. 4.10 for cohesionless soils. Better predictions were achieved using a ξ value of 1.0 to predict the M_R of the decomposed tuff (R^2 = 0.9 which indicates excellent prediction as per Witczak et al. 2002). This indicates that the mechanical behavior of the decomposed tuff (soil 11) may be more close to cohesionless soils. In general, summarized results in Table 4.3 suggest that ξ value of 2.0 is suitable for compacted fine-grained soils.

Table 4.3 The ξ values for different subgrade soils and the goodness of prediction

Soil No. and ID	ξ from regression analysis			ξ = 2.0	
	ξ	R^2	Comments[1]	R^2	Comments[1]
2. Burleson, Approach (i)	2.1	0.94	Excellent	0.94	Excellent
2. Burleson, Approach (ii)	2.1	0.87	Good	0.83	Good
2. Burleson, Approach (iii)	2.1	0.92	Excellent	0.91	Excellent
4. Weathered shale	2.8	0.80	Good	0.74	Good
5. Lateritic soil, RC = 100%	2.0	0.98	Excellent	0.98	Excellent
5. Lateritic soil, RC = 95%	2.0	0.96	Excellent	0.96	Excellent
7. Red wing soil	2.24	0.97	Excellent	0.97	Excellent
8. Red lake falls soil	1.2	0.73	Good	0.67	Fair
11. Decomposed tuff	0.6	0.98	Excellent	0.63	Fair

Note: [1]Comments are based on Witczak et al. (2002) criteria for goodness of prediction: Excellent ($R^2 \geq 0.9$), Good ($0.7 \leq R^2 \leq 0.89$), Fair ($0.4 \leq R^2 \leq 0.69$).

All soils assigned in group 2 (i.e., soils 1, 3, 6, 9 and 10, with 7 sets of data) are clayey fine-grained soils (see Table 4.1). Based on the summarized discussions, a unique ξ value of 2.0 is used in Eq. 4.18 along with the information of M_{ROPT}, ψ_{OPT}, M_{RSAT} and SWCC for predicting the M_R - ψ relationships.

4.6 Performance of the proposed model

The testing methods and M_{RSAT} values of the Renfrow (soil 3), Mudstone (soil 6), MnRoad (soil 9) and Duluth slope (soil 10) soils are detailed in earlier sections of this chapter. The glacial till (soil 1) tested by Fredlund et al. (1977) was compacted at different moisture contents and dry densities before performing the M_R tests. Specimens were subjected to stress levels of σ_d = 20.6 kPa, 48.2 kPa, 82.7 kPa, 103.4 kPa and σ_c = 20.7 kPa. A M_R value of 7 MPa, which was determined from specimens with S close to100%, was used as the M_{RSAT} value. The M_{ROPT} values are predicted using Eq. 4.1. The SWCC of the glacial till is shown in Figure 4.11A. Predictions using Eq. 4.18 and ξ = 2.0 are shown in Figure 4.11B.

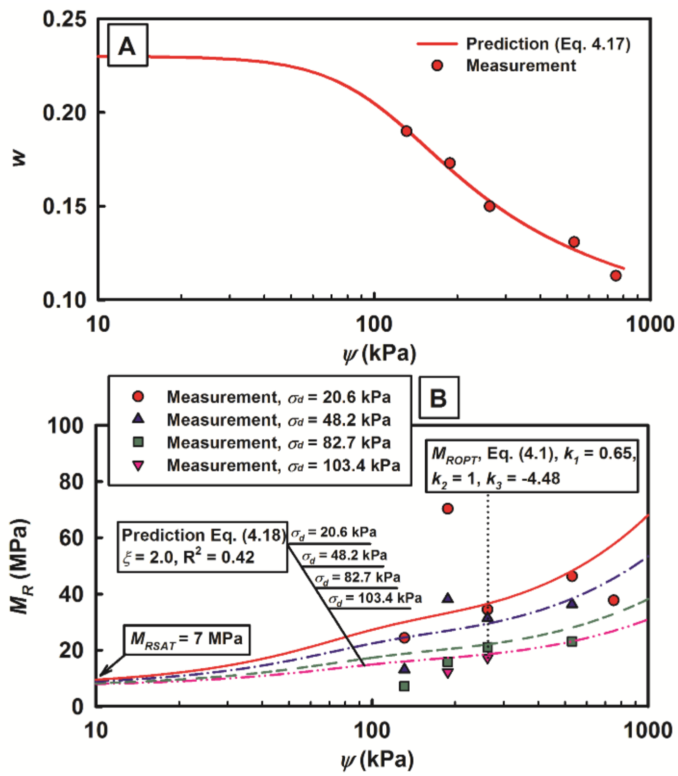

Figure 4.11 Measured and predicted (A) SWCC and (B) the variation of M_R with respect to ψ for a glacial till from Saskatchewan (Data from Fredlund et al. 1977)

Fredlund et al. (1977) are one of the earliest investigators to study the variation of the M_R with ψ from laboratory tests. The measured M_R values show an increasing trend with ψ although they are a little scattered (see Figure 4.11B). The scatter may be attributed to (i) the limitations of the available experimental facilities and testing protocols close to four decades ago, and (ii) the differences in the soil structure amongst specimens. Specimens used in Fredlund et al. (1977) study were compacted at different moisture contents instead of compacted at OMC then dried or wetted to other moisture contents. The later preparation method is believed to provide more unique soil structure and was used to prepare other soils listed in Table 4.1. Eq. 4.18 predicts M_R - ψ relationships using ξ = 2.0 with R^2 = 0.42, which is a fair prediction as per Witczak et al. (2002) guidelines.

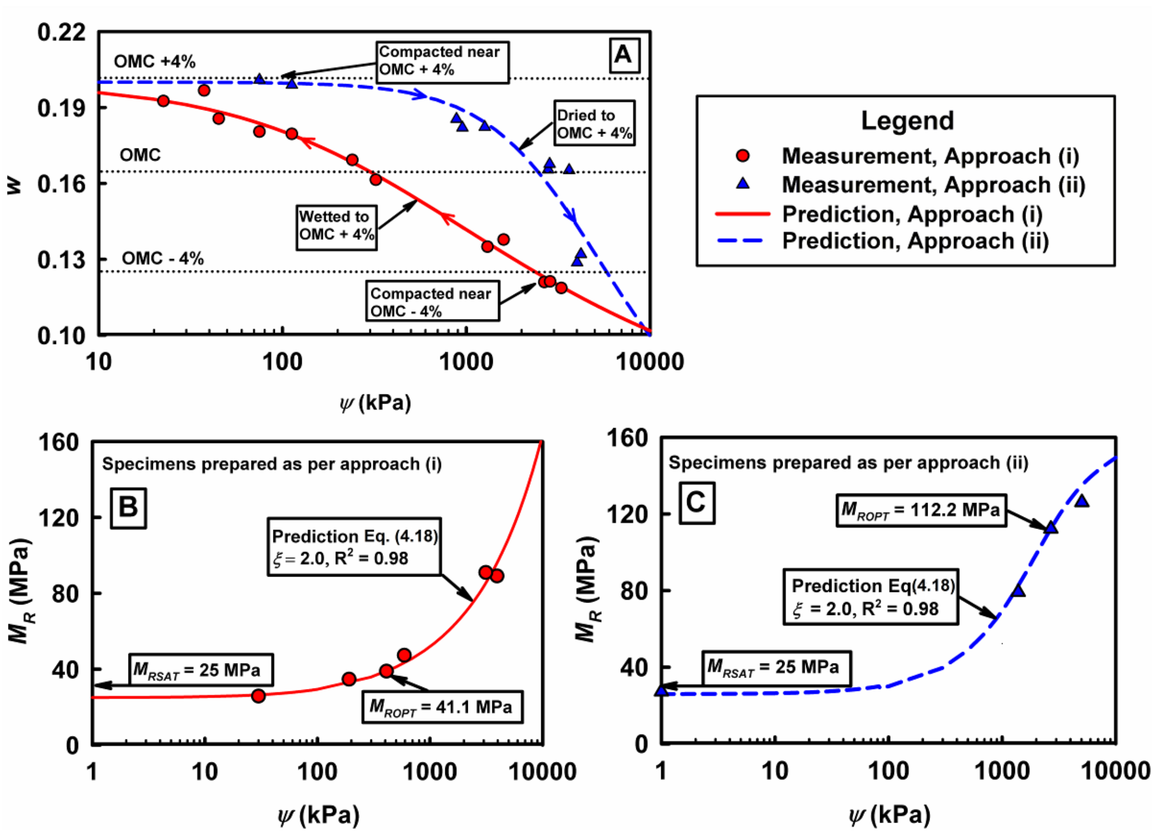

Figure 4.12 Measured and predicted (A) SWCC and (B), (C) variation of M_R with respect to ψ for Renfrow soil from Oklahoma (Data from Zaman and Khoury 2007)

The SWCCs of the Renfrow (soil 3) specimens prepared using approaches (i) and (ii) are shown in Figure 4.12A. The predictions are shown in Figures 4.12B and 4.12C. Excellent predictions with an R^2 = 0.98 was achieved by Eq. 4.18 using ξ = 2.0 for both specimens prepared as per approach (i) and (ii). Similarly, using the SWCC shown in Figure 4.13A, Eq. 4.18 provides excellent predictions for the mudstone (soil 6) compacted at RC = 100% and RC = 95%. Figure 4.13B shows an example of the predictions for the specimens compacted at σ_d = 103 kPa and σ_c = 21 kPa. Figure 4.14 shows the M_R - ψ - σ_d relationships predicted using Eq. 4.18 and ξ = 2.0. The SWCCs of the MnRoad (soil 9) and Duluth slope (soil 10) soils are shown in Figure 4.15A. Predictions by Eq. 4.18 for the MnRoad and Duluth slope soils are shown in Figures 4.15B and 4.15C respectively. Note that Eq. 4.18 provides good predictions for MnRoad (R^2 = 0.78) and excellent predictions for Duluth slope (R^2 = 0.92) soils using ξ = 2.0. Figure 4.16 shows the prediction of the M_R - ψ - σ_d relationships by Eq. 4.18 for the Duluth slope soil. As can be seen from Figure 4.11 through Figure 4.16 that Eq. 4.18, using a unique model parameter ξ = 2.0, provides reasonable predictions for soils 1, 3, 6, 9, and 10 (fair predictions for soil 1, good predictions for soil 9 and excellent predictions for soils 3 and 6).

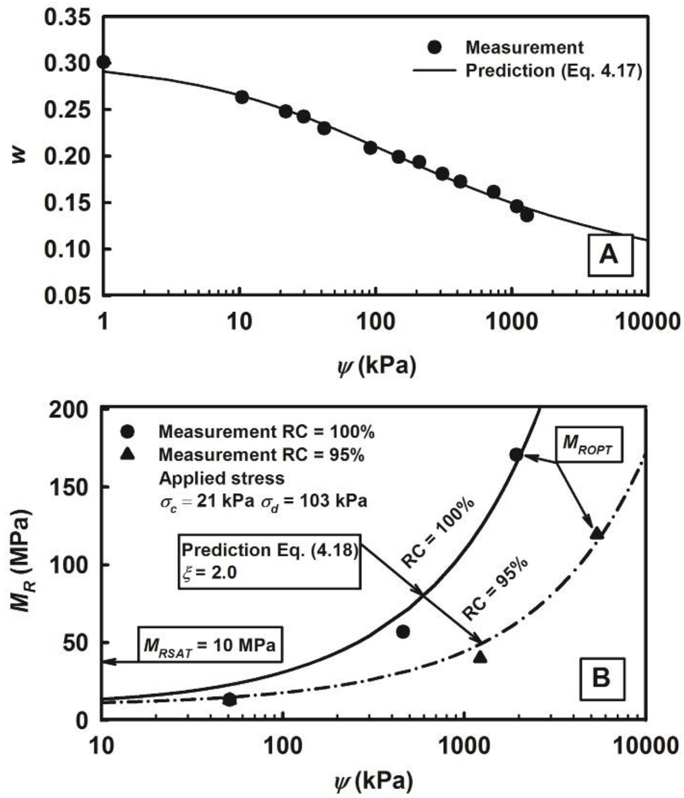

Figure 4.13 Measured and predicted (A) SWCC and (B) variation of M_R with respect to ψ for a mudstone from Taiwan (Data from Yang et al. 2005)

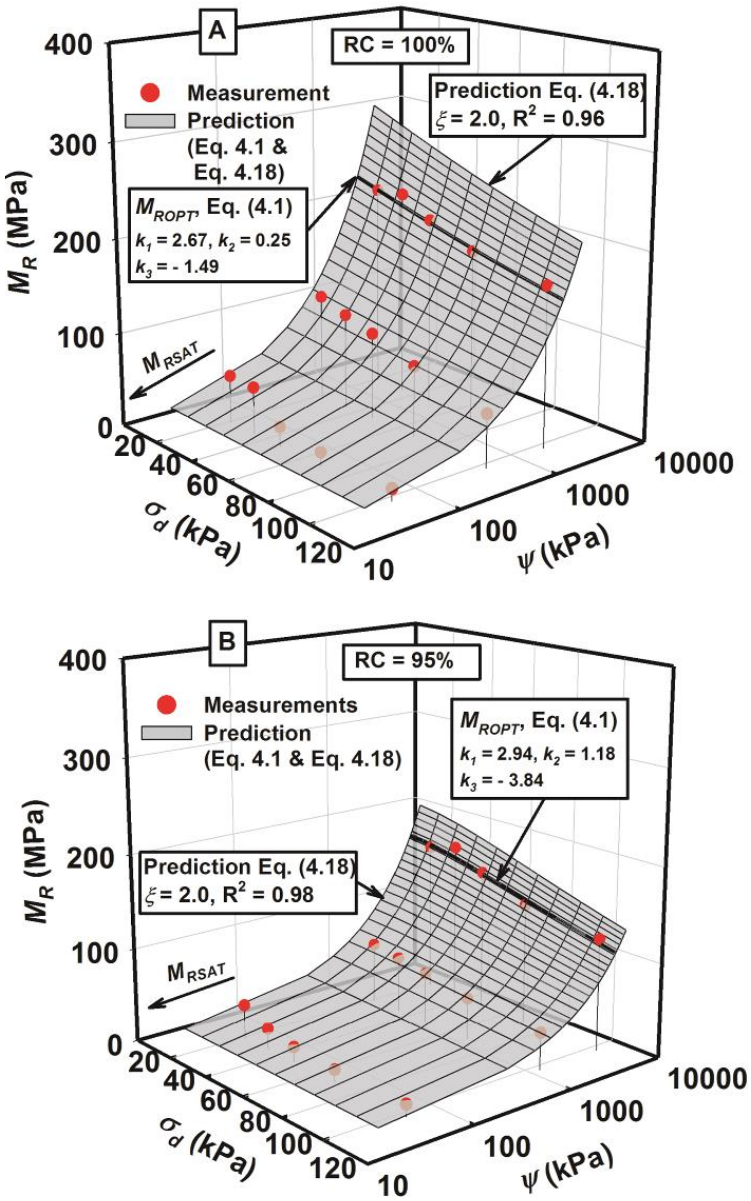

Figure 4.14 Comparisons between the measured and predicted M_R - ψ - σ_d relationships for a mudstone from Taiwan compacted at (A) RC = 100% and (B) RC = 95% (Data from Yang et al. 2005)

Figure 4.17 shows the comparisons between the measured and predicted M_R values using Eq. 4.18 and a unique model parameter ξ = 2.0 for all the soils listed in Table 4.1 (Totally 210 measured data points are included) along with the associated R^2 values. The proposed Eq. 4.18 provides predictions for these 210 data points with an overall R^2 value of 0.9 which indicates excellent prediction as per Witczak et al. (2002) guidelines.

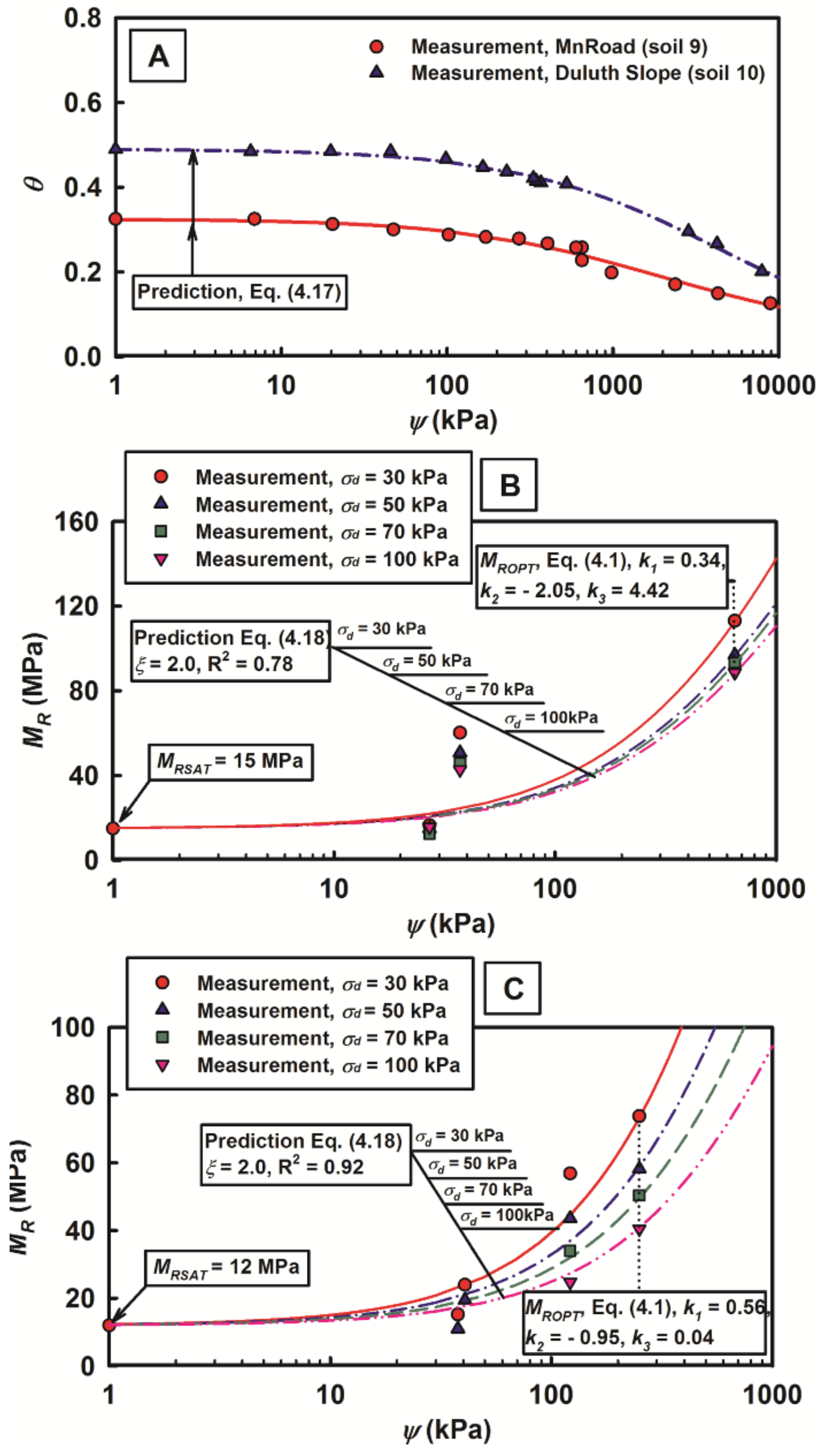

Figure 4.15 Measured and predicted (A) SWCC and the variation of M_R with respect to ψ for (B) MnRoad soil and (C) Duluth slope soil (Data from Gupta et al. 2007)

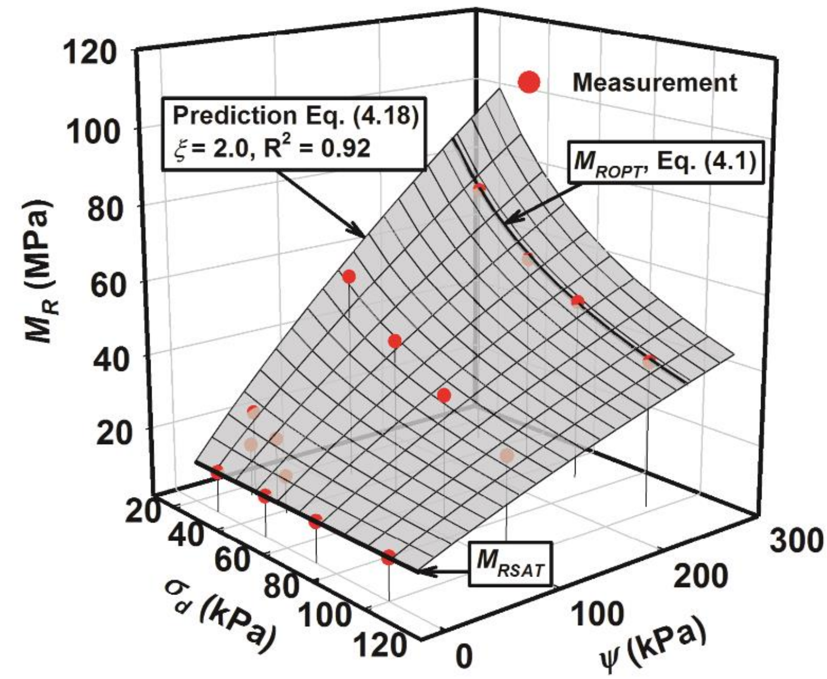

Figure 4.16 Comparisons between the measured and predicted M_R - ψ - σ_d relationships for Duluth slope soil from Minnesota (Data from Gupta et al. 2007)

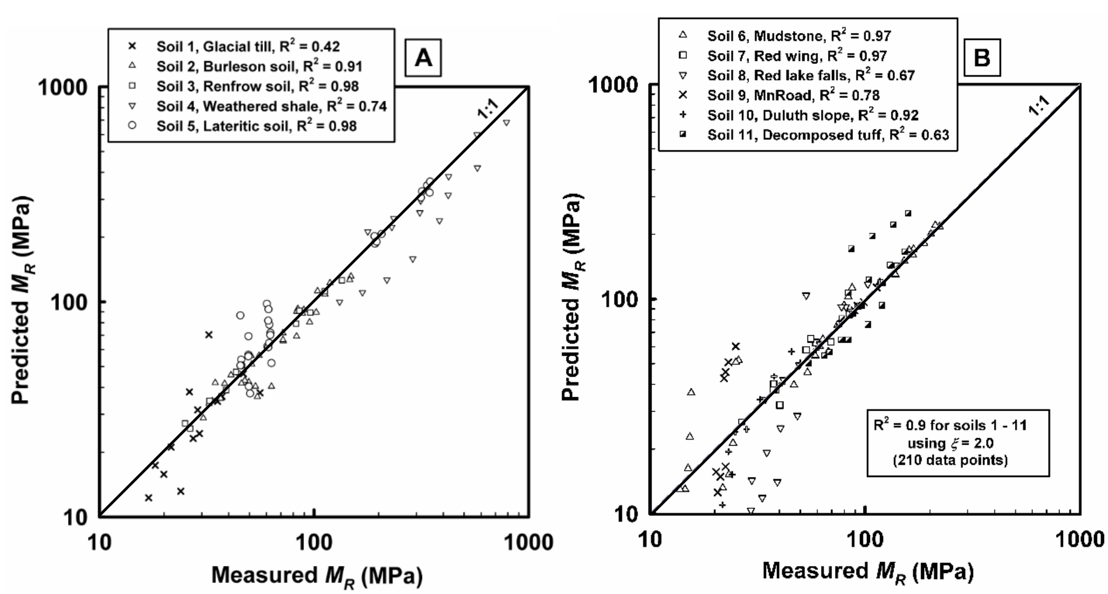

Figure 4.17 Comparisons between the measured and predicted M_R values for (A) soils 1 - 5 and (B) soils 6 - 11

4.7 Summary and conclusions

A simple model is proposed in this chapter to predict the variation of the resilient modulus with respect to the soil suction for compacted fine-grained subgrade soils. The proposed model requires the determination of the M_{RSAT}, M_{ROPT}, ψ_{OPT} values, the SWCC and the model parameter ξ. A total of 16 sets of experimental data derived from 11 different subgrade soils following different testing protocols are selected to provide comparisons between the experimental measurements and the predictions by the proposed model. The comparisons show that the proposed model is capable of reliably predicting the variation of the M_R with respect to the ψ using a single-valued model parameter ξ equal to 2.0. Some key details with respect to the proposed model are summarized below:

(i) The M_{RSAT}, M_{ROPT} values required in the proposed model are conventionally determined for use in the pavement design practice with the aid of the RLLTs. The M_{RSAT} is less sensitive to the applied stress levels and can be assumed as a constant value. The M_{ROPT}, on the other hand, can be predicted using existing models such as Eq. 4.1.

(ii) The proposed model is formulated as the ratio of the moisture contents (i.e., S / S_{OPT} or w / w_{OPT} or θ / θ_{OPT}, see Eq. 4.14, Eq. 4.15, and Eq. 4.16) to allow the use of SWCC with respect to S, as well as w and θ, to estimate the moisture contents corresponding to different soil suction values for convenience in practice. The SWCCs with respect to w and θ summarized in Table 4.2 for different soils used in this study are either measured following the desaturation path (drying SWCC) or formed by the moisture content - soil suction relationships measured after the RLTTs (apparent SWCC). The measurement of drying SWCC or apparent SWCC is relatively quicker and can be conducted using conventional techniques. The proposed model, using drying SWCC or the apparent SWCC, provides reliable predictions for all the soils used in this study. Further studies using SWCC models taking account of the influence of cyclic loading, hysteresis and soil structure for predicting the M_R are encouraged to improve the performance of the proposed model.

(iii) The measured M_R - ψ and M_R - σ_d relationships summarized in Figures 4.6, 4.8, 4.9, 4.14, and 4.16 highlight coupled characteristics. The proposed model predicts smooth *3D* surfaces for the M_R - ψ - σ_d plots that well reproduce the coupled characteristics of the measured data. The predicted smooth *3D* surfaces also help to reduce the possible numerical problems when the proposed model is used for numerical simulations.

(iv) A value of ξ equals to 2.0 can be used in the proposed model to provide excellent predictions (as per Witczak et al. 2002) for the 11 soils (16 sets of experimental data tested as per various testing protocols within different soil suction ranges; see Table 4.1 and Table 4.3). A unique value for model parameter ξ helps to alleviate the need for extensive amount of testing data and regression analysis to provide acceptable predictions using the proposed model. However, lower ξ values may provide better predictions for soils that show higher sensitivity to the ψ and some silty soils with low plasticity.

CHAPTER FIVE

EXPERIMENTAL INVESTIGATIONS ON THE RESILIENT MODULUS OF COMPACTED SUBGRADE SOILS

5.0 Background-Information

The contents presented in this chapter are from the manuscript of the publication:

Han, Z., and Vanapalli, S. K. (2016). Relationship between resilient modulus and suction for compacted subgrade soils. *Engineering Geology*, 211: 85-97.
DOI: 10.1016/j.enggeo.2016.06.020

The symbols used in this chapter are summarized in Table 5.0.

Table 5.0 Symbols used in Chapter Five

Symbols	
a, n, m	model parameters for Fredlund & Xing (1994) SWCC equation
e	void ratio
G_s	specific gravity
I_p	plastic index
k_1, k_2 and k_3	model parameters for stress-dependent equations
M_R	resilient modulus
M_{Rrep}	representative resilient modulus
p_a	atmosphere pressure
R^2	coefficient of determination
s	soil suction
s_{ae}	air-entry value
s_c	soil suction after curing
s_{fp}	soil suction derived from filter paper method
S_r	water degree of saturation
subscript $_{opt}$	corresponding parameters at optimum moisture content condition
subscript $_{sat}$	corresponding parameters at saturation condition
u_a	pore-air pressure
u_w	pore-water pressure
w	gravimetric moisture content
w_{avg}	averaged water content
w_c	water content after curing

Table 5.0 Symbols used in Chapter Five

Symbols	
w_{fp}	water content of the sandwiched filter paper
w_L	liquid limit
γ_{dmax}	maximum dry unit weight
ε_r	axial resilient strain
ε_v	volumetric strain
θ	bulk stress
θ'	net bulk stress
ξ	model parameter
σ_c	confining pressure
$\sigma_{c,net}$	net confining stress
σ_d	deviator stress
τ_{oct}	octahedral shear stress

5.1 Introduction

The resilient modulus (M_R) is defined as the ratio of the cyclic deviator stress (σ_d) to the axial resilient strain (ε_r). It indicates the stiffness of pavement materials under cyclic loading conditions and is a key parameter required in mechanistic pavement design methods. The M_R is mainly used for analyzing and predicting the fatigue cracking failure of the pavement surfacing associated with the resilient strain (Brown 1996). The development of the rutting failure, which results from the accumulation of permanent deformation, is also related to the M_R. This is due to the fact that lower layer stiffness leads to inadequate spreading of traffic loading and greater stress concentration which contribute to the excessive permanent strain (Brown and Selig 1991).

Pavement subgrade and base-course layers are typically compacted at optimum moisture content (w_{opt}) to achieve maximum dry unit weight (γ_{dmax}) and to ensure better engineering performance (Yang et al. 2005, Coronado et al. 2011). Compacted pavement materials are subjected to post-compaction seasonal moisture content variations due to their exposure to the external environment. Like other stiffness and shear strength properties, the M_R is sensitive to changes in the moisture content and suction (s) (Miao et al. 2002, Yang et al. 2008, Rahardjo et al. 2011, Khosravi and McCartney 2012, Han and Vanapalli 2015, Hoyos et al. 2015, Puppala et al. 2016). Recent experimental studies have demonstrated that the M_R - s relationship, for both unbounded subgrade soils and base-course aggregates, is essentially non-linear and is influenced by many factors including the external stress, soil fabric / structure, hydraulic hysteresis and temperature (Ekblad and Isacsson 2006, Yang et al. 2008, Caicedo et al. 2009, Sawangsuriya et al. 2009, Cary and Zapata 2011, Coronado et al. 2011, Khoury et al. 2011, Ba et al. 2013, Ng et al. 2013, Nowamooz et al. 2013, Ng and Zhou 2014, Nokkaew et al. 2014, Salour et al. 2014, Xiao et al. 2014, Salour and Erlingsson 2015, Cary and Zapata 2016). Several models were proposed to predict the influence of the s on the M_R either by considering the direct contribution of the s to the M_R (Caicedo et al. 2009, Cary and Zapata 2011, Khoury et al. 2011, Ng et al. 2013) or by quantifying the s as a contributor to external confining or shearing stresses (Heath et al. 2004, Yang et al. 2005, Liang et al. 2008, Nowamooz et al. 2013, Nokkaew et al. 2014, Gu et al. 2014). A comprehensive summary of various prediction models in the literature is available in Han and Vanapalli (2016a).

This chapter investigates the M_R - s relationship for three Canadian subgrade soils with different geological histories. Two widely used experimental methods were followed to determine the M_R - s relationship under various external stress conditions. Experimental results suggest varying non-linearity between the resilient modulus and the suction, gravimetric water content and external stress for different soils. A simple model proposed by Han and Vanapalli (2015) and two rigorous models proposed by Liang et al. (2008) and Ng et al. (2013) were used for predicting the experimental measurements of three soils investigated. It is shown that all three models provide equally good predictions for the three soils. The model proposed by Han and Vanapalli (2015) needs less experimental data for prediction compared to the other two models and is suitable for different subgrade soils. For this reason, this model can be a useful tool for predicting the M_R - s relationship for subgrade soils for use in mechanistic pavement design methods.

5.2 Experimental program

5.2.1 Materials

Three natural subgrade soils collected from three different locations in Canada (Toronto, Ottawa and Indian Head) are tested in this Chapter. All three soils were collected from 0 to 3m below natural ground surface which is the typical depth of pavement subgrade. The collected soils possibly should have been exposed to erosion, weathering, and leaching over a long period of geological history. The soil collected from Indian Head near Regina in Saskatchewan is a glacial till deposited in the last glacier age 14,000 to 20,000 years ago (denoted as Indian Head Till, IHT). The soil collected from Toronto is a silty clay (denoted as Toronto Silty Clay, TSC). The soil collected from Ottawa is a marine clay sediment of the ancient Champlain Sea formed 10,000 to 12,000 years ago (denoted as Ottawa Champlain Sea Clay, OCSC; it is also known as Leda clay). The Champlain Sea sediment in Ottawa region typically shows an increase in the clay content with increasing depth due to deposition and desiccation processes (Brydon and Patry 1961).

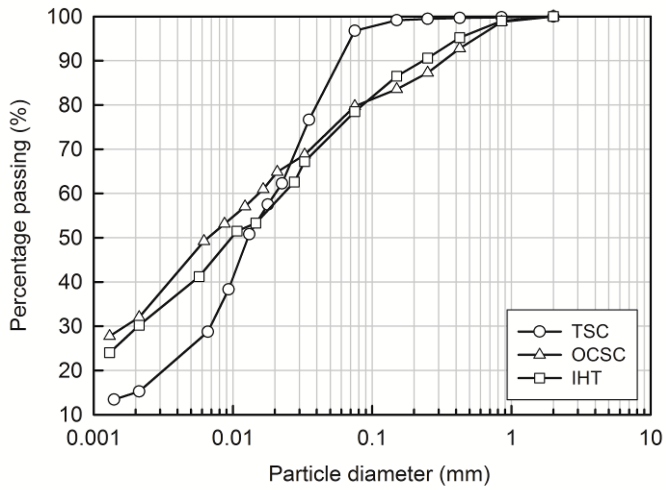

Figure 5.1 Gradation curves for the three soils

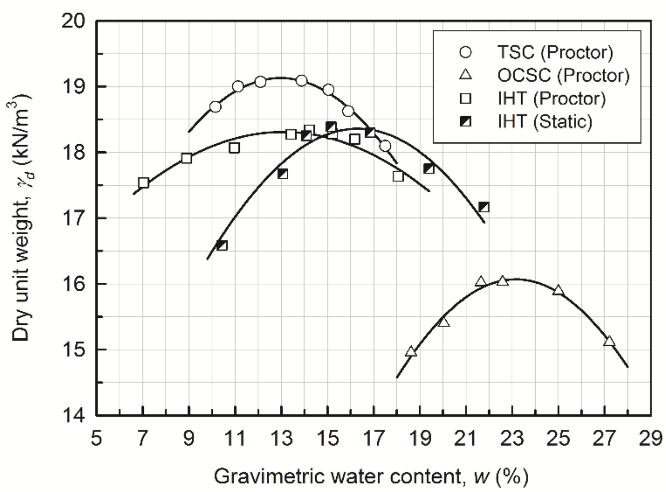

Figure 5.2 Compaction curves for the three soils

The collected soil samples were air dried, grinded and passed through a 2 mm sieve. The prepared dry soil for the IHT, TSC and OCSC was brownish, greyish and dark-greyish in color, respectively. Figure 5.1 shows the gradation curves derived from the sieve analysis and hydrometer analysis as per ASTM D6913-04 (ASTM 2009) and ASTM D422-63 (ASTM 2007), respectively. Figure 5.2 shows compaction curves of the three prepared soils derived from standard Proctor tests as per ASTM D698-12 (ASTM 2012). In addition, static compaction tests using a split brass mould (50 mm of inner diameter) were performed on the IHT. The IHT that was initially prepared at known gravimetric water contents was compacted in five layers (each layer was approximately 20 mm thick) using a compressive stress of 750 kPa, for each layer. The volume and mass of the resulting specimens were measured to calculate the γ_d. The static compaction curve for the IHT is also shown in Figure 5.2. Table 5.1 summarizes basic soil properties of the three soils. It can be observed from Table 5.1 and Figures 5.1 and 5.2 that i) the IHT and OCSC are plastic clays with similar particle size distributions. However, their compaction characteristics such as the w_{opt} and γ_{dmax} are quite different. Comparatively, the TSC is lower in clay content and therefore less plastic; ii) the IHT compacted using two different methods presents similar γ_{dmax} but lower w_{opt} for the Proctor compaction compared to static compaction. Differences in the w_{opt} and γ_{dmax} values are associated with the different soil structure / fabric formed during the static and dynamic compactions (Sivakumar and Wheeler 2000).

Table 5.1 Basic properties of the three soils

Properties	Toronto Silty Clay (TSC)	Indian Head Till (IHT)		Ottawa Champlain Sea Clay (OSCS)
w_L (%)	19.6	35.5		48
I_p (%)	6	19		26
G_s	2.68	2.72		2.75
w_{opt} (%)	13.5[1]	13.9[1]	15.5[2]	23[1]
γ_{dmax} (kN/m^3)	19.15[1]	18.39[1]	18.46[2]	16.16[1]
Sand %	3.5	28		20
Silt %	81.5	42		48
Clay %	16	30		32
USCS	CL-ML	CL		CL
AASHTO	A-4	A-6		A-6

Notes: [1]derived from standard Proctor tests; [2]derived from static compaction tests. Notations: w_L = liquid limit, I_p = plasticity index, G_s = specific gravity, w_{opt} = optimum moisture content, γ_{dmax} = maximum dry unit weight, USCS = unified soil classification system (ASTM D2487-11, 2011), AASHTO = American association of state highway and transportation officials soil classification system (AASHTO M145-91, 2008).

Table 5.2 Conditions of IHT specimens

Sample ID	w_{opt} (%)	Initial γ_d (kN/m^3)	Initial e	Initial S_r	Target s_0 (kPa)	Duration of equilibrium (day)
IHT-1	15.5	18.4620	0.473	0.888	0	25
IHT-2	15.5	18.3915	0.479	0.877	30	21
IHT-3	15.5	18.3693	0.481	0.874	60	18
IHT-4	15.5	18.4527	0.474	0.887	90	14
IHT-5	15.5	18.4344	0.476	0.884	120	6

Specimens (50 mm in diameter and 100 mm in height) of the IHT, TSC and OCSC for cyclic loading tests were statically compacted in the same split brass mould. Two different approaches were used to compact the specimens. For the IHT, prepared soil was compacted in 5 layers using a compression stress of 750 kPa for each layer. For the TSC and the OCSC, prepared soil was also compacted in 5 layers; however, each layer was compacted to achieve the γ_{dmax} determined from Proctor tests by controlling the volume. The measured compression stress was approximately 1100 kPa and 700 kPa for the TSC and the OCSC, respectively. The w_{opt} values derived from different compaction methods were used to prepare soil-water mixtures for compacting specimens (i.e. 13.9% derived from static compaction was used for the IHT; 13.5% and 23% derived from Proctor compaction were used for the TSC and the OCSC). Oven-dried soil was thoroughly mixed with de-aired distilled water to achieve the w_{opt}. The soil-water mixture was passed through a 2 mm sieve, sealed in double-layered plastic bags and stored for a period of 24 hours for achieving uniform moisture content. The w thereafter was measured to check whether the required w_{opt} had been achieved. If there were differences, calculated amount of dry soil or de-aired distilled water was added to adjust the w. Such procedures were repeated until the measured w fell within ± 0.1% of the w_{opt}. The prepared moisturized soil was again passed through a 2 mm sieve to remove any soil clods that may have formed.

In total, five specimens were compacted for the IHT (denoted as IHT-1 through IHT-5) and eight specimens were compacted respectively for the TSC (denoted as TSC-1 through TSC-8) and the OCSC (denoted as OCSC-1 through OCSC-8). Compacted specimens were measured for their mass and volume, wrapped using two layers of plastic film and stored in plastic containers for further moisture equalization. Tables 5.2 and 5.3 summarize the initial conditions of the compacted specimens including the initial dry unit weight γ_d, void ratio e and degree of saturation S_r. Compacted specimens of the same soil with similar initial γ_d and e values suggest that they have an identical initial soil fabric / structure within the specimens.

Table 5.3 Conditions of TSC and OCSC specimens

Sample ID	Compaction				Curing		SWCC	
	w_{opt} (%)	Initial γ_d (kN/m^3)	Initial e	Initial S_r	w_c (%)	s_c (kPa)	w_{avg} (%)	s_{fp} (kPa)
TSC-1	13.5	19.1775	0.397	0.910	14.65	0	14.65	0
TSC-2	13.5	19.1657	0.398	0.908	14.48	9	14.24 14.25	14 15
TSC-3	13.5	19.1833	0.397	0.911	14.27	13	13.92 13.88	19 21
TSC-4	13.5	19.1863	0.397	0.912	13.98	18	13.71 13.82	19 25
TSC-5	13.5	19.1616	0.399	0.908	13.75	21	13.68 13.60	21 24
TSC-6	13.5	19.0759	0.405	0.894	13.62	23	13.43 13.51	25 26
TSC-7	13.5	19.1347	0.401	0.903	13.48	25	13.21 13.14	30 31
TSC-8	13.5	19.0902	0.404	0.896	12.50	48	12.35 12.38	54 56
OCSC-1	23.0	16.2000	0.698	0.907	24.85	0	24.85	0
OCSC-2	23.0	16.2409	0.693	0.912	24.72	41	24.64 24.54	88 74
OCSC-3	23.0	16.2073	0.697	0.908	24.55	68	24.50 24.45	77 87
OCSC-4	23.0	16.2248	0.695	0.910	24.00	147	23.94 23.90	100 184
OCSC-5	23.0	16.2239	0.695	0.910	23.60	219	23.52 23.50	226 251
OCSC-6	23.0	16.2358	0.694	0.912	23.30	290	23.29 23.20	307 388
OCSC-7	23.0	16.2086	0.697	0.908	22.91	428	22.86 22.74	431 578
OCSC-8	23.0	16.2289	0.695	0.911	22.66	558	22.57 22.60	610 749

Notations: w_c = water content after curing, s_c = soil suction after curing, w_{avg} = averaged water content of the two soil slides sandwiching the filter paper, s_{fp} = soil suction derived from filter paper method using Equation 5.1.

5.2.2 Testing equipment

GDS Entry Level Dynamic triaxial testing system (ELDyn) was used to investigate the influence of the suction, gravimetric water content and external stress (i.e., confining and deviator stresses) on the M_R for the three soils. Figure 5.3 shows the layout and components of the ELDyn system. Similar to some triaxial systems used for testing the M_R of unsaturated subgrade soils in the literature (e.g., Yang et al. 2008, Ng et al. 2013, Salour et al. 2014), the ELDyn system controls the pore-air pressure (u_a) and the pore-water pressure (u_w) and therefore the suction ($s = u_a - u_w$) using the axis-translation technique (Hilf 1956). The u_w is controlled by a pore-water pressure controller and is applied to the bottom of the specimen through a high air-entry value ceramic disk (air-entry value s_{ae} = 500 kPa) embedded in the pedestal. The saturated ceramic disk acts like a membrane that only allows the exchange of water when s is lower than its s_{ae}. A pore-water pressure sensor is connected to the water inlet of the pedestal to measure the applied u_w at the bottom of the ceramic disk. The u_a is controlled by a two-channel pneumatic regulator and acts on the top of the specimen through a coarse porous stone. The confining pressure (σ_c) is applied using air pressure which is also controlled by the pneumatic regulator.

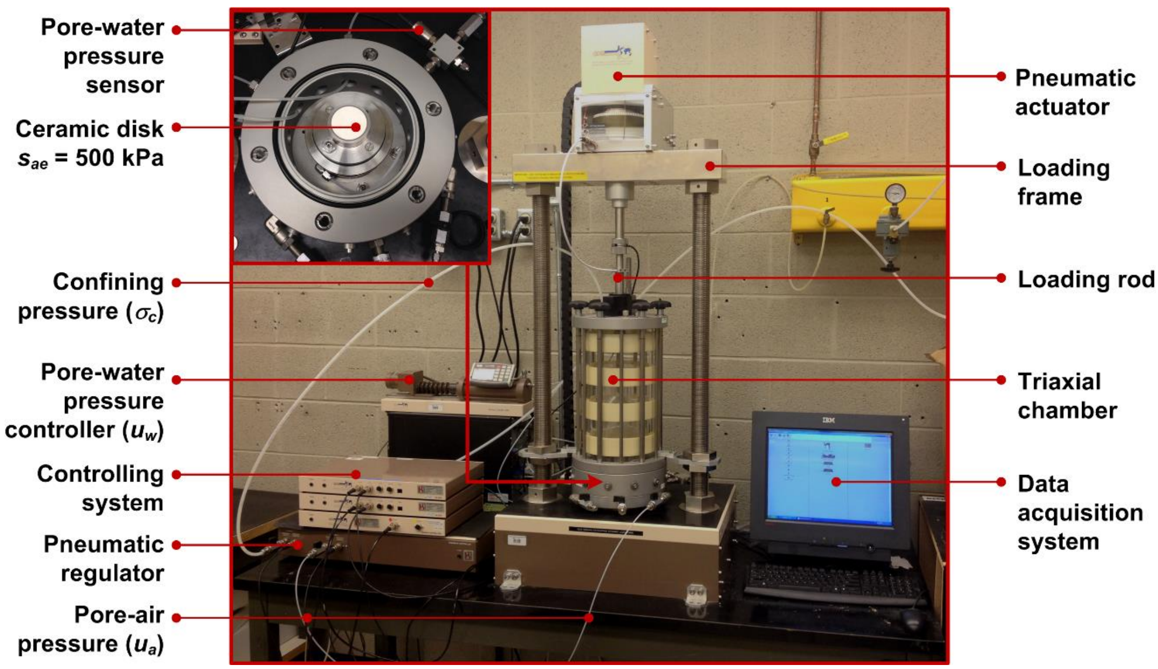

Figure 5.3 GDS ELDyn system used for cyclic loading tests

Cyclic loadings are applied by a pneumatic actuator mounted on the loading frame through a rigid loading rod. An optical encoder is embedded inside the pneumatic actuator to measure the displacement of the loading rod and therefore, the axial deformation of the specimen. The sensitivity of the optical encoder is 0.00020833 mm and the ELDyn system can identify a displacement as low as 0.001 mm. A 5kN load cell with an accuracy of ±5 N (±2.5 kPa for specimen 50 mm in diameter) is mounted at the lower end of the loading rod inside the triaxial chamber to measure the force. This arrangement alleviates the need for calibrating the induced force acting on the loading rod by the cell pressure when load cell is mounted outside the triaxial chamber. It also eliminates possible errors in the measured force associated with the mechanical friction between the loading rod and the triaxial chamber. The load cell and pneumatic actuator, along with the data acquisition systems, form a looped system to enable the application of the stress-controlled cyclic loading.

5.2.3 Testing procedure

Two procedures were used to equilibrate the compacted specimens from w_{opt} to different w and s values for different soils before the cyclic loading tests. Most of the specimens were wetted from w_{opt} to higher w values highlighting the importance of the wetting process. This is based on the consideration that subgrade soils are more likely to increase in moisture content after compaction and reach an equilibrium moisture content with the external environment (Quintus and Killingsworth 1998, Uzan 1998, Yang et al. 2005).

The axis-translation technique was used to control the s of the IHT specimens. After saturating the ceramic disk and mounting the IHT specimens onto the pedestal, a constant u_w of 50 kPa was maintained at the bottom of the specimen through the ceramic disk. The u_a of different values was applied at the top of the specimens to impose different s on the specimens. The s of the IHT specimens statically compacted at w_{opt} (i.e. at s_{opt}) was measured using a revised null pressure plate apparatus devised by Power and Vanapalli (2010). The measured s_{opt} is approximately 120 kPa. Five target suction values of 120, 90, 60, 30, and 0 kPa were respectively imposed on the five prepared IHT specimens (see Table 5.2). IHT specimens during the axis-translation were loaded under a net confining stress $\sigma_{c,net}$ ($\sigma_{c,net} = \sigma_c - u_a$) of 27.6 kPa and a static deviator stress of 5 kPa to simulate the in-situ static stress condition and to maintain good contact between the specimen and the ceramic disk. The water drainage system was flushed at 36 hours intervals to remove any possible air bubbles accumulated beneath the ceramic disk or in the drainage tubes. The completion of suction equilibrium was assumed when the daily water exchange measured by the pore-water pressure controller was less than 0.04% of the specimen water content (typically 150 - 200 mm^3/day for the IHT specimens) referencing to the protocols followed by Wheeler and Sivakumar (1995) and Ng et al. (2013) who reliably achieved suction equilibrium using the axis-translation technique within fine-grained soil specimens with dimensions similar to the specimens in the present study (50 mm in diameter and 100 mm in height). A period of 6 to 25 days was required to achieve the equilibrium for different specimens. Details of the equilibrium time for various IHT specimens are summarized in Table 5.2. It is important to note that the five imposed target suction values are the initial suction (s_0) of the specimens before cyclic loading tests. It is well recognized that the s_0 of fine-grained soil specimens decreases during the cyclic loading due to the generation of the non-recoverable plastic strain and the excitation of the excessive pore-water pressure (Thom et al. 2008, Yang et al. 2008, Sawangsuriya et al. 2009, Sivakumar et al. 2013). The actual s level within the specimen during cyclic loading however could be difficult to precisely control or predict as the degradation in the s is related to many factors such as the external stress level, number and rate of cyclic loading and drainage condition (Cary and Zapata 2016). In addition, the variation in the M_R with increasing cyclic loadings (i.e. decreasing s) is also not consistent for different soils. For example, Thom et al. (2008) and Sivakumar et al. (2013) reported an increase in the M_R during the cyclic loading with measured decreasing s for a kaolinite. Butalia et al. (2003), on the other hand, reported a decrease in the M_R with increasing cyclic loadings for a cohesive soil from Ohio. Ng et al. (2013) showed for a decomposed tuff from Hong Kong that, with increasing cyclic loadings, the M_R increased when soil contracted but slightly decreased when soil dilated. Given the difficulties in relating the M_R to the "real-time" s during the cyclic loading, it is a simplified practice to use either the s_0 (such as Ng et al. 2013, Ng and Zhou 2014) or the s measured after the cyclic loading tests (such as Khoury and Zaman 2004, Yang et al. 2005, Sawangsuriya et al. 2009) to indicate the suction level within the specimens. Both approaches have been successfully used for analyzing the M_R - s relationships and hence adopted in this study (i.e. the s_0 is used to indicate the suction level within IHT specimens while the s measured after the cyclic loading tests is used to indicate the suction level within TSC and OCSC specimens). More discussions with respect to both these approaches are provided in a later section of this chapter.

A simpler and more straightforward procedure to alter the specimens' moisture content from w_{opt} was performed on TSC and OCSC specimens. Among the eight specimens prepared for the TSC and the OCSC, one specimen (TSC-1 and OCSC-1) was saturated to achieve the saturated water content (w_{sat}), one specimen (TSC-7 and OCSC-7) was kept at w_{opt}, one specimen (TSC-8 and OCSC-8) was dried to a lower w, and the remainder five specimens (TSC-2 to TSC-6 and OCSC-2 to OCSC-6) were wetted to different higher w values between w_{opt} and w_{sat}. In this procedure, Whatman 42 filter papers were cut into rectangles (100 mm by 165 mm) and circles (50 mm in diameter) such that one rectangular and two circular filter papers can be used to entirely wrap one cylindrical specimen. The various equipment and tools used for compacting and curing test specimens are shown in Figure 5.4.

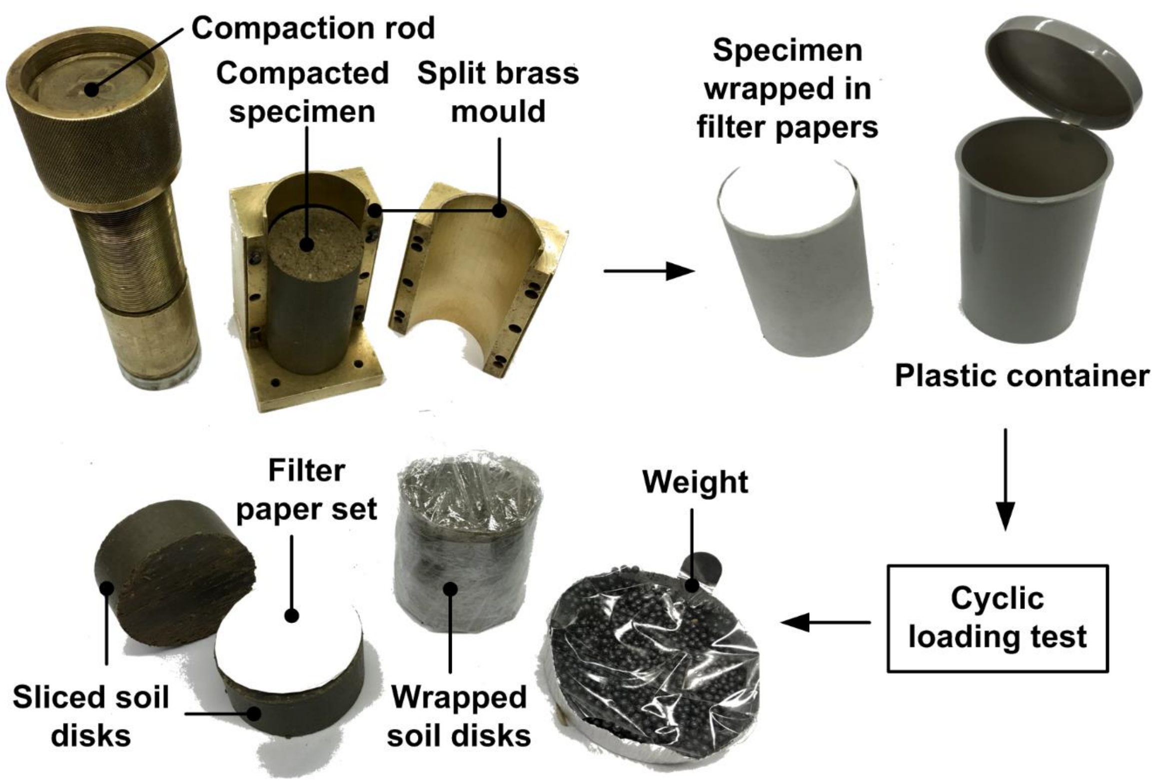

Figure 5.4 Procedure for preparing and testing specimens

In order to saturate the TSC-1 and OCSC-1, each specimen was wrapped within filter papers. A rubber membrane was used to confine the specimen and assure a close contact between the filter paper and the specimen. This approach also prevents any possible moisture loss. The specimen was then placed on a saturated ceramic disk to imbibe water. At 8 hours intervals, the specimen was reversed to ensure that water enters both ends of the specimen uniformly. The filter papers also imbibe water from the saturated ceramic disk and provide access of water along the length of the soil specimen. This procedure helps to accelerate the saturation process without introducing excessive water and protect the specimen from peeling off. The mass of the specimen was measured at 16 hours intervals until the variation between two consecutive measurements was less than 0.2 g (approximately 0.07 - 0.08% of the specimen water content), which is used as a criterion to indicate the full saturation of the specimen. The w_{sat} using this method was found to be 14.65% for the TSC-1 and 24.85% for the OCSC-1, both are lower than the w_{sat} calculated using volume-mass relationship $w_{sat} = e / G_s$ (14.80% for the TSC and 25.20% for the OCSC; the e values are summarized in Table 5.3). This can be explained by the fact that the soil pores of gradually wetted specimens are less likely to be entirely saturated due to the influence of entrapped air within some of the soil pores. The saturation was checked by performing Skempton's B-test prior to the cyclic loading tests using the ELDyn system. The determined B-value was 0.96 and 0.97 for the TSC-1 and OCSC-1, respectively. The w_{sat} was also checked after the cyclic loading test by slicing the specimen into four disks and measuring the average w values. There was good agreement between the w_{sat} and the averaged w for specimens of TSC-1 and OCSC-1.

Five different w values between w_{sat} and w_{opt} were chosen for TSC and OCSC specimens. In order to wet the specimens, each specimen was wrapped in filter papers. De-aired distilled water was evenly sprayed on the filter papers. The amount of sprayed water was approximately 0.5% of the specimen water content (typically 1.5 - 1.7 g). The specimen and the wetted filter papers were further wrapped in two layers of plastic film, stored in a plastic container and placed in a moisture chamber for 24 hours to achieve moisture equilibrium. The mass of specimen was thereafter measured without the filter papers. It was found that procedure followed increased the specimen gravimetric water content by 0.2 - 0.3% each time (i.e. for 24 hour intervals) and ensured a uniform moisture content distribution within the specimen. This procedure was repeated until the specimen reached the desired gravimetric water content w_c, which is summarized in Table 5.3.

Procedure used to dry the TSC-8 and OCSC-8 was similar to that used for wetting the specimens except that air-dried filter papers were used instead of wetted filter papers to wrap the specimens. Air-dried filter papers typically absorb about 0.6 g of water from the specimen and correspondingly reduce the specimen's water content by approximately 0.18 to 0.2% each time (i.e. for 24 hour intervals). Such a slow rate helps to minimize the development of cracks and fissures associated with drying. No cracks or fissures were observed on the surface of the specimens due to drying in the present study.

All specimens of the TSC and the OCSC after achieving the desired w_c were measured for their dimensions (diameter and height) using a caliper readable to 0.01 mm. They were afterward wrapped in two layers of plastic film, sealed in individual plastic containers and stored in a moisture chamber for at least 7 days to allow moisture equilibrium before performing cyclic loading tests. The mass of specimen was measured again prior to performing cyclic loading tests. It was found that moisture loss during the moisture equilibrium was insignificant and could be ignored. Measurements on specimen dimensions indicated that there was slight volumetric strain ε_v for both the TSC (the maximum ε_v was 0.14% for specimen TSC-1 where positive ε_v indicates volumetric expansion) and the OCSC (the maximum ε_v was 1.5% for specimen OCSC-1). It should be noted that the specimens have relatively similar initial soil fabric / structure after compaction as can be assumed from the identical compaction methods and moisture contents and the resulting identical initial γ_d and e values. However, the soil fabric / structure changes during the wetting / drying procedures owing to the expansion or collapse of the soil microstructure upon wetting and the shrinkage upon drying (Alonso et al. 1990). Therefore, the soil fabric / structure within the specimens before cyclic loading tests can be different from the initial soil fabric / structure.

Cyclic loading tests were performed after achieving the desired s_0 (for the IHT) or w_c (for the TSC and OCSC) in the specimens. Haversine form of cyclic loadings were applied at a frequency of 1Hz using the pneumatic actuator. Constant water content condition was maintained during the tests considering the low hydraulic conductivity of the compacted fine-grained soils which does not allow effective dissipation of the excessive pore-water pressure generated during the cyclic loading (Cary and Zapata 2011, Ng et al. 2013). The loading scheme suggested by AASHTO T307-99 (AASHTO 2003) was followed to determine the M_R.

For the TSC and the OCSC, each specimen was initially conditioned by applying 1000 cyclic loadings (σ_d) of 27.6 kPa under a confining stress (σ_c) of 41.4 kPa to minimize the influence of the initial imperfect contact between the loading cap / pedestal and the specimen (i.e. seating errors). After the conditioning phase, four levels of σ_d (27.6, 41.4, 55.2 and 68.9 kPa which were applied in sequence) were used to load the specimen confined under three σ_c levels (41.4, 27.6 and 13.8 kPa which were applied in sequence) for 100 cycles. In total, 12 external stress levels (i.e. 12 combinations of σ_c and σ_d) were applied to test TSC and OCSC specimens. Same σ_d levels were applied on IHT specimens during conditioning phase and testing phase, however, only one net confining stress $\sigma_{c,net}$ of 27.6 kPa was applied during both phases. As the axis-translation technique was used, the applied σ_c was elevated to keep the $\sigma_{c,net}$ at 27.6 kPa. In total, four external stress levels (i.e. four combinations of $\sigma_{c,net}$ and σ_d) were applied to test IHT specimens. The M_R at each stress level was determined using the applied σ_d and the average ε_r values measured from the last five loading cycles for all the three soils.

5.2.4 Soil suction measurement and the soil-water characteristic curve

Contact filter paper method was performed using Whatman 42 filter paper as per ASTM D5298-10 (ASTM 2010) protocol to measure the suction of the TSC and OCSC specimens after the completion of the cyclic loading tests (shown in Figure 4). The test specimen was evenly sliced into four disks. Two disks were used to sandwich a filter paper set (a smaller circular filter paper sandwiched by two larger circular filter papers) and were wrapped tightly in two layers of plastic film. A stress of 1 kPa was applied (by placing an aluminium container filled with calculated mass of metal pellets) to ensure good contact between soil disks and filter papers (Power et al. 2008). This whole setup was thereafter sealed in a container to allow equilibrium for seven days prior to measuring the water content of the sandwiched filter paper (w_{fp}). The calibration equation suggested by ASTM D5298-10 (ASTM 2010) (Equation 5.1) was used to calculate the corresponding s values (denoted as s_{fp}) based on the w_{fp}.

$$\log s_{fp} = \begin{cases} 5.327 - 0.0779 w_{fp} & (w_{fp} < 45.3\%) \\ 2.412 - 0.0135 w_{fp} & (w_{fp} \geq 45.3\%) \end{cases} \tag{5.1}$$

The gravimetric water content of soil disks was also measured. The average gravimetric water content (w_{avg}) of the two soil disks and the corresponding s_{fp} value measured from the sandwiched filter paper are summarized in Table 5.3. These measured w_{avg} - s_{fp} relationships can be used as the soil-water characteristic curve (SWCC) for the TSC and the OCSC. It can be observed from Table 5.3 that i) the two w_{avg} values that were determined from the four disks of the specimen are quite close. This suggests that a uniform moisture content distribution profile was achieved within all specimens; and ii) the w_{avg} values are generally lower than the w_c values. This may be attributed to the moisture loss during the operation of the filter paper method.

The SWCC of the IHT was measured using the modified null pressure plate apparatus devised by Power and Vanapalli (2010). Three specimens (specimens A, B and C; 50 mm in diameter and 20 mm in height), which were prepared following similar procedures for the specimens used for cyclic loading tests, were wetted gradually to different lower suction values using the axis-translation technique to measure the w - s relationships (Specimens A and B were consecutively wetted to s values of 90, 60, 30 and 0 kPa while specimen C was wetted to s values of 100, 70, 50, 20 and 0 kPa). The w corresponding to each s was determined when the variation in the measured w in 24 hours was less than 0.1% (0.05 g variation in specimen mass). No significant volumetric change was observed during the wetting of the three specimens, which is consistent with the observation on the same IHT reported by Oh and Vanapalli (2013).

5.3 Experimental results

5.3.1 Soil-water characteristic curve

Figure 5.5 shows the measured SWCC data using symbols for the three soils. Measurements are also fitted using the Fredlund and Xing (1994) model (Equation 5.2) which uses three fitting parameters a, n and m.

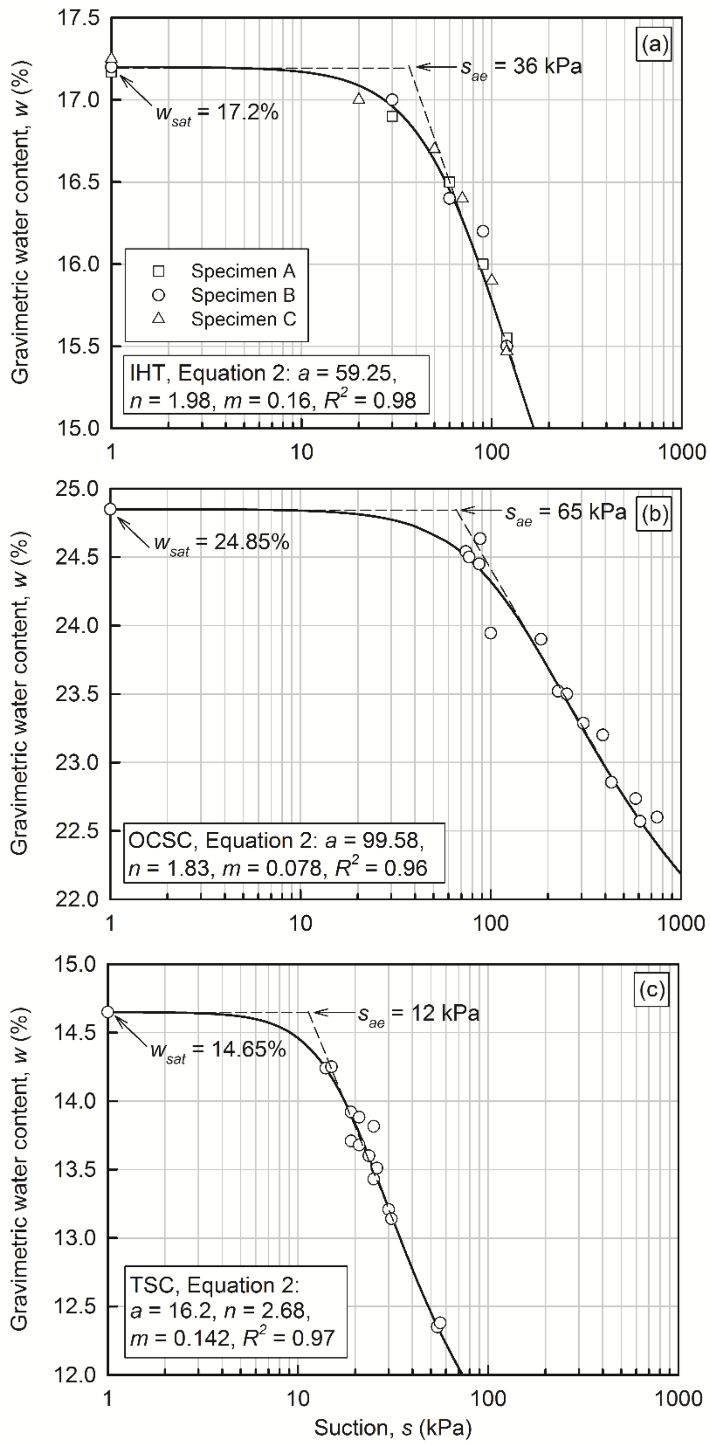

Figure 5.5 SWCC for the (a) IHT, (b) OCSC and (c) TSC

$$\frac{w}{w_{sat}} = \{\ln[2.718 + (\frac{s}{a})^n]\}^{-m} \tag{5.2}$$

The fitted SWCC curves are shown as solid lines in Figure 5.5 along with values of fitting parameters and the coefficient of determination (R^2). The air-entry value (s_{ae}) for each SWCC is determined using the graphical construction method suggested by Vanapalli et al. (1999). It can be observed from Figure 5.5 that there is an increase in the water-retention capacity (either indicated by the s_{ae} or by the slope of the SWCC when s exceeds the s_{ae}) from the TSC to the IHT and to the OCSC. This is consistent with the increase in the plasticity index and fines content for the three soils. Similar results are also reported by several other studies (e.g., Vanapalli et al. 1996, Chin et al. 2010, Chiu et al. 2012, Rahardjo et al. 2013). The suction of TSC and OCSC specimens were determined from the fitted SWCC shown in Figures 5.5(b) and 5.5(c) at their respective w_c values and are summarized in Table 5.3 as s_c. The s_c is used in this study to indicate the suction levels within the TSC and OCSC specimens as per earlier discussions.

5.3.2 Stress-dependent resilient modulus and the influence of soil suction

Similar to other soil stiffness properties, the M_R is sensitive to external shearing (e.g., σ_d) and confining stresses (e.g., σ_c and $\sigma_{c,net}$). The M_R - shearing stress relationship (e.g., M_R - σ_d relationship) is soil-type-dependent and is influenced by several factors associated with the application of the cyclic loadings which include: i) the increase in the density which contributes to an increase in the M_R, ii) the decrease in the suction which contributes to a decrease in the M_R and iii) the breakage of inter-particle bonds which contributes to a decrease in the M_R. The eventual M_R - shearing stress relationship for a specific soil is the result of the interplay among these factors (Sivakumar et al. 2013). For example, for fine-grained soils, studies such as Ng et al. (2013) and Salour et al. (2014) reported a decrease in the M_R with increasing shearing stress, while Parreira and Gonçalves (2000) reported an increase in the M_R with increasing shearing stress. Yang et al. (2008), however, reported that the M_R decreases with increasing shearing stress at lower suction range while a reverse trend was observed at higher suction range. The M_R - confining stress relationship, on the other hand, is quite consistent for different soils. Experimental data in the literature generally suggest an increase in the M_R with increasing confining stress. This can be attributed to the reason that the confining stress prevents the lateral expansion during axial cyclic loadings and contributes to the stiffness.

Exponential functions are usually used to predict the stress-dependent M_R. For example, Equation 5.3, which is recommended in the Mechanistic-Empirical Pavement Design Guide (MEPDG) (ARA, Inc., ERES Consultants Division 2004), links the M_R to the bulk stress θ and the octahedral shear stress τ_{oct} ($\theta = 3\sigma_c + \sigma_d$ and $\tau_{oct} = 0.471\sigma_d$ for conventional triaxial tests; if the axis-translation technique is used, θ should be replaced by the net bulk stress θ' and $\theta' = 3\sigma_c + \sigma_d - 3u_a$) using three model parameters k_1, k_2 and k_3 and the atmospheric pressure p_a. More comprehensive discussions on stress-dependent models are available in LeKarp et al. (2000) and Puppala (2008).

$$M_R = k_1 p_a \left(\frac{\theta}{p_a}\right)^{k_2} \left(\frac{\tau_{oct}}{p_a} + 1\right)^{k_3} \tag{5.3}$$

Equation 5.3 is used in this study to predict the M_R - external stress relationship. Table 5.4 summarizes k_1, k_2 and k_3 values of Equation 5.3 for all the specimens along with the respective R^2 values. In addition, representative resilient modulus (M_{Rrep}) values (sometimes also referred to as summary resilient modulus in the literature) are calculated for all specimens at σ_d = 48.2 kPa and σ_c or $\sigma_{c,net}$ = 27.6 kPa (mean values of σ_d and σ_c applied during the cyclic loading tests; in such case, θ or θ' = 131 kPa and τ_{oct} = 22.7 kPa) using Equation 5.3 and the respective k_1, k_2 and k_3 values and summarized in Table 5.4. The M_{Rrep} indicates an average M_R value of pavement materials under a certain external stress range. The M_{Rrep} is typically used as the M_R of pavement layers for which the influence of external stress on the M_R is not considered (e.g., in simplified method for the design of pavement of less significance) or is not significant (e.g., for pavement layers at greater depth where the external stress level is low).

Figure 5.6 shows the measured M_R - σ_d relationships for IHT specimens (using symbols) and the predictions using Equation 5.3 (using continuous lines). It can be observed that the M_R slightly decreases with increasing σ_d and increases with increasing s_0. Figures 5.7 and 5.8 show measured M_R - σ_d - σ_c relationships (using symbols) for the TSC and the OCSC respectively at w_{sat}, w_{opt} and an intermediate w ($w_{opt} < w < w_{sat}$). Predictions using Equation 5.3 are also shown in a mesh format in Figures 5.7 and 5.8. Similar to the IHT, the M_R of the TSC and the OCSC increases with increasing s_c and decreasing w. The M_R increases with increasing σ_c for both soils. However, the M_R of the TSC increases with increasing σ_d while the M_R of the OCSC decreases with increasing σ_d. Factors such as densification outweigh the factors such as the degradation in the particle bond and suction, which results in an overall increase in the M_R with increasing shearing stress for the TSC. Results of such interplay for the OCSC was however opposite to that of the TSC. Also, the M_R - σ_d and M_R - σ_c relationships are influenced by s_c and w levels. This can be observed from Figures 5.6, 5.7 and 5.8 that the variation of the measured and predicted M_R with respect to the σ_d and σ_c axis varies at different s_c and w values. Generally, the M_R is more sensitive to σ_d and σ_c changes at higher s_c levels. Such a trend suggests that the M_R - external stress and M_R - suction relationships have mutual-influence and therefore show coupled characteristics (Han and Vanapalli 2016a).

Table 5.4 Model parameters of Equation 5.3 and the M_{Rrep} for the three soils

Sample ID	k_1	k_2	k_3	R^2	M_{Rrep} (MPa)
IHT-1 (M_{Rsat})	76.1	-6.02	10.09	0.99	11.80
IHT-2	1620	9.44	-20.88	0.99	28.94
IHT-3	602	2.21	-4.75	0.92	41.38
IHT-4	695.8	0.87	-2.95	0.99	48.13
IHT-5 (M_{Ropt})	505.4	-2.25	4.08	0.99	63.43
TSC-1 (M_{Rsat})	321.5	0.31	-0.17	0.97	33.76
TSC-2	387.2	0.39	-0.34	0.98	40.13
TSC-3	401.5	0.46	-0.34	0.96	42.41
TSC-4	407.6	0.47	-0.45	0.98	42.21
TSC-5	469.5	0.50	-0.75	0.99	46.09
TSC-6	436.1	0.45	-0.29	0.99	46.41
TSC-7 (M_{Ropt})	476.4	0.39	-0.53	0.93	47.49
TSC-8	418.1	0.24	0.67	0.97	51.16
OCSC-1 (M_{Rsat})	273	1.20	-4.12	0.96	16.25
OCSC-2	267.4	0.40	-0.78	0.94	25.40
OCSC-3	247.9	0.21	-0.15	0.89	25.44
OCSC-4	533.8	0.39	-1.33	0.97	45.18
OCSC-5	469.5	0.22	-1.07	0.67	40.03
OCSC-6	720.9	-0.07	-0.02	0.80	70.45
OCSC-7 (M_{Ropt})	1170	0.29	-1.79	0.94	87.73
OCSC-8	1279	0.15	-1.76	0.86	92.92

Note: In Equation 5.3, θ, τ_{oct} and M_R are in kPa, and P_a = 100 kPa when determining the model parameters.

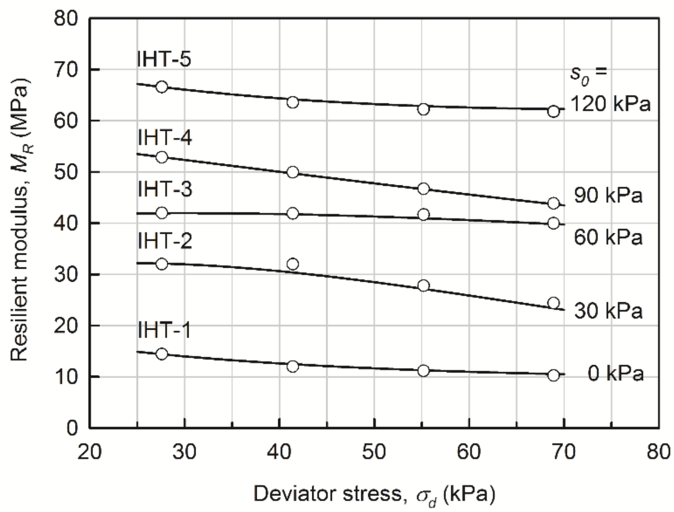

Figure 5.6 M_R - σ_d relationships for the IHT at various s_0 levels

Note that the s_0 and s_c are used to indicate suction levels in IHT specimens (using s_0, see in Table 5.2) and TSC and OCSC specimens (using s_c, see in Table 5.3), respectively. In order to avoid complexity and possible confusion in the notation, the suction (s) is used as the s_0 or s_c for all specimens in the interpretation that follows. Figure 5.9 shows the measured variation of the M_{Rrep} with respect to the s and w (using symbols). The use of s / s_{opt} and (w – w_{opt}) / (w_{sat} – w_{opt}) in Figure 5.9 is to unify the scales of the s and w for the three soils and to highlight the variation of the M_{Rrep} from saturated condition ($M_{Rrep,sat}$) to optimum moisture content condition ($M_{Rrep,opt}$). It can be observed that both M_{Rrep} - s and M_{Rrep} - w relationships are non-linear, and the sensitivity of the M_{Rrep} to the s, which can be indicated by the increase in the M_{Rrep} from $M_{Rrep,sat}$ to $M_{Rrep,opt}$, increases with the soil plasticity (larger increase is observed for the OCSC while slight increase is observed for the TSC). This is consistent with the experimental observations reported in several other studies in the literature (Drumm et al. 1997, Khoury and Zaman 2004, Sawangsuriya et al. 2009, Salour et al. 2014).

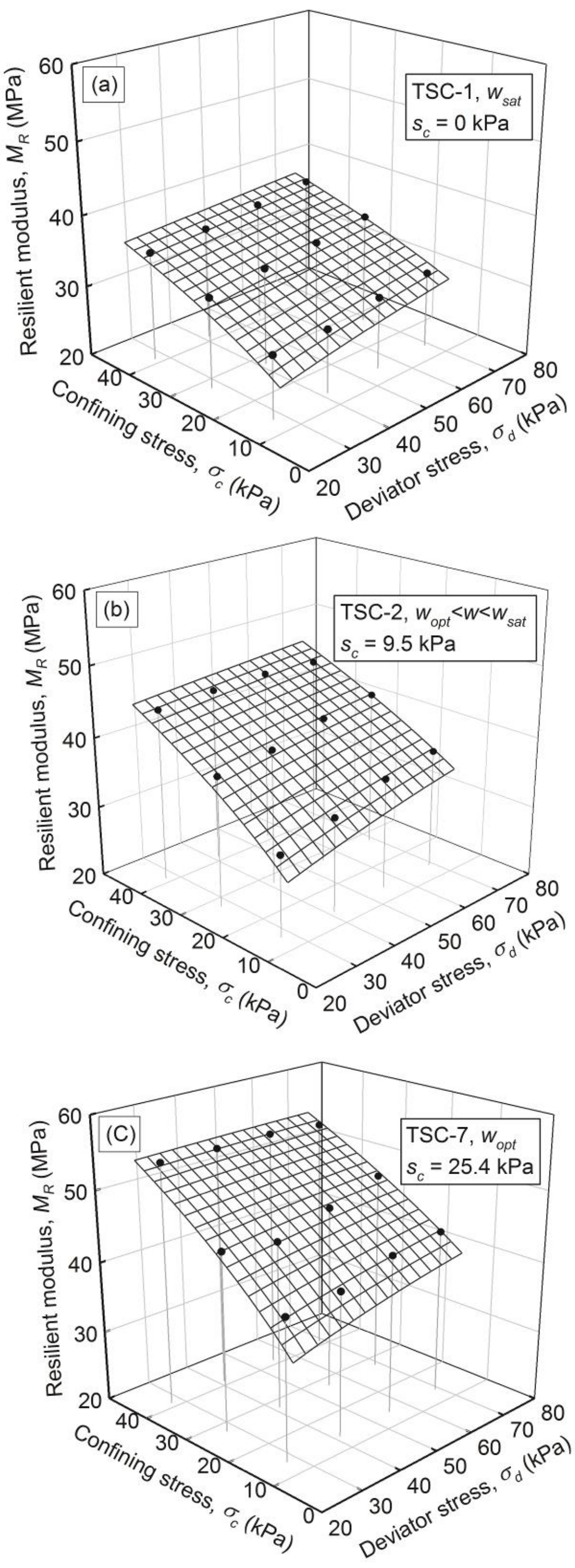

Figure 5.7 M_R - σ_d - σ_c relationships for: (a) TSC-1, (b) TSC-2 and (c) TSC-7

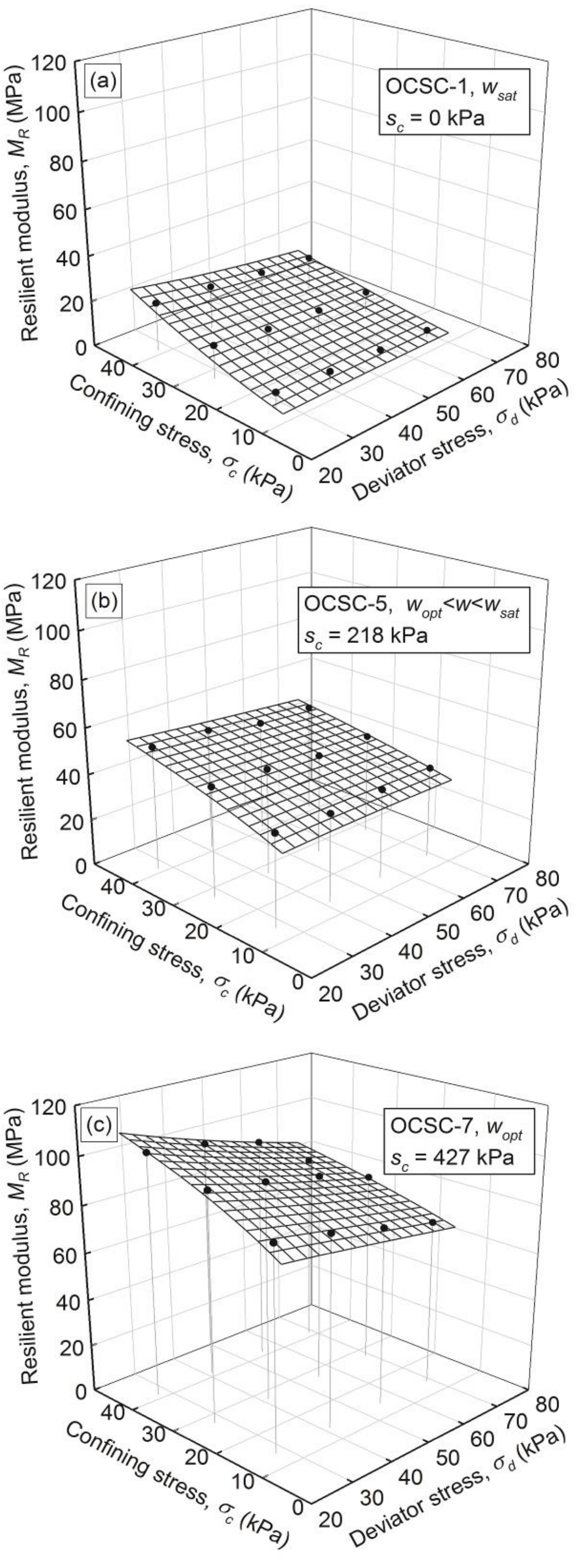

Figure 5.8 M_R - σ_d - σ_c relationships for: (a) OCSC-1, (b) OCSC-5 and (c) OCSC-7

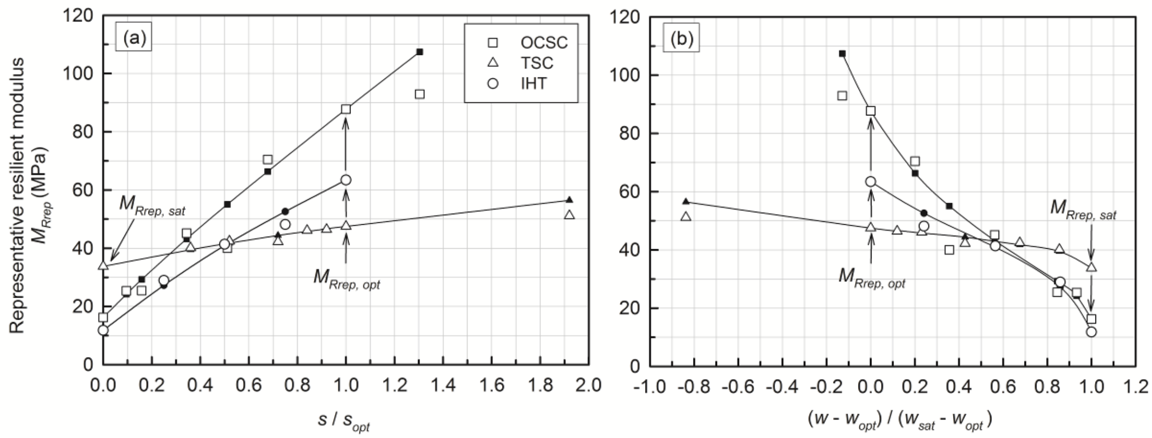

Figure 5.9 Variation of M_{Rrep} with (a) s / s_{opt} and (b) ($w - w_{opt}$) / ($w_{sat} - w_{opt}$) for the three soils

5.4 Model for predicting the resilient modulus

Han and Vanapalli (2015) proposed a normalized model (Equation 5.4) to predict the M_R - s relationship. This model is formed using values of M_R and soil physical states at saturated condition (indicated by subscript $_{sat}$; i.e. M_{Rsat}) and optimum moisture content condition (indicated by subscript $_{opt}$; i.e. M_{Ropt}, s_{opt} and S_{ropt}), and a model parameter ξ for predicting the M_R - s relationship:

$$\frac{M_R - M_{Rsat}}{M_{Ropt} - M_{Rsat}} = \frac{s}{s_{opt}} \left(\frac{S_r}{S_{ropt}}\right)^{\xi} \tag{5.4}$$

If e variation is negligible within the specimens, the volume-mass relationship $S_r = wG_s / e$ can be substituted into Equation 5.4 to yield Equation 5.5. Equation 5.5 is simpler to use as the gravimetric water content w can be easily and reliably measured.

$$\frac{M_R - M_{Rsat}}{M_{Ropt} - M_{Rsat}} = \frac{s}{s_{opt}} \left(\frac{w}{w_{opt}}\right)^{\xi} \tag{5.5}$$

There are several advantages of using Equation 5.4 and Equation 5.5 for predicting the M_R - s relationship:

i) The S_r or w corresponding to the s can be estimated using the SWCC;

ii) This model was validated by Han and Vanapalli (2015) using the M_R - s relationship derived from 11 different compacted subgrade soils. Han and Vanapalli (2015) suggested that the model parameter ξ, which should be determined from regression analysis performed on a large number of testing data at various s levels, typically falls within a narrow range between 1.0 and 3.0. However, an intermediate ξ value of 2.0 provides reasonable predictions for different subgrade soils. Therefore, if a constant ξ value of 2.0 is used in Equations 5.4 and 5.5, the required information in the model for prediction is reduced only to the SWCC, M_{Rsat}, M_{Ropt}, and s_{opt}. The experimental data on the M_R - s relationship at suction levels other than s_{opt} and s = 0 are required by other models in the literature for prediction. However, these information is not required for using Equations 5.4 and 5.5. In other words, this model significantly simplifies the prediction procedure. More details are provided to highlight the advantages of the model in a later section;

iii) The M_{Rsat} and M_{Ropt}, which are required for using Equation 5.5, can be measured using conventional cyclic loading tests without suction control. They are also the key information required in the mechanistic pavement design methods to analyze the as-compacted pavement layers (using M_{Ropt}) and the layers under the worst scenario (using M_{Rsat} for layers that are totally saturated);

iv) If M_{Rsat} and M_{Ropt} in Equations 5.4 and 5.5 are fitted using stress-dependent model, the influence of external stress on the M_R - s relationship can also be predicted. In this chapter, Equation 5.3 is used to describe the stress-dependent M_{Rsat} and M_{Ropt} and is substituted into Equation 5.5 to predict the measured M_R - external stress - suction relationship for the three soils.

5.4.1 Model performance

An examination on the performance of the simple model is shown in Figure 5.9 where measurements on the M_{Rrep} - s and M_{Rrep} - w relationship shown as symbols are predicted using Equation 5.5. Measured $M_{Rrep,opt}$ and $M_{Rrep,sat}$ values and fitted SWCC curves shown in Figure 5.6 for the three soils and a ξ value of 2.0 are used in Equation 5.5 for prediction.

It can be observed that predictions shown as continuous lines with closed symbols well simulate the measured variations of M_{Rrep} with s and w for all the three soils.

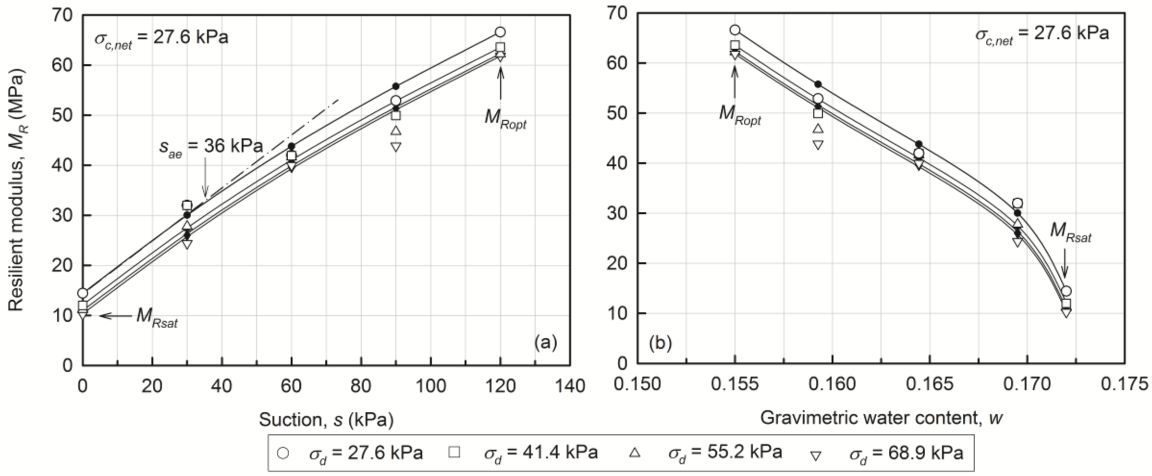

Figure 5.10 Measurements and predictions on the (a) M_R - s and (b) M_R - w relationships for the IHT

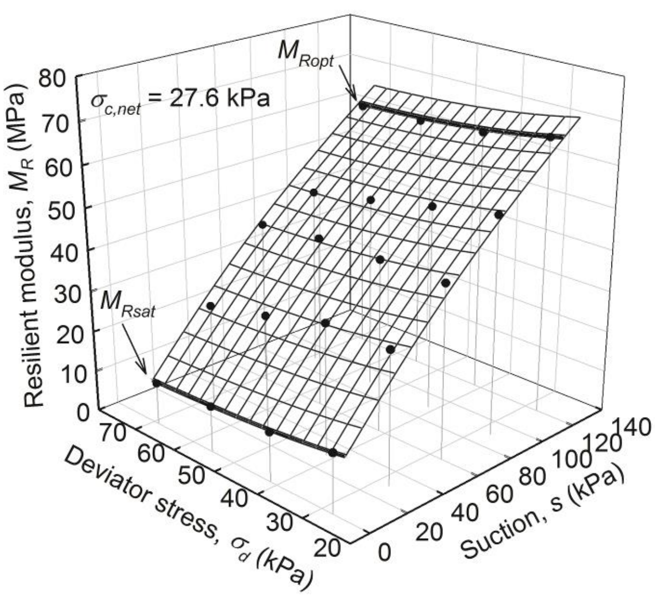

Figure 5.11 Measurements and predictions on the M_R - σ_d - s relationships for the IHT

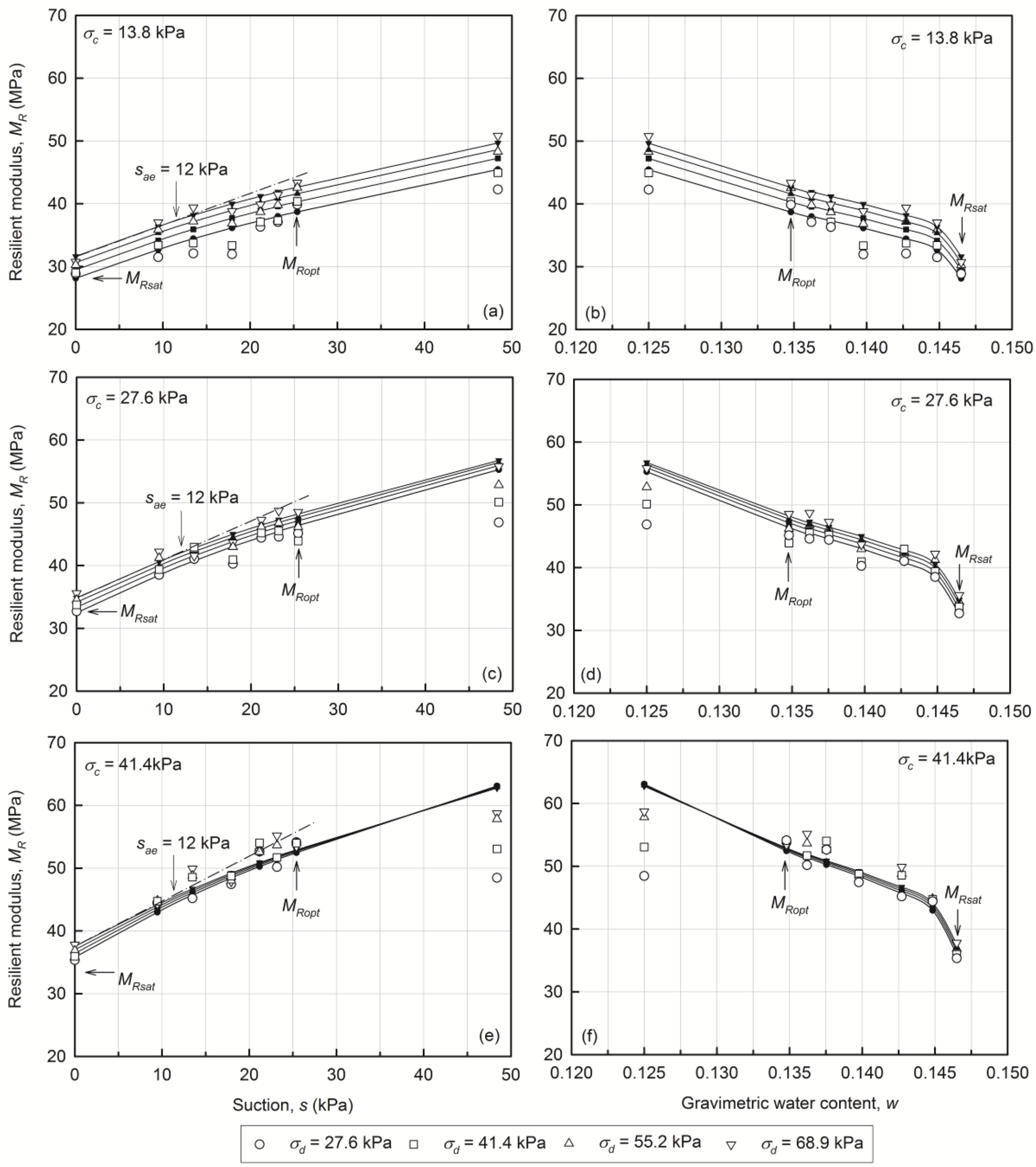

Figure 5.12 Measurements and predictions on the (a), (c), (e) M_R - s and (b), (d), (f) M_R - w relationships under different σ_c levels for the TSC

Detailed predictions are carried out by substituting Equation 5.3 into Equation 5.5 to describe the M_{Ropt} and M_{Rsat} and using $\xi = 2.0$. The k_1, k_2 and k_3 values for M_{Ropt} and M_{Rsat} summarized in Table 5.4 are used in Equation 5.3. Figure 5.10 shows comparisons between measurements (in open symbols) and predictions (in continuous lines with closed symbols) on M_R - s and M_R - w relationships under a $\sigma_{c,net}$ of 27.6 kPa for the IHT. Same comparisons are also shown in Figure 5.11 in the M_R - σ_d - s space as mesh (predictions) versus symbols (measurements). It can be observed from Figure 5.10 that the predicted M_R - s curves at each σ_d level are non-linear. The measured M_R - s and M_R - w relationships at various external stress levels for the IHT are well predicted as can be observed from Figures 5.10 and 5.11.

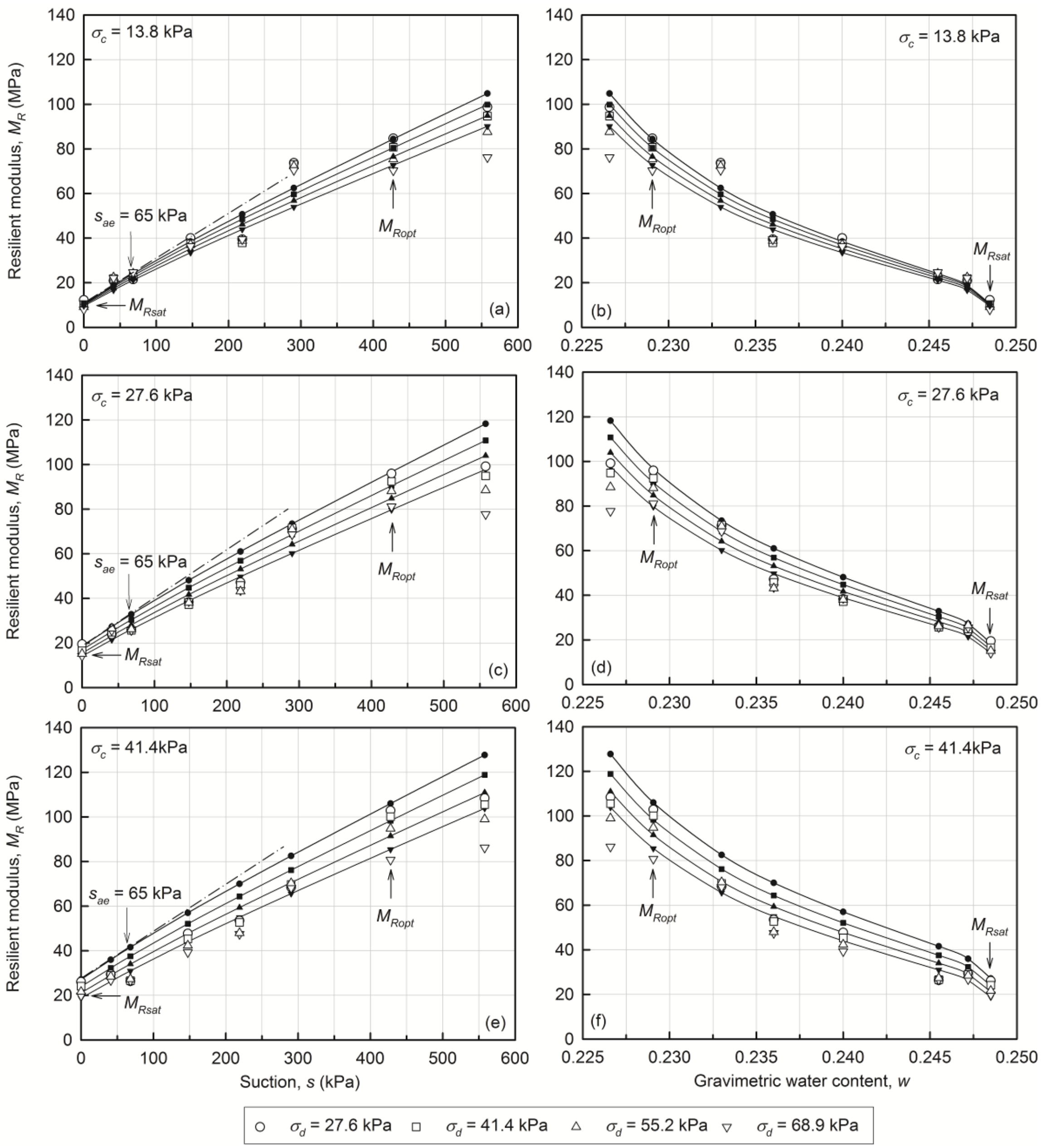

Figure 5.13 Measurements and predictions on the (a), (c), (e) M_R - s and (b), (d), (f) M_R - w relationships under different σ_c levels for the OCSC

Similarly, predictions on the M_R - s and M_R - w relationships under different external stress levels are shown in Figures 5.12 and 5.13 for the TSC and the OCSC, respectively. Predicted M_R - s curves shown in Figures 5.12 and 5.13 present similar non-linear characteristics as shown in Figure 5.10 for the IHT. In addition, it has been shown in Figures 5.7 and 5.8 that the M_R of the TSC and the OCSC respond differently to the increasing σ_d. It can be observed from Figures 5.12 and 5.13 that the M_R of the two soils are reasonably predicted.

In total, under different external stress and suction levels, 20 measurements on the M_R were made for the IHT, 96 measurements on the M_R were made for the TSC and OCSC, respectively. The R^2 values achieved using Equations 5.3 and 5.5 and a constant ξ value of 2.0 are 0.97 for the IHT, 0.93 for the OCSC and 0.88 for the TSC, which suggest reasonably good predictions. In addition, regression analysis was also performed using the whole range of experimental data at all s and w levels for each soil to determine the ξ value that yields the highest R^2. Determined values are: ξ = 1.65, R^2 = 0.98 for the IHT, ξ = 1.92, R^2 = 0.93 for the OCSC, and ξ = 2.6, R^2 = 0.90 for the TSC. Results suggest that i) optimum ξ values for the three soils vary between 1.0 and 3.0 which is consistent with the ξ range reported by Han and Vanapalli (2015); ii) there will be an increase in the R^2 if ξ values determined by performing regression analysis on the entire range of experimental data are used; however, a unique value of ξ of 2.0 also provides comparatively good predictions.

5.4.2 Comparison with other models

Two rigorous models that were developed based on different principles are used to predict the measurements of the three soils investigated in this study. Ng et al. (2013) proposed Equation 5.6, which formulates the s into an independent item that is parallel to the items representing the influence of the external stresses (i.e. net mean stress p, $p = \theta / 3$ for conventional triaxial tests and $p = \theta' / 3$ if the axis-translation technique is used; and cyclic shear stress q_{cyc}, $q_{cyc} = 0.9\sigma_d$ as per AASHTO 2003), to predict the M_R - s - external stress relationship.

$$M_R = k_{1N} (\frac{p}{p_r})^{k_{2N}} (1+\frac{q_{cyc}}{p_r})^{k_{3N}} (1+\frac{s}{p})^{k_{4N}} \tag{5.6}$$

where k_{1N}, k_{2N}, k_{3N} and k_{4N} = model parameters, p_r = reference pressure = 1 kPa.

Yang et al. (2008) proposed Equation 5.7, which incorporates the contribution of s to the confining stress θ (or θ' if the axis-translation technique is used) using Bishop's effective stress parameter χ (Bishop 1959) for predicting the M_R - s - external stress relationship. They suggested using the empirical relationship proposed by Khalili and Khabbaz (1998) (Equation 5.8) to estimate the χ value.

$$M_R = k_{1L} p_a \left(\frac{\theta + \chi s}{p_a}\right)^{k_{2L}} \left(1 + \frac{\tau_{oct}}{p_a}\right)^{k_{3L}} \tag{5.7}$$

where k_{1L}, k_{2L} and k_{3N} = model parameters.

$$\chi = \begin{cases} (s / s_{ae})^{-0.55} & (s > s_{ae}) \\ 1 & (s \le s_{ae}) \end{cases} \tag{5.8}$$

Equations 5.6 and 5.7 were formulated following two typical approaches that are used in the literature to consider the influence of suction (Han and Vanapalli 2016a). Both equations have provided reasonable predictions for the soils for which they were developed as well as for several other soils (Yang et al. 2008, Ng et al. 2013, Salour and Erlingsson 2015, Han and Vanapalli 2016a). They are therefore used to predict the M_R - s - external stress relationship for the IHT, the TSC and the OCSC. It is noted that the SWCC is not required in Equation 5.6; however, it is necessary in Equations 5.7 and 5.8 to determine the s_{ae} and χ values. The s_{ae} values shown in Figure 5.5 are used in Equation 5.8 to determine the χ for Equation 5.7.

Table 5.5 summarizes model parameters values in Equations 5.6 and 5.7, achieved R^2 values and the Required Number of Testing Data (RNTD) for prediction for the three soils. Equations 5.6 and 5.7 have formulations similar to that of Equation 5.3; however, their respective model parameters (k_{1N}, k_{2N}, k_{3N} and k_{4N} in Equation 5.6 and k_{1L}, k_{2L} and k_{3N} in Equation 5.7) are different from those used in Equation 5.3 (k_1, k_2 and k_3) and should be determined from regression analysis using the M_R values measured at the entire suction and external stress levels (compare model parameter values summarized in Table 5.4 and Table

5.5). Therefore, 20 measured data of IHT (5 specimens, 4 data for each specimen) and 96 measured data of TSC and OCSC each (8 specimens, 12 data for each specimen) are required for using Equations 5.6 and 5.7. On the other hand, using Equations 5.3 and 5.5 with a ξ value of 2.0 for prediction requires only the data of M_{Rsat} and M_{Ropt}. In this case, only 8 measured data of IHT (specimens IHT-1 and IHT-5, 4 data for each specimen), 24 measured data of TSC (specimens TSC-1 and TSC-7, 12 data for each specimen) and 24 measured data of OCSC (specimens OCSC-1 and OCSC-7, 12 data for each specimen) are required for prediction.

Table 5.5 Details of using three different models for prediction

Models	Details	IHT	TSC	OCSC
Equation 5.6 (Ng et al. 2013)	RNTD	20	96	96
	R^2	0.97	0.89	0.94
	k_{1N}	1800	5050	1462
	k_{2N}	0.71	0.564	0.831
	k_{3N}	-0.143	-0.042	-0.231
	k_{4N}	1.064	0.503	0.733
Equation 5.7 (Liang et al. 2008)	RNTD	20	96	96
	R^2	0.97	0.8	0.87
	k_{1L}	152.4	390.7	185.2
	k_{2L}	4.253	0.514	1.821
	k_{3L}	-6.916	-0.375	-2.683
Equations 5.3 and 5.5 ($\xi = 2.0$) (Han and Vanapalli 2015)	RNTD	8	24	24
	R^2	0.97	0.88	0.93

Notation: RNTD = Required Number of Testing Data for prediction.
Note: θ, τ_{oct} and M_R are in kPa, and p_a = 100 kPa when determining the model parameters for Equations 5.6 and 5.7.

All three models have provided good predictions for all three soils with a minimum R^2 value of 0.8 as can be observed from Table 5.5. Figure 5.14 shows an example of predictions of Equations 5.6 and 5.7 for the IHT. From comparison of predictions shown in Figures 5.11 and 5.14, it can be observed that the three models extend meshes of different characteristics in the M_R - s - σ_d space and well predict the measured variation of the M_R with suction and external stress levels for the IHT. It is encouraging to note that the simple model requires remarkably less testing data than the other two models to provide equally good predictions. The performance of the simple model using constant model parameter ξ

= 2.0 was validated by 11 different subgrade soils in Han and Vanapalli (2015) as well as three subgrade soils in this study. It is therefore suggested that this model with a ξ value of 2.0 is suitable for predicting M_R - s relationships for different fine-grained subgrade soils. This model simplifies the prediction procedures for M_R - s relationship and reduces the experimental work and associated costs while ensuring the reliability of the prediction.

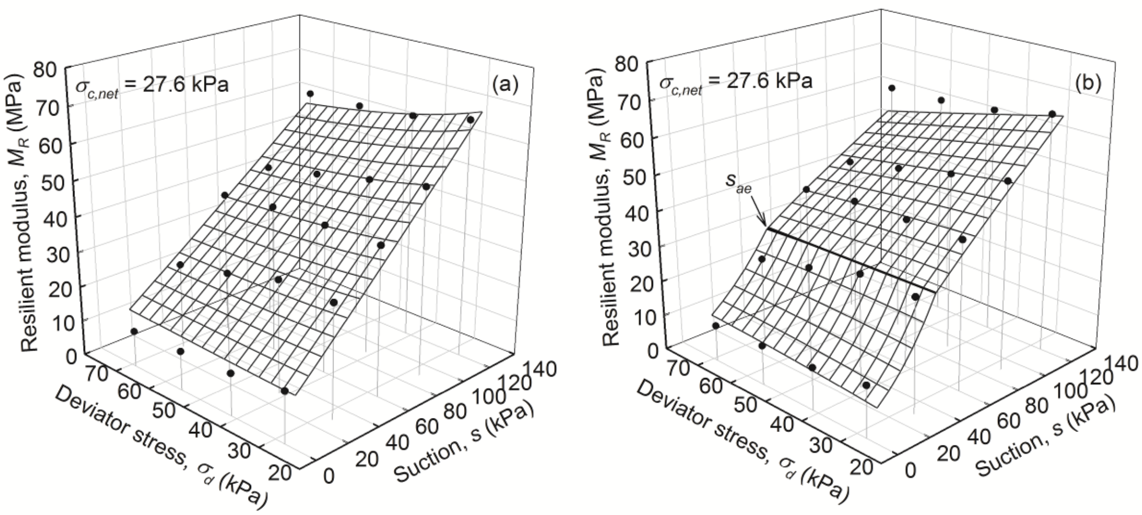

Figure 5.14 Measurements and predictions on the M_R - σ_d - s relationships for the IHT using (a) Equation 5.6 and (b) Equation 5.7

5.5 Discussion and conclusion

The axis-translation technique and filter paper method, which are frequently used in unsaturated soils testing, were adopted to control or measure the suction of the specimens. The ELDyn system that accommodates the axis-translation technique is used to consolidate the IHT specimen to a specified initial suction (s_0) and stress level prior to the cyclic loading test. Such system has been widely used in recent years to determine the M_R - s_0 relationships (Khoury et al. 2011, Ng and Zhou 2014) as well as to determine the influence of s on other mechanical properties (e.g., Khalili and Zargarbashi 2010, Gui and Wu 2014, Hoyos et al. 2015). There are however concerns regarding the use of the axis-translation technique with respect to the time required for suction equilibrium, which is typically excessive, especially for clays (Tinjum et al. 1997, Yang et al. 2008, Khoury et al. 2011; also see the equilibrium time summarized in Table 2). In addition, the elevation of both u_a

and u_w to positive values to supress cavitation effects is not a representative scenario of in-situ condition and may alter the interaction between soil particles and air-water menisci and lead to different soil behavior in comparison to the in-situ behavior (Baker and Frydman 2009).

In several studies, including the current study (for the TSC and OCSC), filter paper method was used to measure the *s* after the cyclic loading test (Khoury and Zaman 2004, Yang et al. 2005, Liang et al. 2008, Azam et al. 2013). The SWCC determined for the TSC and OCSC (Figures 5.5b and 5.5c) also represents the relationship between the *s* and *w* after the cyclic loading test. There are concerns that the *s* measured using this procedure may not precisely represent the suction level of the specimen because i) filter paper method is usually performed regardless of the stress condition applied during the cyclic loading tests, which however influences the *s* (Vanapalli et al. 1999, Ng and Pang 2000, Power and Vanapalli 2010) and ii) filter paper method results are user-dependent and also sensitive to testing procedure and equipment precision (Power et al. 2008). The suction levels and SWCC derived i) before cyclic loading for the IHT and ii) after cyclic loading for the TSC and OCSC are both devoted to indicate or approximate the actual suction levels and SWCC within the specimen during the cyclic loading that are required in Equation 5.5. In spite of the limitations of these experimental procedures, it has been shown in the current study that Equation 5.5 provides reasonable predictions of M_R - *s* relationships for different soils tested using two different methods for control / measure the suction (i.e. the axis-translation technique and the filter paper method). More reliable determination or estimation methods of the suction levels and SWCC during the cyclic loadings will be useful for better understanding the M_R - *s* relationships.

Certain experimental efforts are necessary to reliably determine the M_{Rsat} and M_{Ropt} values. This is because that i) the M_{Rsat} and M_{Ropt} values directly influence the predicted M_R - *s* relationships and ii) the variation of the M_{Rsat} and M_{Ropt} with external stress influences the predicted M_R - external stress relationships at other suction levels. There are several empirical relationships that can be used for estimating the model parameters of stress-dependent models and therefore the M_R. These relationships typically relate the model parameters to soil physical properties such as w, γ_d, I_p, percentage of fines and unconfined compression strength (Malla and Joshi 2008, Zaman et al. 2010). These relationships have greatly contributed to simplify the estimation of the M_R. However, they should be used with greatest caution by checking whether or not the experimental procedure, equipment and target soils are consistent with those used for developing these empirical relationships. If not, experimental determination of the M_{Rsat} and M_{Ropt} is recommended.

In summary, the variation of M_R with respect to the suction for three Canadian subgrade soils was investigated in this chapter. The M_R - s relationships are typically non-linear and are influenced by the external stress level and soil type. The M_R of soil with higher plasticity is more sensitive to the changes in the s and w. Experimental results are reasonably well predicted using a simple model proposed by Han and Vanapalli (2015) that provides predictions based on the SWCC, M_{Rsat}, M_{Ropt} and s_{opt}, which are easy to obtain. It is demonstrated that this simple model, compared with two other rigorous models in the literature, provides equally good predictions but requires remarkably less experimental data. Experimental studies in this chapter presents useful experimental evidence on the resilient behavior of several Canadian subgrade soils. The simple model is encouraging for reliably predicting the M_R of compacted subgrade soils for the design of pavements taking account of the influence of moisture regime and suction.

CHAPTER SIX

NORMALIZING VARIATION OF SOIL STIFFNESS AND SHEAR STRENGTH WITH MOISTURE CONTENT

6.0 Background-Information

The contents presented in this chapter are from the submitted manuscript currently under review:

Han, Z., and Vanapalli, S. K. Normalizing variation of soil stiffness and shear strength with moisture content. Submitted to *ASCE Journal of Geotechnical and Geoenvironmental Engineering* in March 2016.

The symbols used in this chapter are summarized in Table 6.0.

Table 6.0 Symbols used in Chapter Six

Symbols	
a_f, n_f, m_f	model parameters for Fredlund and Xing (1994) SWCC equation
a_v, n_v, m_v	model parameters for van Genuchten (1980) SWCC equation
E	elastic modulus
e	base of natural logarithm
e_0	void ratio
G	shear modulus
G_s	specific gravity
I_p	plasticity index
k_1, k_2, k_3	model parameters for stress-dependent equations
M	constraint modulus
m', n', ξ'	model parameters
M_R	resilient modulus
M_{Rrep}	representative resilient modulus
p_a	atmosphere pressure
q_u	unconfined compression strength
R^2	coefficient of determination
s	soil suction
s_{ae}	air-entry value

Table 6.0 Symbols used in Chapter Six

Symbols	
S_r	water degree of saturation
$S_{u1\%}$	σ_a at ε_a = 1% during UC tests
subscript $_{opt}$	corresponding parameters at optimum moisture content condition
subscript $_{ref}$	corresponding parameters at referencing condition
subscript $_{sat}$	corresponding parameters at saturation condition
u_a	pore-air pressure
u_w	pore-water pressure
w	gravimetric water content
w_L	liquid limit
γ_{dmax}	maximum dry unit weight
ε_a	axial strain
ε_r	resilient strain
θ	bulk stress
θ'	net bulk stress
ξ	model parameter
σ_a	axial stress
σ_c	confining stress
$\sigma_{c,net}$	net confining stress
σ_d	deviator stress
σ_{dmax}	maximum deviator stress
τ_{oct}	octahedral shear stress
Ω	stiffness or shear strength properties

6.1 Introduction

Stiffness and shear strength of unsaturated soils, which are collectively denoted as Ω in this chapter, are sensitive to the moisture content and soil suction (s). The Ω - moisture content relationships show remarkable diversity for different soil types and are difficult to describe using the empirical equations (Heath et al. 2004, Ng et al. 2013). Considerable success has been achieved in recent years in the interpretation of the Ω - moisture content relationships by quantifying s as a contributor to the external stress or to the Ω and modelling the Ω - s relationships (Lu and Likos 2006, Yang et al. 2008, Sawangsuriya et al. 2009b, Khosravi and McCartney 2012, Tang et al. 2015, Han and Vanapalli 2016b). Meniscus water lenses within unsaturated soils restrain the loading-induced straining processes including (i) the bending of soil particles and the flattening of the inter-particle and inter-packet contacts that lead to elastic deformation, and (ii) slippage and friction at contacts and particle crushing and rearrangement that lead to shear failure, and therefore influence the Ω (Wheeler et al. 2003, Sheng 2011). There is significant evidence in the literature suggesting that the restraining effects are similar for both stiffness and shear strength behavior. Due to this reason, different Ω - s and Ω - moisture content relationships can be possibly analyzed using a common approach (Khalili et al. 2004, Alonso et al. 2010, Han and Vanapalli 2016b).

This chapter aims at developing a unified approach for describing the various Ω - moisture content relationships. Experimental investigations are undertaken to determine the variation of the resilient modulus (M_R), elastic modulus (E) and unconfined compression strength (q_u) with respect to s and gravimetric water content (w) for four unbound subgrade soils collected from various locations in Canada. These soils include, namely; a silty clay from Toronto (TSC), a lean clay from Kincardine (KLC), a glacial till from Indian Head (IHT) and a marine clay (Leda clay) from Ottawa (OLC). The M_R, which is the key property used in the mechanistic pavement design methods, is defined as the ratio of the cyclic deviator stress (σ_d) to the resilient strain (ε_r). The M_R is determined using an advanced triaxial equipment that facilitates the application of cyclic loading and soil suction. The E and q_u, which are widely used in conventional geotechnical design and material characterization, are determined using the same triaxial equipment from modified unconfined compression tests (modified UC tests) which allow an unloading-reloading loop starting at an axial strain (ε_a) level of 1%. Identical specimens are prepared for each soil by compacting them at their respective optimum moisture content (w_{opt}) and maximum dry unit weight (γ_{dmax}). Specimens are thereafter wetted or dried to different *w* and *s* levels before testing. The *s* of the IHT specimens for the M_R tests is imposed using the axis-translation technique while *s* of specimens of other three soils is measured using the filter paper method. Experimental investigations reveal that the variation of M_R, *E* and q_u with respect to the *s* and *w* is different for the same soil. Also, distinct Ω - *w* relationships are observed for the four different soils.

The methodology proposed by Han and Vanapalli (2016b) for predicting the Ω - *s* relationships is extended to normalize and interpret the experimentally determined M_R - *w*, *E* - *w* and q_u - *w* relationships. Similar characteristics are observed from the normalized M_R - *w*, *E* - *w* and q_u - *w* relationships. Such similarities can be used to predict the M_R - *w* relationships which are cumbersome and time-consuming to determine from the *E* - *w* and q_u - *w* relationships which can be determined from simple and conventional tests. In this study, the measured M_R - *w* relationships are reasonably well predicted from the measured *E* - *w* and q_u - *w* relationships for the four soils tested. Experimental data on various Ω - moisture content relationships for several soils reported in the literature are also collected and normalized using the proposed approach. Similarities are also observed from these normalized relationships. Studies presented in this chapter are encouraging for rationally estimating the soil stiffness and shear strength properties taking account of the influence of moisture content using simple yet reliable technique.

6.2 Theoretical development

Han and Vanapalli (2016b) proposed a methodology that normalizes the Ω - *s* and the degree of saturation (S_r) - *s* relationships (defined by the soil-water characteristic curve, SWCC) to the same scale.

$$\frac{\Omega-\Omega_{sat}}{\Omega_{ref}-\Omega_{sat}}=\frac{s}{s_{ref}}\left(\frac{S_r}{S_{rref}}\right)^{\xi} \tag{6.1}$$

where subscripts *ref* and *sat* indicate the corresponding parameters at a random referencing unsaturated condition and saturated condition, respectively. The ξ is a model parameter that typically varies between 1.0 and 3.0 for different soil types. The S_r corresponding to each s can be estimated from the SWCC using equations such as those proposed by van Genuchten (1980) (Equation 6.2) or Fredlund and Xing (1994) (Equation 6.3).

$$S_r = [1+(a_v s)^{n_v}]^{-m_v} \tag{6.2}$$

$$S_r = \left\{ \ln[e+(s/a_f)^{n_f}] \right\}^{-m_f} \tag{6.3}$$

where a_v, n_v, m_v and a_f, n_f, m_f are model parameters and e is the base of natural logarithm. In Equation 6.2, empirical relationship $n_v = 1 / (1 - m_v)$ can be used for simplification.

Han and Vanapalli (2016b) suggested that the reference unsaturated condition (i.e. Ω_{ref}, S_{rref} and s_{ref}) does not influence the validity of Equation 6.1. For compacted soils, optimum moisture content condition (parameters correspond to this condition are denoted using subscript *opt*) is suitable to be used as the reference unsaturated condition because such soils are usually compacted at w_{opt} to achieve γ_{dmax} and favorable engineering performance. For such a scenario, Equation 1 becomes Equation 6.4.

$$\frac{\Omega - \Omega_{sat}}{\Omega_{opt} - \Omega_{sat}} = \frac{s}{s_{opt}} \left(\frac{S_r}{S_{ropt}}\right)^{\xi} \tag{6.4}$$

If a constant void ratio e_0 is assumed for compacted soils, the relationship $S_r = wG_s / e_0$ (G_s is specific gravity) can be substituted into Equation 6.4. Thus, Equation 6.4 can be rewritten in terms of w as Equation 6.5.

$$\frac{\Omega - \Omega_{sat}}{\Omega_{opt} - \Omega_{sat}} = \frac{s}{s_{opt}} \left(\frac{w}{w_{opt}}\right)^{\xi} \tag{6.5}$$

Figure 6.1(a) shows typical SWCCs for a sand (sand% = 98, silt% = 2), a silt (sand% = 52.5, silt% = 37.5, clay% = 10, liquid limit w_L = 22%, plasticity index I_p = 5.4%) and a clay (sand% = 28, silt% = 42, clay% = 30, w_L = 35.5%, I_p = 18.7%) (data from Vanapalli et al. 1999). The S_{ropt} for soils compacted at w_{opt} generally varies between 0.8 and 0.9 (Barden 1965, Fredlund and Rahardjo 1993). Let us consider a hypothetical case by assuming S_{ropt} = 0.85 and ξ = 2. The s_{opt} values corresponding to S_{ropt} = 0.85 are approximately 5 kPa, 30 kPa and 300 kPa for the sand, silt and clay respectively (see Figure 6.1a).

Figure 6.1(b) shows the variation of (s / s_{opt}) (S_r / S_{ropt})^2 (i.e. normalized SWCC calculated using the right-hand side of Equation 6.4 from the SWCCs shown in Figure 6.1a) with (s / s_{opt}) for the sand, silt and clay. The s ranges shown in Figure 6.1(b) are approximately 0 - 10kPa for the sand, 0 - 60kPa for the silt and 0 - 600kPa for clay, which are the typical s ranges encountered in practice (Khalili et al. 2004, Fredlund 2006, Oh et al. 2009). The nonlinear variation shown in Figure 6.1(b) is similar to the measurements on the variation of different Ω with respect to s. Generally, the Ω increases nonlinearly from Ω_{sat} to Ω_{opt}. At higher s beyond s_{opt}, Ω tends to (i) reduce for sands, (ii) gradually approach a constant value for silt, and iii) continue to increase for clay (Ng and Yung 2008, Oh et al. 2009, Sawangsuriya et al. 2009b, Lu et al. 2010, Ghayoomi and McCartney, 2011, Hoyos et al. 2012, Hoyos et al. 2015, Puppala et al. 2016). Evidence shown in Figure 6.1(b) supports the rationale of using Equation 6.1 for predicting the normalized Ω - s relationships (left-hand side of Equation 6.1) from the normalized SWCC (right-hand side of Equation 6.1 and shown in Figure 6.1b).

Figure 6.1(c) shows the variation of (s / s_{opt}) (S_r / S_{ropt})^2 with S_r. The curves shown in Figure 6.1(c) are similar to the measured Ω - moisture content relationships for various soils reported in the literature (Khoury and Zaman 2004, Alramahi et al. 2010, Lu and Kaya 2014). The relationship between the Ω and the moisture content is more widely used in practice as the measurement of moisture content is more reliable and simple than the measurement of s (Fredlund 2006). The various curves for different soils shown in Figure 6.1(c) may not be well reproduced using a single empirical equation. However, such curves can be described by substituting the SWCC into Equation 6.4 or 6.5 to replace the s and s_{opt}. For example, if Equation 6.2 is used for the SWCC and substituted into Equation 6.4, Equations 6.6 is obtained to describe the Ω - S_r relationship.

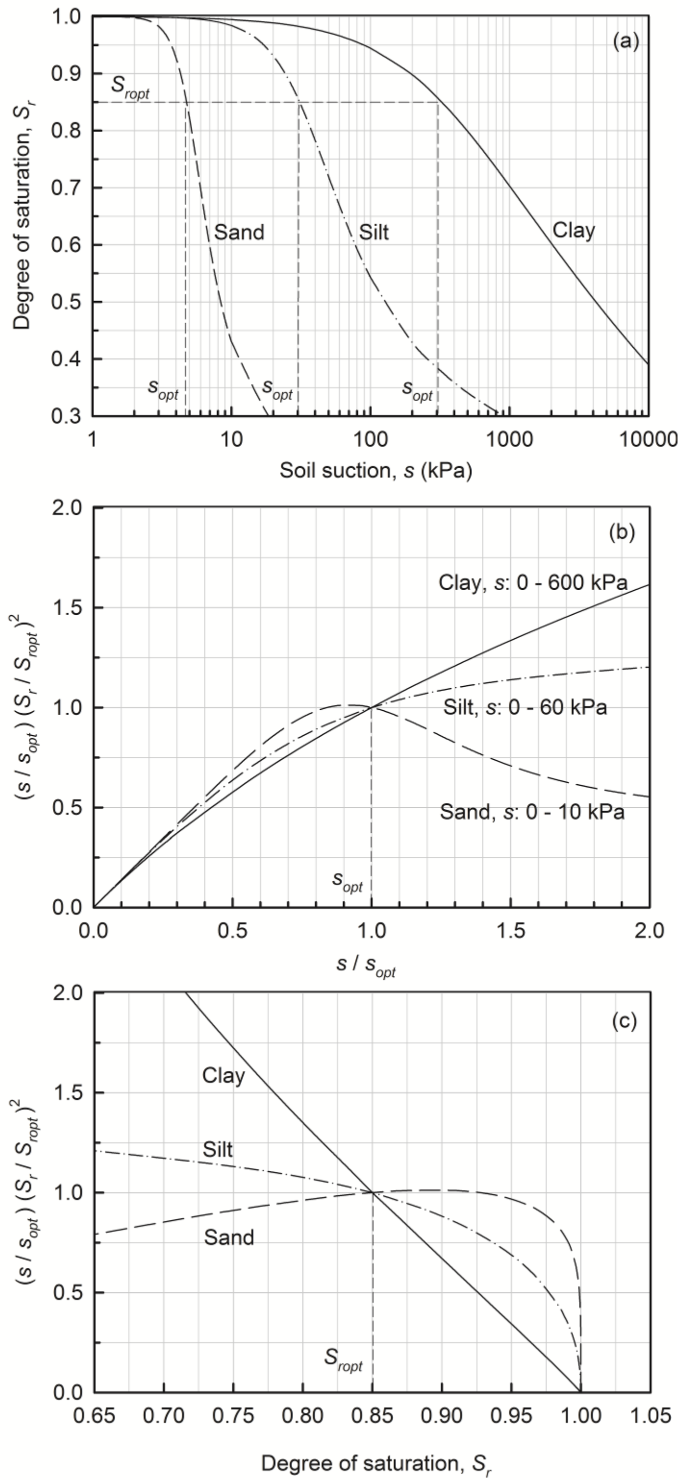

Figure 6.1 (a) SWCC and the variation of (s / s_{opt}) (S_r / S_{ropt})^2 with (b) s / s_{opt} and (c) S_r for sand, silt and clay

$$\frac{\Omega-\Omega_{sat}}{\Omega_{opt}-\Omega_{sat}}=\left(\frac{S_r^{-m_v^{-1}}-1}{S_{ropt}^{-m_v^{-1}}-1}\right)^{n_v^{-1}}\left(\frac{S_r}{S_{ropt}}\right)^{\xi} \tag{6.6}$$

If Equation 6.3 is used for the SWCC and substituted into Equation 6.4, Equation 6.7 is obtained to describe the Ω - S_r relationship:

$$\frac{\Omega-\Omega_{sat}}{\Omega_{opt}-\Omega_{sat}}=\left[\frac{e^{(S_r^{-m_f^{-1}}-1)}-1}{e^{(S_{ropt}^{-m_f^{-1}}-1)}-1}\right]^{n_f^{-1}}\left(\frac{S_r}{S_{ropt}}\right)^{\xi} \tag{6.7}$$

Equation 6.6 is comparatively simpler than Equation 6.7 and therefore is used in this study to describe the Ω - S_r relationship. It should be noted that Equations 6.2 and 6.3 are capable for reasonably fitting the SWCC in the lower soil suction range. For a higher suction range, Equations 6.2 and 6.3 may not be suitable for fitting the SWCC. For example, Equation 6.2 may not well-fit the SWCC when s is higher than 1500 kPa (Fredlund and Xing 1994). For such a scenario, there are some uncertainties using Equations 6.6 and 6.7 or other similar formulations for describing the Ω - moisture content relationships.

Equation 6.6 is rewritten as Equation 6.8 using new parameters $m' = -m_v^{-1}$, $n' = n_v^{-1}$, and $\xi' = \xi$ for differentiating with other equations.

$$\frac{\Omega-\Omega_{sat}}{\Omega_{opt}-\Omega_{sat}}=\left(\frac{S_r^{m'}-1}{S_{ropt}^{m'}-1}\right)^{n'}\left(\frac{S_r}{S_{ropt}}\right)^{\xi'} \tag{6.8}$$

Again, Equation 6.8 can be written in terms of w by assuming a constant e_0 and introducing relationship $S_r = wG_s / e_0$.

$$\frac{\Omega-\Omega_{sat}}{\Omega_{opt}-\Omega_{sat}}=\left(\frac{w^{m'}-w_{sat}}{w_{opt}^{m'}-w_{sat}}\right)^{n'}\left(\frac{w}{w_{opt}}\right)^{\xi'} \tag{6.9}$$

Equations 6.8 and 6.9 can be further simplified into Equations 6.10 and 6.11 using empirical relationship $n_v = 1 / (1 - m_v)$ (van Genuchten 1980) which, in terms of n' and m', equals to $n' = 1 + (1 / m')$. It should be noted that the use of this empirical relationship to reduce parameter n' for simplification purposes however may reduce the flexibility of

Equations 6.10 and 6.11 to fit various Ω - moisture content relationships, especially when they are highly nonlinear. In such cases, Equations 6.8 and 6.9 are more preferable.

$$\frac{\Omega - \Omega_{sat}}{\Omega_{opt} - \Omega_{sat}} = (\frac{S_r^{\ m'} - 1}{S_{ropt}^{\ \ m'} - 1})^{1+\frac{1}{m'}} (\frac{S_r}{S_{ropt}})^{\xi'} \tag{6.10}$$

$$\frac{\Omega - \Omega_{sat}}{\Omega_{opt} - \Omega_{sat}} = (\frac{w^{m'} - w_{sat}^{\ \ m'}}{w_{opt}^{\ \ m'} - w_{sat}^{\ \ m'}})^{1+\frac{1}{m'}} (\frac{w}{w_{opt}})^{\xi'} \tag{6.11}$$

There are two methods to estimate the m', n', and ξ' for Equations 6.8, 6.9, 6.10, and 6.11. The first method is to derive the m_v and n_v of Equation 6.2 from the SWCC and the ξ of Equations 6.1 or 6.4 or 6.5, and use their relationships to the m', n', and ξ' for estimation. In this case, parameters m', n', and ξ' are related to the m_v n_v, and ξ. The second method is to fit Equations 6.8, 6.9, 6.10, or 6.11 to measured Ω - moisture content relationships to directly determine the m', n', and ξ' from regression analysis. In this case, m', n', and ξ' are merely fitting parameters and are not necessarily related to the m_v n_v, and ξ. This chapter discusses (i) the similar characteristic behavior in the $(\Omega - \Omega_{sat}) / (\Omega_{ref} - \Omega_{sat})$ versus moisture content relationships for different stiffness and shear strength properties for the same soil, and (ii) the feasibility of determining n', m' and ξ' from easy-to-obtain Ω - moisture content relationships as per the second method and using them to predict Ω - moisture content relationships which are difficult to obtain.

6.3 Experimental investigations

6.3.1 Materials and equipment

Four natural subgrade soils collected from shallow depth (0 - 3m below natural ground surface) at various locations in Canada (Toronto silty clay - TSC, Kincardine lean clay - KLC, Ottawa Leda clay - OLC from Ontario; and Indian Head till - IHT from Saskatchewan) are investigated. The TSC, KLC and IHT soils are glacial deposits and the OLC is a marine clay of the ancient Champlain Sea basin. Table 6.1 summarizes properties of the four soils. The soil samples collected from various sites are air-dried, grinded and passed through 2mm sieve. The soil passing the 2mm sieve is oven-dried and then mixed with distilled and de-aired water to achieve their respective w_{opt} values (see Table 6.1) and stored in double-layered bags for a period of 24 to 48 hours for achieving moisture equilibrium. The w of the soil is measured and adjusted (by adding water or dry soil) at 24 hours' interval such that the final w is within ± 0.1% of the w_{opt}.

Table 6.1 Properties of the soils tested in the present study

Soils	ID	w_L (%)	I_p (%)	G_s	*w_{opt} (%)	*γ_{dmax} (kN/m^3)	Sand %	Silt %	Clay %	USCS	AASHTO
Toronto silty clay	TSC	19.6	6	2.68	13.5	19.15	3	81	16	CL-ML	A-4
Kincardine lean clay	KLC	31	10	2.71	20.3	16.31	15	60	25	CL	A-4
Indian Head till	IHT	35.5	19	2.72	15.5	18.46	28	42	30	CL	A-6
Ottawa Leda clay	OLC	48	26	2.75	23.0	16.16	20	48	32	CL	A-6

Note: *Determined from soils passing through 2mm sieves.
Notations: USCS = Unified Soil Classification System (ASTM D2487-11, ASTM 2011), AASHTO = American Association of State Highway and Transportation Officials soil classification system (AASHTO M145-91, AASHTO 2008).

Cylindrical specimens which are 50mm in diameter and 100mm in length are statically compacted in a brass split mould in 5 layers. The compaction effort is controlled such that each layer, and the specimen, is compacted to the γ_{dmax} corresponding to the w_{opt} (see Table 6.1). Dimensions and mass of the compacted specimens are measured using a caliper (readable to 0.01mm) and an electronic balance (readable to 0.01g) to calculate their S_r, e_0 and γ_d. The average S_r and e_0 values are: 0.9 and 0.39 for the TSC, 0.85 and 0.65 for the KLC, 0.88 and 0.47 for the IHT, and 0.91 and 0.69 for the OLC.

Figure 6.2 shows the GDS Entry Level Dynamic (ELDyn) triaxial testing system used in this study (i) to preform cyclic loading tests to determine the M_R and (ii) to perform modified UC tests to determine the E and q_u. The ELDyn system facilitates independent control of the pore-air pressure (u_a) using a two-channel pneumatic regulator via a porous stone placed on top of the specimen and the pore-water pressure (u_w) using a pore-water pressure controller via a ceramic stone (whose air-entry value s_{ae} is 500 kPa) embedded in the base pedestal. The pore-water pressure controller can also measure the volume of water flow into or out of the drainage system at a precision of 1mm^3. Such arrangement allows the use of axis-translation technique (Hilf 1956) to control the s ($s = u_a - u_w$) of the specimens. The confining stress (σ_c) is also controlled by the two-channel pneumatic regulator.

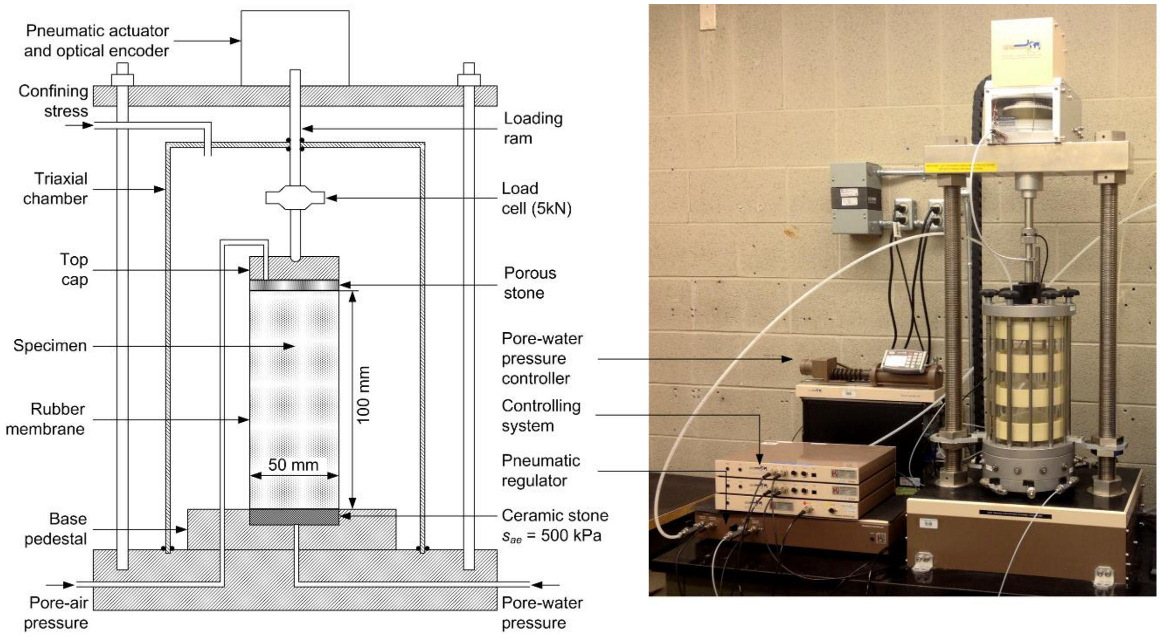

Figure 6.2 GDS Entry Level Dynamic (ELDyn) triaxial testing system used for testing

The ELDyn system facilitates application of load through the pneumatic actuator. An optical encoder embedded in the pneumatic actuator measures the displacement of the loading ram to determine the specimen deformation. The lowest displacement readable from the optical encoder is 0.001mm. A 5kN submersible load cell is mounted on the loading ram inside the triaxial chamber. Such arrangement eliminates the need for adjusting the measured force considering the confining stress-induced force and the mechanical friction that act on the loading ram.

6.3.2 Specimen moisture equilibrium

Compacted specimens of the same soil have the same w_{opt} and dry unite weight which assure relatively "identical" initial soil structure. Specimens are thereafter (i) directly tested, or (ii) saturated or wetted to higher w and tested, or (iii) dried to lower w and tested. Specimens are divided into two groups for performing cyclic loading tests and modified UC tests, respectively. Tables 6.2 and 6.3 provide details of tested specimens including the final w values achieved for each specimen. Emphasis is given to the wetting process from w_{opt} to higher w considering that wetting process is more frequently experienced in the subgrade soils after compaction (Uzan 1998, Houston and Ge 2014). Two different procedures are used to achieve different s or w values, namely; the axis-translation technique (Hilf 1956; applied on specimens IHT-1 to IHT-5 used for determining the M_R) and a manual procedure using filter paper (applied on other specimens for determining the M_R, E and q_u).

Table 6.2 Summary of the M_R test results

Soil	No.	*w (%)	s (kPa)	k_1	k_2	k_3	R^2	M_{Rrep} (MPa)
TSC	1	14.65	0	321.5	0.31	-0.17	0.97	33.76
	2	14.48	9	387.2	0.39	-0.34	0.98	40.13
	3	14.27	13	401.5	0.46	-0.34	0.96	42.41
	4	13.98	18	407.6	0.47	-0.45	0.98	42.21
	5	13.75	21	469.5	0.50	-0.75	0.99	46.09
	6	13.62	23	436.1	0.45	-0.29	0.99	46.41
	7	13.48	25	476.4	0.39	-0.53	0.93	47.49
	8	12.50	48	418.1	0.24	0.67	0.97	51.16
KLC	1	23.50	0	119.9	0.39	-0.47	0.84	12.12
	2	23.19	16	222.3	0.42	-1.89	0.87	16.91
	3	21.37	35	241.9	0.53	0.23	0.92	29.29
	4	20.70	50	236.7	0.37	1.10	0.97	32.79
	5	20.55	55	241.7	0.52	1.33	0.99	36.49
	6	20.30	67	325.1	0.23	0.44	0.96	37.90
	7	19.63	136	426.4	0.24	0.87	0.96	54.33
IHT	1	17.20	0	76.1	-6.02	10.09	0.99	11.80
	2	16.96	30	1620	9.44	-20.88	0.99	28.94
	3	16.46	60	602	2.21	-4.75	0.92	41.38
	4	15.91	90	695.8	0.87	-2.95	0.99	48.13
	5	15.50	120	505.4	-2.25	4.08	0.99	63.43
OLC	1	24.85	0	273	1.20	-4.12	0.96	16.25
	2	24.72	41	267.4	0.40	-0.78	0.94	25.40
	3	24.55	68	247.9	0.21	-0.15	0.89	25.44
	4	24.00	147	533.8	0.39	-1.33	0.97	45.18
	5	23.60	219	469.5	0.22	-1.07	0.67	40.03
	6	23.30	290	720.9	-0.07	-0.02	0.80	70.45
	7	22.93	420	1170	0.29	-1.79	0.94	87.73
	8	22.66	558	1279	0.15	-1.76	0.86	92.92

Note: In Equation 6.12, θ, τ_{oct} and M_R are in kPa, and p_a = 100 kPa for determining the model parameters.
*w values shown are the w before cyclic loading tests.

Table 6.3 Summary of the q_u and E test results of the soils

Soil	No.	*w (%)	s (kPa)	q_u (kPa)	E (MPa)
TSC	9	14.65	0	60	5.2
	10	14.53	8.4	143	15.35
	11	14.49	9.3	144	18.2
	12	13.92	18.8	172	25
	13	13.5	25	240	32
	14	13.5	25	243	N/A
	15	12.66	43	300	39.45
KLC	8	23.5	0	87	2.7
	9	23.1	17	130	6
	10	22.29	24	158	7.75
	11	21.3	36	205	11.3
	12	20.3	67	285	16
	13	20.3	67	290	N/A
	14	19.74	118	360	22
IHT	6	17.2	0	140	9
	7	16.85	37	195	16
	8	16.55	54	210	25
	9	16.1	80	250	30
	10	15.5	120	316	36.92
	11	15.5	120	316	N/A
	12	14.89	180	387	50.98
	13	14.58	224	415	57
OLC	9	24.85	0	82	5.28
	10	24.07	137	210	20.46
	11	23.77	186	225	24
	12	23.31	288	300	32
	13	22.93	420	370	43
	14	22.93	420	374	N/A
	15	22.5	672	545	69

*w values shown are the w before performing the modified UC tests.

The s_{opt} of IHT specimens after compaction is approximately 120kPa, which is measured using "identical" compacted specimens (50mm in diameter and 20mm in height) using a modified null pressure plate apparatus (Power and Vanapalli 2010). Five s levels (i.e. 0, 30, 60, 90 and 120kPa) are designated and imposed on each specimen (i.e. specimens IHT-1 to IHT-5) within the ELDyn system by maintaining an u_w of 50kPa while applying different u_a. Confining stress σ_c is also adjusted such that specimens equilibrate under a constant net confining stress $\sigma_{c,net}$ ($\sigma_{c,net} = \sigma_c - u_a$) of 27.6kPa. The drainage lines of the ELDyn system are flushed at an interval of 36 hours to remove any accumulated air-bubbles below the ceramic disk that may influence the equilibrium process. Equilibrium condition is assumed to have been achieved when water exchange is less than 0.04% of the specimen water content within 24 hours (Wheeler and Sivakumar 1995). Time period for equilibrium varies from 6 days for the IHT-5 equilibrated to s = 120 kPa, to 25 days for the IHT-1 equilibrated to s = 0 kPa.

All other samples, except i) TSC-7, -13, -14, KLC-6, -12, -13, IHT-10, -11, and OLC-7, -13, -14 which are directly tested at w_{opt} after compaction and ii) the TSC-1, -9, KLC-1, -8, IHT-6, and OLC-1, -9 which are saturated and tested, are cured manually to achieve different w values using the filter papers. Cut filter papers are used to entirely wrap the specimens. Specimens subjected to wetting are wrapped, evenly sprayed with de-aired and distilled water, further wrapped by two layers of plastic films and stored in a plastic container for 24 hours for achieving moisture equilibrium. The sprayed water absorbed by the wrapping filter papers each time is approximately 1.5 - 1.7g. Specimen mass measurements after moisture equilibrium suggest that each spray increases the w of a specimen by approximately 0.2 - 0.3%. Such procedure is repeated until designated higher w value is achieved. Specimen subjected to drying is also cured in a similar manner; however, air-dried filter papers are used to absorb moisture from the specimen. Specimen mass measurements after moisture equilibrium suggest that the dry filter papers decrease the w of specimen in a period of 24 hours by approximately 0.18 - 0.32% each time. Both the wetting and drying procedures used in this study alter the w of specimens at a slow rate. This helps to avoid excessive moisture gradient and desiccation cracks / fissures within the specimens.

Specimens that were chosen to be tested under fully saturated condition are wrapped in filter papers, confined within rubber membranes, and placed on a saturated ceramic disk to imbibe water. Specimens are reversed at 8 hours interval to ensure that water enters the specimens evenly from both ends. This procedure is repeated until the variation in specimen mass in 16 hours is less than 0.2g (approximately 0.08% of specimen water content) which is used as a criteria to identify saturation. This procedure avoids introducing excessive water while saturating the specimens which leads to (i) erroneous measurement of w_{sat}, (ii) specimen exterior peeling off and (iii) slump or collapse of the specimens. In addition, Skempton's B-test is performed using the ELDyn system for all saturated soil specimens before performing their respective cyclic loading or modified UC tests. The determined B-values are typically higher than 0.96 which suggests that the soil specimens are saturated.

6.3.3 Cyclic loading and modified UC tests

Cyclic loading tests referencing AASHTO T307-99 protocol (AASHTO 2003) and modified UC tests referencing ASTM D2166-13 protocol (ASTM 2013) are performed to determine the M_R, q_u and E for the four soils. Cyclic loading tests are carried out under constant water content condition considering that fine-grained subgrade soils are low in hydraulic conductivity and the dissipation of excessive pore-water pressure generated during the rapid cyclic loadings is less likely (Brown 1996, Cary and Zapata 2016). The TSC, KLC and OLC specimens listed in Table 6.2 are initially subjected to a conditioning phase during which 1000 cyclic loadings (σ_d) of 27.6 kPa under a constant σ_c of 41.4 kPa are applied to minimize the bedding and seating errors. Thereafter, testing phase follows during which 100 cyclic loadings are applied using four σ_d levels (27.6, 41.1, 55.2 and 68.9kPa) under three σ_c levels (41.1, 27.6 and 13.8kPa). In total, 12 external stress conditions (i.e. 12 combinations of σ_d and σ_c) are applied on each specimen. Same σ_d levels are used to load the IHT specimens, however, $\sigma_{c,net}$ is used instead of σ_c to confine the specimens as axis-translation technique is used. Only one $\sigma_{c,net}$ level is used for the IHT specimens during both conditioning and testing phases considering the long equilibrium period required for the axis-translation technique. Therefore, four different external stress conditions are applied on the IHT specimens during the testing phase. For all the four soils, the M_R at each external stress condition is determined as the ratio of the σ_d to the average ε_r of the last five loading cycles.

Figure 6.3 shows typical axial stress (σ_a) - axial strain (ε_a) relationship from the modified UC tests used in this study for illustration purposes. The loading and unloading rate is set to be 1mm/min as per ASTM D2166-13 protocol (ASTM 2013). Unlike traditional UC tests that directly load the specimens to failure, the modified UC tests allow an unloading-reloading loop starting at ε_a = 1%. There are several approaches to determine the E from the UC test results. The E can be the tangent modulus determined as the slope of the initial linear portion of the σ_a - ε_a curve (i.e. slope of line OA in Figure 6.3) (Duncan and Chang 1970, Atkinson 2000). The *E* can also be the secant modulus determined as the slope of the line linking the origin O and the point on the curve at ε_a = 1% (slope of line OB in Figure 6.3) (Lee et al. 1997, Lu and Kaya 2014, Hossain and Kim 2015). Both approaches however are subjected to uncertainties associated with seating and bedding errors that arise from the imperfect specimen end surfaces, cap-specimen and specimen-pedestal contacts and the alignment of loading system and specimen (Jardine et al. 1984).

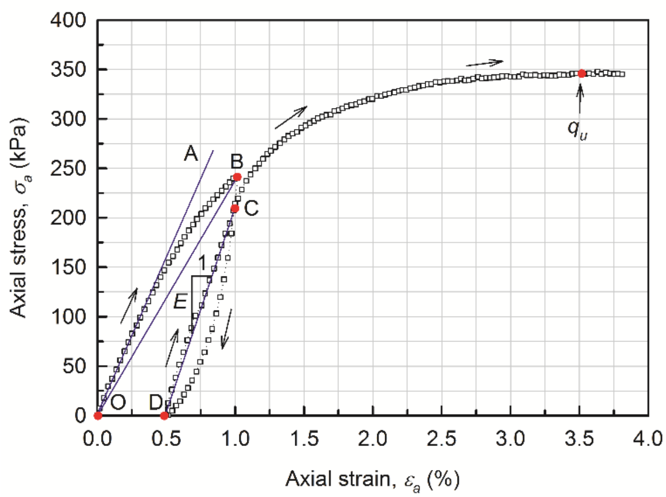

Figure 6.3 Axial stress - axial strain relationships for the modified UC tests

Figures 6.4(a) and 6.4(b) show the typical σ_a - ε_a curves derived from the modified UC tests for the IHT and OLC at three different *w* values. Figures 6.4(c) and 6.4(d) show details of the same curves at a ε_a range between 0 and 1.2%. It can be observed from Figures 6.4(c) and 6.4(d) that the virgin loading curves within low strain range are nonlinear in nature due to the influence of possible bedding and seating errors. The slope of the virgin loading curves does increase with decreasing *w*, however, adjusting these nonlinear curves to calculate the *E* might be largely based on users' discretion and therefore is subjective.

Such limitation could be alleviated if an unloading-reloading loop is allowed at a certain low strain level (e.g., ε_a = 1% in this study). As shown in Figure 6.3, the unloading process starts at point B at ε_a = 1% and ends at point D at σ_a = 0kPa, and the reloading process starts at point D and the reloading curve intersects the unloading curve at point C. The reloading from D to C is mostly elastic and the slope of line DC can be reliably used as the elastic modulus. It can be observed from Figure 6.3 and the experimental results shown in Figures 6.4(c) and 6.4(d) that (i) points D and C are easy to identify from experimental results which makes the determination of E more objective and convenient; (ii) E determined from line DC is generally higher than that determined from the virgin loading curve, which is possibly due to the accumulation of plastic deformation that increases the density of the specimens; and (iii) the reloading curve beyond ε_a = 1% continues the trend exhibited in the virgin loading curve, which suggests that the unloading-reloading loop does not influence the soil behavior at higher ε_a level and the q_u.

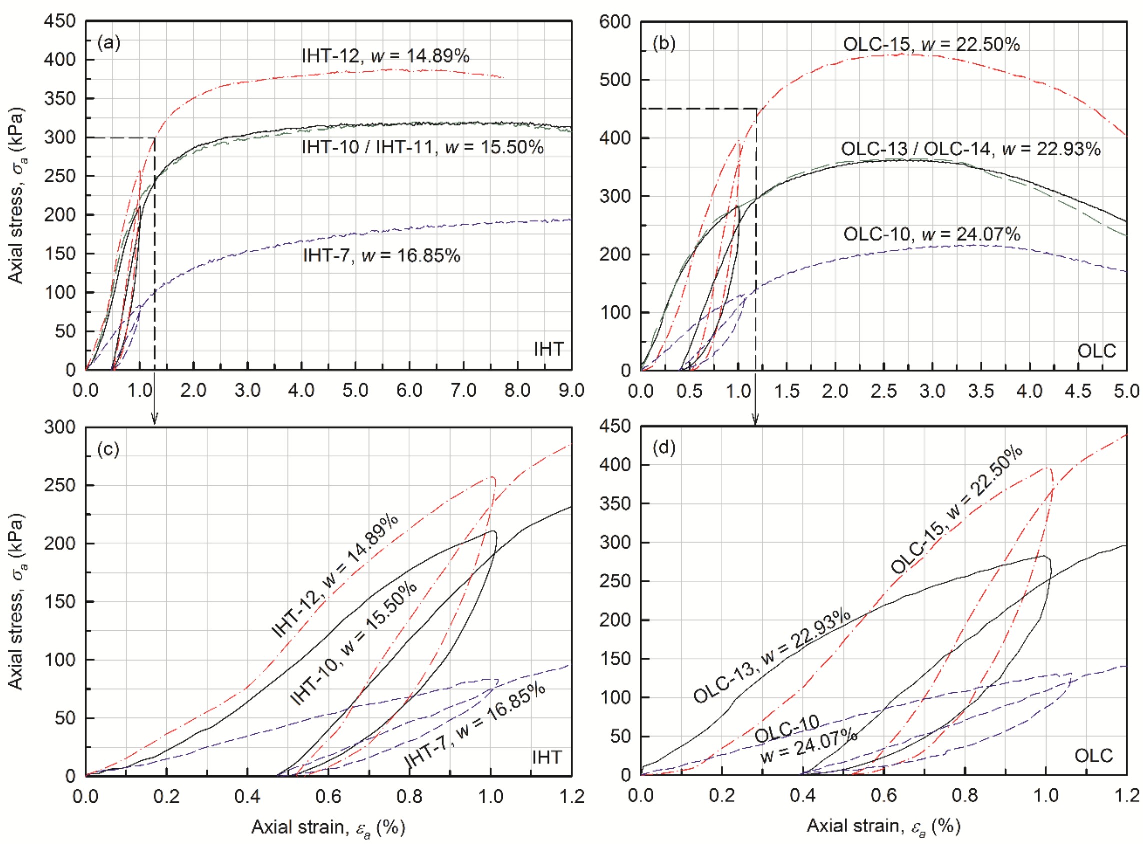

Figure 6.4 Modified UC test results for the (a) (c) IHT and the (b) (d) OLC

The q_u of specimens compacted at w_{opt} and subjected to the conventional UC tests without the unloading-reloading loop (i.e. TSC-14, KLC-13, IHT-11 and OLC-14, see Table 6.3) are compared to the q_u of specimens compacted at w_{opt} and subjected to the modified UC tests (i.e. TSC-13, KLC-12, IHT-10 and OLC-13, see Table 6.3). Figures 6.4(a) and 6.4(b) also show the σ_a - ε_a curves for IHT-10 / IHT-11 and OLC-13 / OLC-14. It can be seen that the q_u values derived from the conventional UC and the modified UC tests are consistent and therefore the modified UC tests does not influence the q_u. For this reason, the E and q_u values derived from the modified UC tests are used in this study.

6.3.4 Soil suction and SWCC measurement

The specimens of the TSC, KLC and OLC after cyclic loading tests are further used to measure their respective w - s relationships using the contact filter paper method as per ASTM D5298-10 protocol (ASTM 2010). The w - s relationships derived from all the specimens of the same soil are used to obtain the SWCC. The SWCC of the IHT is measured using a modified null pressure plate apparatus devised by Power and Vanapalli (2010).

For the filter paper method (used for TSC, KLC and OLC), the specimens are evenly sliced into four disks. A filter paper set (a smaller circular filter paper placed between two larger circular filter papers) is sandwiched between two sliced disks. Equilibrium moisture conditions are typically achieved after a time period of seven days. A stress of 1kPa is applied to ensure good contact between the soil disks and the filter papers (Power et al. 2008). The average w of the two disks and the s measured from the sandwiched filter paper are used as the w - s relationship. Two w - s relationships are measured from each specimen and all the measured w - s relationships for one soil are used to form its SWCC. On the other hand, three identically compacted IHT specimens (20mm in length, 50mm in diameter) are wetted using a modified pressure plate apparatus (Power and Vanapalli 2010) from a s of 120 kPa to different lower s levels and eventually to saturation to measure the SWCC of the IHT following wetting path.

6.4 Presentation and analyses of the experimental results

6.4.1 Soil-water characteristic curve

The measured w - s relationships for the four soils are shown in symbols in Figure 6.5. Measurements are fitted using Equation 6.3 assuming $S_r = w / w_{sat}$. The fitted SWCCs are shown as continuous lines in Figure 6.5 along with the fitting parameter and coefficient of determination (R^2) values. It can be observed that the measured w - s relationships, which range from the w_{sat} to the w_{opt} or w slightly lower than w_{opt}, generally locate within the boundary effect and transition zones of the SWCCs. The corresponding s levels are mostly within 0 to 600kPa where soil suction changes are associated with soil moisture content changes via liquid phase flow (Vanapalli et al. 1996, Khalili and Khabbaz 1998). The water retention capacity, either evaluated by the s_{ae} or by the level of s to desaturate the soil as shown in Figure 6.5, increases with the plasticity of soil (indicated by the I_p and clay%, see Table 6.1). The s values of all specimens used for the modified UC tests and the TSC, KLC and OLC specimens used for the cyclic loading tests are determined from the fitted SWCC shown in Figure 6.5 corresponding to their respective w values (see in Tables 6.2 and 6.3 for the w and s values).

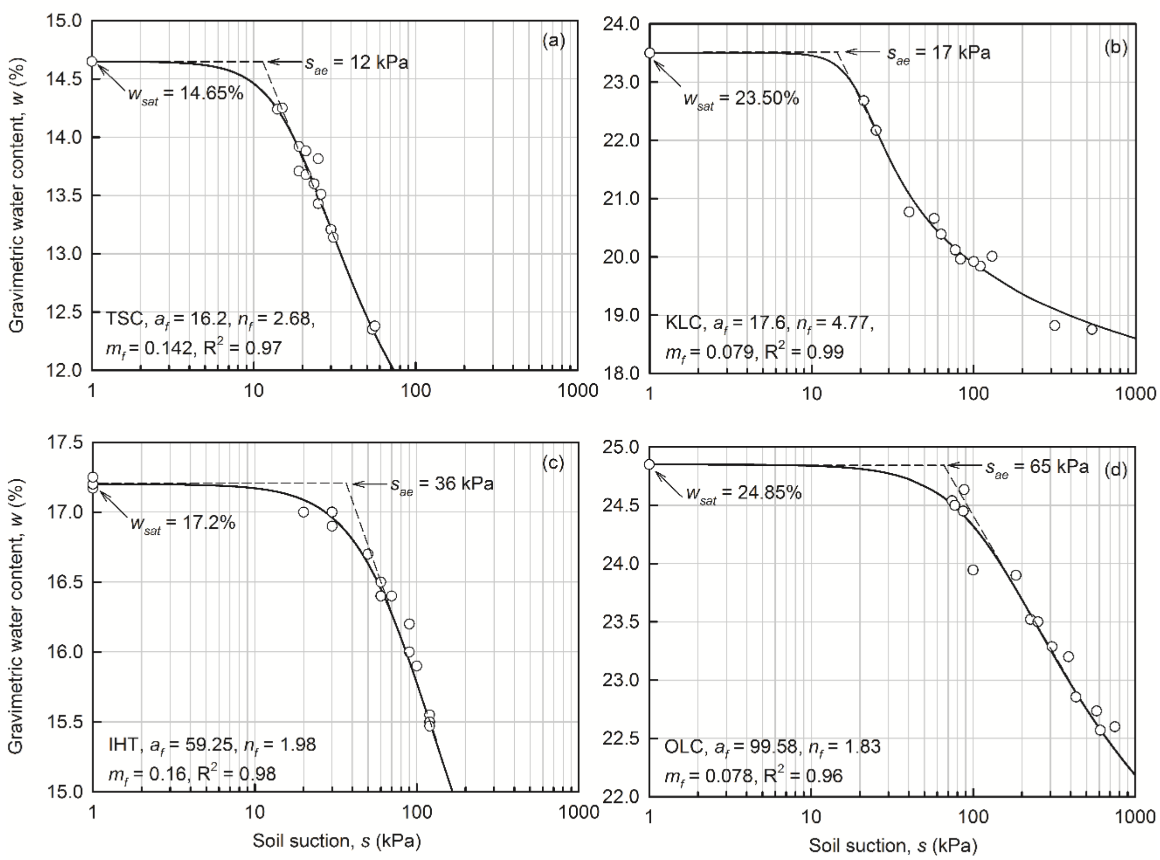

Figure 6.5 SWCCs of the (a) TSC, (b) KLC, (c) IHT and (d) OLC

6.4.2 Predicting the variation of M_R, E and q_u with s

The measured M_R values at various external stress conditions for each specimen are fitted by a widely used stress-dependent model suggested by ARA, INC., ERES (2004).

$$M_R = k_1 p_a (\frac{\theta}{p_a})^{k_2} (\frac{\tau_{oct}}{p_a} + 1)^{k_3} \tag{6.12}$$

where θ is the bulk stress and τ_{oct} is the octahedral shear stress ($\theta = 3\sigma_c + \sigma_d$ and $\tau_{oct} = 0.471\sigma_d$ for conventional triaxial tests performed on TSC, KLC and OLC specimens; θ should be replaced by net bulk stress $\theta' = 3\sigma_{c,net} + \sigma_d$ for the IHT specimens as axis-translation technique is used); p_a is the atmosphere pressure and k_1, k_2 and k_3 are model parameters. The k_1, k_2 and k_3 values derived for each specimen are summarized in Table 6.2 along with the corresponding R^2 values. Equation 6.12 can suitably describe the variation of the M_R with respect to external stress with R^2 values generally higher than 0.9. Instead of using the M_R values measured at all external stress conditions, the representative resilient modulus (M_{Rrep}) values, which are calculated by Equation 6.12 using the mean values of σ_d and σ_c or $\sigma_{c,net}$ applied during the cyclic loading tests (i.e. σ_d = 48.2kPa and σ_c or $\sigma_{c,net}$ = 27.6kPa; τ_{oct} = 22.7kPa and θ or θ' = 131kPa) and the respective k_1, k_2 and k_3 values, are used in this study to investigate the variation of M_R with s and w. The measured E and q_u values for specimens subjected to the modified UC tests are summarized in Table 6.3.

Figure 6.6 shows using different symbols the measured variation of E / E_{sat}, q_u / q_{usat} and M_{Rrep} / $M_{Rrep,sat}$ with respect to the s and w for the four soils. In addition, predictions provided using Equation 6.5 are shown as continuous lines. The fitted SWCCs shown in Figure 6.5 and a ξ value of 2.0, which is suggested by Han and Vanapalli (2016b) for cohesive soils, are used in Equation 6.5 for prediction. The predictions reasonably reproduce the measured variation of the E, q_u and M_{Rrep} with s and w for all the four different soils investigated in the present study.

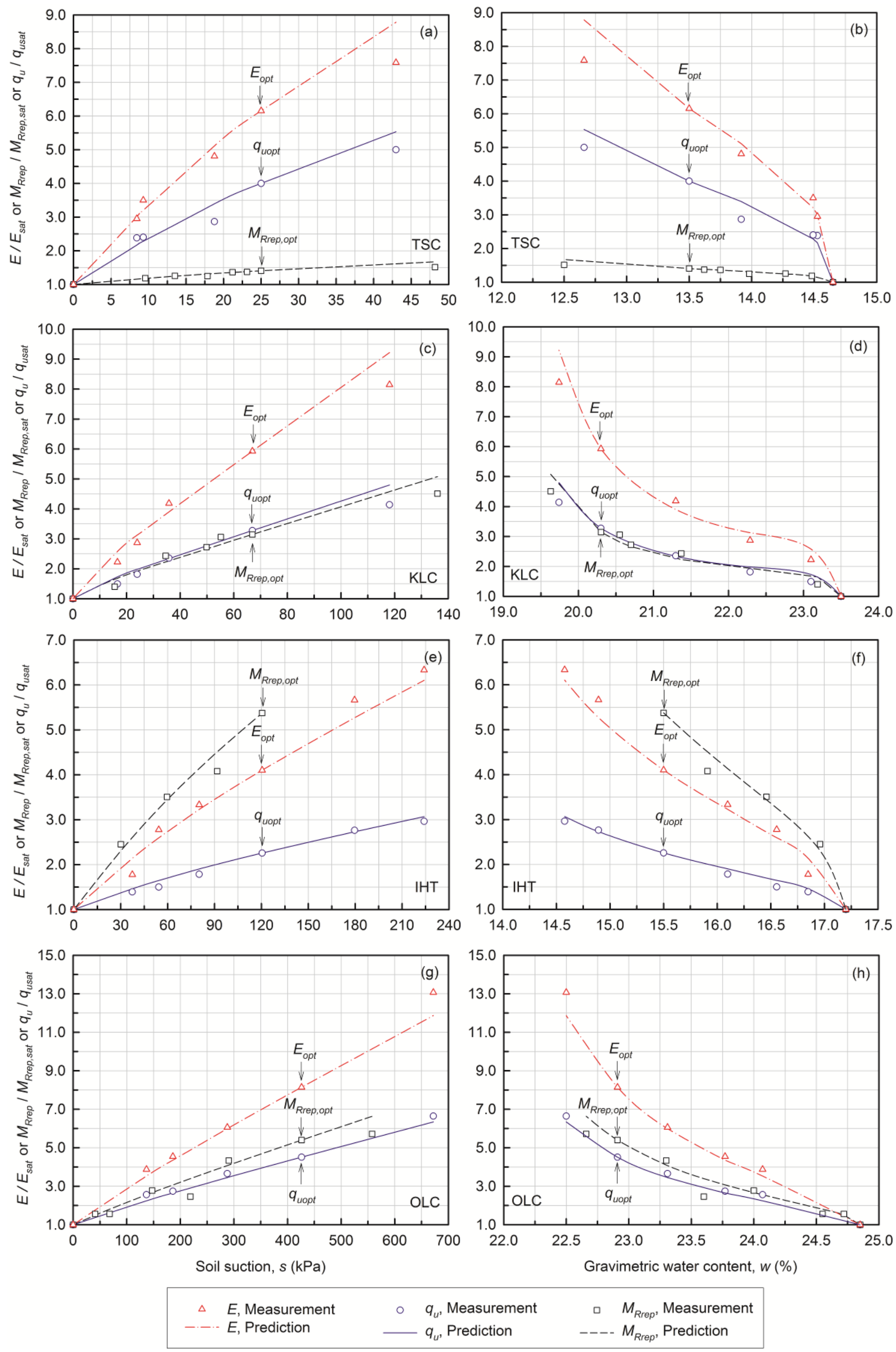

Figure 6.6 Measured and predicted variations in the E, q_u and M_R with s for (a) TSC, (c) KLC, (d) IHT, (f) OLC and with w for (b) TSC, (d) KLC, (f) IHT, (g) OLC

Several features of the Ω - s and Ω - w relationships can be observed from Figure 6.6:

(i) Mechanical properties are sensitive, at different levels, to both the s and w for all the four soils. For example, the increment in the M_{Rrep} of the IHT from $M_{Rrep,sat}$ to $M_{Rrep,opt}$ is more prominent compared with that of the E and q_u while increment in the M_{Rrep} of the TSC is far less significant than that of the E and q_u; the variations of q_u with s and w are similar to that of the M_{Rrep} for the KLC and OLC while the variations of q_u and M_{Rrep} are quite different for the TSC and IHT. Such differences could be difficult to predict without proper experimental investigations;

(ii) All the Ω - s relationships show nonlinear behavior: the Ω initially increases remarkably with s up to approximately s_{ae}; beyond s_{ae}, the rate of increase is less significant. This is associated with the variation in the amount of capillary water from the boundary effect zone to the transition zone. The soil is in a state of capillary saturation in the boundary effect zone and hence soil suction fully contributes to the skeleton stress which results in a significant increase in the Ω with s. However, in the transition zone beyond s_{ae}, the contribution of soil suction reduces due to the decrease in the capillary water and this results in a lower rate of increase in the Ω. Similar observations and interpretations on the Ω - s relationships are also widely reported in the literature (Vanapalli et al. 1996, Ng and Yung 2008, Ghayoomi and McCartney 2011, Sivakumar et al. 2013, Puppala et al. 2016). The differences between the E - s, q_u - s and M_{Rrep} - s relationships are mostly their inclinations with respect to the s axis (i.e. the sensitivities of the E, q_u and M_{Rrep} to the s);

(iii) The Ω - w relationships however show different nonlinear features. The Ω - w relationships of the TSC are upper convex. The upper convex shape of the Ω - w relationships become less prominent for the KLC and IHT and eventually turn to linear or slightly lower convex shape for the OLC. Comparing Figure 6.6 with Figure 6.1(c), it can be observed that the TSC, which is high in silt content (silt% = 81) and low in plasticity (I_p% = 6), exhibits similar Ω - w relationships to that of the “silt curve” in Figure 6.1(c). With an increase in the clay content and I_p, the behavior of the KLC and IHT starts to turn from the “silt curve” to the “clay curve”. The OLC, which is rich in clay content (clay% = 32) and high in plasticity (I_p% = 26), shows linear Ω - w relationships which resemble the “clay curve” in Figure 6.1(c).

It should be noted that the nonlinearity of the prediction curves shown in Figure 6.6 is extrapolated from the SWCCs shown in Figure 6.5 through the use of Equation 6.5, which was initially developed for Ω - s relationships based on the mechanics of unsaturated soils. The measurements of Ω - s relationships and the SWCC need supervision of highly trained personnel and hence are expensive. In addition, the results are user- and equipment-dependent and sensitive to many other factors such as the temperature and the relative humidity. There are also possible discrepancies between the s - moisture content relationships described by the SWCCs and the actual relationships within the specimens during the tests due to the influence of external stress and drainage conditions (Han and Vanapalli 2016b). Due to these reasons, the determination, prediction and use of the Ω - s relationships remain a challenge for geotechnical practitioners, especially when compared with the Ω - moisture content relationships which are easier to determine.

6.4.3 Fitting the variation of M_R, E and q_u with w

The left-hand side four figures in Figure 6.7 show the variations of the normalized M_{Rrep}, E and q_u computed using the relationship$(\Omega - \Omega_{sat}) / (\Omega_{opt} - \Omega_{sat})$ (i.e. $(M_{Rrep} - M_{Rrep,sat}) / (M_{Rrep,opt} - M_{Rrep,sat})$, $(E - E_{sat}) / (E_{opt} - E_{sat})$, and $(q_u - q_{usat}) / (q_{uopt} - q_{usat})$; such a ratio is termed as the "normalized ratio" for brevity) in this chapter. The normalized ratio - w relationships for the M_{Rrep}, E and q_u exhibit similar characteristics to that shown in Figure 6.1c and the right-hand side four figures in Figure 6.6. The similar characteristics shown in the normalized ratio - w relationships for the different Ω types highlights the possibility of determining the normalized ratio - w relationships from easy to perform tests and using them in predicting the Ω - w relationships that are difficult and cumbersome to obtain. For this study specifically, the $(E - E_{sat}) / (E_{opt} - E_{sat})$ - w and $(q_u - q_{usat}) / (q_{uopt} - q_{usat})$ - w relationships which can be measured using conventional UC tests with some modifications can be used as the $(M_{Rrep} - M_{Rrep,sat}) / (M_{Rrep,opt} - M_{Rrep,sat})$ - w relationships to further predict the M_{Rrep} - w relationships, given the $M_{Rrep,sat}$ and $M_{Rrep,opt}$ are measured or predicted. Actually, the E (or the $S_{u1\%}$ which is the σ_a at ε_a = 1% during UC tests) and q_u values derived from the UC tests are frequently used to predict the M_{Rsat} and M_{Ropt} (Lee et al. 1997, Khoury et al. 2013, Hossain and Kim 2015).

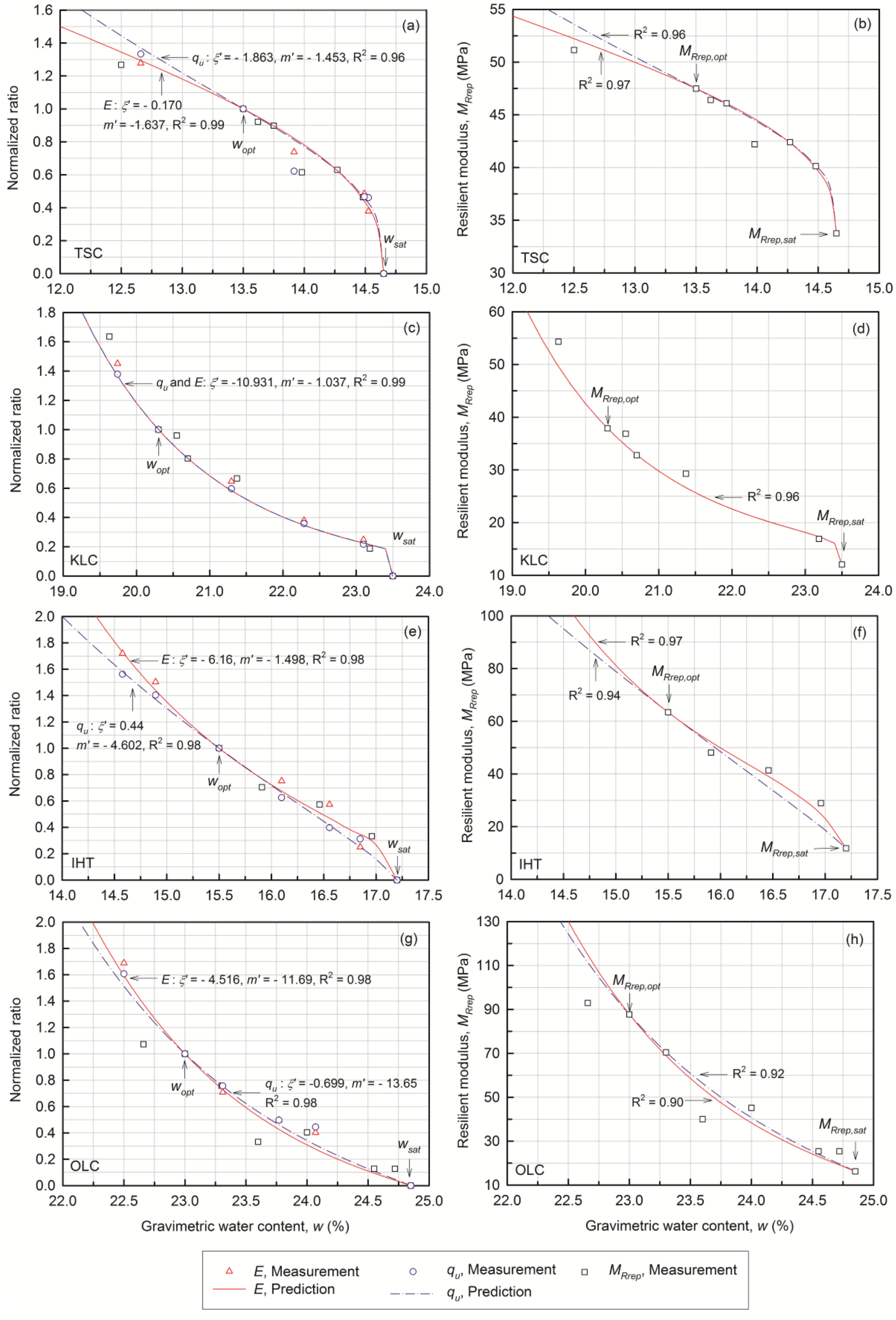

Figure 6.7 Measured and fitted variations in the normalized ratio with *w* for (a) TSC, (c) KLC, (d) IHT, (f) OLC and in the M_{Rrep} with w for (b) TSC, (d) KLC, (f) IHT, (g) OLC

Equation 6.9 (with three parameters n', m' and ξ') or Equation 6.11 (with two parameters m' and ξ') can be used to predict the normalized ratio - w relationships. Equation 6.11 is used to fit the normalized ratio - w relationships for the E and q_u separately considering its simplicity. The fitted curves are also shown in the left-hand side four figures in Figure 6.7 along with the values for the m', ξ' and R^2. As can be observed that Equation 6.11 well captures the various nonlinear characteristics of the measurements on both E and q_u of all soils. There are slight differences between the fitted curves for the E and q_u due to the scatter in the measurements. The fitted normalized ratio - w relationships for the E and q_u are then respectively used as the normalized ratio - w relationships for the M_{Rrep} to predict the M_{Rrep} - w relationships. Results are shown in four figures on the right-hand side of Figure 6.7. Reasonable predictions are achieved for the M_{Rrep} using the fitted normalized ratio - w curves from both the E and the q_u relationships.

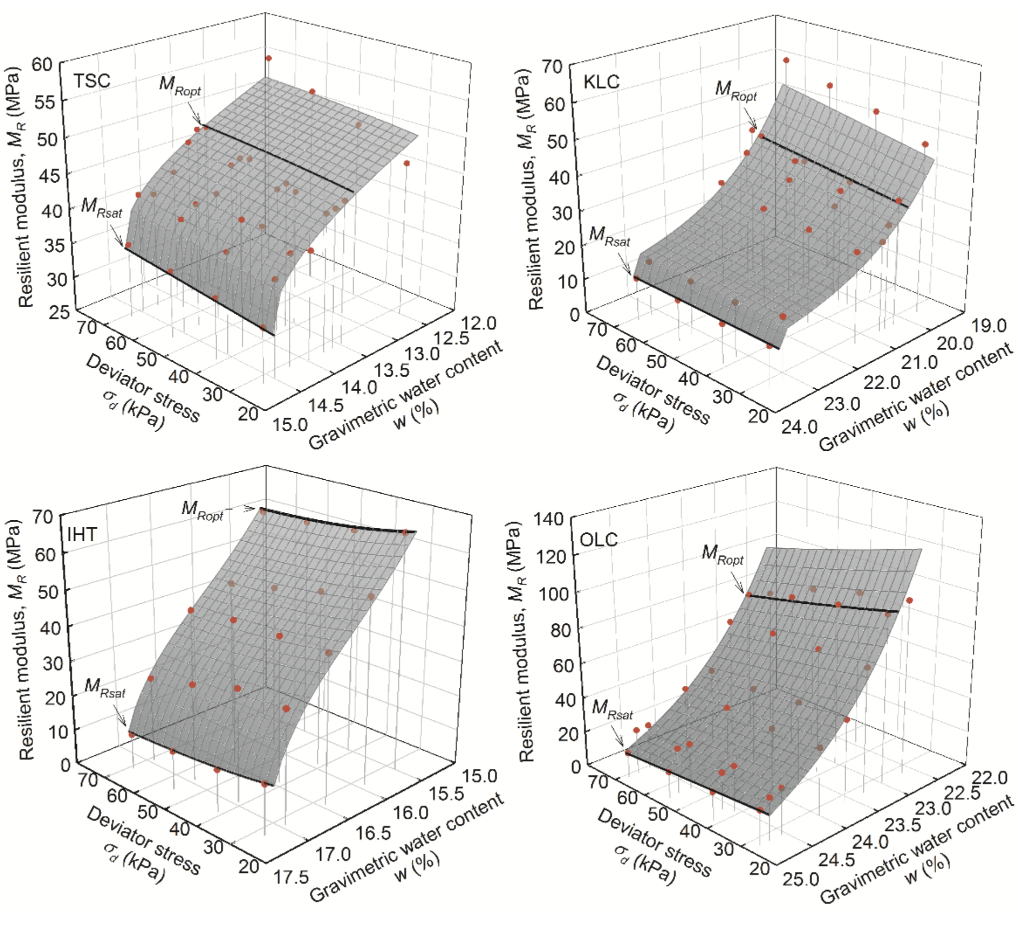

Figure 6.8 Measured and predicted M_R - σ_d - w relationships

It is of interest to note that the predicted M_{Rrep} - w relationships shown in Figure 6.7 are extrapolated from the fitted E - w or q_u - w relationships using Equation 6.11. There is no need of the information of the SWCC for this prediction method. The nonlinearity used to predict the Ω - w relationships shown in Figure 6.6 however is derived from the SWCC. Therefore, the prediction methods shown in Figure 6.6 (Equation 6.5 and its similar formulations) and Figure 6.7 (Equations 6.9 and 6.11 and their similar formulations) are different. Equations 6.8, 6.9, 6.10 and 6.11 appear to be entirely empirical, however, it should be noted that they are essentially developed based on the mechanics of unsaturated soils considering the variations in the soil stiffness and strength properties with moisture content.

Such an approach can be further extended to incorporate the influence of external stress by expressing the Ω_{sat} and Ω_{opt} in Equations 6.8, 6.9, 6.10 and 6.11 using the stress dependent model. For instance, if M_{Rsat} and M_{Ropt} on the left-hand side of Equation 6.11 are expressed using Equation 6.12 and the corresponding k_1, k_2 and k_3 values summarized in Table 6.2 while the right-hand side of Equation 6.11 is calculated using m' and ξ' values derived from the normalized ratio - w relationships for the E (i.e. the fitted curves shown in continuous lines in Figure 6.7), the M_R - external stress - w relationships can be predicted. Figure 6.8 shows examples of the predicted M_R - σ_d - w relationships at σ_c or $\sigma_{c,net}$ of 27.6 kPa for the four tested soils. For each soil, the predicted non-linear M_R - w relationship, which is extrapolated from the E - w relationship, is extended along the σ_d axis following the M_{Rsat} - σ_d and M_{Ropt} - σ_d relationships predicted by Equation 6.12, and form a smooth surface in the M_R - σ_d - w space that reasonably fits the measurements.

6.5 Further validation of the proposed approach using published data from the literature

In order to further validate (i) similarities in the normalized Ω - moisture content relationships for different stiffness and strength properties and for different soil types, and (ii) flexibility of Equations 6.8, 6.9, 6.10 and 6.11 in fitting the normalized Ω - moisture content relationships, published experimental data reported from three different studies (Zhan 2003, Alramahi et al. 2010, Khoury et al. 2013) are collected and interpreted.

6.5.1 Zhan (2003) study on Zaoyang expansive clay

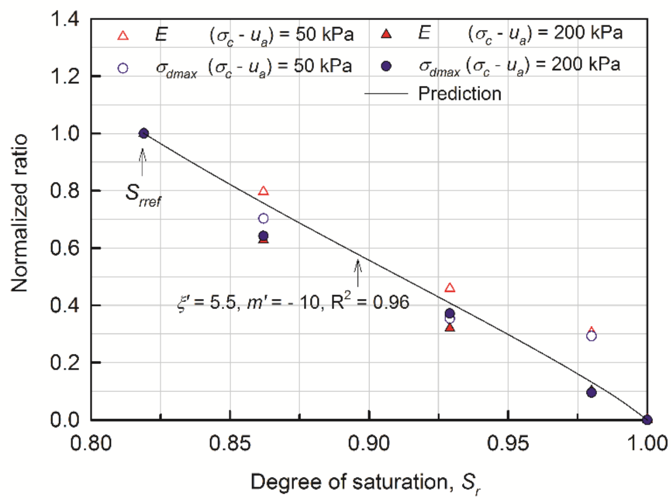

Figure 6.9 Measured and fitted variations in the normalized ratio with S_r for Zaoyang expansive soil

Zhan (2003) conducted soil suction-controlled triaxial tests on an expansive clay collected from Zaoyang, China (w_L% = 50.5, I_p% = 31, sand% = 3, silt% = 48, clay% = 39, CH, A-7-6). Specimens after compaction (s = 540 kPa) were wetted to higher S_r values up to saturation and sheared in drained condition under two $\sigma_{c,net}$ of 50 and 200 kPa. The E and maximum deviator stress (σ_{dmax}, used to indicate the peak shear strength) can be determined from the resulting stress-strain curves. The E, σ_{dmax} and S_r values at S_r = 0.819 (lowest S_r experienced during tests) are used as reference values Ω_{ref} and S_{rref} to replace the Ω_{opt} and S_{ropt} in Equation 6.10 since no triaxial tests were performed at compaction moisture content and S_r = 0.819 is closest to S_{ropt}. Figure 6.9 shows the normalized ratio (i.e. $(E - E_{sat}) / (E_{ref} - E_{sat})$ and $(\sigma_{dmax} - \sigma_{dmax,sat}) / (\sigma_{dmax,ref} - \sigma_{dmax,sat})$) versus S_r relationships measured by Zhan (2003) (shown as symbols) and fitted using Equation 6.10 (shown as a continuous line). For this example and the examples in later sections, all the measured normalized ratio - moisture content relationships are collectively fitted without distinguishing different mechanical properties. It is observed that the measured normalized ratio - S_r relationships for E and σ_{dmax} under both $\sigma_{c,net}$ levels show quite similar characteristic relationships. The features of this relationship are linear and are consistent with the "clay curve" in Figure 6.1(c), and can be fitted using Equation 6.10.

6.5.2 Alramahi et al. (2010) study on glass beads with different pore fluids

Alramahi et al. (2010) used uniform spherical glass beads that were saturated with deionized, silt-slurry and clay-slurry pore fluids to prepared specimens. Prepared saturated specimens were drained by evaporation to different lower S_r values until $S_r = 0$. Piezoelectric transduces were used to generate P and S waves to measure the shear modulus (G) and constraint modulus (M) of the specimens at different S_r during the drying process. Both Equations 6.8 and 6.10 are used for this case. As specimens were dried from saturated condition, the Ω_{ref} and S_{rref} should be used instead of Ω_{opt} and S_{ropt} in Equations 6.8 and 6.10. The G and M values at S_r values near 0.6 (S_{rref}) are used as G_{ref} and M_{ref}. It is noted that the choice of the Ω_{ref}, s_{ref} and S_{rref} does not significantly influence the performance of Equation 6.1 (Han and Vanapalli 2016b) and therefore will not significantly influence the performance of Equations 6.8 and 6.10 at lower s and higher S_r levels. Figure 6.10 shows the measured and fitted normalized ratio (i.e. $(G - G_{sat}) / (G_{ref} - G_{sat})$ and $(M - M_{sat}) / (M_{ref} - M_{sat})$) versus S_r relationships for the glass beads with different pore fluids. Measurements on the normalized G and M are quite uniform throughout the entire S_r range especially for the higher S_r range (say from 0.5 to 1.0). The fitted curves using Equations 6.8 and 6.10 capture the nonlinear characteristics of the measurements. Equation 6.8, which uses three parameters, is more flexible to better fit the measurements at higher S_r range (from 0.5 to 1.0) compared with Equation 6.10 which uses two parameters. It is also interesting to see that the glass beads, although they are non-plastic artificial materials, exhibit normalized ratio - S_r curves similar to "clay curve" shown in Figure 6.1(c) at higher S_r range when mixed with clay-slurry pore fluid. They however exhibit normalized ratio - S_r curves similar to "silt curve" or "sand curve" shown in Figure 6.1(c) at higher S_r range when mixed with silt-slurry and de-ionized pore fluids.

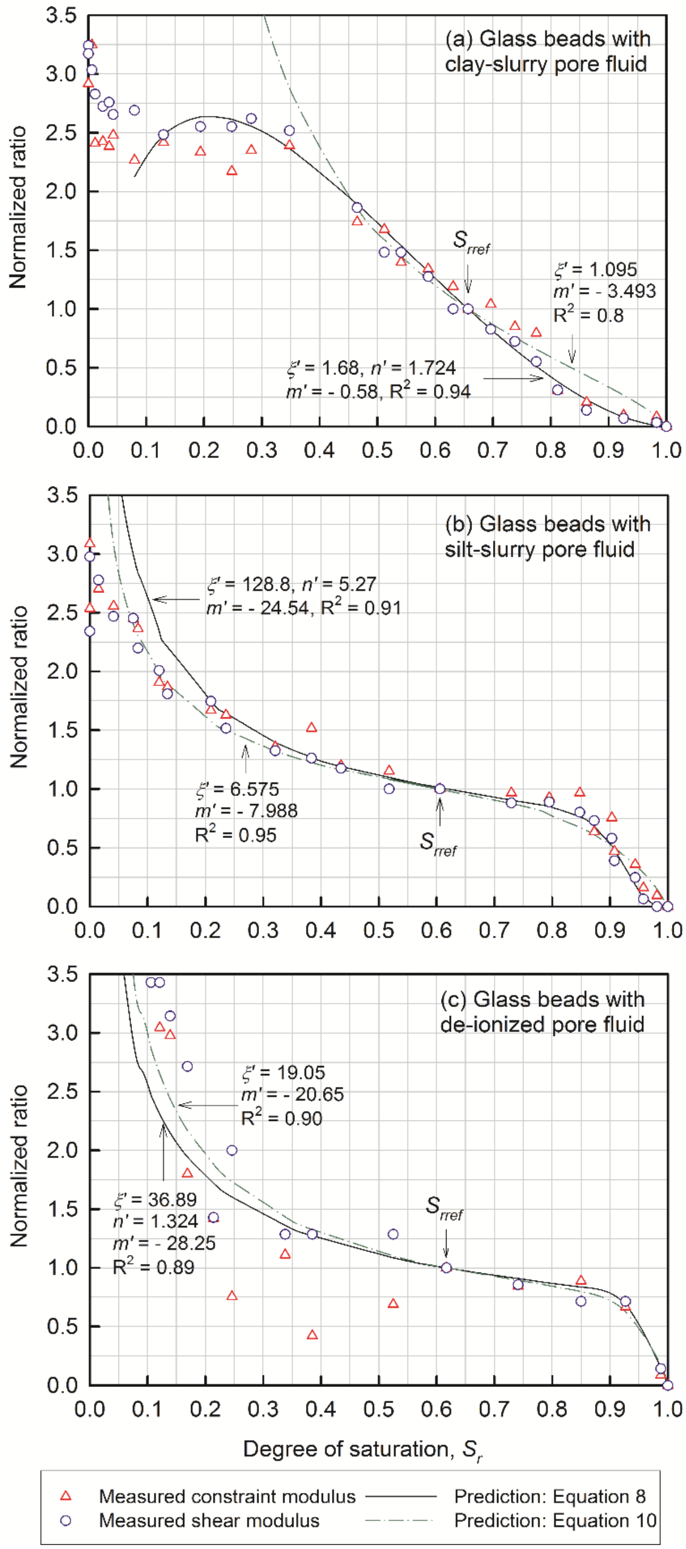

Figure 6.10 Measured and fitted variations in the normalized ratio with S_r for the glass beads with (a) clay-slurry, (b) clay-slurry and (c) de-ionized pore-fluids

6.5.3 Khoury et al. (2013) study on Alloway clay

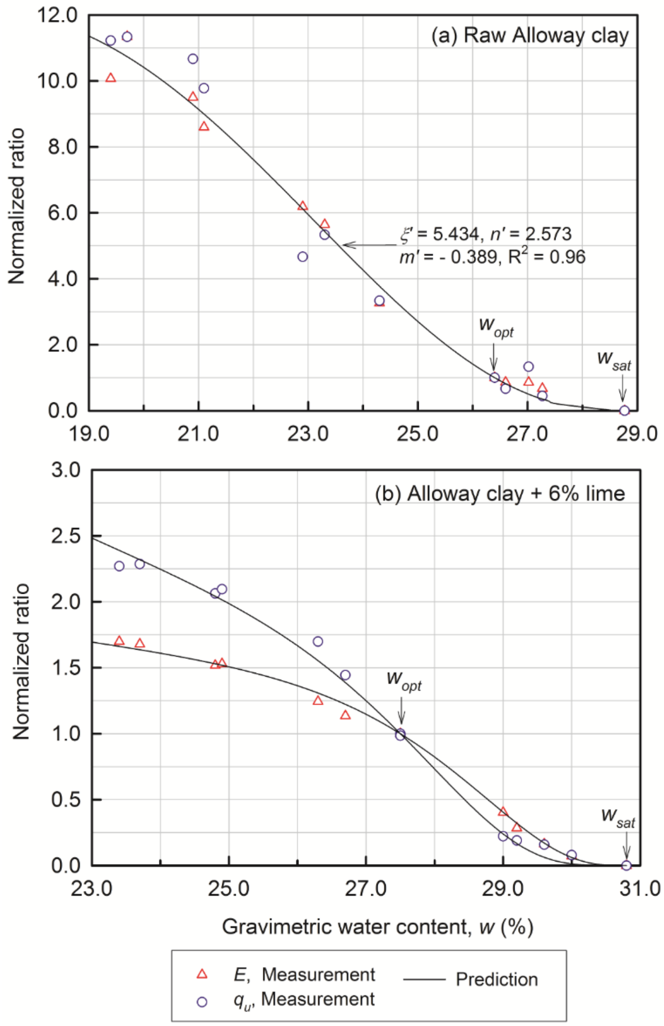

Figure 6.11 Measured and fitted variations in the normalized ratio with *w* for (a) raw Alloway clay and (b) Alloway clay with 6% lime

Khoury et al. (2013) performed UC tests to determine the E and q_u on a raw Alloway clay (w_L% = 51, I_p% = 29, sand% = 6, silt% = 48, clay% = 46, w_{opt} = 26.5%, CH, A-7-6) and Alloway clay stabilized by 6% of lime (Alloway clay + 6% lime, w_{opt} = 27.5%). Specimens were compacted at w_{opt} and tested or compacted at w_{opt} and brought to different w values using approaches suggested by Khoury and Zaman (2004) and tested. Figure 6.11(a) shows the comparisons between the measured and fitted (using Equation 6.9) normalized ratio (i.e. $(E - E_{opt}) / (E_{opt} - E_{sat})$ and $(q_u - q_{usat}) / (q_{uopt} - q_{usat})$) versus w relationships for the raw Alloway clay. Excellent consistency is observed between the behavior of the q_u and E and they can be reasonably fitted using Equation 6.9. Same comparisons are shown in Figure 6.11(b) for the Alloway clay stabilized by 6% lime. It can be observed that q_u and E are consistent at higher w range (say w between w_{opt} and w_{sat}); however distinct and increasing discrepancy between q_u and E appears at lower w range (say w lower than w_{opt}). For this scenario, Equation 6.9 is used to separately fit the q_u and E measurements. The behavior shown in Figure 6.11(b) can be attributed to the cementation forces that are associated with the stabilizing agents, such as the lime for the Alloway clay, which influence the stiffness and strength behavior differently at lower w range as can be observed from the different E and q_u behaviors in Figure 6.11(b).

6.6 Discussion and conclusion

This chapter summarizes extensive experimental investigations on the variation of the stiffness and shear strength (Ω) of compacted soils with moisture content determined from cyclic loading and modified UC tests performed on four subgrade soils from Canada (for which M_R, E and q_u are determined). The above measured data along with the published data from the literature on several soils (for which G and M, σ_{dmax} and E are determined) are normalized as $(\Omega - \Omega_{sat}) / (\Omega_{opt} - \Omega_{sat})$ versus w or S_r relationships or $(\Omega - \Omega_{sat}) / (\Omega_{ref} - \Omega_{sat})$ versus w or S_r relationships. It is found that such normalized relationships for different stiffness and strength properties are similar for a particular soil. An approach (represented by Equations 6.8, 6.9, 6.10 and 6.11), which is developed based on the mechanics of unsaturated soils, has been used to successfully fit such normalized relationships for all the soils. The similarity associated with the various properties are extrapolated to predict the M_R - w relationships which are cumbersome and time-consuming to determine from the easy-to-obtain E - w and q_u - w relationships.

Discussions are provided regarding the feasibility of the proposed approach:

(i) The key assumption in the proposed approach is that the soil suction is the key factor that influences the stiffness and shear strength behavior in response to moisture content changes in a similar fashion. Such an assumption is particularly valid for lower soil suction range (say 0 to 600kPa). Soil suction changes in this range are typically associated with the moisture content changes in liquid phase and are of greater importance in conventional geotechnical practice. At higher soil suction and lower moisture content range, physicochemical inter-particle forces such as the van der Waals and cementation forces have more significant influence compared to the soil suction. For such moisture content range, the similarity maybe valid but less pronounced for some unbonded soils such as the glass beads mixed with different pore fluids as shown in Figure 6.10 and the unbounded Alloway clay shown in Figure 6.11(a). The similarity also may not be valid for bonded soils such as the stabilized Alloway clay shown in Figure 6.11(b) due to the reason that the cementation forces introduced by the bounding agents govern the soil behavior at lower moisture content range and the effects of the cementation forces on the stiffness and strength behavior are different;

(ii) Stiffness and shear strength properties for a particular soil investigated in this study are determined under the same drainage conditions. For example, the M_R, E and q_u for the TSC, KLC, IHT and OLC are determined from cyclic loading and UC tests under undrained condition; the E and σ_{dmax} for the Zaoyang expansive soil are determined from triaxial tests under drained condition by Zhan (2013); the G and M for the glass beads are determined under small strain condition by Alramahi et al. (2010); and the E and q_u for the Alloway clay are determined from UC tests under undrained condition [.by Khoury et al. (2013). It is shown for all the investigated soils in this study that the stiffness / shear strength - moisture content relationships derived under the same drainage condition for the same soil, if normalized, exhibit remarkable similarity. However, such similarity between stiffness / shear strength - moisture content relationships derived from different drainage conditions needs to be verified using more experimental investigations. Therefore, it is suggested to use the similarity for mechanical properties derived under similar drainage conditions.

CHAPTER SEVEN

SUMMARY AND CONCLUSIONS

7.1 Summary

Studies presented in this thesis aim at providing a simple approach for geotechnical practitioners to predict the stiffness and shear strength properties (Ω) of unsaturated compacted soils. To achieve this objective, a unified methodology for modeling the non-linear variation of the Ω with soil suction is developed. Experimental data on various stiffness and shear strength properties including the peak and critical shear strength, elastic modulus, small strain shear modulus, resilient modulus, which are available in the literature, are used to validate the proposed methodology. It is found that the proposed methodology can provide reasonable predictions taking account of various influencing factors such as the external stress level, soil structure and fabric, type of soil, and hydraulic hysteresis.

In addition, comprehensive experimental program is performed to determine the resilient modulus, elastic modulus and unconfined compression strength of four typical Canadian subgrade soils taking account of the influence of soil suction and gravimetric water content. The measured Ω - soil suction relationships for the four soils are reasonably modeled using the proposed methodology. In addition, the measured Ω - gravimetric water content for the four soils also are well modeled using an approach that is developed based on the proposed methodology. The data gathered from the experimental program not only validate the proposed methodology but also are valuable for characterizing the local subgrade soils to facilitate implementation of the mechanistic pavement design method in Ontario.

7.2 Major conclusions

7.2.1 State-of-the-art review:

Various equations available in the literature to predict the variation of the resilient modulus with respect to soil suction are summarized into three groups:

Group A: Empirical relationships;

Group B: Constitutive models incorporating the soil suction into the applied shearing or confining stresses;

Group C: Constitutive models extending the independent stress state variable approach.

Several suggestions on the presently available equations in the literature are provided:

(i) Empirical relationships are easy and economical for use in practice; however, they are only suitable for certain soils and for limited soil suction ranges. Constitutive models are more flexible to consider various influencing factors and provide reasonably good predictions if the model parameters are calibrated using extensive experimental data. The calibrated model parameters for a particular soil within specific soil suction and applied stress ranges may not be suitable for other soils or even for the same soil subjected to different applied stress and soil suction ranges;

(ii) Most constitutive models proposed in the presently available literature to predict the resilient modulus - soil suction relationships are revised and improved from conventional stress-dependent constitutive models. However, model parameters for conventional models cannot be directly used in the improved models for prediction;

(iii) It is important to incorporate moisture content (i.e., gravimetric / volumetric water contents or degree of saturation) as a parameter into the constitutive models. Neglecting the influence of moisture content may result in unreasonable predictions of the resilient modulus when they are applied for a large soil suction range and not being able to take account the influence of hysteresis effects.

7.2.2 Predicting stiffness and shear strength of unsaturated soils

A new methodology is proposed in this thesis for predicting the stiffness and shear strength properties of unsaturated soils using a unified normalized function. The methodology relates the non-linearity of the soil-water characteristic curve (SWCC) to the non-linearity of the Ω - soil suction relationships using i) a parameter ξ and ii) measurements of Ω at saturation condition and one unsaturated condition (i.e., reference condition). Validations of the proposed methodology using the experimental data of different stiffness and shear strength properties for 8 cohesionless and 17 cohesive soils suggest that the methodology can reasonably well interpret and predict the behaviour of stiffness and shear strength within lower suction range taking account of various influencing factors. A unique ξ value of 1.0 and 2.0 are respectively suggested for cohesionless (%clay < 10) and cohesive soils (%clay ≥ 10 and / or I_p% ≥ 12). The proposed methodology can be used as a convenient prediction model in geotechnical engineering practice as it only requires limited testing results and does not need calibration.

7.2.3 Predicting the resilient modulus of compacted subgrade soils

The proposed methodology is examined for its strengths and limitations for predicting the variation of the resilient modulus with respect to soil suction for compacted fine-grained subgrade soils. The optimum moisture content condition is used as the reference unsaturated condition in the proposed methodology for predicting the resilient modulus. A total of 16 sets of experimental data derived from 11 different subgrade soils following different testing protocols are selected to test the performance of the methodology. The comparisons show that the proposed model is capable of reliably predicting the variation of the resilient modulus with respect to soil suction using a single-valued model parameter ξ equal to 2.0.

Several discussions are provided towards using the methodology for predicting the resilient modulus - soil suction relationships:

(i) The resilient modulus at saturated and optimum moisture content conditions required in the proposed methodology are conventionally determined for use in the pavement design practice with the aid of the repeated loading triaxial tests. The resilient modulus at saturated condition is less sensitive to the applied stress levels and can be assumed as a constant value. The resilient modulus at optimum moisture content conditions, on the other hand, can be predicted using the existing conventional stress-dependent models;

(ii) The proposed methodology, using the drying SWCC or the apparent SWCC, provides reliable predictions. Further studies using the SWCC taking account of the influence of cyclic loading, hysteresis and soil structure for predicting the M_R are encouraged to improve the performance of the proposed methodology;

(iii) The measured resilient modulus - soil suction - external stress relationships highlight coupled characteristics. The proposed model predicts smooth *3D* surfaces for the resilient modulus - soil suction - external stress plots that well reproduce the coupled characteristics of the measured data. The predicted smooth *3D* surfaces also help to reduce the possible numerical problems when the proposed model is used for numerical simulations;

7.2.4 Experimental investigations on the resilient modulus of compacted subgrade soils

The variation of resilient modulus with respect to moisture content and soil suction for several Canadian subgrade soils is determined using two different testing techniques: axis-translation technique which imposes soil suction on specimen before the cyclic triaxial tests and filter paper method which measures soil suction from specimens subjected to cyclic triaxial tests. It is found that the resilient modulus - soil suction relationships are non-linear and are influenced by the external stress level as well as the soil type. Soil with higher plasticity is more sensitive to the changes in the soil suction and moisture content. Experimental results are reasonably well predicted using the proposed methodology based on limited and easy-to-obtain experimental data. This experimental investigation is of interest for better understanding the resilient behavior of unsaturated subgrade soils in Canada.

7.2.5 Normalizing variation of soil stiffness and strength with moisture content

Modified unconfined compression tests are performed to determine the elastic modulus - moisture content and unconfined compression strength - moisture content relationships for the compacted Canadian subgrade soils. These relationships, together with the measured resilient modulus - moisture content relationship, are normalized using an approach that is developed based on the proposed unified methodology. There are significant similarities in the characteristics of these normalized relationships. It is shown for unbound soils within higher moisture content range (lower soil suction range), such similarities can be used to predict the variation of the Ω with moisture content that is cumbersome and time-consuming to measure or predict (such as the resilient modulus - moisture content relationship) from the Ω - moisture content relationships that are easy and convenient to measure (such as elastic modulus - and unconfined compression strength - moisture content relationships).

7.3 Suggestions for future studies

Several suggestions are provided for implement and improve the methodology introduced in this thesis:

(i) The accuracy of using moisture content - soil suction relationships defined by SWCC to simulate the actual moisture content - soil suction relationships within the soil specimens subjected to stiffness / shear strength experiments is dependent on the similarity between the experimental conditions applied during the SWCC tests and that applied during the stiffness / shear strength experiments. Soil suction is sensitive to changes during monotonic and cyclic loading tests especially under undrained condition. The rational understanding of the variation of the soil suction during the stiffness / shear strength experiments helps to better highlight the moisture content - soil suction relationships and to improve the performance of the proposed methodology;

(ii) There are several methods available in the literature to estimate the SWCC with different levels of accuracy. These methods, if used to estimate the SWCC required in the proposed method, can further simplify and reduce the procedures and experimental data required to implement the proposed methodology;

(iii) The proposed methodology for stiffness and shear strength properties of unsaturated soils should be jointly used with advanced hydraulic models that can suitably describe the distribution and variation in the soil suction and moisture content in response to various environmental boundary conditions. This can be possibly accomplished by incorporating the proposed methodology into existing numerical software that already possess advanced hydraulic analysis functions for unsaturated soils.

REFERENCES

AASHTO. (1986). *Guide for Design of Pavement Structures*. American Association of State Highway and Transportation Officials. Washington, D.C.

AASHTO. (1992). Designation T292-91: *Standard Method of Test for Resilient Modulus of Subgrade Soils and Untreated Base/Sub-Base Materials*. American Association of State Highway and Transportation Officials. Washington, D.C.

AASHTO. (1996). Provisional Standard TP46-94: *Provisional Method for Determining the Resilient Modulus of Soils and Aggregate Materials*. American Association of State Highway and Transportation Officials. Washington, D. C.

AASHTO. (2003). Designation T307-99: *Determining the Resilient Modulus of Soils and Aggregate Materials*. American Association of State Highway and Transportation Officials. Washington, D.C.

AASHTO. (2008). Designation M-145: *Classification of Soil and Soil-Aggregate Mixtures for Highway Construction*. American Association of State Highway and Transportation Officials. Washington, D.C.

Abu-Farsakh, M. Y., Mehrotra, A., Mohammad, L., and Gaspard, K. (2015). "Incorporating the effect of moisture variation on resilient modulus for unsaturated fine-grained subgrade soils." In *Proceedings of Transportation Research Board 94th Annual Meeting* (No. 15-1149).

Alonso, E. E., Gens, A., and Josa, A. (1990). "A constitutive model for partially saturated soils." *Géotechnique,* 40(3): 405-430.

Alonso, E. E., Pereira, J. M., Vaunat, J., and Olivella, S. (2010). "A microstructurally based effective stress for unsaturated soils." *Géotechnique*, 60(12): 913-925.

Alonso, E. E., Pinyol, N. M., and Gens, A. (2013). "Compacted soil behaviour: initial state, structure and constitutive modelling." *Géotechnique*, 63(6): 463-478.

Alramahi, B., Alshibli, K. A., and Fratta, D. (2010). "Effect of fine particle migration on the small-strain stiffness of unsaturated soils." *Journal of Geotechnical and Geoenvironmental Engineering*, 136(4): 620-628.

ARA, Inc., ERES Consultants Division. (2004). *Guide for Mechanistic - Empirical Design of New and Rehabilitated Pavement Structures*. Final report, NCHRP Project 1-37A. Transportation Research Board, Washington, D.C.

ASTM. (2007). Designation: D422-63: *Standard Test Method for Particle-Size Analysis of Soils*. American Society for Testing and Materials. West Conshohocken, PA.

ASTM. (2009). Designation: D6913-04: *Standard Test Methods for Particle-Size Distribution (Gradation) of Soils Using Sieve Analysis*. American Society for Testing and Materials. West Conshohocken, PA.

ASTM. (2010). Designation: D5298-10: *Standard Test Method for Measurement of Soil Potential (Suction) Using Filter Paper*. American Society for Testing and Materials. West Conshohocken, PA.

ASTM. (2011). Designation: D2487-11: *Standard Practice for Classification of Soils for Engineering Purposes (Unified Soil Classification System)*. American Society for Testing and Materials. West Conshohocken, PA.

ASTM. (2012). Designation: D698-12: *Standard Test Methods for Laboratory Compaction Characteristics of Soil Using Standard Effort (12400 ft-lbf/ft^3 (600 kN-m/m^3))*. American Society for Testing and Materials. West Conshohocken, PA.

ASTM. (2013). Designation: D2166-13: *Standard Test Method for Unconfined Compressive Strength of Cohesive Soil*. American Society for Testing and Materials. West Conshohocken, PA.

Atkinson, J. H. (2000). "Non-linear soil stiffness in routine design." *Géotechnique*, 50(5): 487-508.

Azam, A. M., Cameron, D. A., and Rahman, M. M. (2013). "Model for prediction of resilient modulus incorporating matric suction for recycled unbound granular materials." *Canadian Geotechnical Journal*, 50(11): 1143-1158.

Ba, M., Nokkaew, K., Fall, M., and Tinjum, J. M. (2013). "Effect of matric suction on resilient modulus of compacted aggregate base courses." *Geotechnical and Geological Engineering*, 31(5): 1497-1510.

Baker, R., and Frydman, S. (2009). "Unsaturated soil mechanics: Critical review of physical foundations." *Engineering Geology*, 106(1): 26-39.

Barbour, S. L. (1998). Nineteenth Canadian geotechnical colloquium: The soil-water characteristic curve: a historical perspective. *Canadian Geotechnical Journal,* 35(5): 873-894.

Barden, L. (1965). “Consolidation of compacted and unsaturated clays.” *Géotechnique*, 15(3): 267-286.

Barrera, M. (2002). *Estudio experimental del comportamiento hidromecánico de suelos colapsados*. PhD thesis, Universitat Politècnica de Catalunya, Barcelona, Spain (in Spanish).

Bishop, A. W. (1959). “The principle of effective stress.” *Tecknish Ukebland*, 106(39): 859-863.

Blight, G. E. (2013). *Unsaturated Soil Mechanics in Geotechnical Practice*. CRC Press.

Brooks, R. H., and Corey, A. T. (1964). “Hydraulic properties of porous medium.” Colorado State University (Fort Collins), Hydrology Paper 3.

Brown, S. F. (1996). “Soil mechanics in pavement engineering.” *Géotechnique*, 46(3): 383-426.

Brown, S. F., and Selig, E. T. (1991). ‘‘The design of pavement and rail track foundations.’’ *Cyclic loading of soils: From theory to design*, M. P. O’Reilly and S. F. Brown, eds., Blackie and Son Ltd., Glasgow, Scotland, 249-305.

Brydon, J. E., and Patry, L. M. (1961). “Mineralogy of Champlain Sea sediments and a Rideau clay soil profile.” *Canadian Journal of Soil Science*, 41(2): 169-181.

Caicedo, B., Coronado, O., Fleureau, J. M., and Correia, A. G. (2009). “Resilient behaviour of non-standard unbound granular materials.” *Road Materials and Pavement Design*, 10(2): 287-312.

Caliendo, C. (2012). “Local calibration and implementation of the mechanistic-empirical pavement design guide for flexible pavement design.” *Journal of Transportation Engineering*, 138(3): 348-360.

Cary, C. E. (2011). *Pore Water Pressure Response of a Soil Subjected to Traffic Loading under Saturated and Unsaturated Conditions*. Ph.D. thesis, Arizona State University, Phoenix, Arizona.

Cary, C. E. and Zapata, C. E. (2011). “Resilient modulus for unsaturated unbound materials.” *Road Materials and Pavement Design*, 12(3): 615-638.

Cary, C. E., and Zapata, C. E. (2016). “Pore water pressure response of soil subjected to dynamic loading under saturated and unsaturated conditions." *International Journal of Geomechanics*, DOI: 10.1061/(ASCE)GM.1943-5622.0000642.

Ceratti, J. A., Gehling, W. Y. Y., and Núñez, W. P. (2004). "Seasonal variations of a subgrade soil resilient modulus in southern Brazil." *Transportation Research Record. 1874*, Transportation Research Board, Washington, D. C., 165-173.

Chin, K. B., Leong, E. C., and Rahardjo, H. (2010). "A simplified method to estimate the soil-water characteristic curve." *Canadian Geotechnical Journal*, 47(12): 1382-1400.

Chiu, C. F., Yan, W. M., and Yuen, K. V. (2012). "Reliability analysis of soil–water characteristics curve and its application to slope stability analysis." *Engineering Geology*, 135: 83-91.

Coronado, O., Caicedo, B., Taibi, S., Correia, A. G., and Fleureau, J. M. (2011). "A macro geomechanical approach to rank non-standard unbound granular materials for pavements." *Engineering Geology*, 119(1): 64-73.

Coussy, O. (2004). *Poromechanics*. John Wiley & Sons.

Craciun, O., and Lo, S. C. R. (2010). "Matric suction measurement in stress path cyclic triaxial testing of unbound granular base materials." *Geotechnical Testing Journal*, 33(1): 33-44.

Cui, Y. J., and Delage, P. (1996). "Yielding and plastic behaviour of an unsaturated compacted silt." *Géotechnique*, 46(2): 291-311.

Cunningham, M. R., Ridley, A. M., Dineen, K., and Burland, J. B. (2003). "The mechanical behaviour of a reconstituted unsaturated silty clay." *Géotechnique*, 53(2): 183-194.

Delage, P., Audiguier, M., Cui, Y. J., and Howat, M. D. (1996). "Microstructure of a compacted silt." *Canadian Geotechnical Journal*, 33(1): 150-158.

Doucet, F., and Doré, G. (2004). "Module réversible et coefficient de poisson réversible des matériaux granulaires C-LTPP." *Proc. 57th Canadian Geotechnical Conference and the 5th Joint CGS/IAH-CNC Conference*, Québec, Canada.

Drumm, E. C., Reeves, J. S., Madgett, M. R., and Trolinger, W. D. (1997). "Subgrade resilient modulus correction for saturation effects." *Journal of Geotechnical and Geoenvironmental Engineering*, 123(7): 663-670.

Duncan, J. M., and Chang, C. Y. (1970). "Nonlinear analysis of stress and strain in soils."

Journal of the Soil Mechanics and Foundations Division, 96(5): 1629-1653.

Edil, T. B., and Motan, S. E. (1979). "Soil-water potential and resilient behavior of subgrade soils." *Transportation Research Record, 705,* Transportation Research Board, Washington, D. C., 54-63.

Edil, T. B., Motan, S. E., and Toha, F. X. (1981). "Mechanical behavior and testing methods of unsaturated soils." *Laboratory Shear Strength of Soil. ASTM STP 740*, American Society for Testing and Materials, 114-129.

Edris, E. V., and Lytton, R. L. (1976). *Dynamic Properties of Subgrade Soils, Including Environmental Effects*. Report Number: TTI-2-18-74-164-3, Texas A&M University, Texas, USA.

Ekblad, J., and Isacsson, U. (2006). "Influence of water on resilient properties of coarse granular materials." *Road materials and pavement design*, 7(3): 369-404.

Escario, V., and Saez, J. (1986). "The shear strength of partly saturated soils." *Géotechnique*, 36(3): 453-456.

Escario, V., Juca, J. F. T., and Coppe, M. S. (1989). "Strength and deformation of partly saturated soils." In *Proceedings of the 12th ICSMFE,* Rio de Janeiro, 1, 43-46.

Fredlund, D. G. (2006). "Unsaturated soil mechanics in engineering practice." *Journal of Geotechnical and Geoenvironmental Engineering*, 132(3): 286-321.

Fredlund, D. G., and Rahardjo, H. (1993). *Soil Mechanics for Unsaturated Soils*, John Wiley and Sons, Inc. NY, USA.

Fredlund, D. G., and Xing, A. (1994). "Equations for the soil-water characteristic curve." *Canadian Geotechnical Journal,* 31(4): 521-532.

Fredlund, D. G., Bergan, A. T., and Wong, P. K. (1977). "Relation between resilient modulus and stress research conditions for cohesive subgrade soils." *Transportation Research Record*, *642*, Transportation Research Board, Washington, D. C., 73-81.

Fredlund, D. G., Morgenstern, N. R., and Widger, R. A. (1978). "The shear strength of unsaturated soils." *Canadian Geotechnical Journal,* 15(3): 313-321.

Fredlund, D. G., Xing, A., and Huang, S. (1994). "Predicting the permeability function for unsaturated soils using the soil-water characteristic curve." *Canadian Geotechnical Journal*, 31(4): 533-546.

Fredlund, D. G., Xing, A., Fredlund, M. D., and Barbour, S. L. (1996). "The relationship of the unsaturated soil shear to the soil-water characteristic curve." *Canadian Geotechnical Journal*, 33(3): 440-448.

Fung, Y. C. (1977). *A First Course in Continuum Mechanics*. Englewood Cliffs, NJ, Prentice-Hall, Inc.

Gallipoli, D. (2012). "A hysteretic soil-water retention model accounting for cyclic variations of suction and void ratio." *Géotechnique*, 62, No. 7, 605-616.

Gallipoli, D., Bruno, A. W., D'onza, F., and Mancuso, C. (2015). "A bounding surface hysteretic water retention model for deformable soils." *Géotechnique*, 65(10): 793-804.

Gallipoli, D., Gens, A., Sharma, R., and Vaunat, J. (2003). "An elasto-plastic model for unsaturated soil incorporating the effects of suction and degree of saturation on mechanical behaviour." *Géotechnique*, 53(1): 123-136.

Gan, J. K. M., Fredlund, D. G., and Rahardjo, H. (1988). "Determination of the shear strength parameters of an unsaturated soil using the direct shear test." *Canadian Geotechnical Journal*, 25(3): 500-510.

Garven, E. A., and Vanapalli, S. K. (2006). "Evaluation of empirical procedures for predicting the shear strength of unsaturated soils." *Proceedings of the 4th International Conference on Unsaturated Soils*, Carefree, USA, 2570-2581.

Geiser, F., Laloui, L., and Vulliet, L. (2006). "Elasto-plasticity of unsaturated soils: laboratory test results on a remoulded silt." *Soils and Foundations*, 46(5): 545-556.

Gens, A., and Alonso, E. E. (1992). "A framework for the behaviour of unsaturated expansive clays." *Canadian Geotechnical Journal*, 29(6): 1013-1032.

Gens, A. (2010). "Soil–environment interactions in geotechnical engineering." *Géotechnique*, 60(1): 3-74.

George, K. P. (2004). *Prediction of Resilient Modulus from Soil Index Properties*. Rep. No. FHWA/MS-DOT-RD-04-172, Federal Highway Administration, U.S. Department of Transportation, Washington, D.C.

Ghayoomi, M., and McCartney, J. S. (2011). "Measurement of small-strain shear moduli of partially saturated sand during infiltration in a geotechnical centrifuge." *Geotechnical Testing Journal*, 34(5): 1-11.

Gu, F., Sahin, H., Luo, X., Luo, R., and Lytton, R. L. (2014). “Estimation of resilient modulus of unbound aggregates using performance-related base course properties.” *Journal of Materials in Civil Engineering*. DOI: 10.1061/(ASCE)MT.1943-5533.0001147.

Gui, M. W., and Wu, Y. M. (2014). “Failure of soil under water infiltration condition.” *Engineering Geology*, 181: 124-141.

Gupta, S. C., Ranaivoson, A., Edil, T. B., Benson, C. H., and Sawangsuriya, A. (2007). *Pavement Design using Unsaturated Soil Technology*, Report number: MN/RC-2007-11, Minnesota Department of Transportation, St. Paul, Minnesota.

Hamid, T. B., and Miller, G. A. (2009). “Shear strength of unsaturated soil interfaces.” *Canadian Geotechnical Journal*, 46(5): 595-606.

Han, Z., and Vanapalli, S. K. (2014). “Semi-empirical model for predicting the resilient modulus of unsaturated fine-grained soils using the soil-water characteristic curve.” *Proceeding of the 6th International Conference on Unsaturated Soils*, Sydney, Australia, 797-803.

Han, Z., and Vanapalli, S. K. (2015). “Model for predicting the resilient modulus of unsaturated subgrade soil using the soil-water characteristic curve.” *Canadian Geotechnical Journal*, 52(10): 1605-1619.

Han, Z., and Vanapalli, S. K. (2016a). “State-of-the-Art: Prediction of resilient modulus of unsaturated subgrade soils.” *International Journal of Geomechanics*. DOI: 10.1061/(ASCE)GM.1943-5622.0000631.

Han, Z., and Vanapalli, S. K. (2016b). “Stiffness and shear strength of unsaturated soils in relation to soil-water characteristic curve.” *Géotechnique*. DOI: 10.1680/geot./15-P-104.

Heath, A. C., Pestana, J. M., Harvey, J. T., and Bejerano, M. O. (2004). “Normalizing behavior of unsaturated granular pavement materials.” *Journal of Geotechnical and Geoenvironmental Engineering*, 130(9): 896-904.

Hilf, J.W. (1956). “An investigation of pore water pressure in compacted cohesive soils.” *Technical memorandum 654*. United State Department of the Interior. Bureau of Reclamation, Denver Colorado.

Ho, X. N., Nowamooz, H., Chazallon, C., and Migault, B. (2014a). “Influence of fine content and water content on the resilient behaviour of a natural compacted sand.” *Road Materials and Pavement Design*, 15(3): 606-621.

Ho, X. N., Nowamooz, H., Chazallon, C., and Migault, B. (2014b). “Effective stress concept for the effect of hydraulic hysteresis on the resilient behaviour of low traffic pavements.” *International Journal of Pavement Engineering*, DOI: 10.1080/10298436.2014.973025.

Hossain, M. S. (2008). *Characterization of Subgrade Resilient Modulus for Virginia Soils and Its Correlation with the Results of Other Soil Tests*. Report number: VTRC 09-R4, Virginia Transportation Research Council, Virginia.

Hossain, M. S., and Kim, W. S. (2015). “Estimation of subgrade resilient modulus for fine-grained soil from unconfined compression test.” *Transportation Research Record, 2473*, Transportation Research Board, Washington, D.C., 126-135.

Houston, S. L., and Ge, D. (2014). “Characterization of unsaturated soils: The importance of response to wetting.” In *Proceedings of the ASCE Geo-Congress 2014 Conference*, 77-96.

Hoyos, L. R., Pérez-Ruiz, D. D., and Puppala, A. J. (2011). “Refined true triaxial apparatus for testing unsaturated soils under suction-controlled stress paths.” *International Journal of Geomechanics*, 12(3): 281-291.

Hoyos, L. R., Suescún-Florez, E. A., and Puppala, A. J. (2015). “Stiffness of intermediate unsaturated soil from simultaneous suction-controlled resonant column and bender element testing.” *Engineering Geology*, 188(7): 10-28.

Jardine, R. J., Symes, M. J., and Burland, J. B. (1984). “Measurement of soil stiffness in the triaxial apparatus.” *Géotechnique*, 34(3): 323-340.

Jin, M. S., Lee, K. W., and Kovacs, W. D. (1994). “Seasonal variation of resilient modulus of subgrade soils.” *Journal of Transportation Engineering*, 120(4): 603-616.

Johnson, T. C., Berg, R. L., Chamberlain, E. L., and Cole, D. M. (1986). *Frost Action Predictive Techniques for Roads and Airfields. A Comprehensive Survey of Research Findings*. CRREL Report 86–18. U.S. Army Corps of Engineers, Cold Regions Research and Engineering Laboratory, Hanover, NH.

Jotisankasa, A., Coop, M., and Ridley, A. (2009). “The mechanical behaviour of an unsaturated compacted silty clay." *Géotechnique*, 59(5): 415-428.

Khalili, N., and Khabbaz, M. H. (1998). "A unique relationship of χ for the determination of the shear strength of unsaturated soils." *Géotechnique,* 48(5): 681-687.

Khalili, N., and Zargarbashi, S. (2010). "Influence of hydraulic hysteresis on effective stress in unsaturated soils." *Géotechnique*, 60(9): 729-734.

Khalili, N., Geiser, F., and Blight, G. E. (2004). "Effective stress in unsaturated soils: review with new evidence." *International Journal of Geomechanics*, 4(2): 115-126.

Khazanovich, L., Celauro, C., Chadbourn, B., Zollars, J., and Dai, S. (2006). "Evaluation of subgrade resilient modulus predictive model for use in mechanistic-empirical pavement design guide." *Transportation Research Record, 1947*, Transportation Research Board, Washington, D.C., 155-166.

Khosravi, A., and McCartney, J. S. (2012). "Impact of hydraulic hysteresis on the small-strain shear modulus of low plasticity soils." *Journal of Geotechnical Engineering*, 138(11): 1326-1333.

Khoury, C. N., Brooks, R., Boeni, S. Y., and Yada, D. (2013). "Variation of resilient modulus, strength, and modulus of elasticity of stabilized soils with postcompaction moisture contents." *Journal of Materials in Civil Engineering*, 25(2): 160-166.

Khoury, C. N., Khoury, N. N., and Miller, G. A. (2011). "Effect of cyclic suction history (hydraulic hysteresis) on resilient modulus of unsaturated fine-grained soil." *Transportation Research Record*, *2232*, Transportation Research Board, Washington, D. C., 68-75.

Khoury, N. N., and Zaman, M. M. (2004). "Correlation between resilient modulus, moisture variation, and soil suction for subgrade soils." *Transportation Research Record*, *1874*, Transportation Research Board, Washington, D.C., 99-107.

Khoury, N. N., Brooks, R., and Khoury, C. N. (2009). "Environmental influences on the engineering behavior of unsaturated undisturbed subgrade soils: effect of soil suctions on resilient modulus." *International Journal of Geotechnical Engineering*, 3(2): 303-311.

Khoury, N., Brooks, R., Boeni, S. Y., and Yada, D. (2013). "Variation of resilient modulus, strength, and modulus of elasticity of stabilized soils with postcompaction moisture contents." *Journal of Materials in Civil Engineering*, 25(2): 160-166.

Khoury, N., Brooks, R., Khoury, C., and Yada, D. (2011). “Modeling resilient modulus hysteretic behavior with moisture variation.” *International Journal of Geomechanics*, 12(5): 519-527.

Kim, W. S., and Borden, R. H. (2011). Influence of soil type and stress state on predicting shear strength of unsaturated soils using the soil-water characteristic curve. *Canadian Geotechnical Journal*, 48(12): 1886-1900.

Lee, W., Bohra, N. C., Altschaeffl, A. G., and White, T. D. (1997). “Resilient modulus of cohesive soils.” *Journal of Geotechnical and Geoenvironmental Engineering*, 123(2): 131-136.

LeKarp, F., Isacsson, U., and Dawson, A. (2000). “State of the art. I: Resilient response of unbound aggregates.” *Journal of Transportation Engineering*, 126(1): 66-75.

Li, D., and Selig, E. T. (1994). “Resilient modulus for fine-grained subgrade soils.” *Journal of Geotechnical Engineering*, 120(6): 939-957.

Liang, R. Y., Rabab’ah, S., and Khasawneh, M. (2008). “Predicting moisture-dependent resilient modulus of cohesive soils using soil suction concept.” *Journal of Transportation Engineering*, 134(1): 34-40.

Loach, S. C. (1987). *Repeated Loading of Fine Grained Soils for Pavement Design*. Ph.D. Thesis, University of Nottingham, Nottingham, UK.

Lu, N., and Kaya, M. (2013). “A drying cake method for measuring SSCC, SWRC and hydraulic conductivity function.” *Geotechnical Testing Journal*, 36(1): 1-19.

Lu, N. (2008). “Is matric suction a stress variable?” *Journal of geotechnical and Geoenvironmental Engineering*, 134(7): 899-905.

Lu, N., and Kaya, M. (2014). “Power law for elastic moduli of unsaturated soil.” *Journal of Geotechnical and Geoenvironmental Engineering*, 140(1): 46-56.

Lu, N., and Likos, W. J. (2006). “Suction stress characteristic curve for unsaturated soil.” *Journal of Geotechnical and Geoenvironmental Engineering*, 132(2): 131-142.

Lu, N., Godt, J. W., and Wu, D. T. (2010). “A closed-form equation for effective stress in unsaturated soil.” *Water Resources Research*, DOI: 10.1029/2009WR008646.

Lytton, R. L. (1995). “Foundations and pavements on unsaturated soils.” *Keynote Address, Proc. 1st International Conference on Unsaturated Soils*, Paris, France, 3:1201-1220.

Malla, R. B., and Joshi, S. (2008). "Subgrade resilient modulus prediction models for coarse and fine-grained soils based on long-term pavement performance data." *International Journal Pavement Engineering*, 9(6): 431-444.

Miao, L., Liu, S., and Lai, Y. (2002). "Research of soil-water characteristics and shear strength features of Nanyang expansive soil." *Engineering Geology*, 65(4): 261-267.

Mitchell, J. K., and Soga, K. (2005). *Fundamental behaviour of soils*. Hoboken, NJ, John Wiley & Sons.

Moossazadeh, J., and Witczak, M. W. (1981). "Prediction of subgrade moduli for soil that exhibits nonlinear behavior." *Transportation Research Record*, 810, Transportation Research Board, Washington, D. C., 9-17.

Morales, L., Romero, E., Jommi, C., Garzón, E., and Giménez, A. (2015). "Ageing effects on the small-strain stiffness of a bio-treated compacted soil." *Géotechnique Letters*, 5(3), 217-223.

Ng, C. W. W., and Pang, Y. W. (2000). "Influence of stress state on soil-water characteristics and slope stability." *Journal of Geotechnical and Geoenvironmental Engineering*, 126(2): 157-166.

Ng, C. W. W., and Yung, S. Y. (2008). "Determination of the anisotropic shear stiffness of an unsaturated decomposed soil." *Géotechnique*, 58(1): 23-35.

Ng, C. W. W., and Zhou, C. (2014). "Cyclic behaviour of an unsaturated silt at various suctions and temperatures." *Géotechnique*, 64(9): 709-720.

Ng, C. W. W., Lai, C. H., and Chiu, C. F. (2012). "A modified triaxial apparatus for measuring the stress path-dependent water retention curve." *Geotechnical Testing Journal*, 35(3): 490-495.

Ng, C. W. W., Zhou, C., Yuan, Q., and Xu, J. (2013). "Resilient modulus of unsaturated subgrade soil: experimental and theoretical investigations." *Canadian Geotechnical Journal*, 50(2): 223-232.

Nokkaew, K., Tinjum, J. M., Likos, W. J., and Edil, T. B. (2014). "Effect of matric suction on resilient modulus for compacted recycled base course in postcompaction state." *Transportation Research Record 2433*, Transportation Research Board, Washington, D.C., 68-78.

Nowamooz, H., Chazallon, C., Arsenie, M. I., Hornych, P., and Masrouri, F. (2011).

"Unsaturated resilient behavior of a natural compacted sand." *Computers and Geotechnics*, 38(4): 491-503.

Nowamooz, H., Jahangir, E., and Masrouri, F. (2013). "Volume change behaviour of a swelling soil compacted at different initial states." *Engineering Geology*, 153: 25-34.

Nuth, M., and Laloui, L. (2008). "Effective stress concept in unsaturated soils: Clarification and validation of a unified framework." *International Journal for Numerical and Analytical Methods in Geomechanics*, 32(7): 771-801.

Odezugo, L. O., Donald, I. B., and Parkin, A. K. (1994). "The effect of traffic loads and environmental conditions on resilient modulus." *Proceeding of the 17th Australian Road Research Board Conference*, Gold Coast, Australia, 2: 191-198.

Oh, J. H., Fernando, E. G., Holzschuher, C. and Horhota, D. (2012). "Comparison of resilient modulus values for Florida flexible mechanistic-empirical pavement design." *International Journal of Pavement Engineering*, 13(5): 472-484.

Oh, W. T., and Vanapalli, S. K. (2011). "Modelling the applied vertical stress and settlement relationship of shallow foundations in saturated and unsaturated sands." *Canadian Geotechnical Journal*, 48(3): 425-438.

Oh, W. T., and Vanapalli, S. K. (2013). "Interpretation of the bearing capacity of unsaturated fine-grained soil using the modified effective and the modified total stress approaches." *International Journal of Geomechanics*, 13(6): 769-778.

Oh, W. T., and Vanapalli, S. K. (2014). "Semi-empirical model for estimating the small-strain shear modulus of unsaturated non-plastic sandy soils." *Geotechnical and Geological Engineering*, 32(2), 259-271.

Oh, W. T., Vanapalli, S. K., and Puppala, A. J. (2009). "Semi-empirical model for the prediction of modulus of elasticity for unsaturated soils." *Canadian Geotechnical Journal*, 46(8): 903-914.

Oloo, S. Y., and Fredlund, D. G. (1998). "The application of unsaturated soil mechanics theory to the design of pavements." *Proceedings of the 5th International Conference on the Bearing Capacity of Roads and Airfields*. Trondheim, Norway, 1419-1428.

Parreira, A. B., and Gonçalves, R. F. (2000). "The influence of moisture content and soil suction on the resilient modulus of a lateritic subgrade soil." *International Conference on Geotechnical and Geological Engineering*, Melbourne, Australia.

Power, K. C., and Vanapalli, S. K. (2010). "Modified null pressure plate apparatus for measurement of matric suction." *Geotechnical Testing Journal*, 33(4): 335-341.

Power, K. C., Vanapalli, S. K., and Garga, V. (2008). "A revised contact filter paper method." *Geotechnical Testing Journal*, 31(6): 461-469.

Puppala, A. J. (2008). *Estimating Stiffness of Subgrade and Unbound Materials for Pavement Design.* NCHRP Synthesis 382, Transportation Research Board, Washington D. C.

Puppala, A. J., Pedarla, A., Hoyos, L. R., Zapata, C., and Bheemasetti, T. V. (2016). "A semi-empirical swell prediction model formulated from clay mineralogy and unsaturated soil properties." *Engineering Geology*, 200: 114-121.

Quintus, H. V., and Killingsworth, B. (1998). *Analyses Relating to Pavement Material Characterizations and Their Effects on Pavement Performance*. Report number: FHWA-RD-97-085. Federal Highway Administration, US Department of Transportation, Washington, D. C.

Rahardjo, H., Melinda, F., Leong, E. C., and Rezaur, R. B. (2011). "Stiffness of a compacted residual soil." *Engineering Geology*, 120(1): 60-67.

Rahardjo, H., Satyanaga, A., and Leong, E. C. (2013). "Effects of flux boundary conditions on pore-water pressure distribution in slope." *Engineering Geology*, 165: 133-142.

Rassam, D. W., and Williams, D. J. (1999). "A relationship describing the shear strength of unsaturated soils." *Canadian Geotechnical Journal*, 36(2): 363-368.

Romero, E., and Simms, P. H. (2008). "Microstructure investigation in unsaturated soils: a review with special attention to contribution of mercury intrusion porosimetry and environmental scanning electron microscopy." *Geotechnical and Geological Engineering*, 26(6): 705-727.

Romero, E., and Vaunat, J. (2000). "Retention curves in deformable clays." In *Experimental evidence and theoretical approaches in unsaturated soils* (eds A. Tarantino and C. Mancuso), pp. 91–106. Rotterdam, the Netherlands: A. A. Balkema.

Romero, E., Gens, A., and Lloret, A. (1999). "Water permeability, water retention and microstructure of unsaturated compacted Boom clay." *Engineering Geology*, 54(1): 117-127.

Rosenbalm, D. C., and Zapata, C. E. (2013). "Incorporation of the soil-water characteristic curve hysteresis in pavement design." *Proceedings of the 1st Pan-Am Conference on Unsaturated Soils*, Cartagena de Indias, Colombia.

Sahin, H., Gu, F., Tong, Y., and Lytton, R. L. (2013). "Unsaturated soil mechanics in the design and performance of pavements." *Keynote Address, Proceedings of the 1st Pan-Am. Conference on Unsaturated Soils*, Cartagena de Indias, Colombia.

Salour, F., and Erlingsson, S. (2015). "Resilient modulus modelling of unsaturated subgrade soils: laboratory investigation of silty sand subgrade." *Road Materials and Pavement Design*, 16(3): 553-568.

Salour, F., Erlingsson, S., and Zapata, C. E. (2014). "Modelling resilient modulus seasonal variation of silty sand subgrade soils with matric suction control." *Canadian Geotechnical Journal*, 51(12): 1413-1422.

Sauer, E. K., and Monismith, C. L. (1968). "Influence of soil suction on behavior of a glacial till subjected to repeated loading." *Highway Research Record, 215,* Highway Research Board, Washington, D. C., 8-23.

Sawangsuriya, A., Edil, T. B., and Benson, C. H. (2009a). "Effect of suction on resilient modulus of compacted fine-grained subgrade soils." *Transportation Research Record, 2101,* Transportation Research Board, Washington, D. C., 82-87.

Sawangsuriya, A., Edil, T. B., and Bosscher, P. J. (2009b). "Modulus-suction-moisture relationship for compacted soils in postcompaction state." *Journal of Geotechnical and Geoenvironmental Engineering*, 135(10): 1390-1403.

Seed, H. B., Chan, C. K., and Lee, C. E. (1962). "Resilience characteristics of subgrade soils and their relation to fatigue failures in asphalt pavements." *Proceedings of the International Conference on the Structural Design of Asphalt Pavements*, Michigan, USA, 611-636.

Shaqlaih, A., White, L., and Zaman, M. (2012). "Resilient modulus modeling with information theory approach." *International Journal of Geomechanics,* 13(4): 384-389.

Sheng, D. (2011). "Review of fundamental principles in modelling unsaturated soil behaviour." *Computers and Geotechnics*, 38(6): 757-776.

Sheng, D., Fredlund, D. G., and Gens, A. (2008). "A new modelling approach for unsaturated soils using independent stress variables." *Canadian Geotechnical*

Journal, 45(4): 511-534.

Simms, P. H., and Yanful, E. K. (2001). “Measurement and estimation of pore shrinkage and pore distribution in a clayey till during soil-water characteristic curve tests.” *Canadian Geotechnical Journal*, 38(4): 741-754.

Sivakumar, V., Kodikara, J., O'Hagan, R., Hughes, D., Cairns, P., and McKinley, J. D. (2013). “Effects of confining pressure and water content on performance of unsaturated compacted clay under repeated loading.” *Géotechnique*, 63(8): 628-640.

Smith, G. N. (1986). *Probability and statistics in civil engineering*, Collins, London.

Stolle, D., Guo, P., and Liu, Y. (2009). “Resilient modulus properties of granular highway materials.” *Canadian Journal of Civil Engineering*, 36(4): 639-654.

Suriol, J., and Lloret, A. (2007). “Cambios en la estructura de suelos compactados frente a humedecimiento y secado.” *Ingenierı´a Civil, Madrid*, 147, 67-76 (in Spanish).

Suriol, J., Gens, A., and Alonso, E. E. (1998). “Behaviour of compacted soils in suction controlled oedometer.” In *Proceedings of the 2nd International Conference on Unsaturated Soils*, Beijing, 1, 463-443.

Tang, C. S., Pei, X. J., Wang, D. Y., Shi, B., and Li, J. (2015). “Tensile strength of compacted clayey soil.” *Journal of Geotechnical and Geoenvironmental Engineering*, 141(4), 04014122.

Tarantino, A., and Tombolato, S. (2005). “Coupling of hydraulic and mechanical behaviour in unsaturated compacted clay.” *Géotechnique*, 55(4): 307-317.

Thom, R., Sivakumar, V., Brown, J. and Hughes, D. (2008). “A simple triaxial system for evaluating the performance of unsaturated soils under repeated loading.” *Geotechnical Testing Journal*, 31(2): 1-8.

Thu, T. M., Rahardjo, H., and Leong, E. C. (2007). “Elastoplastic model for unsaturated soil with incorporation of the soil-water characteristic curve.” *Canadian Geotechnical Journal*, 44(1): 67-77.

Tian, P., Zaman, M. M., and Laguros, J. G. (1998). “Gradation and moisture effects on resilient moduli of aggregate bases.” *Transportation Research Record, 1619*, Transportation Research Board, Washington, D. C., 75-84.

Tinjum, J. M., Benson, C. H., and Blotz, L. R. (1997). “Soil-water characteristic curves for compacted clays.” *Journal of Geotechnical and Geoenvironmental Engineering*, 123(11): 1060-1069.

Uzan, J. (1985). "Characterization of granular material." *Transportation Research Record, 1022*, Transportation Research Board, Washington, D. C., 52-59.

Uzan, J. (1998). "Characterization of clayey subgrade materials for mechanistic design of flexible pavements." *Transportation Research Record, 1629*, Transportation Research Board, Washington, D. C., 189-196.

van Genuchten, M. T. (1980). "A closed-form equation for predicting the hydraulic conductivity of unsaturated soils." *Soil Science Society of America Journal*, 44(5): 892-898.

Vanapalli, S. K. (2009). "Shear strength of unsaturated soils and its applications in geotechnical engineering practice." *In Proceedings of the 4th Asia-Pacific Conference on Unsaturated Soils*. 579-598, New Castle, Australia.

Vanapalli, S. K., and Han, Z. (2014). "Application of the unsaturated soil mechanics in the design of pavements." *Proceedings of the 6th International Conference on Unsaturated Soils*, Sydney, Australia, 1799-1805.

Vanapalli, S. K., and Fredlund, D. G. (2000). "Comparison of empirical procedures to predict the shear strength of unsaturated soils uses the soil-water characteristic curve." *Proceedings of the Geo-Denver 2000*, Denver, USA, 195-209.

Vanapalli, S. K., and Mohamed, F. M. (2007). "Bearing capacity of model footings in unsaturated soils." *Experimental Unsaturated Soil Mechanics*, Springer Berlin Heidelberg, 483-493.

Vanapalli, S. K., and Oh, W. T. (2010). "A model for predicting the modulus of elasticity of unsaturated soils using the soil-water characteristic curve." *International Journal of Geotechnical Engineering*, 4(4): 425-433.

Vanapalli, S. K., and Oh, W. T. (2011). "Simple techniques for the estimation of suction in compacted soils in the range of 0 to 60,000 kPa." *Geotechnical Testing Journal*, 34(6): 765-774.

Vanapalli, S. K., Fredlund, D. G., and Pufahl, D. E. (1999). "Influence of soil structure and stress history on the soil-water characteristics of a compacted till." *Géotechnique*, 49(2): 143-159.

Vanapalli, S. K., Fredlund, D. G., Pufahl, D. E., and Clifton, A. W. (1996). "Model for the prediction of shear strength with respect to soil suction." *Canadian Geotechnical Journal*, 33(3): 379-392.

Wheeler, S. J., and Sivakumar, V. (1995). "An elasto-plastic critical state framework for unsaturated soil." *Géotechnique*, 45(1): 35-53.

Wheeler, S. J., Sharma, R. S., and Buisson, M. S. R. (2003). "Coupling of hydraulic hysteresis and stress–strain behaviour in unsaturated soils." *Géotechnique*, 53(1): 41-54.

Witczak, M. W. (2003). NCHRP 1-28A: *Harmonized Test Method for Laboratory Determination of Resilient Modulus for Flexible Pavement Design*. Final Report. TRB, National Research Council, Washington, D.C.

Witczak, M. W., Pellinen, T., and El-Basyouny, M. (2002). "Pursuit of the simple performance test for asphalt concrete fracture/cracking." *Journal of Association of Asphalt Paving Technologists*, 71: 767-778.

Wu, S., Gray, D. H., and Richart Jr, F. E. (1984). "Capillary effects on dynamic modulus of sands and silts." *Journal of Geotechnical Engineering*, 110(9): 1188-1203.

Xiao, J., Juang, C. H., Xu, C., Li, X., and Wang, L. (2014). "Strength and deformation characteristics of compacted silt from the lower reaches of the Yellow River of China under monotonic and repeated loading." *Engineering Geology*, 178: 49-57.

Yang, C., Cui, Y. J., Pereira, J. M., and Huang, M. S. (2008b). "A constitutive model for unsaturated cemented soils under cyclic loading." *Computers and Geotechnics*, 35(6): 853-859.

Yang, S. R., Huang, W. H., and Tai, Y. T. (2005). "Variation of resilient modulus with soil suction for compacted subgrade soils." *Transportation Research Record, 1913*, Transportation Research Board, Washington, D. C., 99-106.

Yang, S. R., Kung, J. H. S., Huang, W. H., and Lin, H. D. (2006). "Resilient modulus of unsaturated cohesive subgrade soils." *Chinese Journal of Geotechnical Engineering*, 28(2): 225-229. (In Chinese)

Yang, S. R., Lin, H. D., Kung, J. H., and Huang, W. H. (2008). "Suction-controlled laboratory test on resilient modulus of unsaturated compacted subgrade soils." *Journal of Geotechnical and Geoenvironmental Engineering*, 134(9): 1375-1384.

Zaman, M., and Khoury, N. (2007). *Effect of Soil Suction and Moisture on Resilient*

Modulus of Subgrade Soils in Oklahoma. Report number: ORA 125-6662, Oklahoma Department of Transportation, Norman, Oklahoma.

Zaman, M., Solanki, P., Ebrahimi, A., and White, L. (2010). "Neural network modeling of resilient modulus using routine subgrade soil properties." *International Journal of Geomechanics*, 10(1): 1-12.

Zapata, C. E., Andrei, D., Witczak, M. W., and Houston, W. N. (2007). "Incorporation of environmental effects in pavement design." *Road Materials and Pavement Design*, 8(4): 667-693.

Zhan, T. L., and Ng, C. W. W. (2006). "Shear strength characteristics of an unsaturated expansive clay." *Canadian Geotechnical Journal*, 43(7): 751-763.

Zhan, T. L. T. (2003). *Field and Laboratory Study of an Unsaturated Expansive Soil Associated with Rain-Induced Slope Instability*. Ph.D. thesis, Hong Kong University of Science and Technology, Hong Kong, China.

APPENDICES

Table A.1 Resilient modulus data of IHT specimens

Net confining stress, σ_{cnet} (kPa)	Deviator stress, σ_d (kPa)	Net bulk stress, θ_{net} (kPa)	Octahedral shear stress, τ_{oct} (kPa)	Resilient modulus, M_R (MPa)
Specimen: IHT-1, *w* = 17.2%, *s* = 0 kPa				
27.6	27.6	110.4	13.01	14.43
27.8	41.4	124.8	19.52	12.00
27.8	55.2	138.6	26.02	11.16
27.8	68.9	152.3	32.48	10.24
Specimen: IHT-2, *w* = 16.96%, *s* = 30 kPa				
27.6	27.6	110.4	13.01	32.00
27.8	41.4	124.8	19.52	31.98
27.8	55.2	138.6	26.02	27.78
27.8	68.9	152.3	32.48	24.39
Specimen: IHT-3, *w* = 16.46%, *s* = 60 kPa				
27.6	27.6	110.4	13.01	41.98
27.8	41.4	124.8	19.52	41.89
27.8	55.2	138.6	26.02	41.67
27.8	68.9	152.3	32.48	39.98
Specimen: IHT-4, *w* = 15.91%, *s* = 90 kPa				
27.6	27.6	110.4	13.01	52.87
27.8	41.4	124.8	19.52	49.95
27.8	55.2	138.6	26.02	46.71
27.8	68.9	152.3	32.48	43.85
Specimen: IHT-5, *w* = 15.50%, *s* = 120 kPa				
27.6	27.6	110.4	13.01	66.60
27.8	41.4	124.8	19.52	63.56
27.8	55.2	138.6	26.02	62.23
27.8	68.9	152.3	32.48	61.80

Table A.2 Resilient modulus data of TSC specimens: TSC-1 and TSC-2

Confining stress, σ_{cnet} (kPa)	Deviator stress, σ_d (kPa)	Bulk stress, θ_{net} (kPa)	Octahedral shear stress, τ_{oct} (kPa)	Resilient modulus, M_R (MPa)
Specimen: TSC-1, *w* = 14.65%, *s* = 0 kPa				
13.80	27.60	69.00	13.01	28.86
13.80	41.40	82.80	19.52	29.02
13.80	55.20	96.60	26.02	30.24
13.80	68.90	110.30	32.48	30.74
27.60	27.60	110.40	13.01	32.71
27.60	41.40	124.20	19.52	33.73
27.60	55.20	138.00	26.02	34.53
27.60	68.90	151.70	32.48	35.61
41.40	27.60	151.80	13.01	35.35
41.40	41.40	165.60	19.52	35.95
41.40	55.20	179.40	26.02	36.86
41.40	68.90	193.10	32.48	37.80
Specimen: TSC-2, *w* = 14.48%, *s* = 9 kPa				
13.80	27.60	69.00	13.01	31.49
13.80	41.40	82.80	19.52	33.40
13.80	55.20	96.60	26.02	35.85
13.80	68.90	110.30	32.48	37.04
27.60	41.40	124.20	19.52	39.37
27.60	55.20	138.00	26.02	41.21
27.60	68.90	151.70	32.48	42.21
41.40	41.40	165.60	19.52	44.72
41.40	55.20	179.40	26.02	44.81
41.40	68.90	193.10	32.48	44.32
27.60	27.60	110.40	13.01	38.50
41.40	27.60	151.80	13.01	44.41

Table A.3 Resilient modulus data of TSC specimens: TSC-3 and TSC-4

Confining stress, σ_{cnet} (kPa)	Deviator stress, σ_d (kPa)	Bulk stress, θ_{net} (kPa)	Octahedral shear stress, τ_{oct} (kPa)	Resilient modulus, M_R (MPa)
Specimen: TSC-3, w = 14.27%, s = 13 kPa				
13.80	27.60	69.00	13.01	32.08
13.80	41.40	82.80	19.52	33.74
13.80	55.20	96.60	26.02	37.18
13.80	68.90	110.30	32.48	39.39
27.60	27.60	110.40	13.01	41.04
27.60	41.40	124.20	19.52	42.94
27.60	55.20	138.00	26.02	42.53
27.60	68.90	151.70	32.48	41.54
41.40	27.60	151.80	13.01	45.20
41.40	41.40	165.60	19.52	48.55
41.40	55.20	179.40	26.02	48.79
41.40	68.90	193.10	32.48	49.90
Specimen: TSC-4, w = 13.98%, s = 18 kPa				
13.80	27.60	69.00	13.01	31.96
13.80	41.40	82.80	19.52	33.36
13.80	55.20	96.60	26.02	36.83
13.80	68.90	110.30	32.48	38.82
27.60	27.60	110.40	13.01	40.28
27.60	41.40	124.20	19.52	40.93
27.60	55.20	138.00	26.02	42.96
27.60	68.90	151.70	32.48	43.67
41.40	27.60	151.80	13.01	47.44
41.40	41.40	165.60	19.52	48.75
41.40	55.20	179.40	26.02	48.03
41.40	68.90	193.10	32.48	47.87

Table A.4 Resilient modulus data of TSC specimens: TSC-5 and TSC-6

Confining stress, σ_{cnet} (kPa)	Deviator stress, σ_d (kPa)	Bulk stress, θ_{net} (kPa)	Octahedral shear stress, τ_{oct} (kPa)	Resilient modulus, M_R (MPa)
Specimen: TSC-5, w = 13.75%, s = 21 kPa				
13.80	27.60	69.00	13.01	36.32
13.80	41.40	82.80	19.52	37.11
13.80	55.20	96.60	26.02	38.69
13.80	68.90	110.30	32.48	39.87
27.60	27.60	110.40	13.01	44.42
27.60	41.40	124.20	19.52	45.18
27.60	55.20	138.00	26.02	46.15
27.60	68.90	151.70	32.48	47.27
41.40	27.60	151.80	13.01	52.63
41.40	41.40	165.60	19.52	54.01
41.40	55.20	179.40	26.02	52.59
41.40	68.90	193.10	32.48	52.70
Specimen: TSC-6, w = 13.62%, s = 23 kPa				
13.80	27.60	69.00	13.01	37.09
13.80	41.40	82.80	19.52	37.33
13.80	55.20	96.60	26.02	39.80
13.80	68.90	110.30	32.48	41.46
27.60	27.60	110.40	13.01	44.59
27.60	41.40	124.20	19.52	45.54
27.60	55.20	138.00	26.02	46.76
27.60	68.90	151.70	32.48	48.71
41.40	27.60	151.80	13.01	50.18
41.40	41.40	165.60	19.52	51.70
41.40	55.20	179.40	26.02	53.64
41.40	68.90	193.10	32.48	55.18

Table A.5 Resilient modulus data of TSC specimens: TSC-7 and TSC-8

Confining stress, σ_{cnet} (kPa)	Deviator stress, σ_d (kPa)	Bulk stress, θ_{net} (kPa)	Octahedral shear stress, τ_{oct} (kPa)	Resilient modulus, M_R (MPa)
Specimen: TSC-7, *w* = 13.48%, *s* = 25 kPa				
13.80	27.60	69.00	13.01	39.86
13.80	41.40	82.80	19.52	40.37
13.80	55.20	96.60	26.02	42.56
13.80	68.90	110.30	32.48	43.35
27.60	27.60	110.40	13.01	45.14
27.60	41.40	124.20	19.52	43.91
27.60	55.20	138.00	26.02	46.17
27.60	68.90	151.70	32.48	48.53
41.40	27.60	151.80	13.01	54.13
41.40	41.40	165.60	19.52	53.98
41.40	55.20	179.40	26.02	54.03
41.40	68.90	193.10	32.48	53.46
Specimen: TSC-8, *w* = 12.50%, *s* = 48 kPa				
13.80	27.60	69.00	13.01	42.28
13.80	41.40	82.80	19.52	44.96
13.80	55.20	96.60	26.02	48.30
13.80	68.90	110.30	32.48	50.80
27.60	27.60	110.40	13.01	46.86
27.60	41.40	124.20	19.52	50.11
27.60	55.20	138.00	26.02	52.83
27.60	68.90	151.70	32.48	55.82
41.40	27.60	151.80	13.01	48.46
41.40	41.40	165.60	19.52	53.06
41.40	55.20	179.40	26.02	57.81
41.40	68.90	193.10	32.48	58.73

Table A.6 Resilient modulus data of OLC (OCSC) specimens: OLC-1 and OLC-2

Confining stress, σ_{cnet} (kPa)	Deviator stress, σ_d (kPa)	Bulk stress, θ_{net} (kPa)	Octahedral shear stress, τ_{oct} (kPa)	Resilient modulus, M_R (MPa)
Specimen: OLC-1, *w* = 24.85%, *s* = 0 kPa				
13.80	27.60	69.00	13.01	12.26
13.80	41.40	82.80	19.52	10.23
13.80	55.20	96.60	26.02	9.18
13.80	68.90	110.30	32.48	8.00
27.60	27.60	110.40	13.01	19.48
27.60	41.40	124.20	19.52	16.49
27.60	55.20	138.00	26.02	15.13
27.60	68.90	151.70	32.48	14.18
41.40	27.60	151.80	13.01	26.10
41.40	41.40	165.60	19.52	24.12
41.40	55.20	179.40	26.02	21.63
41.40	68.90	193.10	32.48	19.90
Specimen: OLC-2, *w* = 24.72%, *s* = 41 kPa				
13.80	27.60	69.00	13.01	20.89
13.80	41.40	82.80	19.52	21.86
13.80	55.20	96.60	26.02	22.42
13.80	68.90	110.30	32.48	22.16
27.60	27.60	110.40	13.01	23.90
27.60	41.40	124.20	19.52	24.89
27.60	55.20	138.00	26.02	26.53
27.60	68.90	151.70	32.48	25.60
41.40	27.60	151.80	13.01	29.41
41.40	41.40	165.60	19.52	28.95
41.40	55.20	179.40	26.02	28.46
41.40	68.90	193.10	32.48	26.80

Table A.7 Resilient modulus data of OLC (OCSC) specimens: OLC-3 and OLC-4

Confining stress, σ_{cnet} (kPa)	Deviator stress, σ_d (kPa)	Bulk stress, θ_{net} (kPa)	Octahedral shear stress, τ_{oct} (kPa)	Resilient modulus, M_R (MPa)
Specimen: OLC-3, w = 24.55%, s = 68 kPa				
13.80	27.60	69.00	13.01	21.51
13.80	41.40	82.80	19.52	22.81
13.80	55.20	96.60	26.02	24.14
13.80	68.90	110.30	32.48	24.66
27.60	27.60	110.40	13.01	25.80
27.60	41.40	124.20	19.52	25.71
27.60	55.20	138.00	26.02	26.18
27.60	68.90	151.70	32.48	25.74
41.40	27.60	151.80	13.01	26.37
41.40	41.40	165.60	19.52	26.60
41.40	55.20	179.40	26.02	27.32
41.40	68.90	193.10	32.48	26.61
Specimen: OLC-4, w = 24%, s = 147 kPa				
13.80	27.60	69.00	13.01	39.46
13.80	41.40	82.80	19.52	37.91
13.80	55.20	96.60	26.02	38.87
13.80	68.90	110.30	32.48	39.47
27.60	27.60	110.40	13.01	47.22
27.60	41.40	124.20	19.52	45.81
27.60	55.20	138.00	26.02	43.19
27.60	68.90	151.70	32.48	43.63
41.40	27.60	151.80	13.01	53.53
41.40	41.40	165.60	19.52	52.70
41.40	55.20	179.40	26.02	47.99
41.40	68.90	193.10	32.48	47.50

Table A.8 Resilient modulus data of OLC (OCSC) specimens: OLC-5 and OLC-6

Confining stress, σ_{cnet} (kPa)	Deviator stress, σ_d (kPa)	Bulk stress, θ_{net} (kPa)	Octahedral shear stress, τ_{oct} (kPa)	Resilient modulus, M_R (MPa)
Specimen: OLC-5, w = 23.6%, s = 219 kPa				
13.80	27.60	69.00	13.01	40.00
13.80	41.40	82.80	19.52	37.42
13.80	55.20	96.60	26.02	37.08
13.80	68.90	110.30	32.48	36.35
27.60	27.60	110.40	13.01	38.30
27.60	41.40	124.20	19.52	37.22
27.60	55.20	138.00	26.02	38.09
27.60	68.90	151.70	32.48	38.71
41.40	27.60	151.80	13.01	47.71
41.40	41.40	165.60	19.52	45.36
41.40	55.20	179.40	26.02	42.38
41.40	68.90	193.10	32.48	39.36
Specimen: OLC-6, w = 23.3%, s = 290 kPa				
13.80	68.90	110.30	32.48	70.48
13.80	55.20	96.60	26.02	72.22
13.80	41.40	82.80	19.52	73.02
13.80	27.60	69.00	13.01	73.72
27.60	68.90	151.70	32.48	68.67
27.60	55.20	138.00	26.02	70.98
27.60	41.40	124.20	19.52	71.53
27.60	27.60	110.40	13.01	71.28
41.40	68.90	193.10	32.48	68.21
41.40	55.20	179.40	26.02	70.31
41.40	41.40	165.60	19.52	69.73
41.40	27.60	151.80	13.01	68.50

Table A.9 Resilient modulus data of OLC (OCSC) specimens: OLC-7 and OLC-8

Confining stress, σ_{cnet} (kPa)	Deviator stress, σ_d (kPa)	Bulk stress, θ_{net} (kPa)	Octahedral shear stress, τ_{oct} (kPa)	Resilient modulus, M_R (MPa)
Specimen: OLC-7, w = 22.93%, s = 420 kPa				
13.80	68.90	110.30	32.48	70.31
13.80	55.20	96.60	26.02	75.33
13.80	41.40	82.80	19.52	80.75
13.80	27.60	69.00	13.01	84.71
27.60	68.90	151.70	32.48	81.18
27.60	55.20	138.00	26.02	88.08
27.60	41.40	124.20	19.52	92.44
27.60	27.60	110.40	13.01	95.94
41.40	68.90	193.10	32.48	80.75
41.40	55.20	179.40	26.02	94.78
41.40	41.40	165.60	19.52	100.12
41.40	27.60	151.80	13.01	102.83
Specimen: OLC-8, w = 22.66%, s = 558 kPa				
13.80	68.90	110.30	32.48	76.19
13.80	55.20	96.60	26.02	87.64
13.80	41.40	82.80	19.52	94.69
13.80	27.60	69.00	13.01	98.73
27.60	68.90	151.70	32.48	77.69
27.60	55.20	138.00	26.02	88.48
27.60	41.40	124.20	19.52	94.84
27.60	27.60	110.40	13.01	99.16
41.40	68.90	193.10	32.48	86.20
41.40	55.20	179.40	26.02	98.95
41.40	41.40	165.60	19.52	105.52
41.40	27.60	151.80	13.01	108.37

Table A.10 Resilient modulus data of KLC specimens: KLC-1 and KLC-2

Confining stress, σ_{cnet} (kPa)	Deviator stress, σ_d (kPa)	Bulk stress, θ_{net} (kPa)	Octahedral shear stress, τ_{oct} (kPa)	Resilient modulus, M_R (MPa)
Specimen: KLC-1, *w* = 23.5%, *s* = 0 kPa				
13.80	27.60	69.00	13.01	9.52
13.80	41.40	82.80	19.52	9.82
13.80	55.20	96.60	26.02	10.93
13.80	68.90	110.30	32.48	12.06
27.60	27.60	110.40	13.01	11.58
27.60	41.40	124.20	19.52	11.29
27.60	55.20	138.00	26.02	11.91
27.60	68.90	151.70	32.48	12.44
41.40	27.60	151.80	13.01	14.00
41.40	41.40	165.60	19.52	13.89
41.40	55.20	179.40	26.02	13.66
41.40	68.90	193.10	32.48	12.74
Specimen: KLC-2, *w* = 23.19%, *s* = 16 kPa				
13.80	27.60	69.00	13.01	15.74
13.80	41.40	82.80	19.52	14.00
13.80	55.20	96.60	26.02	14.42
13.80	68.90	110.30	32.48	14.99
27.60	27.60	110.40	13.01	17.83
27.60	41.40	124.20	19.52	15.67
27.60	55.20	138.00	26.02	15.71
27.60	68.90	151.70	32.48	15.79
41.40	27.60	151.80	13.01	22.29
41.40	41.40	165.60	19.52	19.84
41.40	55.20	179.40	26.02	18.10
41.40	68.90	193.10	32.48	17.09

Table A.11 Resilient modulus data of KLC specimens: KLC-3 and KLC-4

Confining stress, σ_{cnet} (kPa)	Deviator stress, σ_d (kPa)	Bulk stress, θ_{net} (kPa)	Octahedral shear stress, τ_{oct} (kPa)	Resilient modulus, M_R (MPa)
Specimen: KLC-3, *w* = 21.37%, *s* = 35 kPa				
13.80	27.60	69.00	13.01	22.79
13.80	41.40	82.80	19.52	23.59
13.80	55.20	96.60	26.02	23.84
13.80	68.90	110.30	32.48	27.11
27.60	27.60	110.40	13.01	26.37
27.60	41.40	124.20	19.52	27.33
27.60	55.20	138.00	26.02	28.34
27.60	68.90	151.70	32.48	31.19
41.40	27.60	151.80	13.01	30.20
41.40	41.40	165.60	19.52	33.38
41.40	55.20	179.40	26.02	34.99
41.40	68.90	193.10	32.48	39.22
Specimen: KLC-4, *w* = 20.7%, *s* = 50 kPa				
13.80	27.60	69.00	13.01	24.07
13.80	41.40	82.80	19.52	27.23
13.80	55.20	96.60	26.02	31.07
13.80	68.90	110.30	32.48	33.07
27.60	27.60	110.40	13.01	26.09
27.60	41.40	124.20	19.52	31.12
27.60	55.20	138.00	26.02	33.90
27.60	68.90	151.70	32.48	37.48
41.40	27.60	151.80	13.01	31.65
41.40	41.40	165.60	19.52	36.44
41.40	55.20	179.40	26.02	38.00
41.40	68.90	193.10	32.48	41.05

Table A.12 Resilient modulus data of KLC specimens: KLC-5 and KLC-6

Specimen: KLC-5, *w* = 20.55%, *s* = 55 kPa				
Confining stress, σ_{cnet} (kPa)	**Deviator stress, σ_d (kPa)**	**Bulk stress, θ_{net} (kPa)**	**Octahedral shear stress, τ_{oct} (kPa)**	**Resilient modulus, M_R (MPa)**
13.80	27.60	69.00	13.01	23.31
13.80	41.40	82.80	19.52	28.69
13.80	55.20	96.60	26.02	31.90
13.80	68.90	110.30	32.48	36.32
27.60	27.60	110.40	13.01	30.04
27.60	41.40	124.20	19.52	34.88
27.60	55.20	138.00	26.02	38.88
27.60	68.90	151.70	32.48	43.71
41.40	41.40	165.60	19.52	39.95
41.40	55.20	179.40	26.02	44.92
41.40	68.90	193.10	32.48	49.30
41.40	27.60	151.80	13.01	34.31
Specimen: KLC-6, *w* = 20.3%, *s* = 67 kPa				
13.80	27.60	69.00	13.01	32.31
13.80	41.40	82.80	19.52	33.17
13.80	55.20	96.60	26.02	35.09
13.80	68.90	110.30	32.48	38.11
27.60	27.60	110.40	13.01	35.85
27.60	41.40	124.20	19.52	36.35
27.60	55.20	138.00	26.02	37.75
27.60	68.90	151.70	32.48	40.97
41.40	27.60	151.80	13.01	37.77
41.40	41.40	165.60	19.52	39.65
41.40	55.20	179.40	26.02	40.76
41.40	68.90	193.10	32.48	43.79

Table A.13 Resilient modulus data of KLC specimens: KLC-7

Specimen: KLC-7, w = 19.63%, s = 136 kPa				
Confining stress, σ_{cnet} (kPa)	**Deviator stress, σ_d (kPa)**	**Bulk stress, θ_{net} (kPa)**	**Octahedral shear stress, τ_{oct} (kPa)**	**Resilient modulus, M_R (MPa)**
13.80	27.60	69.00	13.01	44.06
13.80	41.40	82.80	19.52	48.01
13.80	55.20	96.60	26.02	51.07
13.80	68.90	110.30	32.48	53.40
27.60	27.60	110.40	13.01	48.78
27.60	41.40	124.20	19.52	53.77
27.60	55.20	138.00	26.02	57.28
27.60	68.90	151.70	32.48	61.07
41.40	27.60	151.80	13.01	50.00
41.40	41.40	165.60	19.52	56.35
41.40	55.20	179.40	26.02	60.50
41.40	68.90	193.10	32.48	63.70